Aus dem Max Delbrück Centrum für Molekulare Medizin

DISSERTATION

The physiological role of mitochondrial Na^+/Ca^{2+} exchanger NCLX for glial Ca^{2+} homeostasis

Zur Erlangung des akademischen Grades
Doctor of Philosophy in Medical Neurosciences
(PhD in Medical Neurosciences)

vorgelegt der Medizinischen Fakultät
Charité - Universitätsmedizin Berlin

Von
Julia Parnis
aus Kishinev, Republik Moldau

Gutachter/in: 1. : Prof. Dr. H. Kettenmann

2. : Prof. Dr. A. Verkhratsky

3. : Prof. Dr. J. Deitmer

Datum der Promotion: 01.02.2013

Acknowledgements

I would like to express my sincere gratitude to all the people, who designed and participated in the project, giving me interesting insights into the mechanism of glial functions in the brain. I would like to thank my supervisor, Prof. Dr. Helmut Kettenmann for giving me the opportunity to work on this project; I would like to thank Dr. Christiane Nolte for taking a part in designing the project and introducing me into the world of glia and research. Special thanks go to Prof. Israel Sekler for designing the project, for teaching me the principles of Ca^{2+} imaging, for the never ending passion and enthusiasm regarding the great values of the mitochondrial Ca^{2+}. I owe to Prof. Israel Sekler my professional development as a researcher.

I would like to thank my friend and colleague, MD PhD Ignacio Delgado-Martinez, who taught me the infinite possibilities of looking on data, the importance of the analysis, and for his constant support. Thanks to Dr. Vitali Matyash for his constant support, great ideas and fruitful discussions. Special thanks go to my collaborators from the US, Prof. Vlad Parpura and Dr. Vedrana Montana, who contributed greatly to the project and were always ready to help. I would like to thank Kordelia Hummel for teaching me the basics of molecular biology and helping me with the molecular cloning of mitochondrial pericam, which allowed me to look into the microglial mitochondria.

I would like to thank the two students I supervised, Nora Freyer and Johannes Kacerovsky, who contributed to this research with results, brainstorming, and a friendly attitude. My success would be unimaginable without the help from our great technical assistants. Special thanks go to Irene Haupt, who prepared primary microglial and astrocyte cultures, which is very time-consuming. Moreover, Irene helped a lot by always thinking one step ahead and caring. Many thanks to Regina Piske for her enormous help with the experiments, for her great professional skills and understanding. Thanks also to Nadine Scharek, Karin Heufelder and Michaela Seeger-Zografakis for their technical assistance.

I would like to thank German-Israeli Foundation (GIF) for the financial support.

Many thanks go to our secretary Birgit Jarchow, who made our life much easier. Special thanks go to Sylvia Sibilak, responsible for foreign students at MDC, for her help, advices, friendly attitude and her care.

Next in the text, but extremely important, I would like to tell all my friends, my colleagues, who supported me in so many ways: "*Thank you! I would not be able to do anything without you. Thank you for your nice words, thank you for the help and shoulder when needed. Thank you that you were and still are there for me*."

My friends and my colleagues to whom I addressed the lines above are Larisa Bulavina, Bruno Benedetti, Hu Feng, Petya Georgieva, Grietje Krabbe (previously Tessmann), MinChi Ku, Jitender Kumar, Marta Maglione, Daniele Mattei, Maria Pannell, Nadine Richter, Adriana Rocha, Daniel Reyes Haro, Stefanie Seifert, Kristin Stock, Frank Szulzewsky, Susanne Wolf and dear Katyayni Vinnakota. Outside the lab I would like to thank my friend Benjamin Foerstera and many other friends, who are and were there for me.

Enormous thanks I owe to my family for all the support, for all the care, for the unconditional love. I have no enough words to express my gratitude to you. At the end I would like to thank my beloved husband, Lior, for believing in me, always supporting me, for preparing nice meals, always knowing the right words, for the warmth and care, for his LOVE.

Table of Contents

List of Figures

List of Tables

Abbreviations

AMPA	α-amino-3-hydroxy-5-methyl-4-isoxazolepropionic acid
ANT	Adenine nucleotide transporter
ATP	Adenosine 5′-triphosphate
BAPTA	1,2-bis(o-aminophenoxy)ethane-N,N,N',N'-tetraacetic acid
BCA	Bicinchoninate assay
BrdU	5-Bromo-2`-Deoxy-uridine
BSA	Bovine serum albumin
$[Ca^{2+}]_{cyt}$	Cytosolic calcium concentration
CGP37157	7-Chloro-5-(2-chlorophenyl)-1,5-dihydro-4,1-benzothiazepin-2(3*H*)-one
CNS	Central nervous system
DAG	Diacylglycerol
DAPI	4’6-diamidino-2-phenylindole
DMEM	Dulbecco’s modified Eagle medium
DMSO	Dimethyl sulfoxide
E	Embryonic day
EDTA	Ethylenediaminetetraacetic acid
EGTA	Ethylene glycol-bis(2-aminoethylether)-*N,N,N′,N′*-tetraacetic acid
ELISA	Enzyme-linked immunosorbent assay
ER	Endoplasmic reticulum
ERK1/2	Extracellular signal-regulated kinase 1/2
FCCP	Carbonyl cyanide 4-(trifluoromethoxy)phenylhydrazone
FCS	Fetal calf serum
FITC	Fluorescein isothiocyanate
GABA	γ-Aminobutyric acid
GAPDH	Glyceraldehyde 3-phosphate dehydrogenase
GDH	L-Glutamic Dehydrogenase from bovine liver

GFAP	Glial fibrillary acidic protein
GFP	Green fluorescent protein
HBSS	Hank's Balanced Salt Solution
HEK293T	Human embryonic kidney cell line
HRP	Horse radish peroxidase
IFN-γ	Interferon γ
IgG	Immunoglobulin G
IL	Interleukin
IP_3	Inositol 1,4,5-triphosphate
IP_3Rs	IP_3 receptor
LPA	Lysophosphatidic acid
LPS	Lipopolysaccharide
MAPK	Mitogen-activated protein kinase
MCP-1	Monocyte chemotactic protein 1
MCU	Mitochondrial Ca^{2+} uniporter
mGluRs	Metabotropic glutamate receptors
MTE	Mannitol-Tris EDTA solution
mtRP	Mitochondrially targeted ratiometric pericam
NAD^+	β-Nicotinamide adenine dinucleotide hydrate
NCLX	Mitochondrial Na^+/Ca^{2+} exchanger
NCX	Na^+/Ca^{2+} exchanger
NGS	Normal goat serum
NMDA	N-methyl-D-Aspartate
NMRI	Naval Medical Research Institute
P	Postnatal day
P2XR	Purinergic receptor P2X
P2YR	Purinergic receptor P2Y
PAF	Platelet-activating factor
PB	Phosphate buffer
PBS	Phosphate buffered saline
PBS-T	PBS-Tween 20

PCR	Polymerase Chain Reaction
PFA	Paraformaldehyde
PIP_2	Phosphatidylinositol 4,5-bisphosphate
PKB	Protein kinase B
PKC	Protein kinase C
PLC	Phospholipase C
PLL	Poly-L-Lysine
PMCA	Plasmalemmal Ca^{2+}-ATPase
PVDF	Polyvinylidenedifluoride membrane
qRT-PCR	Real-time quantitative RT-PCR
RANTES	Regulated upon Activation- Normal T cell Expressed and Secreted
ROS	Reactive oxygen species
rpm	Revolutions per minute
RT	Room temperature
RT-PCR	Reverse Transcription-Polymerase Chain Reaction
RyR	Ryanodine receptor
SDS-PAGE	Sodium dodecyl sulphate polyacrylamide gel electrophoresis
SEM	Standard error of mean
SERCA	Sarcoplasmic-ER Ca^{2+}-ATPase
SFM	Serum-free medium
siGAPDH	Small interfering RNA vs. GAPDH
siNCLX	Small interfering RNA vs. NCLX
siRNA	Small interfering RNA
SOC	Store-Operated Channels
SOCE	Ca^{2+} entry via SOC
Stim	Stromal interaction molecule
TCA	Tricarboxylic cycle
TLR4	Toll-like receptor 4
TRITC	Tetramethylrhodamine isothiocyanate

TRPC	Transient receptor potential canonical type
UTP	Uridine 5′-triphosphate
VGCC	Voltage-gated Ca2+ channels
YFP	Yellow fluorescent protein
α-MEM	Minimum Essential Media

Chapter 1

Introduction

1.1 The life of calcium signaling

Ja, Kalzium das ist alles!

(1959, Otto Loewi, Nobel laureate from 1936)

Calcium (Ca^{2+})

In the nineteenth century the well-known British clinician and pharmacologist Sidney Ringer revealed the great importance of Ca^{2+} for heart function. The discovery was accidental: he mistakenly used London tap water instead of distilled water and to his surprise observed that isolated rat hearts contracted beautifully in tap water but not in distilled water. Experimenting with different minerals, he revealed that ”calcium salts are necessary for the proper contraction of the heart” (Ringer, 1883). Although this great breakthrough did not win the immediate attention of scientists, this was the beginning of Ca^{2+} signaling era.

Ca^{2+} is one of the most important molecules in biology. Calcium ions were in fact chosen to be the most ubiquitous signaling molecules very early in evolution, maybe as early as ATP (Adenosine 5′-triphosphate) was chosen to be the energy currency in most living creatures. On the one hand, Ca^{2+} affects the properties of biological membranes and readily interacts with different biological molecules, while on the other hand, a majority of reactions utilizing ATP can proceed only at low Ca^{2+} concentration ($[Ca^{2+}]$). High $[Ca^{2+}]$ is harmful for cells causing protein and nucleic acid aggregation, influencing the integrity of biological membranes and initiating the precipitation of phosphates, the source of energy transfer and acid-base buffering properties. Therefore, all life forms tightly control intracellular $[Ca^{2+}]$.

From the middle of twentieth century the information regarding the involvement of Ca^{2+} in a variety of cell activities accumulated with growing speed. Today we know that Ca^{2+} is the most ubiquitous second messenger involved in the regulation of every aspect of life: muscle contraction, oocyte fertilization, endocrine and paracrine secretion, exocytosis, metabolism, cell proliferation, cell death and more (Berridge et al., 2003; Berridge et al., 2000; Clapham, 2007).

However, it was only towards the end of twentieth century that Roger Tsien's brilliant idea to trap Ca^{2+} indicators inside the cell (Tsien, 1981) allowed the measurement of Ca^{2+} concentrations for the first time and enabled the changes to be followed in different cellular processes. Today different Ca^{2+}-sensitive dyes and genetically encoded Ca^{2+}-sensors allow the examination of Ca^{2+} in different organelles and at specific cellular locations in real time. And seeing is believing.

Ca^{2+} signaling toolkit

Keeping low cytosolic free [Ca^{2+}] ([Ca2+]$_{cyt}$) is an universal characteristic of all eukaryotic cells. [Ca^{2+}]$_{cyt}$ is about 10,000 fold lower that [Ca^{2+}] in the extracellular milleau. This is achieved via the interplay between the "ON" reactions, which introduce Ca^{2+} into the cytoplasm, and "OFF" reactions, which extrude Ca^{2+} from the cytoplasm (Berridge et al., 2003). Free cytosolic Ca^{2+} can bind to an array of sensors, further processing the signal to the effectors, which execute Ca^{2+}-dependent processes. Proteins performing the functions of these diverse Ca^{2+} signaling systems constitute the "Ca^{2+} signaling toolkit". Many of the toolkit's components undergo alternative splicing and have several isoforms with different properties, therefore expanding even more the versatility of Ca^{2+} signaling. The components of the Ca^{2+} signaling toolkit are cell-type specific. Figure 1.1 shows the main components of the cellular Ca^{2+} signaling toolkit.

Receptors triggering Ca^{2+} entry - Two types of receptors responsible for the "ON" reaction have been described: ionotropic and metabotropic receptors. Both are located on the plasma membrane. Ionotropic receptors are channels, which are activated and open upon ligand binding. Through them Ca^{2+} enters from the large Ca^{2+} pool in the extracellular space driven by its electrochemical gradient. Metabotropic receptors are also activated upon ligand binding, but unlike ionotropic receptors, they trigger Ca^{2+} mobilization from the endoplasmic reticulum (ER) Ca^{2+} stores via the activation of trimeric G-proteins, which in turn activate phospholipase C (PLC). PLC cleaves phoshphoinositol PIP_2 (Phosphatidylinositol 4,5-bisphosphate), and the product IP_3 (inositol 1,4,5-triphosphate) binds to and opens IP_3 receptors (IP_3Rs) on the ER.

Channels triggering Ca^{2+} entry - Channels responsible for Ca^{2+} entry include voltage-gated and store-operated channels. Voltage-gated channels are located on the plasma membrane of excitable cells, while Store-Operated Channels (SOC) are found on the plasma membrane of the majority of cells. SOC are activated upon depletion of the ER Ca^{2+} store. Ca^{2+} entry via SOC

(SOCE) was shown to be mediated by Orai proteins on the plasma membrane (Orai1, Orai2 and Orai3) and Stim (stromal interaction molecule) proteins on the ER (Stim1 and Stim2). Orais build the channels themselves, while Stim proteins sense ER [Ca^{2+}], and when [Ca^{2+}] in the ER drops below a certain threshold, evoke opening of Orai channels. This is accomplished via the

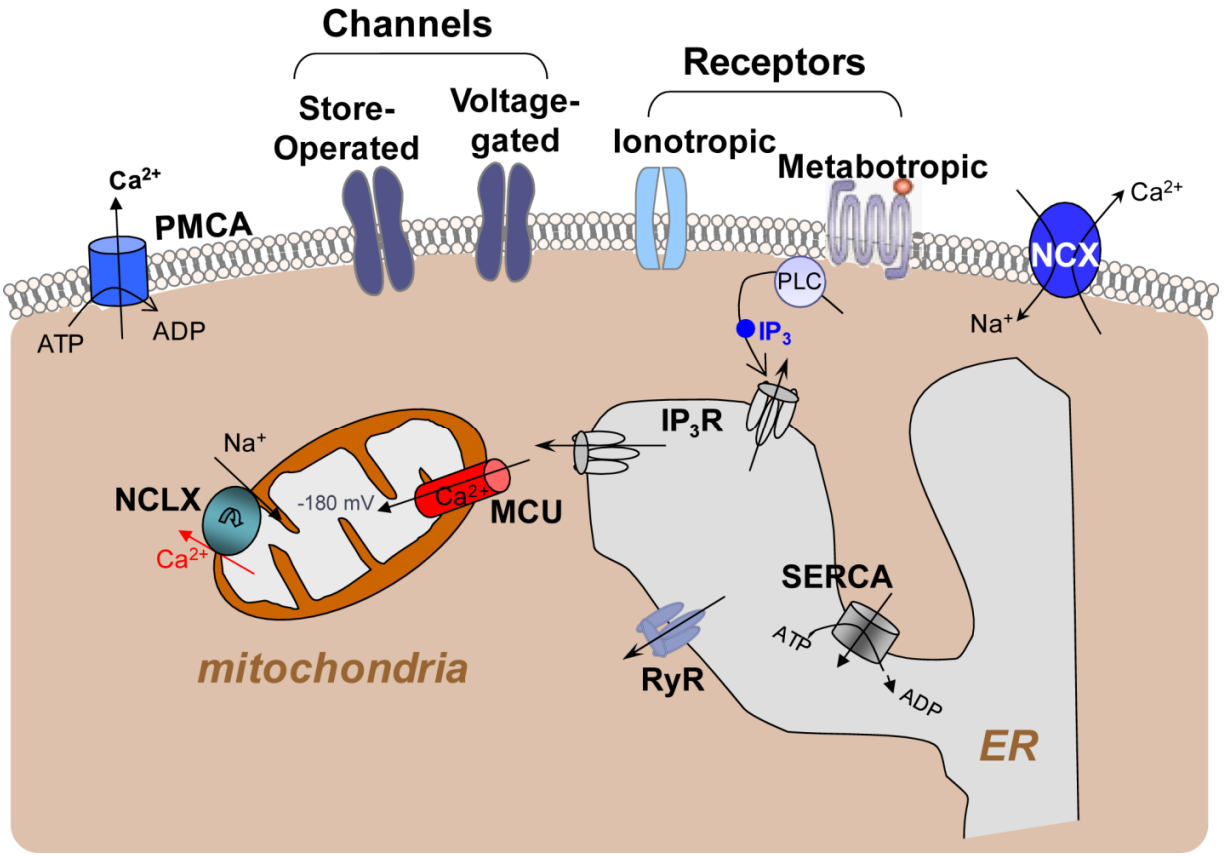

***Figure 1.1.* Principles of cellular Ca^{2+} signaling**

General scheme depicting the main components of the Ca^{2+} signaling toolkit. Some of the components exist in several isoforms, further adding to the versatility of cellular Ca^{2+} signaling. Ca^{2+} entry into the cytosol begins from the activation of channels or receptors on the plasma membrane. Open channels and ionotropic receptors cause Ca^{2+} entry into the cytosol from the extracellular space. Extrusion of Ca^{2+} from the cytosol is mediated by plasmalemmal Ca^{2+}-ATPases (PMCA) or Na^+/Ca^{2+} exchangers (NCX). Additional Ca^{2+} stores in the cell are endoplasmic reticulum (ER) and mitochondria. IP_3, inositol 1,4,5-triphosphate; IP_3R, inositol 1,4,5-triphosphate receptor; PLC, phospholipase C; RyR, ryanodine receptor; SERCA, sarcoplasmic-ER Ca^{2+}-ATPase; MCU, mitochondrial Ca^{2+} uniporter; NCLX, mitochondrial Na^+/Ca^{2+} exchanger.

ability of Stim1 proteins to bind Ca^{2+} in the ER lumen via their N-terminal EF hand motif. When ER Ca^{2+} levels decrease, Ca^{2+}-free Stim1 proteins can oligomerize with other Stim1 molecules, creating large aggregates (Putney, 2009). Multioligomerized Stim1 is translocated to the ER-plasma membrane junction, activating and opening the Orai channels, through which Ca^{2+} enters according to its electrochemical gradient. Stim1 does not only interact with Orais, but also seems to be able to interact with TRPC (transient receptor potential canonical type) channels. Furthermore, Stim1, Orai1 and several TRPCs can oligomerize and create different SOCs with distinguished properties (Huang et al., 2006; Yuan et al., 2007).

Phospholipase C – PLC is a plasma membrane bound enzyme, catalyzing the reaction of cleavage of PIP_2 to IP_3 and diacylglycerol (DAG). IP_3 and DAG are second messengers. DAG activates protein kinase C and IP_3 binds to and opens IP_3R on the ER surface. The PLC family consists of 14 known members and is divided into 6 groups: PLC-β, PLC-γ, PLC-δ, PLC-ε, PLC-ζ and PLC-η (Berridge et al., 2003). PLC isoforms are widely distributed. Most of them are activated by heterotrimeric G-proteins, PLC-ε is activated by small GTPases Rho and Ras (Wing et al., 2003).

IP_3 receptor (IP_3R) – IP_3Rs are located on the ER and ubiquitously expressed in many cell types. IP_3R is a protein, consisting of four subunits of about 310 kDa (Clapham, 2007; Foskett et al., 2007; Parpura and Verkhratsky, 2011). Three isoforms of IP_3Rs are known: IP_3R1, IP_3R2, IP_3R3. Usually most of the cells express more than 1 isoform of IP_3Rs. IP_3R-mediated Ca^{2+} release can be regulated by IP_3 and by Ca^{2+} itself, via phosphorylation and protein-protein interactions (Foskett et al., 2007).

Ca^{2+}-ATPases (PMCA and SERCA) and Ca^{2+}-exchangers (NCX, NCKX) – Following Ca^{2+} entry from the extracellular space or from the internal stores, Ca^{2+} should leave the cytosol to maintain Ca^{2+} homeostasis. Moving Ca^{2+} out of the cell against its electrochemical gradient is performed by two ATPases: plasmalemmal Ca^{2+} ATPase (PMCA) and sarcoplasmic-ER Ca^{2+} ATPase (SERCA). Four PMCA isoforms and three SERCA isoforms are known (Clapham, 2007; Strehler et al., 2007; Strehler and Treiman, 2004). The isoforms are regulated differently and have distinct kinetic characteristics. The isoforms show developmental-, tissue- and cell-type specific expression patterns.

Ca^{2+} exchangers, unlike pumps, use the electrochemical gradient of Na^+ to extrude Ca^{2+} from the cytosol. They consist from Na^+/Ca^{2+} exchangers (NCX) or K^+-dependent Na^+/Ca^{2+} exchangers (NCKX). Mammals express three members of NCX (encoded by Slc8 genes) and

five members of NCKX (encoded by Slc24 genes). NCX1 is the most widely expressed member of NCX family, while NCX2 is abundant in neurons of the brain, and NCX3 is present in the skeletal muscles and in some areas of the brain (Lytton, 2007). NCKX1 is mostly expressed in the eye and to some extent in cells of haemopoietic origins (Lytton, 2007). NCKX2 is highly expressed in the neurons in the brain, retinal ganglion cells and cone photoreceptors. NCKX3 and 4 are expressed in the brain and widely distributed outside of the brain. NCKX5 is very abundant in the eye and skin, strongly expressed in the brain and thymus, and has lower expression in other tissues (Lytton, 2007).

1.2 Ca^{2+} signaling in glia: the source of excitability

"Hitherto, gentlemen, in considering the nervous system, I have only spoken of the really nervous parts of it. But if we would study the nervous system in its real relations in the body, it is extremely important to have a knowledge of that substance also which lies between the proper nervous parts, holds them together and gives the whole its form in a greater or less degree" (Virchow, 1858). With these words the German pathologist Rudolf Virchow first described neuroglia. He presented them as merely connective tissue. The cellular origin of glia was shown later by Camillo Golgi (Golgi, 1873, 1903).

In glial cells, Ca^{2+} homeostasis plays a central role in diverse cellular processes. Glial cells of the central nervous system (CNS) are divided into three major subtypes: astroglia, oligodendroglia and microglia. In the brain, glial cells comprise the largest cellular population. They provide physical and metabolic support for neurons or control immune responses in the brain (microglia). These cells also play important roles in the development of the nervous system and in the regulation of neuron repair mechanisms after injury. Moreover, glial cells, in particular astrocytes, actively participate in synaptic transmission and are involved in the formation of cellular circuits and information processing in the brain (Agulhon et al., 2008; Perea et al., 2009).

Microglia: immune cells of the brain

The immune system is subdivided into innate and adaptive systems. The innate system responds immediately to any foreign particle, while the adaptive system responds later, but has a property of cellular memory. Microglia belong to the innate immune cells of the central nervous system (CNS) and respond to pathogens without prior exposure.

The first description of microglia goes back to around 1920 to Pio Del Rio-Hortega (Del Rio Hortega, 1919, 1920). By using modified silver carbonate impregnation to stain microglia, he could illustrate for the first time the properties of microglia, which still hold true today.

Microglia are derived from primitive myeloid progenitor cells in parallel to monocytes. In 2010 Ginhoux et al. (Ginhoux et al., 2010) found by fate mapping experiments that they originate at a very early developmental stage within the yolk sac. They appear between embryonic day 7 (E7) and E7.5 from yolk sac progenitors. Around E8 these progenitors enter the embryo and at E10 they populate the CNS rudiment. In the healthy mature CNS, microglia have a ramified or "resting" morphology, presented by a small soma and fine processes (Figure 1.2). The term "resting" to describe microglia is no longer true. The in vivo imaging studies of green-EGFP-expressing microglia show constant movement of microglial processes (Davalos et al., 2005; Nimmerjahn et al., 2005). They constantly scan their environment, and any change will trigger their immediate response.

Trauma, infection, ischemia, altered neuronal homeostasis or neurodegenerative diseases activate microglia. Activated microglia change their shape to an amoeboid appearance, which was described as an egg-like shape, i.e. possess less cellular processes and larger somata (Figure 1.2). Moreover, activation of microglia involves changes in gene expression, and reorganization of the cell phenotype. Activated microglia are able to migrate towards the source of "change" following chemotactic gradients and proliferate. They clear damaged cells or debris via phagocytosis. Finally, microglia can secrete an array of pro – and anti – inflammatory molecules, and chemokines (Table 1.1). When the immune reaction is enhanced, microglia also help to recruit other immune cells from the periphery to the CNS, amplifying the immune reaction. Until today the discrimination between microglia and invading monocytes was impossible. However, recent developments in the field reveal changes between these cells in morphology and gene expression (unpublished results, Ransohoff R.M). This hopefully will help to unveil the microglial role in pathology, and would allow seeing the interplay between microglia, monocytes and the resident cells of the CNS.

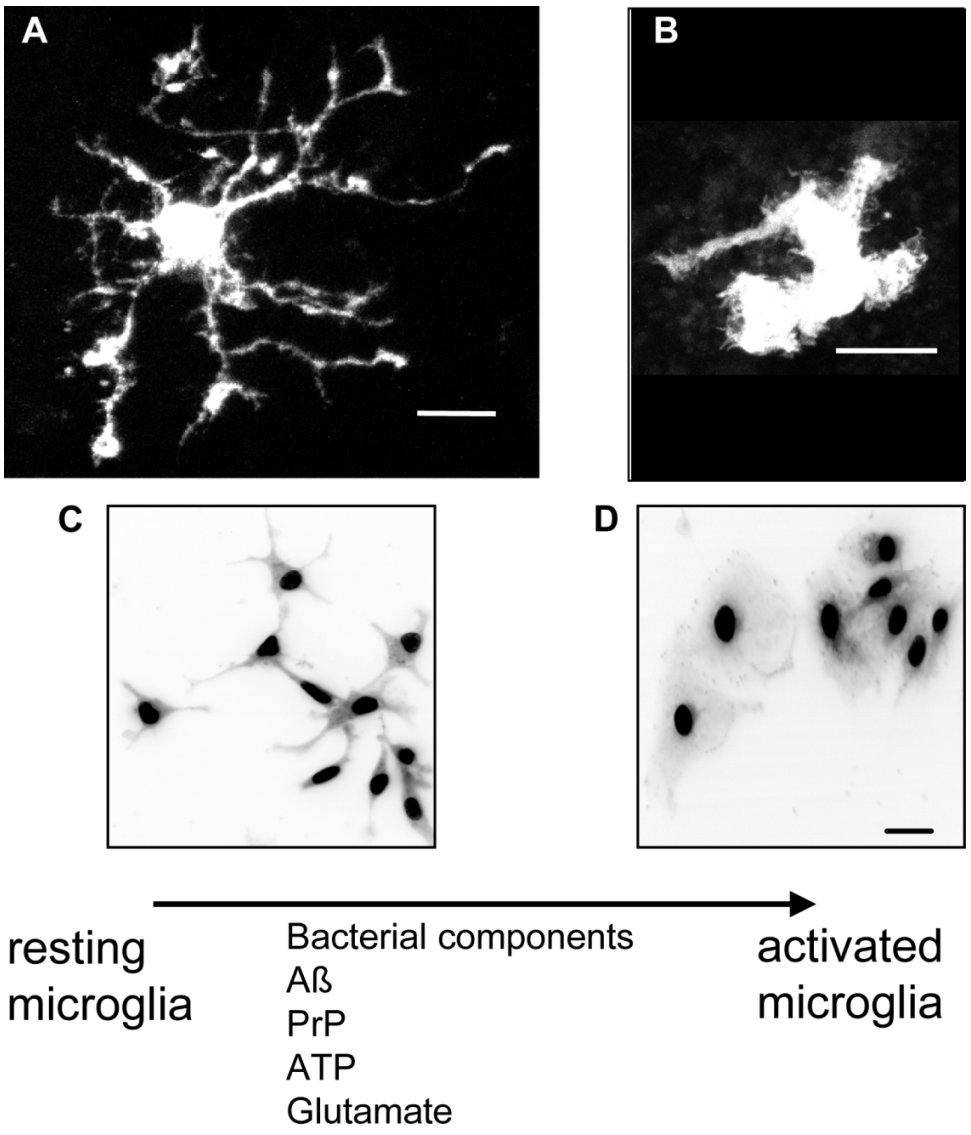

Figure 1.2. ***Resting vs. activated microglial cells***

Microglial cells in tissue ***(A-B)*** in resting or ramified morphology ***(A)*** are activated in response to pathological stimulus and take an amoeboid shape ***(B)***. The same can be observed for microglial cells grown in culture ***(C-D)***. Cultured cells ***(C)*** become more activated under pathological stimuli ***(D)***. ***(A)*** Microglial cell from an acute brain slice was injected with Lucifer Yellow after recording with the patch clamp technique (Boucsein et al., 2003). ***(B)*** The cell in the facial nucleus underwent a change in morphology two days after facial nerve axotomy (Boucsein et al., 2000). ***(C,D)*** Microglial cells isolated from rat brain were cultured for one day (Kingham et al., 1999). Culture conditions do not mimic the normal brain environment, but involve a pathological event and alteration in neuronal homeostasis. Therefore cultured microglia are activated compared to more ramified tissue cells. ***(D)*** Microglial cells exposed to lipopolysaccharide (LPS) (1 µg/ml LPS for 24 h), an immunogenic component of the bacterial cell wall; their appearance changes to an amoeboid one. The scale bars are 10 µm. (Taken from (Pocock and Kettenmann, 2007))

Microglial activation is considered a normal reaction needed for the tissue repair after CNS injury. However, massive or chronic activation of microglial cells can enhance the immune reaction in the CNS, exacerbating CNS injury. This is due to an array of cytotoxic substances, such as free radicals, glutamate, proteases, neurotoxic and pro-inflammatory cytokines secreted by over-activated microglia (Kettenmann et al., 2011; Kreutzberg, 1996). Therefore, microglial activation is tightly regulated. This is not "all-or-nothing" process, but a dynamic response with distinct acquired functions. Microglial function is further controlled by cytokines and neurotransmitters released by neurons and other glial cells, therefore creating diverse possibilities for interactions between neurons, microglia and astrocytes (Hanisch, 2002).

Table 1.1. ***Secretory molecules of microglia***

Class	Substanses/ Proteins	
Cytokines	IL-1, IL-6, IL-10, IL-12, IL-16, IL-23, TNFα, TGFβ	
Chemokines	CC:	CCL2/MCP-1, CCL3/MIP-1α, CCL4/MIP-1β, CCL5/RANTES
	CXC:	CXCL8/IL-8, CXCL9/MIG, CXCL10/IP-10, CXCL12/SDF-1α
	CX3C:	CX3CL1/fractalkine
Matrix metalloproteinases	MMP-2, MMP-3, MMP-9	
Free radicals	ROS (reactive oxygen species), nitric oxide	
Eicosanoids	PGD2, leukotriene C4	
Growth factors	nerve growth factor, fibroblast growth factor	
Proteases	elastase, plasminogen, Cathepsins B and L	
Glutamate receptors/ channels agonists	Quinolinic acid, glutamate	
Complement factors	C1, C3, C4	

Other	Amyloid precursor protein

(secretion of these molecules is modulated either by microglial activation, anatomical location, age or animal species). Taken from Rock et al. (Rock et al., 2004)

Microglial Ca^{2+} signaling

The literature describing microglial Ca^{2+} signaling is mostly based on the studies performed on cultured microglia. Microglia, as immune cells are activated by any isolation or cutting procedure, therefore the majority of the research in the field shows rather activated, but not the ramified microglia present in the healthy brain. *In vivo* recordings from the green GFP-expressing microglia have shown new and very exciting data about microglial function in the healthy brain; however the information regarding microglial Ca^{2+} *in vivo* in healthy brain is still missing (Kettenmann et al., 2011).

To study the role of Ca^{2+} signaling in microglial function, the component of the bacterial wall, lipopolysaccharide (LPS) is often used to trigger microglial activation. It was shown that LPS-evoked microglial activation is paralleled by a chronic increase in the resting Ca^{2+} level and reduced Ca^{2+} signaling following stimulation with UTP (Uridine 5′-triphosphate) and complement C5a (Hoffmann et al., 2003). Lowering the $[Ca2+]_{cyt}$ by chelating Ca^{2+} with BAPTA (1,2-bis(o-aminophenoxy)ethane-N,N,N',N'-tetraacetic acid) restored the strength of the Ca^{2+} signals along with the inhibition of the LPS-induced cytokine release. However, elevation of the resting Ca^{2+} level was not sufficient for evoking cytokine release.

In microglial cells, Ca^{2+} is instrumental in regulating their executive functions, such as release of cytokines and cell toxic molecules, or migration and phagocytosis (Farber and Kettenmann, 2006; Ifuku et al., 2007; Nolte et al., 1996). For example, complement C5a-induced microglial motility was found to be linked to a G-protein coupled receptor and accompanied with $[Ca^{2+}]_{cyt}$ increases. Microglial migration involves $P2Y_{12}$ purinergic receptors and is also linked to PLC-mediated Ca^{2+} increases (Kettenmann et al., 2011). Purinergic metabotropic receptor $P2Y_6$, mobilizing Ca^{2+} from the ER, was shown to participate in the clearance of apoptotic cell debris by microglia (Koizumi et al., 2007).

Microglial Ca^{2+} toolkit

Such precise responses in microglial $[Ca^{2+}]_{cyt}$ require the well-concerted action of Ca^{2+} channels, pumps and exchangers, located within the plasma membrane and the intracellular calcium storage elements, like endoplasmic reticulum (ER) and mitochondria. Here I will present components of the microglial Ca^{2+} toolkit, responsible for these changes.

Plasma membrane- Microglia respond with Ca^{2+} increases to numerous stimuli, like complement C5a, endothelin, lysophosphatidic acid (LPA), platelet-activating factor (PAF), RANTES (Regulated upon Activation- Normal T cell Expressed and Secreted), thrombin and some neurotransmitters (Kettenmann et al., 2011). To respond to these stimuli, microglial cells are equipped with different receptors and channels on the plasma membrane. One of the best characterized systems in microglia is the purinergic signaling system, differentially responding to different derivatives of ATP. Purinoreceptors are divided into metabotropic P1 adenosine receptors, metabotropic P2Y purinoreceptors and ionotropic P2X receptors. Microglia also respond to glutamate, the major neurotransmitter in the brain, via ionotropic AMPA (α-amino-3-hydroxy-5-methyl-4-isoxazolepropionic acid) receptors or metabotropic mGluR receptors. Microglia also express $GABA_B$ (GABA, γ-Aminobutyric acid) receptors, nicotinic Acetylcholine receptors (nAChRs), adrenergic and dopamine receptors. Microglia respond with Ca^{2+} increases to a variety of neurohormones and neuromodulators via receptors to PAF, bradykinin, histamine, endothelin, cannabinoids, angiotensin, opioids etc. (Kettenmann et al., 2011; Pocock and Kettenmann, 2007).

One of the major Ca^{2+} entry pathways in microglia is mediated by SOC on the plasma membrane. Ca^{2+} entry via SOC (SOCE) is triggered by the depletion of the ER Ca^{2+} stores. The first evidence for functional SOCE in microglia derived from Ca^{2+} imaging studies on C5a and C3a-stimulated microglia (Moller et al., 1997) and later from microglia stimulated with purinergic agonists (Toescu et al., 1998). Although the existence of STIM1s and Orais was shown to mediate SOCE in many cells, their expression and function in microglia is still a mystery.

Ca^{2+} extrusion in microglia is mediated via PMCAs and NCXs on the plasma membrane. The expression of PMCAs is not characterized in microglia. Na^+/Ca^{2+} exchange was shown in microglia using Ca^{2+} imaging technique (Nagano et al., 2004). Further studies revealed the expression of all three existing isoforms NCX1, NCX2 and NCX3 in rat microglia *in vitro* at both mRNA and protein levels (Matsuda et al., 2006; Nagano et al., 2004).

PLC was shown to function in microglia. For example, albumin pre-incubation with rat cultured microglia evoked cell proliferation along with $[Ca^{2+}]_{cyt}$ elevation via the Src tyrosine kinase, PLC and IP_3 (Hooper et al., 2005). However, neither the expression of PLC nor the characterization of PLC isoforms was reported in microglia.

ER- To release Ca^{2+} from the major intracellular Ca^{2+} store, ER, functional RyRs and IP_3Rs were shown in microglia (Kettenmann et al., 2011; Klegeris et al., 2007). In human microglia stimulation with RyR agonist cyclic ADP ribose evoked Ca^{2+} elevation (Kettenmann et al., 2011), however the role of RyRs in microglial physiology is unclear. Human microglia express three RyR subunits, while the molecular identity of IP_3Rs in microglia remains unknown. After agonist application and depletion of ER Ca^{2+} stores they are refilled via SERCA. The effectiveness of the SERCA inhibitors thapsigargin and cyclopiazonic acid (CPA) suggests a role for SERCA in microglial Ca^{2+} regulation (Kettenmann et al., 2011). Interestingly, SERCA inhibition by thapsigargin could transfer microglia from the activated into the ramified phenotype (Yagi et al., 1999), suggesting the involvement of ER Ca^{2+} stores in the ramification process of microglia. However, SERCA expression in microglia was never shown.

Astrocytes

Soon after the discovery of neuroglia by Camillo Golgi, a subset of glial cells was called astrocytes by Michael von Lenhossek (Lenhossek, 1891). The astrocytes were further classified into two types. Protoplasmic astrocytes are found in the grey matter, where they ensheathe synapses and blood vessels. Fibrous astrocytes are found in the white matter, where they contact nodes of Ranvier and blood vessels.

It is hard to define astrocytes as one cell population. Astrocytes are very heterogeneous in their morphology, protein composition and function. Only according to astrocytic identifying staining with GFAP (glial fibrillary acidic protein) and S100β, rodent astrocytes can be divided into 9 different population (Emsley and Macklis, 2006): tanycytes, radial glia, Bergmann glia, protoplasmic astrocytes, fibrous astrocytes, velate glia, marginal glia, perivascular glia and ependymal glia. In one brain region several types of astrocytes can co-exist. Figure 1.3 shows some examples of different types of astrocytes in the CNS. The density of astrocytes can vary between different regions. This diversity expands further in primates (Matyash and Kettenmann, 2010).

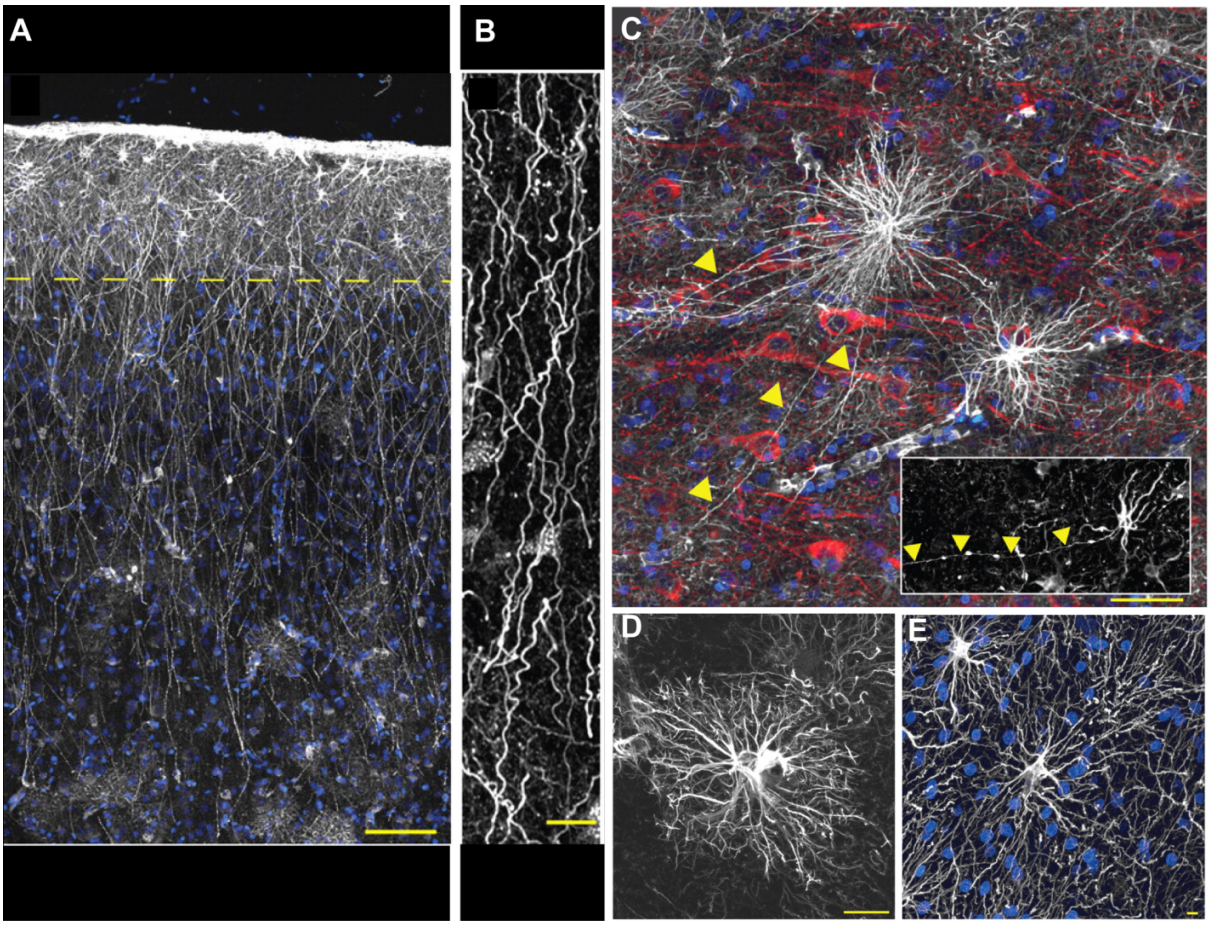

***Figure 1.3.* Morphological heterogeneity of astrocytes**

(A) GFAP-stained astrocytes (*white*) in pial surface and layers 1–2 of human cortex. Cell nuclei are stained with DAPI (*blue*). Scale bar, 100 µm. Yellow line indicates border between layer 1 and 2. ***(B)*** Interlaminar astrocyte processes characterized by their tortuosity. Scale bar, 10 µm. ***(C)*** Varicose projection astrocytes reside in layers 5–6 and extend long processes characterized by evenly spaced varicosities. Inset, Varicose projection astrocyte from chimpanzee cortex. Astrocytic marker GFAP is shown in *white*; Neuronal marker MAP2 is shown in *red*; and nuclear stain DAPI is *blue*. Yellow arrowheads indicate varicose projections. Scale bar, 50 µm. ***(D)*** Typical human protoplasmic astrocyte. Scale bar, 20 µm. ***(E)*** Human fibrous astrocytes in white matter. Scale bar, 10 µm. (Taken from (Matyash and Kettenmann, 2010)).

To meet the extremely high energy demands, brain cells are able to use glucose, lactate, pyruvate and glutamine as their energy sources (Belanger et al., 2011). Despite the fact that in

the extracellular space both glucose and lactate are similarly abundant (concentration of 0.5-1.5 mM) (Belanger et al., 2011), neurons prefer lactate over glucose. Astrocytes and neurons differ metabolically and use discrete metabolic pathways under the same physiological condition, complementing each other's requirements. For example, neurons depend on the mitochondrial oxidative metabolism, while astrocytes are highly glycolytic. As lactate generation depends on glycolysis, astrocytes produce lactate from the majority of their utilized glucose and release it into the extracellular space. Transfer of lactate from astrocytes to neurons was proposed to proceed via the astrocyte-neuron lactate shuttle (Pellerin and Magistretti, 1994). First, glutamate is released upon neuronal activation. The extracellular glutamate is taken up by astrocytes via Na+-dependent process. Na^+ is extruded from astrocytes via Na^+/K^+ ATPase, which requires ATP and consequently, increases the utilization of glucose. The resulting enhancement in glycolysis leads to an elevation in the level of secreted lactate. Then, lactate is utilized by neurons to meet their energy demands.

Astrocytes unlike neurons metabolize glycogen, the largest energy store in the brain. Interestingly, some neurotransmitters promote glycogenolysis in cortical slices and in astrocytes *in vitro* (Belanger et al., 2011). The astrocytic glycogen reservoir was shown to maintain neuronal function and viability, when energy supply is scarce (Belanger et al., 2011).

Moreover, astrocytes are responsible for glutamate replenishment in the brain. First, glutamate uptake is achieved mainly in astrocytes via high affinity glutamate transporters. This glutamate is converted to glutamine by glutamine synthetase, an enzyme specific for astrocytes. Glutamine, secreted by astrocytes is taken up by neurons, which can then convert it back to glutamate. Second, only astrocytes express pyruvate carboxylase, enabling them to produce glutamate from glucose.

Astrocytes can control synaptic communication via different mechanisms. First, astrocytes regulate levels of K^+ ions and neurotransmitters at the synaptic cleft. Second, astrocytes express receptors for numerous neurotransmitters and release neuroactive and trophic factors, helping in the regulation of synapse maturation and functioning, blood flow, and neuronal survival. For example, co-culture of CNS neurons called retinal ganglion cells with astrocytes could increase the neuronal synaptic activity by about 100-fold (Pfrieger and Barres, 1997). Using co-cultures of retinal ganglion cells and astrocytes, Ullian et al. (Ullian et al., 2001) found that astrocytes enhance synaptic function and increase the number of new synapses by about 10-fold. These data support astrocytic function in the formation and maintenance of synaptic connections *in vitro*.

Moreover, astrocytes have been shown to participate in synaptic plasticity. For, example Müller and Best (Muller and Best, 1989) found that ocular dominance plasticity was restored following the transplantation of immature astrocytes into primary visual cortex of adult cats. Not much is known regarding how astrocytes regulate synaptic plasticity. Intermediate filaments, GFAP and vimentin were shown to be involved in astrocytic regulation of neural plasticity and regeneration (Parpura et al., 2012). During development astrocytes cause developing neurons to express complement component C1q, tagging specific synapses for elimination (Stevens et al., 2007). The evidence grows for the support of active astrocytic participation in shaping brain functioning.

Astrocytes are connected to neurons on one side, and on the other side their endfeet cover almost all vascular surfaces in the brain. Astrocytes regulate the change in local cerebral blood flow via triggering constriction or relaxation of smooth muscle cells on the vasculature. Astrocytes, vascular cells and neurons comprising one functional entity are called neurovascular unit. Release of either vasoconstrictors or vasodilators by astrocytes and neurons control the vascular tone and local cerebral blood flow. Astrocytes listen to neuronal activity via responding to neurotransmitters released during neuronal function. Both, vasodilation and vasoconstriction were shown to be triggered following astrocyte activation via metabotropic glutamate receptor and consequent Ca^{2+} elevation (Attwell et al., 2010). However, it is still unclear which mechanisms are involved in vasoconstriction and vasodilation *in vivo*.

Astrocyte Ca^{2+} signaling

Astrocyte Ca^{2+} excitability was first shown in the early 1990s (Cornell-Bell et al., 1990). Using Ca^{2+} imaging of cultured astrocytes, these studies linked astrocyte excitability to elevated Ca^{2+} intracellular levels. Subsequent studies *in vitro*, in brain slices and *in vivo* substantiated that astrocytic activity is paralleled by Ca^{2+} elevations, which mainly come from the ER.

Astrocyte Ca^{2+} signals can be divided into spontaneous oscillations and transients evoked by neurotransmitters (Table 1.2). Moreover, Ca^{2+} signals can propagate to neighboring astrocytes as an intercellular Ca^{2+} wave. Ca^{2+} waves were first shown *in vitro* (Cornell-Bell et al., 1990). In brain slices such Ca^{2+} waves involve fewer astrocytes. Ca^{2+} waves exist also *in vivo* in pathological conditions, like Alzheimer disease (Kuchibhotla et al., 2009; Nimmerjahn et al., 2009), epilepsy or cortical spreading depression (Fiacco and McCarthy, 2006), in the developing

retina (Fiacco and McCarthy, 2006) and under normal physiological conditions in the hippocampus (Kuga et al., 2011) and in cerebellum (Hoogland et al., 2009; Nimmerjahn et al., 2009).

Table 1.2 ***Ca^{2+} signaling in astrocytes***

	Neurotransmitter	Experimental model	Brain area	Refs
Spontaneous activity	Non-applicable	Brain slices	Thalamus	(Aguado et al., 2002; Parri et al., 2001)
			Hippocampus	(Aguado et al., 2002; Nett et al., 2002)
			Cerebellum	(Aguado et al., 2002; Grosche et al., 1999)
			Cortex	(Peters et al., 2003)
			Striatum	(Aguado et al., 2002)
		In vivo	Cortex	(Dombeck et al., 2007; Hirase et al., 2004; Takata and Hirase, 2008)
Synaptically evoked	Norepinephrine	Brain slices	Cerebellum	(Kulik et al., 1999)
		In vivo	Cortex	(Bekar et al., 2008)
	ATP	Brain slices	Hippocampus	(Bowser and Khakh, 2004)
			Cerebellum	(Beierlein and Regehr, 2006; Piet and Jahr, 2007)
			Retina	(Newman, 2005)
			Olfactory bulb	(Rieger et al., 2007)
	GABA	Brain slices	Hippocampus	(Kang et al., 1998; Serrano et al., 2006)
	Glutamate	Brain slices	Hippocampus	(Araque et al., 2002;

			Bezzi et al., 1998; Perea and Araque, 2005b)
		Cortex	(Pasti et al., 1997; Schipke et al., 2008)
		Nucleus accumbens	(D'Ascenzo et al., 2007)
		Cerebellum	(Beierlein and Regehr, 2006; Piet and Jahr, 2007)
		Olfactory bulb	(Rieger et al., 2007)
	In vivo	Cortex	(Schummers et al., 2008; Wang et al., 2006)
Acetylcholine	Brain slices	Hippocampus	(Araque et al., 2002; Perea and Araque, 2005b)
Nitric Oxide	Brain slices	Cerebellum	(Matyash et al., 2001)
Endocannabinoids	Brain slices	Hippocampus	(Navarrete and Araque, 2008)

(Taken from Perea G. et al. (Perea et al., 2009))

Ca^{2+} signals in astrocytes originate at specific intracellular locations, called microdomains (Grosche et al., 1999), located on the astrocyte processes, and from there advance towards other cell regions. Considering that one astrocyte can contact ~100,000 synapses, such spatial regulation of Ca^{2+} signaling would provide much higher flexibility for controlling neuronal activity.

Interestingly, astrocytic Ca^{2+} rises as a response to physiological sensory stimuli. For example, stimulation of whiskers increased astrocyte Ca^{2+} in mouse barrel cortex (Wang et al., 2006), astrocyte Ca^{2+} is also elevated in the mouse sensory cortex in response to running of the animal (Dombeck et al., 2007). Astrocytes in the visual cortex respond to visual stimuli with distinct spatial perceptive fields with tuning sharper than neuronal one (Schummers et al., 2008). All these data support an active astrocytic contribution to the brain activity.

How do astrocytes modulate neuronal activity? They release several gliotransmitters, like glutamate, D-serine, ATP, adenosine, GABA, and other substances like TNFα, prostaglandins and others, affecting neuronal and synaptic activity. Table 1.3 summarizes actions of

gliotransmitters on neuronal activity. The evidence shows that gliotransmitter release can be mediated via several mechanisms. First, some gliotransmitters are released in a Ca^{2+}-dependent manner (Montana et al., 2006; Perea and Araque, 2005a) from synaptic-like vesicles (Araque et al., 2000; Araque et al., 1998b; Montana et al., 2006) or lysosomes (Zhang et al., 2007). Other suggested mechanisms include connexin/pannexin hemichannels, reversal of glutamate transporters, pore-forming $P2X_7$ receptors and cell swelling-induced anion channels (Malarkey and Parpura, 2008).

Table 1.3. ***Gliotransmitters and synaptic transmission***

Gliotransmitter	Experimental preparation	Neuromodulation	Refs
Glutamate	Hippocampus	Depression of evoked EPSCs and IPSCs	(Araque et al., 1998a; Liu et al., 2004b)
		Frequency increase of miniature PSCs	(Araque et al., 1998b)
		Frequency increase of miniature IPSCs	(Kang et al., 1998)
		Frequency increase of spontaneous EPSCs	(Fiacco and McCarthy, 2004; Jourdain et al., 2007)
		Frequency increase of spontaneous IPSCs	(Liu et al., 2004a)
		Postsynaptic SIC	(Araque et al., 1998a; Navarrete and Araque, 2008; Perea and Araque, 2005b)
		Increase of neuronal excitability	(Bezzi et al., 1998)
		Heterosynaptic depression	(Andersson et al., 2007)
	Cortex	Postsynaptic SIC	(Ding et al., 2007)
	Ventro basal thalamus	Postsynaptic SIC	(Parri et al., 2001)
	Nucleus accumbens	Postsynaptic SIC	(D'Ascenzo et al.,

			2007)
	Olfactory bulb	Postsynaptic SIC	(Kozlov et al., 2006)
	Retina	Light-evoked neuronal activity	(Newman and Zahs, 1998)
ATP/Adenosine	Cerebellum	Depression of spontaneous EPSCs	(Brockhaus and Deitmer, 2002)
	Hippocampus	Heterosynaptic depression of spontaneous EPSCs	(Serrano et al., 2006)
		Modulation of LTP	(Pascual et al., 2005)
		Synaptic depression	(Pascual et al., 2005)
	Hypothalamic paraventricular nucleus	Insertion of AMPA receptors	(Gordon et al., 2005)
	Retina	Depression of light-evoked EPSCs	(Newman, 2003)
D-Serine	Hippocampus	Modulation of LTP	(Yang et al., 2003)
	Hypothalamic supraoptic nucleus	Modulation of LTP	(Panatier et al., 2006)
	Retina	Potentiate NMDA receptor transmission	(Newman, 2003)
TNFα	Hippocampus	Insertion of AMPA receptors	(Beattie et al., 2002)
		Increase of synaptic scaling	(Fiacco et al., 2007)
GABA	Olfactory bulb	Postsynaptic SOC	(Kozlov et al., 2006)
Undefined (gluatamate and/or nitric oxide)	Neuromuscular junction	Synaptic depression	(Robitaille, 1998)
		Synaptic potentiation	(Castonguay and Robitaille, 2001)

Abbreviations: *EPSCs*, excitatory postsynaptic currents; *IPSCs*, inhibitory postsynaptic currents; *LTP*, long-term potentiation; *PSCs*, postsynaptic currents; *SIC*, slow inward current; *SOC*, slow outward current. (Taken from Perea et al. (Perea et al., 2009))

Ca^{2+} signaling toolkit in astrocytes

Ionotropic Ca^{2+} receptors – The major ionotropic receptors participating in astrocyte Ca^{2+} signaling are P2X purinoreceptors and glutamatergic receptors, like AMPA, N-methyl-D-Aspartate (NMDA) and kainate receptors. AMPA receptors are the predominant ionotropic glutamate receptors in astrocytes (Parpura and Verkhratsky, 2011). In many types of astroglia AMPA receptors lack GluR2 subunits, therefore making astrocytic AMPA receptors highly permeable to Ca^{2+}, although this property is limited due to rapid receptor desensitization (Verkhratsky et al., 2011). Astrocytic NMDA receptors were shown *in vitro* and in acutely isolated slices (Verkhratsky et al., 2011). They have a distinct pharmacological profile and gating properties, have significantly lower Ca^{2+} permeability than those in neurons. From these properties it may be concluded that astrocytic NMDA receptors are composed of NR1, NR2C/D and NR3 subunits.

Astrocytes express $P2X_1$-$P2X_4$ and $P2X_7$ receptors (Butt, 2011). Additional ATP-sensitive $P2X_{1/5}$ purinoreceptors in astrocytes have a high affinity to ATP, are permeable for Ca^{2+} and weakly desensitize (Verkhratsky et al., 2011). $P2X_7$ receptors are activated upon high [ATP] and are involved in astrogliosis (Butt, 2011). Functional α7 nicotinic Acetylcholine receptors are expressed in cultured astrocytes (Verkhratsky et al., 2011), but their expression *in vivo* was not shown. All the ionotropic receptors in astrocytes are cationic channels, permeable not only to Ca^{2+}. Another ion, entering these channels and affecting Ca^{2+} signaling and astrocytic homeostasis, is Na^+.

Metabotropic Ca^{2+} receptors – Astrocytes respond with Ca^{2+} elevations to neuronal activity mostly via the activation of the metabotropic receptors on the plasma membrane. Astrocytes express metabotropic glutamate receptors (mGluRs), $GABA_B$ receptors, muscarinic Achetylcholine receptors, endocannabinoid receptors and P2Y receptors. The signaling from these receptors down to G_q proteins and activation of PLC elevates $[Ca^{2+}]_{cyt}$ released from ER and mediates Ca^{2+}-dependent functions. Metabotropic Ca^{2+} signaling can be distinguished from the ionotropic one by the fact that Ca^{2+} elevation is seen with no extracellular Ca^{2+} and it is sensitive to the SERCA inhibition. The major metabotropic receptors in astrocytes are mGluRs responding to glutamate and P2YRs responding to ATP and its derivatives. $P2Y_1R$ is the major type mediating metabotropic ATP-evoked Ca^{2+} responses in astrocytes (Butt, 2011). $P2Y_2R$ is also functional in astrocytes and evokes Ca^{2+} signals different from those ones, triggered via $P2Y_1R$ activation (Fam et al., 2003; Gallagher and Salter, 2003). At the vascular surface

astrocyte Ca^{2+} transients are mediated mostly via $P2Y_2Rs$ and $P2Y_4Rs$ (Simard et al., 2003). The most abundant mGluRs in astrocytes *in situ* are mGluR3 and 5, while mGluR1 and 5 trigger PLC and IP_3-mediated Ca^{2+} rises (Parpura and Verkhratsky, 2011).

Voltage-gated Ca^{2+} channels (VGCC) – Astrocytes express 5 types of VGCC: L-, N-, P/Q-, R- and T-type (Verkhratsky et al., 2012). Their expression and function is regulated by different stimuli, like neuronal co-culture and other (Verkhratsky et al., 2012). The function of VGCC was shown in primary cultured and freshly isolated astrocytes (Duffy and MacVicar, 1994; Eriksson et al., 1993). Their role *in situ* was shown in acute slices from the ventrobasal thalamus (Parri and Crunelli, 2003; Parri et al., 2001), where VGCC were shown to contribute to spontaneous Ca^{2+} oscillations.

SOCE - Although SOCE was demonstrated in astrocytes, its molecular identity remains unknown. Astrocytes express functional TRP channels. TRPC1 was described to oligomerize with TRPC4 and/or TRPC5 to build functional channel. TRPC1 was shown to be involved in SOCE and in Ca^{2+} signaling following the activation of purinergic receptors with ATP (Malarkey et al., 2008).

Na^+/Ca^{2+} exchangers - All three members of NCX family are expressed in astrocytes (Minelli et al., 2007). They are placed in the perisynaptic processes and particularly abundant on those processes that envelope excitatory synapses. Na^+/Ca^{2+} exchangers can operate both in forward and reverse modes dependent on the membrane potential and Na^+ and Ca^{2+} gradients across the plasma membrane. Ca^{2+} transients conducted via both modes were detected in astrocytes *in vitro* and *in situ (Verkhratsky et al.,* 2011*)*.

IP_3Rs and RyRs - IP_3Rs in astrocytes are expressed mostly on the distant processes, location matching with the origin of the metabotropic Ca^{2+} signals. IP_3R2 is the most prominent and functional isoform expressed in astroglia (Agulhon et al., 2008). Astrocytes also express RyRs and its activation by caffeine was shown in thalamic astrocytes. RyR3 was shown to be involved in astrocytic migration (Matyash et al., 2002), but the function of RyRs in hippocampal astrocytes is not clear.

1.3 Mitochondrial Ca^{2+} signaling in glia: shedding the light in the darkness

Principles of mitochondrial Ca^{2+} signaling

The widely-known function of mitochondria as a powerhouse of a cell is only one side of mitochondrial physiology. More and more disorders, particularly the chronic neurodegenerative diseases, stroke and heart reperfusion injury, are being associated to a greater or lesser extent with mitochondrial dysfunction, prompting many scientists to investigate the role of mitochondria in the life of a cell.

Mitochondria are very dynamic organelles that regulate plethora of cellular activities. They produce the energy coin of the cell, ATP, and participate in fatty acid oxidation, amino acid metabolism and ketone body synthesis. Additionally, mitochondria are intimately involved in intracellular Ca^{2+} signaling, therefore being also involved in all Ca^{2+}-dependent cell functions with a particular role in cell death. Such versatile functions place mitochondria as a hub of energy requirement of the cell, cell signaling and ion homeostasis.

There is a two-way connection between Ca^{2+} and mitochondria: Ca^{2+} regulates numerous mitochondrial functions and, in turn, Ca^{2+} handling by mitochondria affects cytoplasmic Ca^{2+} transients and behavior of Ca^{2+}-dependent proteins. Ca^{2+} enters the cytosol gradually diffusing from its entry point, therefore $[Ca^{2+}]$ in the vicinity of a Ca^{2+} channel can reach a high concentration, creating so called Ca^{2+} microdomains. Recent evidence shows that the outer mitochondrial membrane senses $[Ca^{2+}]$ in the range of 15-30 μM (Giacomello et al., 2010), which is much higher than the bulk cytosol concentration. Mitochondria can move towards Ca^{2+} gradients in the cell and be immobilized in the regions of very high $[Ca^{2+}]$. Therefore, mitochondria are located just under the mouths of active Ca^{2+} transporters, where $[Ca^{2+}]$ and energy demand are particularly high. Mitochondria rapidly take up Ca^{2+} via the mitochondrial uniporter he mitochondrial matrix buffers Ca^{2+}, which is then extruded from mitochondria via Na^{+}-dependent or -independent (H^{+}-coupled) pathways (Drago et al., 2011). In such a way mitochondria can funnel Ca^{2+} to a specific cellular location, change the activation of certain proteins and shape Ca^{2+} signals.

Mitochondria contain two membranes: the outer membrane is semi-permeable to ions, and the permeability of the inner membrane is regulated by a variety of transporters, carriers, channels etc. (Figure 1.4). Mitochondria create a proton gradient via the electron transport chain (ETC)

and this gradient is used to produce ATP, to maintain ion homeostasis inside the organelle and to move metabolic substrates across the membrane.

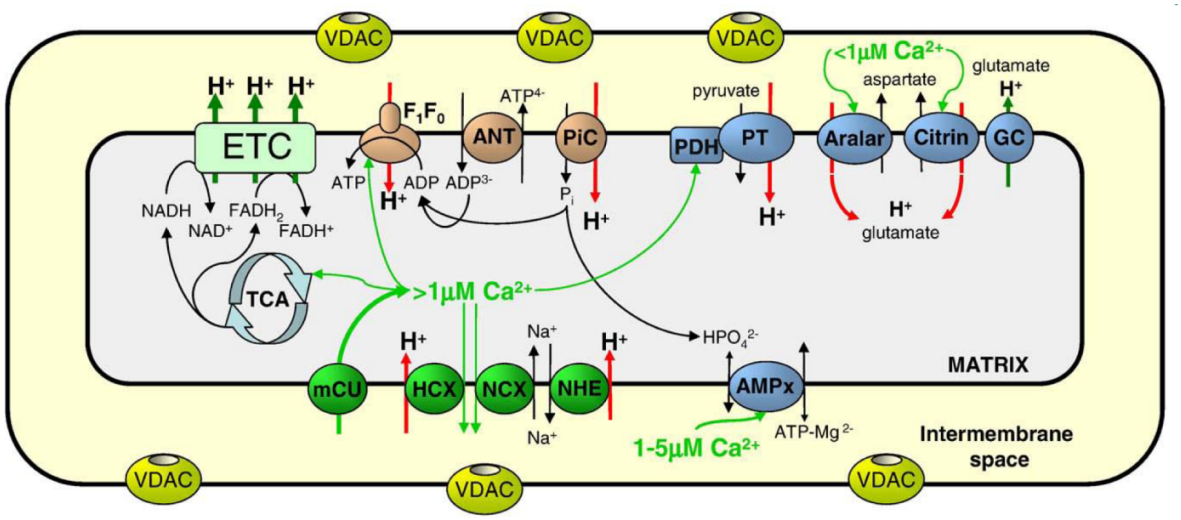

Figure 1.4. ***Mitochondrial ion and energy handling***

The scheme illustrates electron and ATP carriers (light green and brown), proteins transporting metabolic substrates (blue) and ions (green) across the inner and outer mitochondrial membranes. *VDAC*, voltage-dependent anion channel; *ETC*, electron transport chain; *ANT*, adenine nucleotide transporter; P_i, inorganic phosphate; P_iC, phosphate carrier; *TCA*, tricarboxylic acid cycle; *PDH*, pyruvate dehydrogenase; *PT*, pyruvate transporter; *GC*, glutamate carrier; *NHE*, Na^+/H^+ exchanger; *NCX*, Na^+/Ca^{2+} exchanger; *HCX*, H^+/Ca^{2+} exchanger; *mCU*, mitochondrial Ca^{2+} uniporter. (Taken from (Demaurex et al., 2009))

Mitochondrial Ca^{2+} signaling toolkit

Ca^{2+} is sequestered into the mitochondria via the mitochondrial Ca^{2+} uniporter (MCU) or via alternative pathways, like rapid mode of uptake pathway (RaM), which is differentiated by its kinetics, pharmacology and Ca^{2+} affinity. MCU is the most characterized Ca^{2+} uptake pathway. Its activity depends on the membrane potential, can be inhibited by ruthenium red, and has low temperature sensitivity and high transport rate. The molecular identity of MCU has been revealed recently by 2 groups: Baugman et al. and De Stefani et al. (Baughman et al., 2011; De Stefani et al., 2011) characterized a protein known as NP_001028431, coiled-coil domain-

containing protein 109A. MCU has following features: (i) MCU is ubiquitously expressed in all mammalian tissues and the majority of eukaryotic organisms; (ii) the molecular weight of MCU is 40 kDa and it has two transmembrane domains, which may create a pore or Ca^{2+} channel; (iii) knock-down of MCU significantly diminishes the mitochondrial Ca^{2+} influx in isolated mitochondria and in permeabilized cells, and this effect can be rescued by overexpression of MCU; (iv) site-specific mutagenesis causes loss of MCU function; (v) MCU blockade does not affect mitochondrial properties, like morphology, O_2 consumption, $\Delta\psi_m$ and ATP production; (vi) ruthenium red and La^{3+} sensitive Ca^{2+} currents were recorded from bacterially expressed MCU reconstituted in lipid bilayers.

MCU accumulates Ca^{2+} at the micromolar range; however, there is evidence that Ca^{2+} enters the mitochondria at the nanomolar range. Jiang at al. (Jiang et al., 2009) reported that the originally known K^+/H^+ exchanger Letm1 (leucine zipper EF-hand containing transmembrane protein) is also a high affinity mitochondrial Ca^{2+}/H^+ antiporter, transporting one Ca^{2+} in exchange to one H^+ and responsible for mitochondrial Ca^{2+} import at low [Ca^{2+}].

Letm1 activity could be blocked by the MCU inhibitor, ruthenium red, and also by the inhibitor of the mitochondrial Na^+/Ca^{2+} exchanger, CGP37157. Similar results were also observed by another group (Waldeck-Weiermair et al.). However, the role of Letm1 as mitochondrial Ca^{2+}/H^+ exchanger is still a matter of debate for the following reasons: (i) electrogenic H^+/Ca^{2+} exchange cannot be explained physiologically, as import of a net positive charge into the mitochondrial matrix does not support Ca^{2+} influx; (ii) K^+ fluxes via the K^+/H^+ antiporter Letm1 could alter $\Delta\psi_m$, which would contribute to Ca^{2+} influx; (iii) there is no evidence for the weakening of mitochondrial Ca^{2+} transients triggered via IP_3-coupled pathway; (iv) H^+/K^+ ionophore nigericin can rescue Letm1 knock-out phenotype (Dimmer et al., 2008) (reviewed in (Drago et al., 2011)).

In order to maintain ion balance, Ca^{2+} uptake should be accompanied by the transport of anions freely passing the internal mitochondrial membrane. These anions could be acetate or phosphate. With the latter Ca^{2+} spontaneously creates precipitates in the mitochondrial matrix. Such precipitates include a high quantity of Ca^{2+} and their existence was demonstrated in electron microscopy images of isolated mitochondria (Starkov, 2010). Calcium phosphate precipitates are considered to be responsible for mitochondrial Ca^{2+} storage (Starkov, 2010). Ca^{2+}-binding matrix-located proteins were suggested to participate in the generation of Ca^{2+} precipitates, serving as a nucleation center. However, the role for alternative non-proteinaceous factors, such as DNA, which is known to bind Ca^{2+}, in the nucleation process cannot be excluded (Starkov, 2010).

After the sequestration and buffering in the mitochondrial matrix, Ca^{2+} is extruded from mitochondria via Na^+-dependent or -independent (H^+-coupled) pathways (Drago et al., 2011). Existence of the functional Na^+/Ca^{2+} antiporter in mitochondria was known for many years, but the molecular identity of the mitochondrial Na^+/Ca^{2+} exchanger NCLX was revealed only in 2010 in our common study (Palty et al., 2010). These are the characteristics of the protein: (i) NCLX has a molecular weight of about 60 kDa, which is similar to the weight of the mitochondrial protein previously observed to conduct Na^+/Ca^{2+} exchange upon reconstitution into the lipid bilayer (Li et al., 1992; Paucek and Jaburek, 2004); (ii) NCLX exhibits Na^+- and Li^+-dependent Ca^{2+} exchange, previously reported to be a unique property of the mitochondrial Na^+/Ca^{2+} exchanger; (iii) NCLX is enriched in the mitochondrial fractions and specifically located to the mitochondrial cristae; (iv) NCLX mediated Ca^{2+} efflux can be inhibited by the pharmacological inhibitor of the exchanger, CGP37157; (v) transfection of cells with a catalytically inactive mutant of NCLX exhibits a dominant negative effect on the mitochondrial Ca^{2+} efflux.

Mitochondrial Ca^{2+} in glia

Most of the experiments investigating the effect of mitochondrial Ca^{2+} in glia are performed in vitro, therefore limiting the interpretations of what is happening in vivo. Different organelle structure *in vitro* and *in vivo* was shown for astrocytic ER (Pivneva et al., 2008), which coincided also with alteration in Ca^{2+} influx via SOC. Moreover, astrocytes form a very heterogeneous population, both functionally and morphologically, and it is not surprising that they may have different mitochondrial morphology and properties. For example, in the striatum, a brain region prone to neurological disorders, like Huntington disease, astrocytes along with neurons revealed decreased mitochondrial Ca^{2+} buffering capacity when compared to the cells of cortical origin (Oliveira and Goncalves, 2009).

ATP release from astrocytes is a Ca^{2+}-dependent process and mitochondria were shown to play a special role in this process. Mitochondrial Ca^{2+} uptake via the uniporter was reported to be responsible for rhythmic ATP accumulations in the astrocytes of suprachiasmatic nucleus, region regulating circadian neural and neuroendocrine rhythms in the mammalian brain (Burkeen et al., 2011).

Astrocytic mitochondria regulate the spatial spread of Ca^{2+} signals in astrocytes. Boitier et al. (Boitier et al., 1999) inhibited mitochondrial Ca^{2+} uptake via dissipation of the mitochondrial

membrane potential by the application of either mitochondrial respiratory complex III inhibitor antimycin A1 or complex I inhibitor rotenone along with ATP synthase inhibitor oligomycin. Blockade of mitochondrial Ca^{2+} uptake accelerated the intracellular Ca^{2+} wave that is triggered by mechanical or ATP-induced stimulation by about 50%. The dynamic nature of astrocytic mitochondria was shown upon stimulations with transmitters, like ATP or glutamate. The stimulation triggered astrocytic mitochondria to travel to the plasma membrane. This process was Ca^{2+}-dependent, as it was blocked by pre-incubation with Ca^{2+} chelator BAPTA-AM (Kolikova et al., 2006).

Functional mitochondrial Na^+/Ca^{2+} exchange was shown in astrocytes via monitoring changes in Na^+ upon glutamate application (Bernardinelli et al., 2006). Mitochondrial Na^+ accumulation upon glutamate stimulation was Ca^{2+}-sensitive and inhibited by the pharmacological blocker of the mitochondrial Na^+/Ca^{2+} exchanger. According to the new evidence from the same group, spontaneous Na^+ spikes in astrocytic mitochondria originate from different mechanism. The study revealed coincident spontaneous transient increases in mitochondrial $[Na^+]$, $\Delta\psi_m$, matrix pH and mitochondrial reactive oxygen species (ROS) in individual astrocytic mitochondria (Azarias and Chatton, 2011). These changes did not coincide with increases in mitochondrial Ca^{2+} levels. In astrocytic and neuronal mitochondria from rat neocortex and hippocampus the expression of Na^+/Ca^{2+} exchanger NCX1, NCX2 and NCX3 was shown by western blot analysis and *in situ* electron microscopy and immunocytochemistry, however their function in the mitochondrial ion homeostasis was not described (Gobbi et al., 2007).

1.4 NCLX: what do we know?

NCLX or NCKX6 belongs to the Ca^{2+}/cation exchanger (CCX) branch of a large protein superfamily, called Ca^{2+}/cation antiporters. The protein is encoded by the gene SLC24A6 and was cloned independently by 2 groups in 2004 (Cai and Lytton, 2004b; Palty et al., 2004). The protein represents the only member of CCX branch, and it shares only about 20% sequence homology with other members of Na^+/Ca^{2+} superfamily. 3 isoforms of NCLX are known: transcript variant 1 (or long), transcript variant 2 and transcript variant 3 (or short). The long transcript is more abundant and encodes a protein of 585 (mouse) or 584 (human) amino acids. Mouse and human proteins share 83% identity. The topographical analysis of the protein sequence suggests 13 transmembrane domains, including 2 transmembrane α-repeats,

important for the protein activity (Figure 1.5). Both α1 and α2 domains are active, have different pharmacological and kinetic properties, like sensitivity to KB-R9743 and K^+ (Palty, 2006). A functional exchanger is built via homo- or heterooligomerization of a single α-domain (Palty, 2006).

In addition, a very detailed analysis by Cai et al (Cai, 2004) revealed possibilities for protein-protein interaction and post-translational modifications. A potential cleavage site for signal peptidase and two consensus glycosylation sites were found between M0 and M1 transmembrane domains. Several phosphorylation sites were suggested in the large intracellular loop.

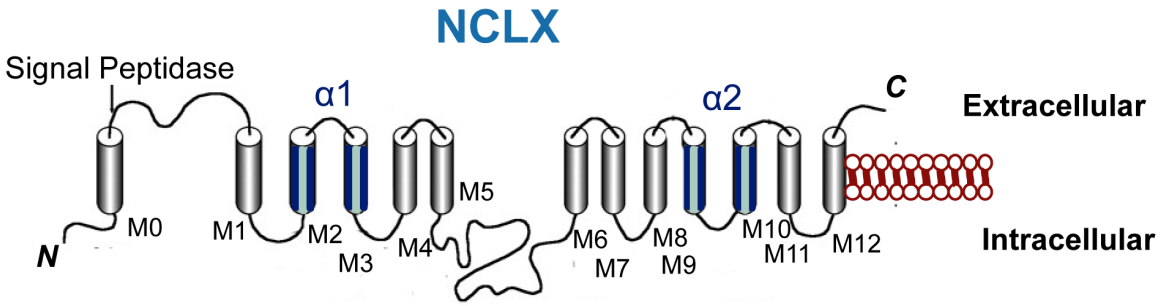

***Figure 1.5.* Putative structure of NCLX**

Putative transmembrane topology model of NCLX with cylinders, representing transmembrane domains, α repeat regions are colored in blue. Signal Peptidase indicates a predicted cleavage site. (Modified from Cai et al. (Cai and Lytton, 2004a))

The mitochondrial Na^+/Ca^{2+} exchange was shown to be a substrate for kinases, like PINK1 and PKC (Gandhi et al., 2009; Palty and Sekler, 2012).

Most of the studies investigating the role of NCLX used pharmacological inhibition of the exchanger with benzothiazepine compounds, such as diltiazem, clonazepam, and CGP37157 (Cox et al., 1993). Although CGP37157 is the most specific pharmacological blocker of the mitochondrial Na^+/Ca^{2+} exchanger, it has been recently reported to have many side effects on different components of Ca^{2+} signaling, such as SERCA, RyRs, L-type Ca^{2+} channels and plasmalemmal Na^+/Ca^{2+} exchangers (Neumann et al., 2011). This means that the data existing

regarding the mitochondrial Na^+/Ca^{2+} exchanger should be taken with caution and further analyzed in light of the lack of specificity of CGP37157.

An interesting observation for the role of the exchanger in Ca^{2+} oscillations comes from Ishii et al. (Ishii et al., 2006). They showed that pharmacological inhibition of the exchanger favors fast refilling of the ER stores, increases $[Ca^{2+}]$ in the vicinity of IP_3Rs and reactivates IP_3Rs, causing an additional Ca^{2+} release from the ER. In cardiac myocytes by using CGP37157 or clonazepam 2 studies showed that NCLX blockade increases mitochondrial Ca^{2+} transients, while decreasing the amplitude of the systolic Ca^{2+} influx (Bell et al., 2006; Maack et al., 2006). Recently, by using NCLX knock-down Kim et al. showed a key role of NCLX in antigen receptor mediated Ca^{2+} signaling in B lymphocytic chick cell lines (Kim et al., 2012) via regulation of the ER Ca^{2+} stores. NCLX knock-down reduced ER Ca^{2+} uptake by about 42%. Finally, after so many years of mitochondrial Ca^{2+} research, the molecular identity of the key players is revealed. Hopefully, this knowledge will boost the investigation of the role of the mitochondrial Ca^{2+} in physiology and pathology and will provide us with the most interesting insights into the mechanisms of mitochondrial involvement in Ca^{2+} signaling.

Chapter 2

Objectives

Despite the fundamental role of Ca^{2+} signaling in glia, little is known about the role of mitochondrial Na^{+}/Ca^{2+} exchangers in shaping glial physiological responses. The presence of both plasmalemmal and mitochondrial Na^{+}/Ca^{2+} exchangers has been demonstrated in astrocytes (Bernardinelli et al., 2006; Minelli et al., 2007). The identification of the mitochondrial exchanger offers a remarkable opportunity to investigate for the first time the role of Ca^{2+} homeostasis, mediated through this compartment, in physiological processes in astro- and microglial cells.

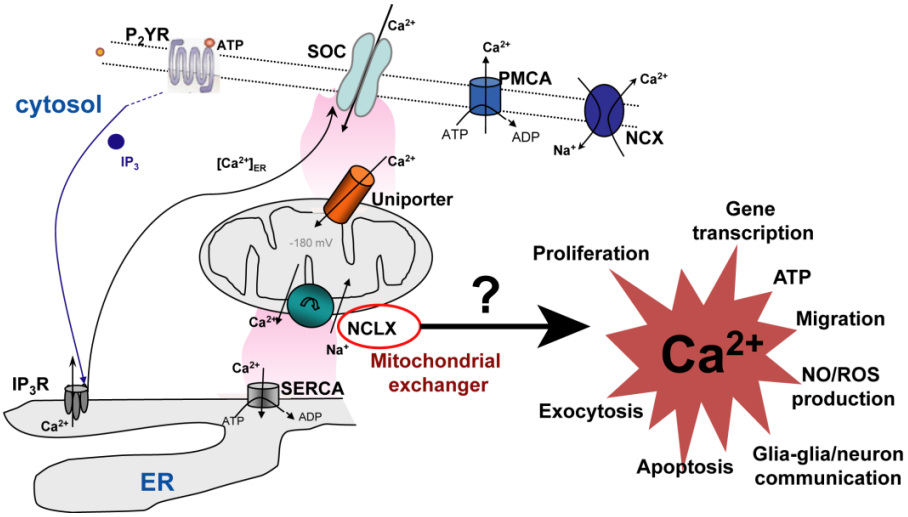

Figure 2.1. ***Simplified scheme representing Ca^{2+} cellular pathway and its effects***

As a result of metabotropic activation (for example, metabotropic purinergic receptor, P2YR), ER Ca^{2+} stores are depleted through IP_3-sensitive Ca^{2+} channel. This is sensed by store-operated Ca^{2+} channels (SOC), which open and enable Ca^{2+} entry into the cell. Mitochondria sense local microdomains of intracellular Ca^{2+} at the mouth of open Ca^{2+} channels (pink gradients). They rapidly take up significant amounts of Ca^{2+} via the uniporter, and via activity of NCLX, Ca^{2+} is "shuttled away" from the Ca^{2+} entry sites to the cytoplasm, thus facilitating prolonged Ca^{2+} entry. At the end, Ca^{2+} in the ER is restored by the efforts of SERCA, ER Ca^{2+} ATP-ase. Ca^{2+} is removed from the cytoplasm by plasmalemmal NCX and PMCA.

The overall hypothesis of this project is that NCLX is the mitochondrial Na^+/Ca^{2+} exchanger in glia and that it is fundamental not only to mitochondrial but also to global Ca^{2+} homeostasis in glia (Figure 2.1). Considering the major role that Ca^{2+} plays in glial physiology, my hypothesis is that the NCLX is critical to major glial activity, ranging from cytokine secretion to chemotactic activity. Combining fluorescent ion measurements and molecular silencing via siRNA approach, I focused on the role of this distinct exchanger in glial Ca^{2+} homeostasis and examined how it affects glial communication or activation under physiological and pathological conditions.

The project aimed to answer the following questions:

1. Is the NCLX found in astro- and microglial cells and in which subcellular compartments?
2. How does the exchanger NCLX affect the cytoplasmic and mitochondrial Ca^{2+} handling in glial cells following physiological stimuli?
3. How does NCLX influence the executive functions of activated microglia?
4. How does NCLX modulate astrocytic intercellular communication and other astrocytic properties?

Addressing these issues and understanding the role of this particular exchanger NCLX in Ca^{2+} pathways inside the glial cells will shed more light on functioning of glia, cells involved in numerous diseases, such as Alzheimer disease, glia tumor (glioma), epilepsy, and neuropathic pain.

Chapter 3

Materials and Methods

3.1 Materials

Drugs and chemicals

Table 3.1. ***Drugs and chemicals***

Material	Company
Adenosine 5'-triphosphate dipotassium salt (ATP)	Sigma-Aldrich, Munich, Germany
Ampicillin	Sigma-Aldrich, Munich, Germany
Blasticidin	Sigma-Aldrich, Munich, Germany
Bovine serum albumin (BSA)	Carl Roth GmbH & Co. KG, Karlsruhe, Germany
CGP37157	Ascent Scientific LTD, Bristol, UK
FCCP	Ascent Scientific LTD, Bristol, UK
Fetal Calf Serum (FCS)	GIBCO®, Invitrogen, Darmstadt, Germany
Glucose	Merck, Damstadt, Germany
Glutamate	Sigma-Aldrich, Munich, Germany
HEPES	Roth, Karlsruhe, Germany

L-Glutamic Dehydrogenase from bovine liver (GDH)	Sigma-Aldrich, St. Louis, USA
L-glutamine	Biochrom AG, Berlin, Germany
Lipopolysaccharide (LPS)	Alexis biochemicals, Lausen, Switzerland
Mannitol	Sigma-Aldrich, Munich, Germany
Milk, powdered`	Roth, Karlsruhe, Germany
Penicillin/Streptomycin	Biochrom AG, Berlin, Germany
Poly-L-Lysine (PLL)	Sigma-Aldrich, Munich, Germany
Protease inhibitor cocktail tablets (complete, mini)	Roche Diagnostics Deutschland GmbH, Mahnheim, Germany
Recombinant Mouse Complement Component C5a, CF	R&D Systems Europe, Ltd., UK
Recombinant mouse IFN-γ, CF (carrier-free)	R&D Systems Europe, Ltd., UK
Sucrose	Sigma-Aldrich, Munich, Germany
SuperSignal® west	Pierce (Thermo Fischer Scientific), Bonn, Germany
Thapsigargin	Tocris Bioscience, Bristol, UK
Tris base	Carl Roth GmbH, Karlsruhe, Germany
Tween® 20	Roth, Karlsruhe, Germany
Zymozan	Sigma-Aldrich, Munich, Germany
β-Nicotinamide adenine dinucleotide hydrate (NAD^+)	Sigma-Aldrich, St. Louis, USA

Dyes and transfection reagents

Table 3.2. ***Dyes and transfection reagents***

Material	Company
4',6-diamidino-2-phenylindole, dihydrochloride (DAPI)	Roche Diagnostics Deutschland GmbH, Mahnheim, Germany
Calcein-AM	Life Technologies Ltd. (Invitrogen), NY, USA
DharmaFECT 1, 2, 3, 4 siRNA transfection reagents	Thermo Fisher Scientific, Dharmacon Products, Lafayette, UK
Diff-Quik staining set	Medion Diagnostics, Langen, Germany
Fluo-3 AM, cell permeant	Life Technologies Ltd. (Invitrogen), NY, USA
Fluo-4 AM, cell permeant	Invitrogen, Karlruhe, Germany
Fura-2 AM, cell permeant	Invitrogen, Karlruhe, Germany
H_2DCFDA (for measurement of Reactive Oxygen Species (ROS))	Invitrogen, Karlruhe, Germany
Lipofectamine™ 2000 transfection reagent	Life Technologies Ltd. (Invitrogen), UK
Lipofectamine™ RNAiMAX	Life Technologies Ltd. (Invitrogen), UK
TransIT-TKO	Mirus, Madison, USA

Media and buffers

Table 3.3. ***Media and buffers***

Media/ Buffer	Composition
5 x siRNA Buffer	Thermo Fisher Scientific, Dharmacon Products, Lafayette, UK

Ca^{2+} Phosphate Transfection Solutions	Solution A	2.5 M $CaCl_2$
	Solution B or Phosphate buffer	274.0 mM NaCl, 9.9 mM KCl, 2.8 mM $Na_2HPO_4x2H_2O$, 42.0 mM HEPES, pH 6.75-6.76, sterile filtered
Dulbecco Phosphate Buffered Saline (PBS)		GIBCO®, Invitrogen, Darmstadt, Germany
Dulbecco's Modified Eagle Medium (DMEM)		Supplemented with 10% heat inactivated fetal calf serum, 2 mM L-glutamine, 100 u/ml penicillin, 100 µg/ml streptomycin
Griess reagent		• Solution A: 1 mg/ml Naphthylethylene in A. dest. • Solution B: 1 g/ml Sulfanilamid, 60 µl/ml H_3PO_4 (85%) in A. dest. • To obtain Griess reagent solutions A and B were freshly mixed 1:2.
Hank's Balanced Salt Solution (HBSS)		GIBCO®, Invitrogen, Darmstadt, Germany
HEPES buffer	2mM Ca^{2+} (normal)	150 mM NaCl , 5.4 mM KCl, 1.0 mM $MgCl_2$, 2.0 mM $CaCl_2$, 10.0 mM HEPES, 10.0 mM Glucose, at pH 7.4
	Ca^{2+}-free	150 mM NaCl , 5.4 mM KCl, 2.0 mM $MgCl_2$, 10.0 mM HEPES, 10.0 mM Glucose, at pH 7.4
	5mM Ca^{2+}	150 mM NaCl , 5.4 mM KCl, 1.0 mM $MgCl_2$, 5.0 mM $CaCl_2$, 10.0 mM HEPES, 10.0 mM Glucose, at pH 7.4
L929 conditioned medium		L929 mouse fibroblasts were grown at T75 flask till 80% confluence, then 30 ml of supplemented DMEM was added. After 2 days the medium was collected, filtered and frozen until usage.
LB medium		1.0% Tryptone, 0.5% Yeast extract, 1.0% NaCl, pH 7.0
Mannitol-Tris EDTA buffer		270 mM D-mannitol, 10 mM Tris, 0.1 mM EDTA, pH 7.4

(MTE)		
Macrophage-SFM, (1X), liquid (serum-free medium)		GIBCO®, Invitrogen, Darmstadt, Germany
Minimum Essential Media (α-MEM)-no phenol red		GIBCO®, Invitrogen, NY, USA
OPTI-MEM® I Reduced Serum Media		GIBCO®, Invitrogen, Darmstadt, Germany
Phosphate Buffered Saline (PBS)		137 mM NaCl, 2.7 mM KCl, 4.3 mM $Na_2HPO_4x2H_2O$, 1.4 mM KH_2PO_4, pH 7.4
Phosphate Buffered Saline-Tween (PBS-T)		137 mM NaCl, 2.7 mM KCl, 4.3 mM $Na_2HPO_4x2H_2O$, 1.4 mM KH_2PO_4, 0.05% Tween 20, pH 7.4
Restore PLUS Western Blot Stripping Buffer		Pierce, Thermo Fisher Scientific, Bonn, Germany
RIPA buffer (lysis buffer)		Sigma-Aldrich, Deisenhofen, Germany
Sucrose gradient solutions	Sucrose, 1.0 M	1.0 M Sucrose, 10mM Tris-base, 0.1 mM EDTA, pH 7.6 (adjusted with HCl)
	Sucrose, 1.3 M	1.3 M Sucrose, 10mM Tris-base, 0.1 mM EDTA, pH 7.6 (adjusted with HCl)
	Sucrose, 1.5 M	1.5 M Sucrose, 10mM Tris-base, 0.1 mM EDTA, pH 7.6 (adjusted with HCl)
	Sucrose, 1.7 M	1.7 M Sucrose, 10mM Tris-base, 0.1 mM EDTA, pH 7.6 (adjusted with HCl)
	Sucrose, 2.0 M	2.0 M Sucrose, 10mM Tris-base, 0.1 mM EDTA, pH 7.6 (adjusted with HCl)

Tissue lysis buffer	20 mM Tris-HCl (pH 7.5), 0.32 M Sucrose, 0.2 mM EDTA, 0.5 mM EGTA
Trypsin/DNase	10 mg trypsin, 0.5 mg DNase per ml PBS

Antibodies

Table 3.4. ***Antibodies***

Name	Host	Company	Dilution
Primary antibodies			
Mc Anti-ComplexIV subunit I OxPhos (Cytochrome C oxidase)	mouse	Invitrogen, Germany	1:1,000
Mc Anti-GFAP	mouse	Millipore GmbH (Chemicon), Germany	1:400
Mc Anti-N-Cadherin	mouse	BD Biosciences, Germany	1:1,000
Mc Anti-neuronal Nuclei (NeuN)	mouse	Millipore GmbH (Chemicon), Germany	1:100
Pc Anti-ANT	goat	Santa Cruz Biotechnology Inc., Germany	1:100
Pc Anti-GAPDH	rabbit	New England Biolabs GmbH, Frankfurt am Main, Germany	1:10,000
Pc Anti-GFAP	rabbit	Millipore GmbH (Chemicon), Germany	1:1,000
Pc Anti-Itgam (CD11b)	rabbit	Abnova GmbH, Germany	1:10,000
Pc Anti-NCLX	rabbit	Prof. Sekler, Ben-Gurion University, Israel	1:300 (IHC);1:500-1:2,000 (WB)

Pc Anti-Sec62	rabbit	Prof. T. Sommer, MDC, Berlin	1:1,000
Secondary antibodies			
Alexa Fluor 488 Anti—rabbit IgG	goat	Life Technologies GmbH, Germany	1:1,000
Alexa Fluor 566 Anti—mouse IgG	goat	Life Technologies GmbH, Germany	1:1,000
HRP Anti-goat IgG	bovine	Jackson ImmunoResearch Europe LTD, UK	1:2,500
HRP Anti-mouse IgG	goat	Sigma-Aldrich, Munich, Germany	1:5,000
HRP Anti-rabbit IgG	goat	Jackson ImmunoResearch Europe LTD, UK	1:5,000

Abbreviations: *Mc*, monoclonal; *Pc*, polyclonal; *HRP*, horse radish peroxidase

Plasmids

Table 3.5. ***Plasmids***

Plasmid	Resistance	Protein expressed
pcDna3.1-mtRP	Ampicillin	Mitochondrial ratiometric pericam (mtRP)
pMP71-mtRP	Ampicillin	Mitochondrial ratiometric pericam (mtRP)
pMP71-GFP	Ampicillin	GFP

Small interfering RNA (siRNA)

Table 3.6. ***siRNAs***

siRNA	Protein targeted	Company
siGLO Red transfection indicator	Fluorescent siRNA, no gene is targeted	Thermo Fisher Scientific Dharmacon Products, Lafayette, UK
ON-TARGETplus Control Non-targeting pool (negative control siRNA)	None	Thermo Fisher Scientific Dharmacon Products, Lafayette, UK
ON-TARGET GAPD Control pool (siRNA vs. GAPDH (siGAPDH))	GAPDH	Thermo Fisher Scientific Dharmacon Products, Lafayette, UK
ON-TARGETplus SMARTpool, Mouse SLC24A6 (siRNA vs. Slc24a6 or NCLX (siNCLX))	NCLX	Thermo Fisher Scientific Dharmacon Products, Lafayette, UK

Commercial kits and home-made assays

Table 3.7. ***Commercial kits and home-made assays***

Kit		Supplier
BCA Protein Assay		Pierce, Thermo Fisher Scientific, Bonn, Germany
Cell surface protein isolation kit		Pierce, Thermo Fisher Scientific, Bonn, Germany
IL-12 ELISA assay	Anti-mouse IL-12 (p40) Capture Antibody	BD Pharmingen ™, NJ, USA

	Anti-mouse IL-12 (p40) detection Antibody	BD Pharmingen ™, NJ, USA
	IL-12 Standard 10 µg	R&D Systems Europe, Ltd., UK
IL-6 ELISA assay	Anti-mouse IL-6 Capture Antibody	R&D Systems Europe, Ltd., UK
	Anti-mouse IL-6 Detection Antibody	R&D Systems Europe, Ltd., UK
	IL-6 Standard 5 µg	R&D Systems Europe, Ltd., UK
InviTrap® Spin Universal RNA mini kit		Invitek (Stratec), Berlin, Germany
MCP-1 ELISA		PeproTech GmbH, Hamburg, Germany
TNFα ELISA kit Duoset		R&D Systems Europe, Ltd., UK

Devices

Table 3.8. ***Devices***

Device		Company
Centrifuge Eppendorf 5403		Eppendorf, Hamburg, Germany
Centrifuge Eppendorf 5417R		Eppendorf, Hamburg, Germany
Centrifuge Eppendorf 5810R		Eppendorf, Hamburg, Germany
Eppendorf BioPhotometer plus		Eppendorf, Hamburg, Germany
Fluorescent imaging setup	Axiovert 135 inverted microscope	Carl Zeiss AG, Jena, Germany
	cooled CCD camera	PCO Imaging, Kelheim, Germany
	PolychromeV	TILL Photonics GmbH, Graefelfing, Germany

	monochromator	
Microplate reader Infinite M200		Tecan, Männedorf, Switzerland
Realplex^2 Mastercycler		Eppendorf, Hamburg, Germany
Sonicator UP 50 H		Dr. Hielscher GmbH, Teltow, Germany
Thermomixer 5355		Eppendorf, Hamburg, Germany
Ultra Centrifuge : Sorvall WX80 Ultra Centrifuge		Fisher Scientific GmbH, Schwerte, Germany

Software

Table 3.9. ***Softwares***

Software	Company
Image J Macbiophotonics	http://www.macbiophotonics.ca/index.htm
Imaging Workbench 6.0	INDEC BioSystems, Santa Clara, USA
KaleidaGraph 4.1	Synergy Software, Reading, USA
Origin 7.0	OriginLab, Northampton, USA
Microsoft Office 2007, 2003	Microsoft Deutschland, Berlin, Germany
Adobe Creative Suite CS	Adobe Systems, San Jose, USA
Thomson Reuters EndNote®	Thomson Reuters, Carlsbad, USA

3.2 Methods

Reagents and plasmids

CGP37157 (7-Chloro-5-(2-chlorophenyl)-1,5-dihydro-4,1-benzothiazepin-2(3*H*)-one; Ascent Scientific, UK) was freshly prepared before each experiment at a stock concentration of 40 mM in DMSO and was used at a final concentration of 20 µM. ATP, FCCP, and all other reagents were obtained from Sigma Aldrich (Deisenhofen, Germany).

The plasmid expressing mitochondrial-targeted ratiometric-pericam (pcDNA3.1 $^{(+)}$-mtRP) was kindly provided by Atsushi Miyawaki (Wako, Japan).

Double-stranded ON-TARGETplus SMARTpool siRNAs, used to silence NCLX expression, and siGLO RISC-Free siRNA were obtained from Dharmacon (Thermo Fisher Scientific; Epsom, UK or Lafayette, CO, USA).

Cells/ transfections

Procedures for animal work were approved by the Federal Ministry of Berlin: “Landesamt für Gesundheit und Soziales” (LaGeSo) allowance T0014/08.

Microglia

Primary microglial cultures- Primary microglia cultures were prepared from cerebral cortex of newborn Naval Medical Research Institute (NMRI) mice (P_0-P_3) as described previously (Prinz et al., 1999). In brief, cortical and midbrain tissue was freed of blood vessels and meninges in Hank’s Balanced Salt Solution (HBSS) (Gibco, Invitrogen, Germany) and trypsinized in 1% trypsin and 0.05% deoxyribonuclease for 5 min at room temperature. Digested tissue was dissociated with a fire-polished pipette, and washed twice in HBSS. Dissociated cells were plated on T75 flasks coated with poly-L-lysine and cultured in normal medium. After 7 days medium was changed to 33% L929-conditioned medium. Microglia were separated from the underlying astrocytic layer by gentle shaking at 200 rpm for 10 min at room temperature. The microglia were seeded 1-1.5 × 10^5 cells per (15 mm diameter) glass coverslips or 5× 10^4 cells/well at 96-well plates. Cultures usually were used for experiments within 1 to 3 days after plating. An example of microglial culture is shown in Figure 3.1A.

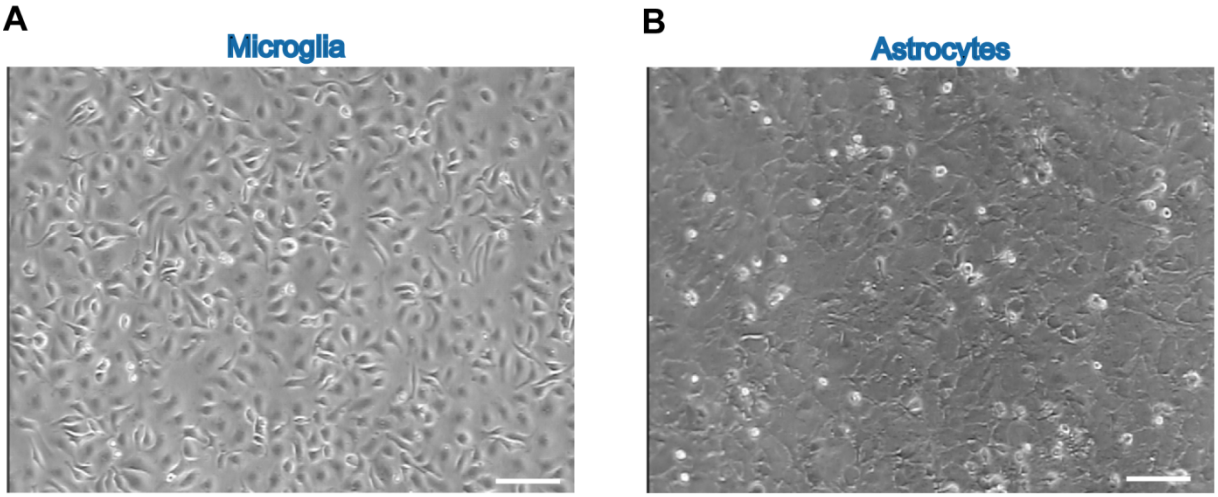

Figure 3.1. ***Primary murine microglia and astrocytes***

Phase contrast image of ***(A)*** primary microglia and ***(B)*** primary cortical astrocytes. Scale bar ***(A)*** 50 µm, ***(B)*** 100 µm.

Microglial stimulation- Before stimulation, microglial cells were allowed to settle for 6 h. Medium was removed by aspiration and macrophage serum free medium (M-SFM) (Invitrogen, Germany) was added. 24 h later cultures were stimulated for 18 h with 100 ng/ml LPS (Sigma-Aldrich, USA) and/or 10 U/ml mouse IFNγ (R&D Systems, USA). The pharmacological inhibitor CGP37157 (Ascent Scientific, UK) was added at a final concentration of 20 µM.

Microglial transduction

Retroviral vectors- The vector pMP71-mtRP was created by subcloning of mitochondrially targeted ratiometric pericam (mtRP) (Nagai et al., 2001) from the pcDNA3.1-mtRP plasmid into the pMP71 vector backbone (Engels et al., 2003). PMP71 backbone was taken from the retroviral vector pMP71-GFP, which was kindly provided by Prof. Dr. Wolfgang Uckert (MDC, Berlin, Germany). PcDNA3.1-mtRP was a present of Prof. Israel Sekler (Ben-Gurion University, Beer-Sheva, Israel).

The retroviral vector pMP71-mtRP was created by cutting the GFP insert from expression vector pMP71-GFP by using EcoRI and NotI restriction enzymes. mtRP was cut from pcDNA3.1-mtRP by HindIII and EcoRI. Restrictions enzymes were from New England Biolabs, UK. The fragments were separated by gel electrophoresis and isolated with Easypure Kit (Biozym, Germany). Klenow Fill-In Kit (Stratagene GmbH, Germany) was used to create blunt ends. PMP71 vector was dephosphorylated by calf alkaline phosphatase (Roche Diagnostics, Germany). The purification of DNA was done by ethanol precipitation.

For this purpose, 20 µl of DNA solution was resuspended in 200 µl ethanol and cooled down at -20°C for 20 min. Then the suspension was centrifuged at 14,000 rpm at 4°C for 20 min, and the remaining pellet was resuspended in 50-100 µl 70% ethanol, centrifuged at 14,000 rpm at 4°C for 10 min, and the remaining dry pellet was resuspended in the desired amount of double distilled water (DDW).

The mtRP fragment was ligated to a pMP71 backbone by using Rapid DNA Ligation Kit (Roche Diagnostics, Germany). Competent *E. coli* cells (Promega, Germany) were used to amplify the ligated vector. The cells were plated on agar plates supplemented with 50 µg/ml ampicillin. Colonies were picked and the plasmid DNA was isolated by Invisorb®SpinPlasmid Mini (Invitek, Germany). The samples were examined in a test restriction with PstI and KpnI. An adequate probe was selected and used for retransformation into competent *E. coli* to amplify the retroviral expression vector. *E. coli* were grown in LB medium supplemented with 50 µg/ml ampicillin overnight. The retroviral expression vector was isolated by EndoFree® Plasmid Maxi Kit (Qiagen, Germany).

Transfection of the packing cell line- For production of the virus particles the retrovirus packing cell line Platinum E (Cell Biolabs, Inc., USA; (Morita et al., 2000)) was used. The virus was produced by transient calcium phosphate transfection (Graham and van der Eb, 1973) of Platinum E cells with pMP71-RPmt vector.

For this purpose, Platinum E cells were seeded at $8.0x10^5$ cells /3.5mm well one day before the transfection. During the transfection Solution A (15µl $CaCl_2$ (2.5M), 18 µg retroviral expression plasmid DNA (pMP71-mtRP) in 150 µl) was mixed drop wisely with 150 µl Solution B or phosphate buffer per well. After the incubation for 20 min at room temperature 300 µl were added to each well of the retrovirus packing cells. The medium was changed to the standard DMEM medium following 5-7 h of incubation at 37°C, 90% humidity. Virus containing medium was harvested 48 h afterwards, filtered through 40 µm filter and used for the transduction.

Transduction of microglia- Virus-containing medium was mixed with fresh standard cell culture medium and L929 conditioned medium (50%, 20%, and 30% respectively), and applied to microglial cells on coverslips. L929 conditioned medium was used to stimulate proliferation (Sawada et al., 1990). 2 days after the infection microglial cells were used for the experiments.

Fluorescent staining

Microglia and RAW264.7 cells were grown on coverslips and transfected with siGLO as described. One day after the transfection, cells were washed 3 times with PBS, fixed with 4%

paraformaldehyde (4% PFA in PBS, pH 7.4) for 15 minutes at room temperature. Following the fixation, cells were washed with PBS, and stained with nuclear dye 4',6-diamidino-2-phenylindole, dihydrochloride (DAPI) at the concentration 1µg/ml diluted in PBS for 15 minutes at room temperature in dark chamber. Afterwards, cells were washed 3 times with PBS, mounted and left to dry for at least 1 day. Images were acquired using DAPI or tetramethylrhodamine isothiocyanate (TRITC) filter to visualize siGLO signal.

Astrocytes

Astrocytic cell culture - Enriched astrocyte cultures were prepared from cortices of 0- to 2-day-old newborn NMRI mice as described previously (Lyons and Kettenmann, 1998). Briefly, mice were sacrificed and cortical tissue was carefully freed from blood vessels and meninges, trypsinized and gently triturated with a fire-polished pipette in the presence of 0.05% DNase (Worthington Biochem. Corp., Freehold, USA). After two washes, cells were cultured in Dulbecco's Modified Eagle Medium (DMEM) with 10% fetal calf serum in 10 cm petri dishes, in 25cm^2 flasks or on poly-L-lysine (PLL)-coated glass coverslips at 37 °C in a humidified 5% CO_2/95% air atmosphere. After one day, cells were washed twice with Hank's balanced salt solution (HBSS) to remove cellular debris. After approximately 10-21 days, when astrocytes reached confluence, they were shaken in order to get rid of microglial cells, which usually grow on top of astrocytic monolayer. Confluent astrocytic cultures were slightly visible in phase contrast image (Figure 3.1B). Astrocytes were harvested for experiments at this stage, or were trypsinized, re-plated and used for experiments. The astrocytes were used within 14-21 days from the preparation of the primary culture.

For glutamate release and associated subset of calcium imaging experiments, which were performed by Dr. V.Montana and Prof. V.Parpura, University of Alabama, Birmingham, USA, astrocyte cultures were prepared from visual cortices of 0- to 2-day-old C57BL/6 mice as previously described (Reyes et al., 2011). Astrocytes were grown in culture medium containing α-minimum essential medium (α-MEM, without phenol red; Invitrogen) supplemented with fetal bovine serum (10% v/v; Thermo Scientific Hyclone, Logan, UT), L-glutamine (2 mM), D-glucose (20 mM), sodium pyruvate (1 mM), penicillin (100 I.U./ml), streptomycin (100 µg/ml) and sodium bicarbonate (14 mM) (pH=7.35). After 7-18 days in culture, cells were purified for astrocytes (>99% for the astrocytes from visual cortices). In some cases, after the purification procedure, astrocytes were returned to the incubator up to 1 day before transfection.

Transfection procedures of astrocytes

For silencing NCLX activity, astrocytes were transfected with ON-TARGET cocktail of siRNAs (siNCLX) to silence NCLX expression, or pool of control ON-TARGETplus non-targeting siRNAs (control), at a final concentration of 10 nM siRNA. siRNAs and transfection reagents were diluted first in OPTI-MEM I reduced serum media (Invitrogen, Darmstadt, Germany). As controls, in some experiments cells treated only with a transfection reagent (mock-treated) or untreated cells were used. Astrocytes were analyzed 3 days after the transfection. Lipofectamine RNAiMAX (1 µl per 1,200 µl of medium) (Invitrogen GmbH, Darmstadt, Germany) or TransIT-TKO (6µl/flask containing 4 mL of medium) (Mirus, Madison, USA) was used to transfect astrocytes with siRNA. Fluorescent transfection marker siGLO RISC-Free siRNA or siGLO red transfection indicator was used in the cytoplasmic Ca^{2+} imaging experiments and glutamate release experiments to identify siRNA-transfected cells. Based on the siGLO fluorescence, cells were visualized using a standard tetramethylrhodamine isothiocyanate (TRITC) filter set (Chroma Technology, Rockingham, VT), siRNA was delivered to all astrocytes and retained intracellularly throughout the duration of experiments.

For mitochondrial Ca^{2+} imaging experiments of NCLX-silenced astrocytes, the siNCLX or control siRNAs were co-transfected with pcDna3.1 $^{(+)}$-mtRP (1 µg) (Figure 4.7A) using Lipofectamine 2000 transfection reagent (1 µl per each 300 µl medium) (Invitrogen GmbH, Darmstadt, Germany) according to the manufacturer's protocol. Transfection efficiency was around 1-5 %.

Calcein and DAPI staining of astrocytes (the experiments were performed by Dr. V. Montana and Prof. V. Parpura, University of Alabama, Birmingham, USA)

Due to the possible harmful effects of transfection on cell viability, cells were evaluated for the accumulation of calcein AM, dye labelling only live cells with active intracellular esterases (Hua et al., 2004). Astrocytes were grown on glass coverslips, transfected as described with siGLO and siNCLX or untransfected. Then cells were incubated with calcein AM (1 µg/ml; Invitrogen) and pluronic acid (0.025% w/v) in complete culture medium at 37°C in a humidified 5% CO_2/95% air atmosphere for 10 minutes. Deesterification of calcein AM was performed by incubating the cells for 10 minutes in external solution at room temperature. During the last 5 minutes of desertification time, nuclei were stained using the cell permanent nuclear stain Hoechst 33342 (5 µg/ml; Invitrogen) for 5 minutes at room temperature. Then, cells were washed in external solution. Calcein was visualized using fluorescein isothiocyanate (FITC) filter set, while a DAPI filter set was used for visualization

of Hoechst. Visualization of siGLO was accomplished using TRITC filter set. Image acquisition was done using a 60x Plan Apo oil-immersion objective (1.4 NA; Nikon).

Biochemical assays

Cell fractionation, Western blot analysis

Cell/ tissue lysis- Cell extracts were washed with PBS and lysed with RIPA buffer (Sigma-Aldrich, Deisenhofen, Germany) supplemented with protease inhibitors (Roche Diagnostics Deutschland GmbH, Mannheim, Germany). After the lysis, cells were agitated at 4^{o}C for 30 min and centrifuged for 20 min at 14,000 rpm. Then the supernatants were collected and frozen at -70 °C until use.

Mice were deeply anesthetized and sacrificed according to the protocol approved by the Committee for the Ethical Care and Use of Animal. Tissues from newborn and 6 weeks old NMRI mice were washed with ice-cold PBS, cut into small pieces and sonicated three times for 30 seconds in the ice-cold lysis buffer containing 20 mM Tris-HCl (pH7.5), 0.32 M Sucrose, 0.2 mM EDTA and 0.5 mM EGTA supplemented with protease inhibitors. 1 ml of lysis buffer was added per each 5 mg of tissue. Following the sonication, homogenate was spun for 15 min at 14,000 rpm, and the supernatants were collected. For the Figure 4.3A in the results section, tissue extract was washed, diced and suspended in RIPA buffer supplemented with protease inhibitors (3 ml per gram of tissue). Then, the tissue was lysed by passing at least 10 times through the needle of 22 gauges, incubated at 4^{o}C for 30 min and centrifuged for 20 min at 14,000 rpm. Then the supernatants were collected and frozen at -70 °C until use.

Subcellular fractionation- ER, cytosol, and mitochondria-enriched fractions from primary astroglia cultures were obtained according to the Bozidis et al. protocol (Bozidis et al., 2007). Briefly, about 4-5x10^{7} cells were washed once with PBS, suspended in Mannitol-Tris EDTA solution (MTE) (270 mM D-mannitol, 10 mM Tris, 0.1 mM EDTA, pH 7.4), and then lysed by sonication. The homogenate was spun at 1,400g for 10 min; the supernatant (total fraction) was recovered and further centrifuged for 10 min at 15,000g. At this stage the resulting pellet (crude mitochondria) and supernatant (crude ER) were separated for further purification.

The supernatant was loaded on the top of sucrose gradient, consisting of layers of 2.0 M sucrose (2.0 M sucrose, 10 mM Tris, 0.1 mM EDTA, pH 7.6), 1.5 M sucrose (1.5 M sucrose, 10 mM Tris, 0.1 mM EDTA, pH 7.6), and 1.3 M sucrose (1.3 M sucrose, 10 mM Tris, 0.1 mM EDTA, pH 7.6), and ultracentrifuged for 70 min at 152,000g. The upper band was collected,

as cytosol-enriched fraction. The ER containing band was extracted, diluted with MTE buffer, and further spun at 126,000 g for 45 min. The resulting pellet (ER) was suspended in PBS.

Crude mitochondrial pellet was diluted in MTE solution, and purified by centrifugation at 44,000g for 22 min on sucrose gradient consisting from layers of 1.7 M (1.7 M sucrose, 10 mM Tris, 0.1 mM EDTA, pH 7.6) and 1.0 M (1.0 M sucrose, 10 mM Tris, 0.1 mM EDTA, pH 7.6) sucrose. Then the band, containing the mitochondrial fraction, was extracted and washed in MTE buffer, followed by centrifugation at 15,000g for 10 min. The resulting pellet (mitochondria) was suspended in PBS.

Purification of the plasma membrane-enriched fraction was done with the Pierce cell surface protein isolation kit (Pierce/ Thermo Fisher Scientific, Bonn, Germany) according to the manufacturer's instructions.

Protein quantification and Immunoblotting- Protein concentration was determined by the bicinchoninate assay (BCA) (Pierce/ Thermo Fisher Scientific, Bonn, Germany). Beforehand, plasma membrane-enriched fraction was dialyzed 3 times vs. PBS to exchange the original buffer, and then assayed by the BCA method.

Extracted proteins (20 µg) were separated by 10 or 12% SDS-PAGE, transferred onto polyvinylidenedifluoride membrane (PVDF, Amersham/ GE Healthcare Europe GmbH, Freiburg, Germany) either via a wet transfer system (constant amperage of 200 mA, 4^{o}C, 75 minutes) or a semi-dry transfer system (constant voltage of 15 V, RT, 75 minutes). Protein transfer was always monitored by staining the membranes with the reversible dye Ponceau-S red (Sigma-Aldrich, Deisenhof, Germany). Membranes were probed using following primary antibodies: anti-NCLX ((Palty et al., 2004) 1:500 for astrocytes and 1:2000 for microglia), anti-ANT (1:100, Santa Cruz Biotechnology Inc., Heidelberg, Germany), anti-Sec62 (1:1,000, kindly provided by Prof. T. Sommer, MDC, Berlin, Germany), anti-N-Cadherin (1:1,000, BD Biosciences, Heidelberg, Germany), anti-Cytochrome C oxidase (anti-complex IV subunit I OxPhos) (1:1,000, Invitrogen, Darmstadt, Germany), anti-CD11b (1:10,000, Abnova GmbH, Heidelberg, Germany), anti-GAPDH (1:10,000, New England Biolabs GmbH, Frankfurt am Main, Germany). Membranes were incubated with primary antibodies diluted in antibody dilution buffer (5% non-fat dried milk in PBS-T) for 2 hours at room temperature, followed by at least three 5 minutes washes in PBS-T and 1 hour incubation with secondary antibody conjugated to horse radish peroxidise (HRP) and subsequently developed with a chemiluminiscent substrate SuperSignal West Pico or Dura Chemiluminiscence substrate kit (Thermo Fisher Scientific, Bonn, Germany) and visualized by the Molecular Imager Gel Doc XR system using the QuantityOne™ software (Bio-Rad Laboratories GmbH, Munich, Germany).

Immunohistochemistry (the experiments were done in collaboration with Dr. C.Nolte, MDC, Berlin, Germany)

Mice were deeply anesthetized with sodium pentobarbital (100 mg/kg body weight; Sanofi) and perfused intracardially with a saline solution (0.9% NaCl). Brains were dissected, washed several times in 0.1 M phosphate buffer (PB, pH 7.4) and quickly frozen in isopentane, cooled by dry ice. Cryosections (14-15 µm thick) were mounted on gelatin-coated slides and allowed to dry for 30 min at room temperature. Sections were permeabilized with 0.1% Triton X-100 in PB for 20 min and incubated in blocking solution (0.5% bovine serum albumin, 4% normal goat serum [NGS], 0.01% Triton X-100 in PB) for 1 hr at room temperature in order to reduce non-specific staining. Antibodies were diluted in 1% bovine serum albumin,1% NGS, 0.01% Triton X -100 in PB. Sections were incubated for 24 h at 4^{o}C with the following primary antibodies: mouse monoclonal anti-GFAP (Sigma-Aldrich) (1:400), rabbit polyclonal anti-GFAP (DAKO) (1:1,000), rabbit polyclonal anti-NCLX (1:300) and mouse monoclonal anti-NeuN (Chemicon) (1:200). The secondary antibodies used to visualize the signals from primary antibodies were Alexa 566 goat anti–mouse IgG (1:1,000, Invitrogen) or Alexa 488 goat anti rabbit IgG (1:1,000, Invitrogen). They were incubated for 2 h at room temperature, then the sections were mounted with Aqua-Polymount (Polyscience Inc.) and the images were acquired with fluorescent Axiovert microscope.

RNA isolation, RT-PCR and qRT-PCR (Real-time quantitative RT-PCR)

RT-PCR (**R**everse **T**ranscription-**P**olymerase **C**hain **R**eaction) is a method used to detect mRNA expression levels. RNA is first transcribed into cDNA using reverse transcriptase, and then the resulting cDNA is amplified by PCR reaction using primers for the genes of interest. Real-time quantitative RT-PCR or qRT-PCR is quantitative RT-PCR, used to quantify PCR templates. For qRT-PCR, probe-based method was used, utilizing two specific primers and a probe complementary to the middle of the PCR product. Fluorescent signal is created only when a probe binds its complementary sequence, therefore separating a fluorophore and a quencher on the different ends of the probe.

To extract RNA from the tissue, isolated tissue was cut with single-edged razor blade and sonicated at 100% power for three times 10 seconds each time. Tissue homogenate was immediately used for RNA isolation. To extract RNA from cells, they were washed in PBS and harvested in RNA lysis buffer. Total RNA from tissues or cells was extracted by RNeasy Mini Extraction Kit or InviTrap Spin universal mini kit (Invitek) according to manufacturer's

instructions. This was followed by first-strand cDNA synthesis using the SuperScript II reverse transcriptase enzyme (Invitrogen) with 1 µg total RNA and oligo-dT primers.

QRT-PCR was performed with gene-specific assays purchased from Dharmacon (Thermo Fisher Scientific, Epsom, UK) according to manufacturer's instructions. β-Actin served as internal control to quantify relative gene expression following silencing of GAPDH gene. For determining a suitable internal control, 3 housekeeping genes: GAPDH, ACTB (encoding for β-Actin) and PPIB (encoding for peptidylprolyl isomerase B (cyclophilin B)) were evaluated for the stability of the expression, and GAPDH had the highest stability score. Therefore, GAPDH served as the internal control to quantify changes in relative gene expression in the rest of the experiments.

The following primers were used for RT-PCR:

Table 3.10. ***RT-PCR primers for detection of NCLX expression***

Primer		Sequence
NCLX AF	forward	5'-TCT ATG GCA TCT ATG AGA TC-3'
	reverse	5'-CCA GGG AGA AGA TCA AGC TG-3'
NCLX E15	forward	5'-CCT GGG GAA ACA GCA TTG GAG-3'
	reverse	5'-CAG TAA TCC GTC TGG CTC CAG-3'
β-Actin	forward	5'- CCC TGA AGT ACC CCA TTG AA -3'
	reverse	5'- GTG GAC AGT GAG GCC AAG AT-3'

The following primers were used for qRT-PCR:

Table 3.11. ***Gene expression assays containing qRT-PCR primers and gene-specific probes for quantification of NCLX expression***

Gene	Encoded protein	Primer	Sequence
SLC24A6	NCLX	Forward	5'-ACA TAT TAC GGT CCC TGG GT-3'
		Reverse	5'-ATC TGA GAA GGC ATC TCC-3'

		Probe	5'-CCT GGG GAA ACA GCA TTG G-3'
Gapdh	GAPDH	Forward	5'-GGC TGG CAT TGC TCT CAA-3'
		Reverse	5'-GCT GTA GCC GTA TTC ATT GTC-3'
		Probe	5'-CAT TTC CTG GTA TGA CA-3'
ACTB	β-Actin	Forward	5'-CTT CTA CAA TGA GCT GCG TGT G-3'
		Reverse	5'-GGT CTC AAA CAT GAT CTG G-3'
		Probe	5'-CCG TGA AAA GAT GAC CC-3'
PPIB	peptidylprolyl isomerase B (cyclophilin B)	Forward	5'-GCA AGT TCC ATC GTG TCA TCA AG-3'
		Reverse	5'-GCT CAC CAT AGA TGC TC-3'
		Probe	5'-TGG CAC AGG AGG AAA GAG C-3'

Functional assays

Executive functions of microglia (this part was performed by Nora Freyer under the supervision of Dr. C.Nolte and myself)

Cytokine release- IL-6 and IL-12 were measured in ELISA, based on capturing and detecting antibody pairs from R & D Systems, following the procedure of the manufacturer. TNF- α was quantified using a complete ELISA kit (R & D Systems, Germany). The color reaction was analyzed in a microplate reader (infinite M200, Tecan Deutschland GmbH, Germany). Total protein was determined using the MicroBCA protein kit (Pierce, USA) (Hausler et al., 2002). Data were normalized to the groups treated with LPS/IFNγ without CGP37157, which was taken as 100%.

Nitric oxide release assay - Upon activation microglial cells produce nitric oxide, NO, from L-Arginine. To assay NO production, the Griess reaction was used (Menaka et al., 2009). This reaction measures the accumulation of nitrite (NO^{2-}), a breakdown product of NO, via color reaction. Microglia were seeded and stimulated as described earlier with or without 20 µM CGP37157. After 24h of stimulation, 100 µl of each supernatant or NO-standard were mixed

with 100 µl of Griess reagent, incubated at room temperature for 10 min and the optical density was determined in a microplate reader at 540 nm.

Reactive oxygen species (ROS) release assay- Activated microglia are the major source of ROS generation in the CNS. To measure ROS generation the carboxylated H_2DCFDA analog (6-carboxy-2',7'-dichlorodihydrofluorescein diacetate) was used (Eruslanov and Kusmartsev, 2010). Removal of the acetate and ester groups by intracellular esterases and oxidation via ROS both impede its leakage out of the cells and readily convert it to a green fluorescent form, which can be measured. Microglia were seeded, incubated with 150 µl/well of 20 µM carboxylated H_2DCFDA for 90 min at 37^{o}C. Zymosan was used as an alternative activation substrate. First, to prepare zymosan particles, 10 mg zymosan powder were suspended in 1 ml DMEM with 50% FCS, vortexed, incubated for at least 1 hour and centrifuged for 30 min at 4,000 rpm. Then the pellet was washed twice with PBS and re-suspended in 1 ml normal growth medium. Zymosan was used at final concentration of 1 mg/ml. Microglia were stimulated as previously described with or without 20 µM CGP37157, washed in PBS. Then the fluorescence was measured in a plate reader at 535 nm upon excitation of 485 nm.

Chemotaxis assay- Microglial chemotaxis was measured in a multiwell microchemotaxis chamber. Polycarbonate filters with pores of 5 µm diameter separated the upper and the lower wells. Chemoattractive agents were added to the lower wells. 50 µl of a cell suspension containing $5x10^4$ microglia/ml were added to the upper wells. Inhibitor was added to both the upper and the lower wells. Experiments were performed in triplicate. After 3 h incubation at 37 °C, filters were fixed and stained with Diff-Quick (Baxter Diagnostics, Switzerland). Non-migrated cells were wiped off with a cotton swab. The rate of migration was determined by counting cells on the lower filter surface in three random fields of each well (Nolte et al., 1996). Data were normalized to the groups stimulated by ATP and without CGP37157 and presented as migration (% of ATP-stimulated migration without CGP37157).

Fluorimetric measurements of cytosolic and mitochondrial Ca^{2+}

Cytosolic Ca^{2+} measurements - Ca^{2+} imaging experiments were carried out at room temperature using an Axiovert 135 inverted microscope (Carl Zeiss AG, Berlin, Germany) equipped with a cooled CCD camera (PCO Imaging, Kelheim, Germany) and a Polychrome V monochromator (TILL Photonics GmbH, Graefelfing, Germany). Fluorescence measurements were acquired using Axon Imaging Workbench 6 software (INDEC BioSystems, Santa Clara, USA). Cells were first evaluated for their appearance (Figure 3.2A) and for the intracellular distribution of the dye (Figure 3.2B). Acquisition speed was 1

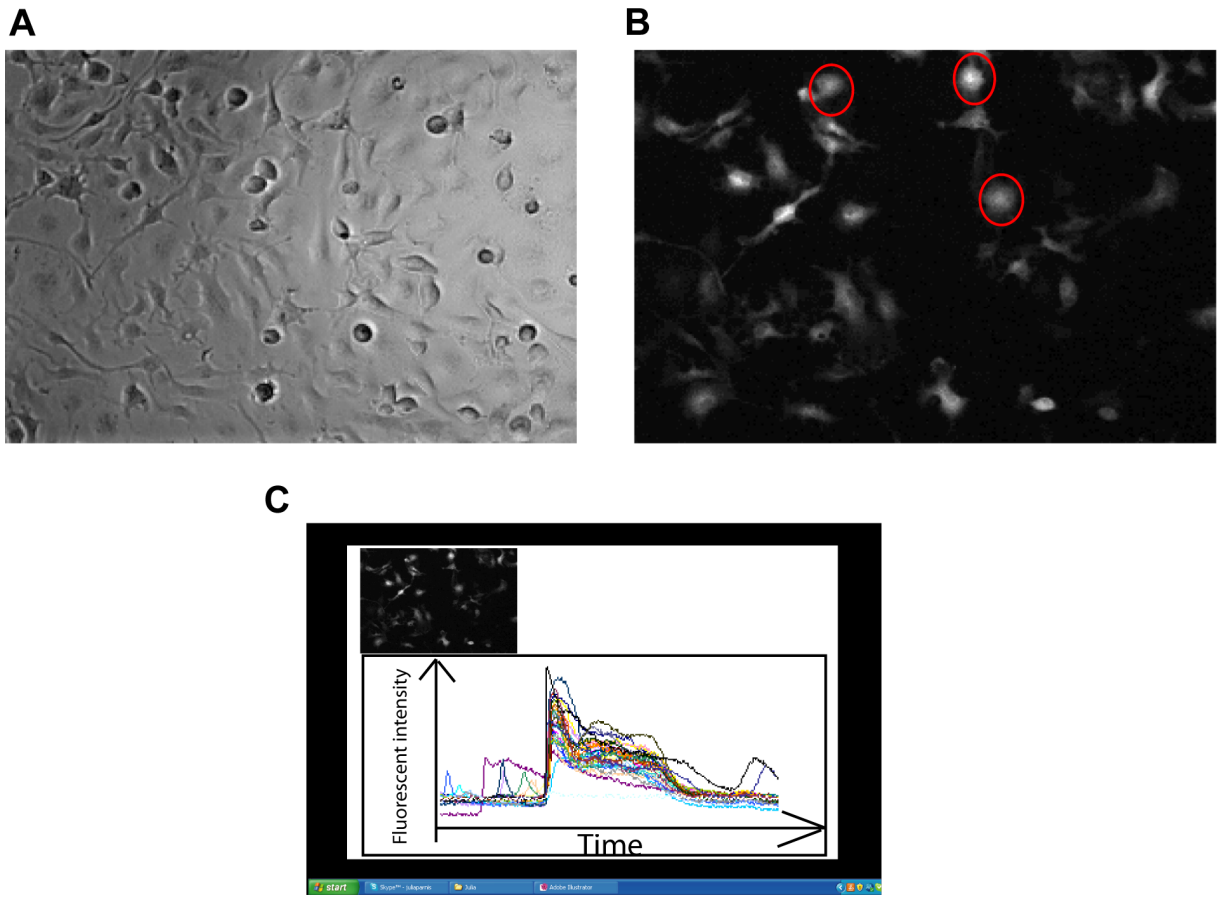

Figure 3.2. Measuring Ca^{2+} changes in glial cells with Ca^{2+}-sensitive dyes

Microglial cells loaded with Fluo-4 AM Ca^{2+}-sensitive dye. ***(A)*** Bright field image of microglial cells taken with 20X objective. ***(B)*** Fluorescent image of Fluo-4 AM-loaded microglia show the cytoplasmic distribution of the dye. Regions of interest (ROIs) are selected (red ovals) and fluorescent intensity in such ROIs is measured. ***(C)*** Imaging software records the images and the data can be presented as fluorescent intensity vs. time. Rise in fluorescent intensity corresponds to the elevation in cytosolic Ca^{2+} concentration, which can be elicited by stimuli application.

frame in 3 sec for the experiments measuring Store-Operated Channel entry following thapsigargin stimulus and 1 frame in 1.2 sec for rest of the experiments. To measure cytosolic Ca^{2+} levels, cells were loaded for 30 min with 5 µm Fluo-4 AM or 2.5 µm Fura-2 AM (Molecular Probes/ Invitrogen). After loading with Fura-2 AM cells were washed for at least 20 min in HEPES buffer ((mM) NaCl 150.0, KCl 5.4, $MgCl_2$ 1.0, $CaCl_2$ 2.0, HEPES 10.0, Glucose 10.0, at pH 7.4) to allow de-esterification. The cells were excited at wavelengths of 480 nm for Fluo-4 AM loaded cells and 340 and 380 nm and the emitted light passed via a longpass emission filter at 520 nm and 510 (± 40)nm for Fluo-4 AM and Fura-2 AM staining, respectively. The data was processed to show fluorescent intensity vs. time in each region of

interest (ROI) selected (Figure 3.2C). Changes in the fluorescence for each ROI were normalized to the average of the fluorescence intensity acquired for 50-200 sec prior stimuli application.

Mitochondrial Ca^{2+} measurements - Mitochondrial Ca^{2+} levels were monitored in cells transiently expressing mtRP using excitation wavelengths of 430 nm (Ca^{2+}-sensitive wavelength (Nagai et al., 2001)), presented as F_0/ F_{430}, and the emission collected using a 535 nm band-pass filter. F_0 was calculated as the average value obtained during 50-100 sec before the stimulus application. MtRP was excited at the pH-insensitive 430 nm wavelength and at the 485/430 nm ratiometric mode. Due to the pH sensitivity of mtRP when excited at the 485 nm wavelength and the potential interference by mitochondrial pH changes (Malli et al., 2003), only signals without changes at 485 nm during the stimulus application, were taken into the analysis.
Ca^{2+}-free HEPES buffer contained (mM) NaCl 150.0, KCl 5.4, $MgCl_2$ 2.0, EGTA 0.5, HEPES 10.0, Glucose 10.0, at pH 7.4.

Astrocytic Ca^{2+} waves- Intercellular propagation of Ca^{2+} elevations in astrocytes can be elicited by mechanical touch of a particular astrocyte grown in a monolayer. Astrocytic Ca^{2+} wave has physiological relevance; therefore assessing different parameters of Ca^{2+} wave propagation could provide insights into the Ca^{2+} excitability and Ca^{2+} store properties of astrocytes. Confluent astrocytes grown on coverslips were loaded with 5 μm Fluo-4 AM for 30 min at room temperature. Following the dye loading and washing, the coverslips were mounted in the bath containing HEPES buffer and Ca^{2+} waves were evoked mechanically by touching a single astrocyte with a micropipette (Cornell-Bell et al., 1990). The changes in Fluo-4 AM fluorescence were acquired with 10x Plan objective (Carl Zeiss Meditec AG, Berlin, Germany) with speed of 1 frame in 1.2 sec.

Glutamate release and cytosolic Ca^{2+} measurements in stimulated solitary astrocytes (this part was performed by Dr. V. Montana and Prof. V. Parpura, University of Alabama, Birmingham, USA)

Stimulation of astrocytes- Astrocytes were stimulated using glass pipettes filled with external solution as described in detail elsewhere (Hua et al., 2004). The advantages of this method are spatio-temporal control of the stimulus application, lack of the plasma membrane damage and the physiological ground (Hua et al., 2004; Malarkey and Parpura, 2011). To control for the contact between the pipette and the solitary astrocyte we monitored pipette resistance using a patch-clamp amplifier (PC-ONE; Dagan, Minneapolis, MN). The strength of the stimulus, measured as increase in the pipette resistance upon establishment

of a pipette-astrocyte contact, was comparable under all conditions tested (Mann-Whitney U-test, p=0.27-0.34).

Cytosolic Ca^{2+} measurements - The intracellular Ca^{2+} levels in somata of solitary astrocytes were recorded using the Ca^{2+} indicator Fluo-3 AM as previously described (Hua et al., 2004; Lee et al., 2008; Montana et al., 2004). Astrocytes were loaded with 1μg/ml Fluo-3 AM (Invitrogen, NY, USA) in external solution containing pluronic acid (0.025% w/v; Invitrogen) for 20 minutes at room temperature. Cells were washed and kept in external solution for 20 minutes at room temperature for de-esterification of intracellularly-trapped Fluo-3 AM. Image acquisition was done using a standard fluorescein isothiocyanate (FITC) filter set (Chroma Technology). All imaging data were background subtracted using regions of the coverslip field containing no cells. Data are expressed as dF/Fo ± SEM (%) in which dF represents the change of fluorescence, while Fo represents the fluorescence of the cell soma at rest. The concentration of cytosolic Ca^{2+} was determined using calibration of Fluo-3 AM as described elsewhere (Malarkey et al., 2008; Parpura and Haydon, 2000).

Glutamate measurements - Ca^{2+}-dependent glutamate release from cultured solitary astrocytes was measured using the L-glutamate dehydrogenase (GDH)-linked assay as previously described (Hua et al., 2004; Lee et al., 2008; Montana et al., 2004). Astrocytes were incubated in an enzymatic assay solution containing external solution supplemented with 1 mM NAD^+ (Sigma-Aldrich, St. Louis, USA) and ~53–137 I.U./ml GDH (Sigma-Aldrich, St. Louis, USA) (pH 7.4). External solution contained (in mM): 140 NaCl, 5 KCl, 2 $CaCl_2$, 2 $MgCl_2$, 5 glucose and 10 HEPES (pH 7.4). When released to the extracellular space, glutamate gets converted by GDH to α-ketoglutarate with the concomitant reduction of the bath supplied coenzyme NAD^+ to NADH, the latter being a fluorescent product when excited by UV light. Images were acquired at room temperature (20–24°C) using a standard 4'6-diamidino-2-phenylindole (DAPI) filter set (Nikon, Melville, NY, USA). Every experiment was preceded by a control run on astrocytes bathed in solution lacking GDH and NAD^+ for photo-bleaching and background subtraction calculation. After correction all imaging data were expressed as dF/Fo (%), in which dF represents the change of fluorescence, while Fo represents the background fluorescence level surrounding the solitary astrocyte, immediately and laterally of its soma, before mechanical stimulation. The concentration of extracellular glutamate was determined as described elsewhere (Innocenti et al., 2000).

Astrocytic wound healing assay

Astrocytic migration and proliferation was evaluated using a scratch assay described by Geback et al. (Geback et al., 2009). Astrocytes were seeded in 4-well plates at 60%

confluence ($6x10^4$ cells/well). The next day cells were transfected with either 10 nM siNCLX, control non-targeting siRNA or mock-transfected as described, or left untreated and cultured for 3 days to reach full confluence. At day 4, astrocytic monolayers were scratched with a 200µl sterile pipette tip in the shape of horizontal double cross (see Figure 4.18B). After two washes with PBS to remove detached cells and debris, cells were incubated in serum-reduced medium containing 1% FCS. To determine the effect of the NCLX inhibitor, either 20 µM CGP37157 or 0.05% DMSO (vehicle) in culture medium plus 1 % FCS were added to the freshly scratched control monolayers. Phase contrast images of the wounds were acquired at 0 – 72 h after scratching using a 5x magnification objective and frame grabber software (InteQ, Berlin, Germany). Care was taken that at each acquisition time point the culture dish and the cross-shaped wound area was exactly centered and images were acquired at identical positions (see Figure 4.18A). TScratch software (Geback et al., 2009) (www.cse-lab.ethz.ch/software.html) was used to determine the open wound area. The results were expressed as % of open wound area at time point 0h. The end point was defined when the initial open wound area was at least 50% closed. At least 6 replicates per condition were analyzed. The results were expressed as % of open wound area.

Cell proliferation assay

Astrocyte proliferation was determined by a colorimetric immunoassay measuring 5-Bromo-2`-Deoxy-uridine (BrdU) incorporation (Roche Diagnostics Deutschland GmbH, Mannheim, Germany) in proliferating cells. Two days after transfection of astrocytes with siRNA, cells were trypsinized and seeded into 96 well-plates at a density of $3.5x10^3$ cells/well. The optimal cell density for this assay was determined in a titration assay utilizing different astrocytic cell densities in 1 and 10% FCS. Serum could interfere with the assay and mask the effects of NCLX knock-down on the proliferation, therefore cells were grown in 1% FCS just prior to BrdU application. 1 day after the re-seeding, medium was changed to medium containing 1% FCS and BrdU was added according to the manufacturer's instructions. The assay was performed 24 h after the addition of BrdU according to the manufacturer's instructions with 5 replicates for each condition.

Data analysis

To analyze the data derived from mitochondrial Ca^{2+} imaging, only curves presenting more than 2% increase in fluorescence upon stimuli application were taken into the analysis. The reason to exclude such curves is low signal to noise ratio in such curves and therefore

difficulty to evaluate different parameters and higher risk to mistaken in the analysis. The rate of Ca^{2+} influx (entry) or efflux was obtained by measuring the initial slope of Ca^{2+} rise or decline, respectively (Figure 3.3A, C). The maximal value of the normalized fluorescent intensity was taken as the peak amplitude or influx (Figure 3.3B). To evaluate the duration of the Ca^{2+} response the width of the peak at its half-amplitude was determined (Figure 3.3D). To find out the cumulative fluorescence, the area under the curve was derived by integration (Figure 3.3E). For mitochondrial Ca^{2+} imaging the area was calculated for 100 sec from the beginning of the Ca^{2+} rise.

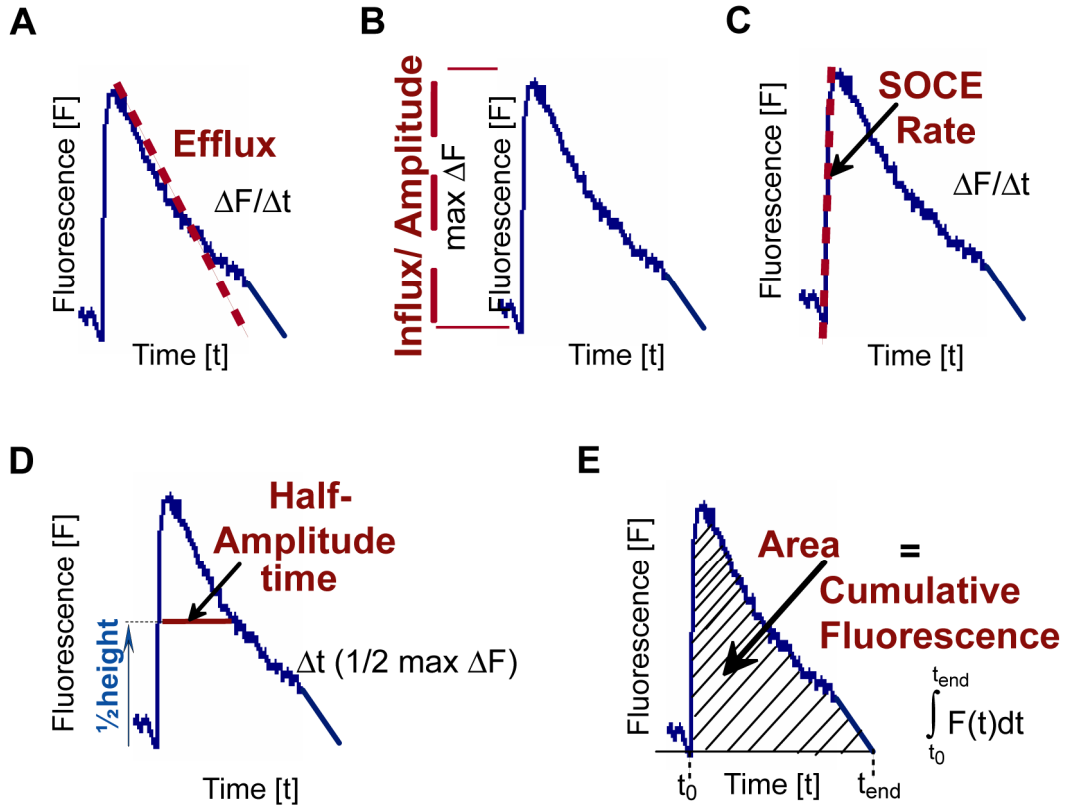

Figure 3.3. Analyzing Ca^{2+} imaging data

An example of Ca^{2+} imaging curve and graphical representation of the analysis of (A) Ca^{2+} efflux, (B) Ca^{2+} influx or peak amplitude, (C) SOCE rate measuring the rate of the Ca^{2+} influx, (D) Half-amplitude time and (E) Area or Cumulative fluorescence of the Ca^{2+} response.

To determine the velocity of astrocytic Ca^{2+} waves, the background image was first subtracted. Next, three concentric circles with radiuses of 23.45, 117.81, and 212.19 μm were drawn centred at the point of stimulation (Figure 4.16B). Then the curve of fluorescent intensity vs. time was acquired for the areas aligned by the circles: (1) small circle, (2) middle circle, and (3) large circle (see Figure 4.16C). The time for the peak amplitude was

determined and applied to the formula in Figure 4.16C to calculate the velocity for each region. Velocity calculated for the middle and large circles was presented in the results.

To calculate the area of the wave, after the background subtraction, the images constructing the Ca^{2+} wave were grouped in one Z-stack, the obtained image was enhanced, and the area was calculated in the image J software.

The data analysis was performed with MS Excel 2003, Origin 7, KaleidaGraph version 4.1, and ImageJ softwares.

Statistics

All experiments evaluated statistically were done at least three times utilizing astrocytic (or microglial) cultures originating from different cell preparations. Data from microglial experiments were evaluated for the outliers. The value which had a z-score of more than 1.96 was considered an outlier and excluded from the analysis. Data are presented as mean $\pm$ SEM for column graphs and as median and 25^{th} and 75^{th} percentiles for boxplots. For the parametrical data the statistical significance was evaluated using Student's t-test, unpaired and double-tailed. For the experiments with more than two test groups to compare, a multiple parameter one-way ANOVA test was used followed by Bonferroni post-test. For the comparison of non-parametric data Mann-Whitney U-test or Kruskall-Wallis test followed by Bonferroni correction and Mann-Whitney U-test pair comparisons were used to evaluate the statistical significance.

NS denotes $p>0.05$, * denotes $p<0.05$, ** denotes $p<0.01$, *** denotes $p<0.001$.

Chapter 4

Results

4.1 NCLX is responsible for mitochondrial Ca^{2+} extrusion in astrocytes

Growing evidence indicates that the mitochondrial Na^+/Ca^{2+} exchanger NCLX mediates mitochondrial Ca^{2+} extrusion in different cell lines (Kim et al., 2012; Palty et al., 2010) and this extrusion plays an essential role in cell physiology. To show the role of NCLX for glial physiology, I first sought to determine NCLX role for mitochondrial Ca^{2+} handling in glia. As a model to explore glial cells I chose the *in vitro* system most closely mimicking the situation *in vivo*, namely primary murine astrocytes and microglia.

NCLX expression profile

NCLX mRNA and protein expression in different tissues and cell types

This part of the project provided insights into NCLX expression in the brain and glia compared to other cells and tissues and into a subcellular localization of NCLX. To evaluate NCLX expression at the mRNA level, two primer pairs were designed: NCLX AF and NCLX E15 (Table 3.10). Na^+/Ca^{2+} exchanger NCLX has three known splice variants: transcript variant 1 (or long), transcript variant 2 and transcript variant 3 (or short). Both sets of primers chosen in this study can identify all three isoforms. When the NCLX AF primers were aligned to the reference mRNA sequence database from *Mus musculus* (http://www.ncbi.nlm.nih.gov/RefSeq/), the resulting transcripts' lengths were 349 bp for the short isoform and 498 bp for the first and second isoforms. Database alignment with the NCLX E15 primer set resulted in product lengths of 191

bp for isoforms 1 (long) and 2 and 42 bp for the isoform 3 or short isoform. First, the exchanger's expression was evaluated in different murine tissues utilizing both primers (Figure 4.1A). RT-PCR reaction employing the NCLX AF primer set generated products of about 350 and 500 bp length in all sampled tissues (*upper panel* Figure 4.1A). These results support that the short and at least one other isoform are expressed by all the sampled tissues. NCLX transcript variant 3 was less abundant in both adult and E15 brain compared to heart, kidney and liver. The transcript variant 3 was enriched in choroid plexus compared to the whole brain extract. As these primers did not allow any distinction between the first and the second isoforms, a conclusion can be drawn only for the common expression of these two isoforms. Their expression was highest in the choroid plexus, followed by E15 total brain, and the lowest expression was seen in adult brain. RT-PCR utilizing the NCLX E15 primer set resulted in a product length of about 200 bp, while the 42 bp product could not be detected due to technical reasons (*middle panel* Figure 4.1A). This means that the RT-PCR with NCLX E15 primers could detect only the first 2 splice variants, but not the third (short) variant. Both adult and E15 brain had the lowest mRNA expression, while choroid plexus had the highest expression. β-Actin was used as a housekeeping gene to control for equal loading (*lower panel* Figure 4.1A). According to these results, NCLX is expressed at the mRNA level in all the tissues, but its expression levels vary in the different tissues.

To assess the NCLX expression in primary astrocytes and microglia, RT-PCR reaction utilizing the NCLX AF primer pair was set (Figure 4.1B) with β-Actin mRNA expression as a loading control (*lower panel* Figure 4.1B). The RT-PCR reaction with NCLX AF primers generated two bands at about 350 and 500 bp (*upper panel* Figure 4.1B). Both bands had comparable intensity in microglia and astrocytes, but much lower intensity in the brain. This indicates that astrocytes and microglia had similar NCLX expression at the mRNA level. However, the reaction yielded an additional product of about 700 bp. This band was very intense in astrocytes, very faint in total brain extract and absent in microglia. One possibility to explain this effect is a genomic DNA contamination; however the use of DNase as a part of the RNA extraction procedures should ensure the absence of genomic DNA. Another possibility may be the creation of secondary structure between the two PCR products, which may result in the hybrid running at a higher length. Nonetheless, these data show a high NCLX expression at the mRNA level both in primary cultures of murine cortical astrocytes and microglia compared to the whole brain.

Next, NCLX expression was investigated by Western blot analysis in cellular extracts from rat and murine primary cells and cell lines, including human embryonic kidney cell line (HEK293T)

(Figure 4.1C). Analysis revealed one band at about 60 kDa present in all the samples and a band at about 100 kDa present in primary murine astrocytes, human and rat astrocytoma cell

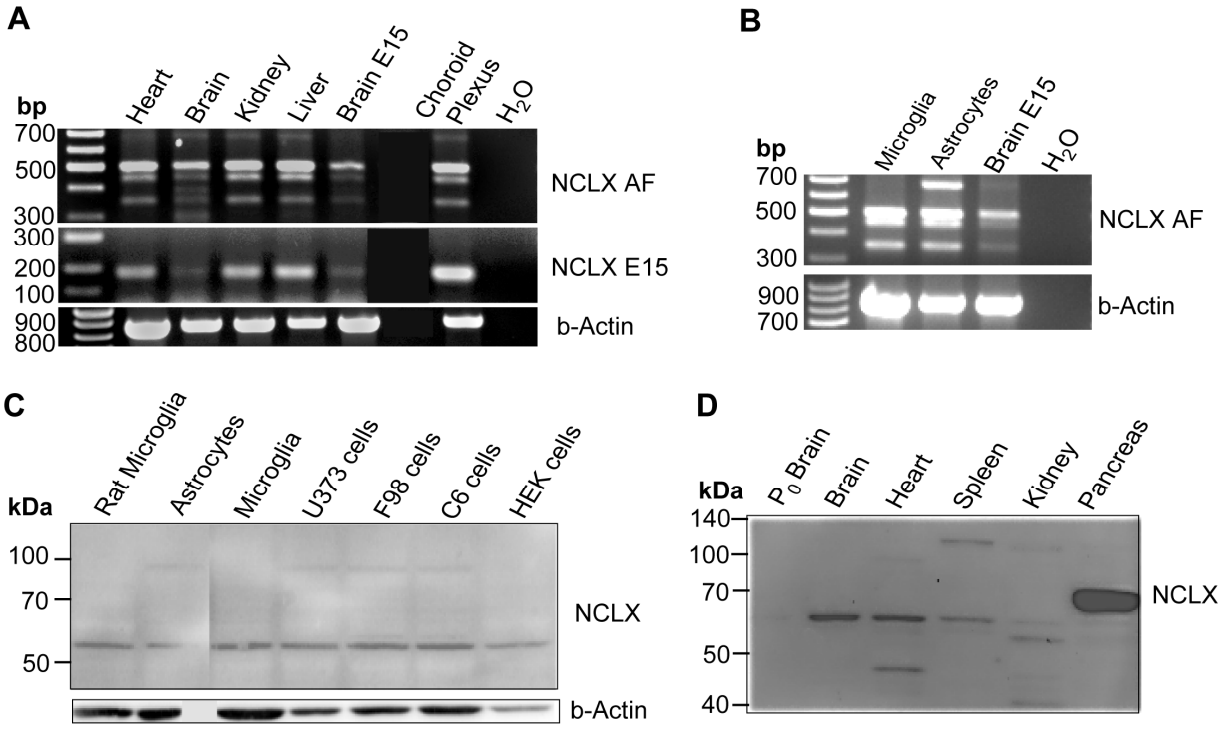

Figure 4.1. NCLX mRNA and protein are expressed in glia

(A-B) NCLX expression was analyzed at mRNA level by RT-PCR in homogenates of different murine tissues and cells as described. NCLX mRNA was evaluated in ***(A)*** different murine tissues or ***(B)*** primary murine glial cells compared to the whole brain extract, using two different sets of primers: NCLX AF (*upper panel* ***A*** and ***B***) and NCLX E15 (*middle panel* ***A***). As a loading control, β-Actin set of primers was used (*lower panel* ***A*** and ***B***). ***(C-D)*** NCLX protein levels were assessed by Western blot analysis in ***(C)*** rat and murine primary glial cells, different astrocytoma cell lines and HEK293T cell line and in ***(D)*** murine tissues as indicated using NCLX antibody and β-Actin for loading marker (*lower panel* ***C***).

lines U373, F98 and C6 (*upper panel* Figure 4.1C). Judging from the 60 kDa form, NCLX expression does not differ much between different samples. The 100 kDa band may represent a dimer, which has been described previously (Palty et al., 2006; Palty et al., 2010). β-Actin served as a loading control and indicated uneven loading of the samples, thus limiting interpretations of these results (*lower panel* Figure 4.1C).

Western blot analysis of different murine tissues revealed a band at about 60 kDa in brain, heart, spleen and kidney (Figure 4.1D). The highest NCLX expression was detected in the pancreas, and the band appeared at about 70 kDa. In the kidney the major band was lower than 60 kDa, in the heart additional bands appeared at about 45 and 100 kDa. Analysis also revealed an additional band in the spleen above 100 kDa. The existence of NCLX protein in different molecular weights may indicate either oligomers or proteins which might have undergone post-translational modification including proteolysis. At the molecular weight of about 60 kDa the most intense band that, NCLX antibody detected, was in the adult brain extract and heart, and the lowest expression was in P_0 brain extract. Predicted molecular weight of NCLX varies between 60, 63 and 64 kDa. These results did not allow us to distinguish between different NCLX isoforms, but showed NCLX expression at protein level in all the tissues with large degree of variation between different tissues.

NCLX expression in the brain

Next, to see in which brain region and in which cell types NCLX is expressed, immunohistochemical analysis was performed on frozen coronal and saggital sections of murine and rat brains (Figure 4.1A-C). This part was done in collaboration with Dr. C.Nolte, MDC, Berlin, Germany. An immunolabeling for NCLX was difficult to achieve; most reproducible results could be achieved on frozen sections that had been permeabilized shortly with ice cold methanol and acetone before immunolabeling. Usually there was a weak, diffuse staining of the entire tissue, and only in some areas a cell specific labeling was seen when using double immunolabeling approach. Double immunolabeling for GFAP and NCLX is shown in Figure 4.1A and indicates that astrocytes specifically express NCLX, at least in the white cerebellar matter from rat, as the co-labeling of NCLX and astrocytic marker GFAP revealed that the GFAP positive cells were also NCLX positive (Figure 4.1A, arrow points to a GFAP positive NCLX positive cell). Such intense labeling of astrocytes for NCLX, however, was not seen that clearly in all brain areas. This may be due to heterogeneous permeability of the tissue for the antibody. Even harsh treatment to permeabilize the tissue, as fixation by methanol or permeabilization by organic solvents (acetone or methanol) did not improve staining, it remained heterogeneous. This may indicate that the NCLX epitope is rather unstable or masked by fixation. In brain sections that had been double immunolabeled for NCLX and a microglial cell marker (Iba-1 antibody) a pronounced NCLX labeling that allowed to distinguish the microglia could not be detected (not shown).

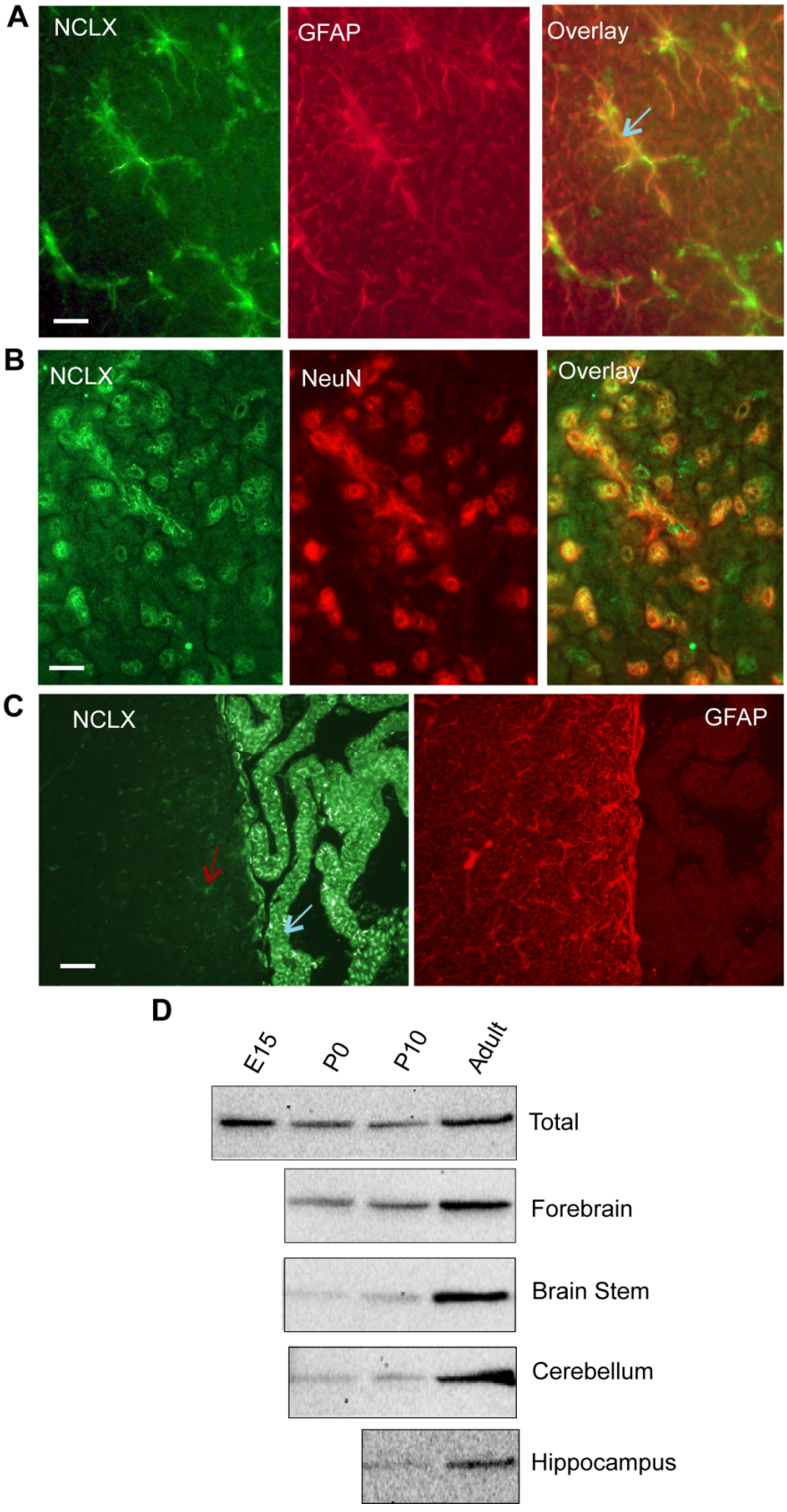
A
NCLX
GFAP
Overlay
B
NCLX
NeuN
Overlay
C
NCLX
GFAP
D
E15
P0
P10
Adult
Total
Forebrain
Brain Stem
Cerebellum
Hippocampus

Figure 4.2. NCLX is expressed in the brain

(A-C) Immunohistochemical expression of NCLX in adult mouse or rat brains (this part was performed in collaboration with Dr. C. Nolte, MDC, Berlin, Germany). 15-µm thick frozen sections were double-immunolabeled with NCLX antibody and neuronal or glial marker as described. ***(A)*** NCLX expression in astrocytes of white cerebellar matter from rat. Sections of rat white cerebellar matter were stained for NCLX and astrocytic marker GFAP (from left to right). The overlay of both images is shown in the right picture. An example of NCLX positive GFAP positive cell is shown (arrow). Scale bar 10 µm. ***(B)*** NCLX expression in neurons of the brain stem. Sections from mouse brain stem were stained with NCLX antibody and Alexa488 conjugated secondary antibody (green), Neuronal marker NeuN was visualized with Alexa 594 conjugated secondary antibody (red). The overlay of both pictures is shown in the right. NCLX positive NeuN negative structures may represent glial cells (arrow) Scale bar 20 µm. ***(C)*** NCLX expression in choroid plexus from mouse brain. Sections were stained for NCLX and astrocytic marker GFAP (from left to right). While the ependymal-like cells of chorioid plexus are intensely labelled for NCLX (blue arrow) there is also weak NCLX staining on astrocytic-like structures in the brain parenchyma (red arrow). Scale bar 20 µm. ***(D)*** NCLX expression in different brain regions is upregulated during adulthood. NCLX expression was analyzed by Western blot in diverse brain regions (total, forebrain, brain stem, cerebellum, and hippocampus) of mice of different ages (E_{15}, P_0, P_{10}, and Adult). β-Actin marker was used as loading control in all experiments, but the images of β-Actin were not incorporated in the figure.

In contrast, NCLX expression was more clearly seen in neurons: for instance in the brain stem there was a clear staining for NCLX on cells positive for the neuronal marker NeuN (Figure 4.1B). While co-staining of NeuN and NCLX was mostly found on the somata, there were additional NCLX-positive structures that were not labeled for NeuN (arrow in Figure 4.1B). Purkinje cells of the cerebellum were more strongly labeled by NCLX antibody than the surrounding tissue (not shown). In sections through the lateral ventricles, NCLX immunostaining revealed a very intense staining in the choroid plexus and in cells reminiscent of ependymal cells (Figure 4.1C, arrow marks ependymal-like cells), while an overall, but faint NCLX immunolabeling could be seen in the brain parenchyma. Staining with the astrocytic marker GFAP exposed a typical astrocytic staining pattern and revealed that ependymal-like cells were GFAP-negative. Taken together, NCLX appeared to be expressed more strongly on neuronal and ependymal-like structures, but was also visible in glial cells in some brain areas.

Primary murine glial cells, as used in this study, are usually derived from cortices of newborn up to maximal 3 days old (P_0-P_3) mice. Since it has been shown that components of cellular calcium handling machinery can be regulated with age (Buchholz et al., 2007; Murchison and Griffith, 2007; Toescu and Verkhratsky, 2007), I wanted to test whether this is also the case for NCLX. I also wanted to verify whether in brains of newborn animals there is already a clear

expression of the mitochondrial exchanger and compare the expression to younger (E15) and older ages (P_{10}, adult). Finally, I wanted to test whether NCLX is differentially expressed in different brain areas. For this purpose, I performed Western blot analysis of mice of brain homogenates from E_{15}, P_0, P_{10} and adult (2 months) mice (Figure 4.1D). At all ages tested, NCLX antibody revealed a band of about 60 kDa, corresponding to the expression of the Na^+/Ca^{2+} exchanger as described above for the cells. In total brain extracts NCLX expression was higher at E15 and in adulthood compared to brains from P_0 and P_{10} mice (*upper panel*, Figure 4.1D). When looking at the different brain regions, NCLX protein levels were up-regulated toward the adulthood in the forebrain, brain stem, cerebellum and hippocampus (*lower panels*, Figure 4.1D). At the adult age NCLX expression was similarly strong in forebrain, brain stem and cerebellum, but weaker in the hippocampus. At P10 and P0 NCLX expression was the highest in the forebrain and much lower in hippocampus, brain stem and cerebellum. However, all the distinct brain regions tested including total brain extract revealed a band, corresponding to the expression of Na^+/Ca^{2+} exchanger NCLX throughout the whole life of the mouse.

NCLX expression in mitochondrial-enriched fractions

Next, I looked at the subcellular localization of NCLX. I started with Western blot analysis of different cell populations compared with the newborn brain. In those Western blot experiments, where I used β-Actin as a loading control, it was difficult to achieve even loading for the different cell types and tissues. In optimization experiments I found GAPDH as the more suitable housekeeping control and used it in the following experiments. Comparison of NCLX expression for different cell populations of the brain vs. whole brain. confirmed a major band of approximately 60 kDa in lysates from cultures of cortical astrocytes, primary murine microglia, primary murine neuroprecursor cells (NPCs) (NPCs was a kind gift from K. Stock, MDC, Berlin, Germany), murine astrocytoma cell line GL261 and brain from newborn mice (*upper panel* Figure 4.3A). Additionally, a fainter band at about 100 kDa related to SDS stable NCLX dimer was detected in both astrocytic and GL261 extracts, but not in other homogenates. GAPDH served as loading control and indicated even sample loading (*lower panel* Figure 4.3A). According to these results, NCLX is expressed in different cellular populations of the brain, including primary astrocytes and microglia.

To analyze NCLX expression in different cellular compartments I performed subcellular fractionation of astrocytic, microglial and HEK293T cell cultures and determined NCLX

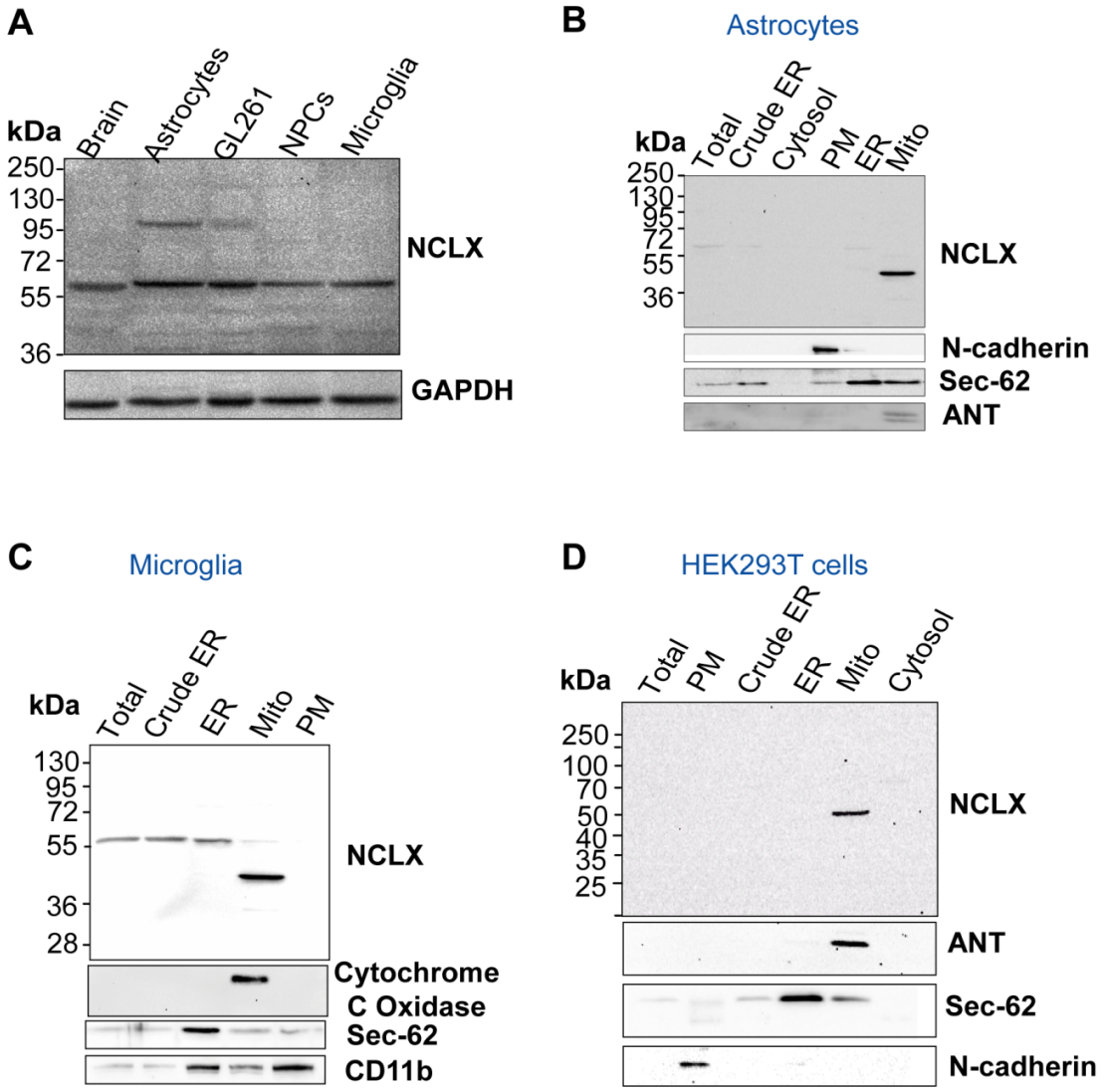

***Figure 4.3.* NCLX is enriched in glial mitochondria**

(A) Immunoblot analysis of NCLX expression in newborn mouse brain, primary murine astrocytes, murine astrocytoma cell line GL261, primary murine neuroprecursor cells (NPCs) and microglia *(upper panel)*. GAPDH served as an internal loading control *(lower panel)*. ***(B)*** NCLX is enriched in the mitochondria of astrocytes. NCLX expression in indicated cellular compartments (total, crude ER, cytosol, plasma membrane (PM), ER and mitochondria (Mito) -enriched fractions) *(upper panel)*. The membranes were stripped and re-probed for PM (N-cadherin), ER (Sec-62) and mitochondrial (ANT) markers *(lower panels)*. **(*C*)** NCLX is enriched in the mitochondria of microglia. NCLX expression in indicated cellular compartments (total, crude ER, plasma membrane (PM), ER and mitochondria (Mito) -enriched fractions) *(upper panel)*. The membranes were stripped and re-probed for mitochondrial (Cytochrome C Oxidase), ER (Sec-62) and PM (CD11b) markers *(lower panels)*. ***(D)*** Expression of NCLX in indicated cellular fractions purified from Human Embryonic Kidney cell line HEK293T (total, crude ER, cytosol, plasma membrane (PM), ER and mitochondria (Mito) -enriched fractions) *(upper panel)*. The membranes were stripped and re-probed for mitochondrial (ANT), ER (Sec-62) and PM (N-cadherin) markers *(lower panels)*.

expression by Western blot analysis. The fractions were counterstained with organelle specific markers (*lower panels* Figure 4.3B-D) to determine the separation quality of the fractions. In murine astrocytes total, crude ER and ER-enriched fractions revealed a faint band at ~ 60 kDa, whereas no band was visible in the plasma membrane or in cytosolic fractions (Figure 4.3B). Interestingly, the mitochondrial fraction showed a strong NCLX positive band of ~ 50kDa, suggesting that the passage of NCLX to the mitochondria may be linked to post-translational proteolysis. Probing the fractions with Anti-ANT and N-Cadherin showed a good separation of the mitochondrial and plasma membrane fractions, respectively. Although some degree of ER cross-contamination was detected in other fractions when probing with the ER marker Sec-62, this is likely to be related to the physical interaction of ER with other organelles. Nonetheless, these data show that the astrocytic Na^+/Ca^{2+} exchanger NCLX is primarily located in mitochondria.

In murine microglia total, crude ER and ER-enriched fractions showed a band at ~ 60 kDa, whereas no band was visible in the plasma membrane (Figure 4.3C). Similar to astrocytes, mitochondrial fractions showed the most intense band compared to other fractions and it also corresponded to ~ 50kDa. Probing the fractions with anti-Cytochrome C Oxidase and anti-Sec-62 indicated a good fractionation of mitochondrial and ER fractions, respectively.

Fractionation of HEK293T cell line was used to evaluate the fractionation protocol for the different subcellular fractions. First, the HEK293T cell line is readily available and easy to grow compared to primary cells. Furthermore, I have established the protocol in collaboration with Prof. I. Sekler and R. Palty for our common publication (Palty et al., 2010), where I showed mitochondrial localization of NCLX in HEK293T cells. The separation of mitochondrial, ER and plasma-enriched fractions was of good quality, as shown from the assessment with corresponding organellar markers: ANT, Sec-62 and N-cadherin (*lower panels* Figure 4.3D). NCLX enrichment in the mitochondria was very obvious for HEK cells (Figure 4.3D). The band was at ~ 50kDa, similarly to astrocytes and microglia. There were no bands detected in other fractions probably due to very brief exposure time. Taken together, as proven in HEK293T cells, primary murine microglia and astrocytes, the Na^+/Ca^{2+} exchanger NCLX is found mainly in mitochondria.

Downregulation of NCLX as a tool to investigate NCLX function

To study gene function RNA interference (RNAi) is commonly used in research to specifically inhibit a target gene's function. RNAi is a sequence specific post-transcriptional gene silencing mechanism that is highly conserved in evolution, allowing very exact targeting of a gene of interest. In my work I used small interfering RNAs (siRNAs) which activate RNAi pathway, specifically targeting murine Slc24a6 gene encoding for NCLX.

Optimization of knock-down conditions in the cell line RAW264.7

To ensure maximum specificity with minimum side effects, a pool of four different siRNAs was used, each one targeting NCLX. To optimize the conditions for silencing NCLX gene, first, siRNA delivery into the cells should be optimized. Then optimal siRNA delivery conditions should be applied to the positive siRNA control, which is known to efficiently downregulate gene expression. As a positive control I used siRNA vs. a housekeeping gene GAPDH (siGAPDH). Only after carefully establishing the conditions for siGAPDH siRNA vs. NCLX (siNCLX) could be tried with the same protocol and its efficiency could be estimated.

First, I evaluated the efficiency of NCLX knock-down by siNCLX in the murine macrophage cell line RAW264.7. Cell lines do not require utilization of animals; they are more available and easier to culture than primary cells. To optimize the delivery of siRNA into the cells, fluorescently tagged red transfection indicator siGLO was transfected by several transfection reagents. Cells were evaluated for viability, morphology and siGLO delivery 1 day after transfection. To visualize the cells and quantify transfection efficiency, cells were fixed with paraformaldehyde and stained with the nuclear dye DAPI (4',6-diamidino-2-phenylindole, dihydrochloride), therefore allowing to assess the amount of cells, which internalized siGLO signal (*right column* Figure 4.4A). From the four different transfection reagents tested DharmaFECT 2 and DharmaFECT 4 reagents both did not affect the viability and morphology of the cells and achieved maximal siGLO delivery. DharmaFECT 2 yelded a slightly higher transfection efficiency (about 91% of cells were siGLO positive) than DharmaFECT 4 (about 84% of cells were siGLO positive). Figure 4.4A shows an example of RAW264.7 cells transfected with siGLO compared to non-transfected cells. Phase contrast image showed that the transfection did not affect cell morphology (*left column* Figure 4.4A).

In the next optimization step, RAW264.7 cells were transfected with 50 nM siGAPDH by DharmaFECT 2 transfection reagent, and this was compared to two conditions: transfection with

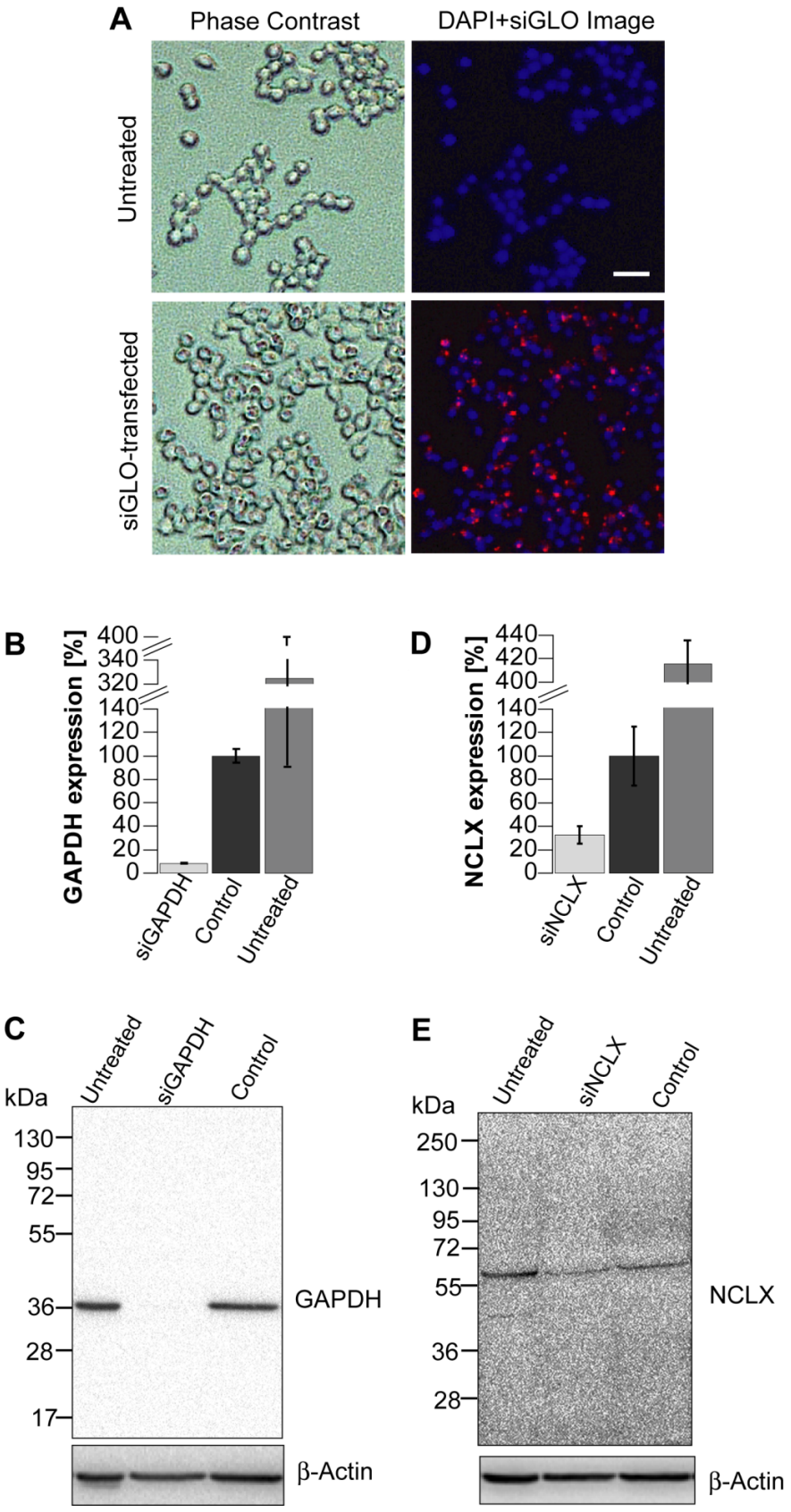
A
Phase Contrast
DAPI+siGLO Image
Untreated
siGLO-transfected
B
GAPDH expression [%]
400
340
320
140
120
100
80
60
40
20
0
siGAPDH
Control
Untreated
D
NCLX expression [%]
440
420
400
140
120
100
80
60
40
20
0
siNCLX
Control
Untreated
C
kDa
Untreated
siGAPDH
Control
130
95
72
55
36
28
17
GAPDH
β-Actin
E
kDa
Untreated
siNCLX
Control
250
130
95
72
55
36
28
NCLX
β-Actin

***Figure 4.4.* Small interfering RNA vs. NCLX (siNCLX) is targeted to almost all cells and efficiently down-regulates NCLX expression**

(A) Evaluation of siRNA delivery in the macrophage cell line RAW267.1 following transfection with fluorescently tagged red siRNA transfection indicator siGLO. Right column shows images of untreated cells, while left column shows images of cells transfected with siGLO (red color, *bottom row*). The nuclei were stained using the cell permeant nuclear stain DAPI (blue color, *bottom row*). Comparison of siGLO-transfected and untreated cultures in the phase contrast images indicates that cell morphology is almost unchanged by the siRNA treatment (*upper row*). Scale bar 50 µm. ***(B, C)*** The optimal siRNA transfection conditions were further evaluated using positive control siRNA vs. GAPDH (siGAPDH). GAPDH mRNA and protein expression were determined following transfection with siRNA vs. GAPDH (siGAPDH) by ***(B)*** quantitative RT-PCR (qRT-PCR) and by ***(C)*** Western blot analysis, respectivley. ***(D, E)*** NCLX mRNA and protein expression were analyzed following transfection with siRNA vs. NCLX (siNCLX) by ***(D)*** qRT-PCR and ***(E)*** Western blot analysis and compared with cells transfected with non-targeted siRNA (control) or untransfected cells (untreated). Values in **B** and **D** were derived from duplicates and are shown as mean ±SEM. For Western blot experiments ***(C, E)*** β-Actin served as loading control (*lower panel*).

non-targeted control siRNA (control) and untreated control. The efficiency of GAPDH knock-down was evaluated at the mRNA level via qRT-PCR (Figure 4.4B) and at the protein level via Western Blot analysis (Figure 4.4C). siGAPDH transfection decreased GAPDH mRNA expression to 8.3±0.3% (GAPDH mRNA expression in control cells was 100.0±5.9%). The mRNA expression level in untransfected RAW264.7 cells was 324.6±75.7%. These results suggest an effect of the transfection procedure on GAPDH mRNA levels compared to the untreated condition. Nevertheless, siGAPDH efficiently knocked down GAPDH mRNA. When the knock down effect was analysed on protein level, GAPDH protein expression was completely abolished by the specific siRNA treatment (Figure 4.4C), while in control cells and the untreated control the expression was comparable (100.0% and 103.3% respectively). These results provided me with the ground to continue with the optimization of knocking down NCLX gene function.

NCLX expression was silenced with 10 or 50 nM siNCLX and the efficiency of silencing was evaluated at the mRNA level (Figure 4.4D) and at the protein level (Figure 4.4E) as described in the previous paragraph. 10 nM siNCLX reduced NCLX mRNA levels to 32.7±7.6% (from 100.0±25.2% in control-treated cells). However, as seen for GAPDH expression (see above), siRNA treatment largely decreased also NCLX mRNA level when compared to untreated cells (from 416.3±20.4% for the untreated cells to 100.0±25.2% for cells transfected with control siRNA) probably due to either a side effect of the control siRNA or an effect of transfection

reagent. Western blot analysis following siNCLX transfection showed a reduction in protein levels from 100.0% to 72.7%, as revealed from densitometry analysis of the bands. SiRNA treatment affected also NCLX protein level: transfection of the cells with control siRNA reduced protein expression by 39.9%. The side effect of siRNA treatment on the protein expression was weaker compared to the effect on mRNA expression. These data showed that siNCLX is effective in inhibiting NCLX expression both on mRNA and protein levels, but care should be taken regarding possible side effects of siRNA transfection.

Optimization of knock-down conditions in primary microglia

In a next step a protocol was established to knock down NCLX expression in microglia. As described for the RAW264.7 cell line, I first optimized the type of transfection reagent and its amount to deliver siRNA to the majority of the cells. Transfection of primary murine microglia with red siGLO transfection indicator (Figure 4.5A) and staining with nuclear dye DAPI revealed that transfecting cells with 1.6 µl/well (400 µl) of DharmaFECT 4 could deliver siGLO signal to 93.0±5.6% of DAPI-stained microglia.

With this knowledge, positive siRNA vs. GAPDH gene (25 nM) was delivered to primary microglia to confirm whether siRNA could inhibit gene function. Effect of GAPDH gene silencing was assessed via qRT-PCR. Both, lipofectamine RNAiMAX and DharmaFECT 4 transfection reagents were very efficient in knocking down GAPDH expression and reduced mRNA expression levels from 100.0±23.8% to 31.4±4.7% and to 35.3±5.5%, respectively (Figure 4.5B). In microglia control siRNA transfection affected GAPDH mRNA levels much less than in RAW264.7 cells: from 73.7±22.7% for untreated microglia to 100.0±23.8% for microglia treated with control siRNA.

Conditions applied to silence GAPDH expression were applied to knock down NCLX gene in microglia. Microglia were transfected with 10 and 50 nM siNCLX by DharmaFECT 4. The siNCLX transfection lead to a decrease in NCLX mRNA expression from 100±10.8% for control-treated microglia to 22.5±4.5% and 37.4±11.1% for microglia transfected with 10 and 50 nM siNCLX, respectively (Figure 4.5C). Control siRNA transfection decreased NCLX mRNA expression from 124.0±60.1% for untreated cells to 100±10.8% for control-treated cells. This set of experiments revealed that 10 nM siNCLX is sufficient to efficiently downregulate NCLX expression at the mRNA level.

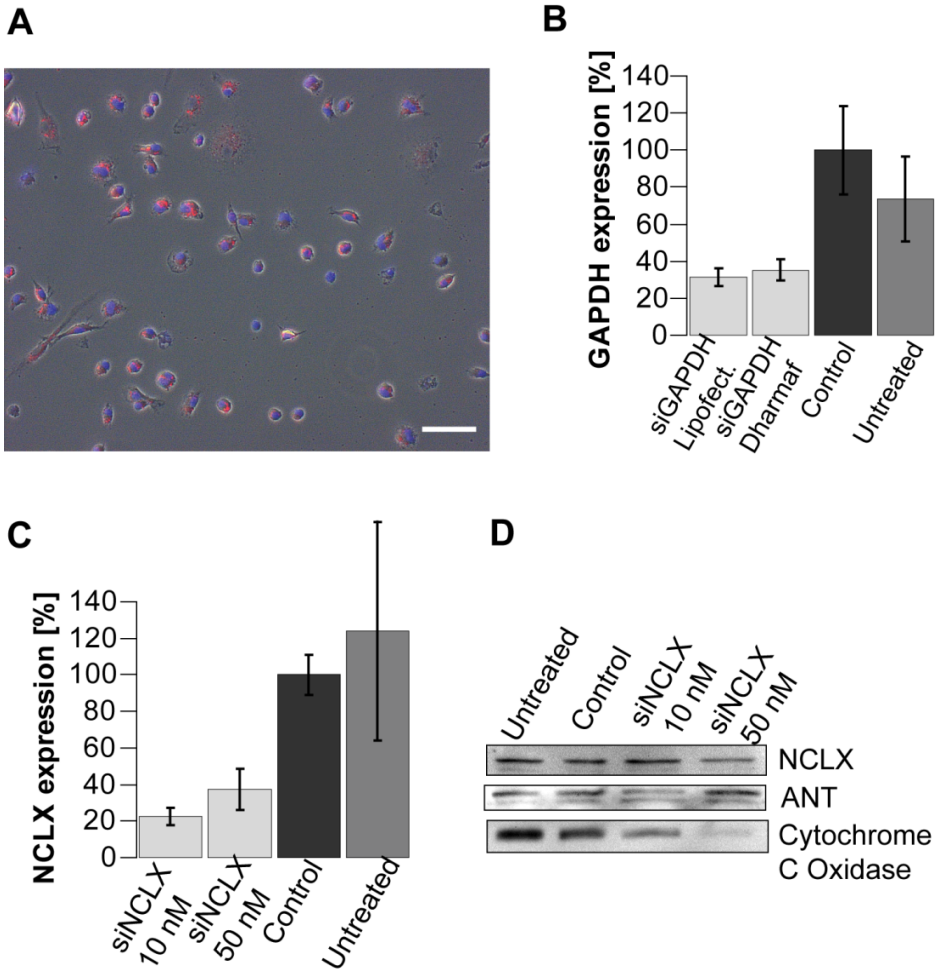

Figure 4.5. Optimization of NCLX expression knock-down in microglia.
(A) SiRNA delivery in primary murine microglia was assessed following cell transfection with fluorescently tagged marker siGLO. The image shows an overlay of bright field image with siGLO (*red color*) and cell permeant nuclear stain DAPI (*blue color*). Scale bar 50 µm. ***(B)*** Optimization of siRNA transfection conditions using siRNA vs. GAPDH (siGAPDH). SiRNA vs. GAPDH or non-targeted siRNA (control) was delivered either by two different transfection reagents, or cells remained untreated. ***(C)*** NCLX mRNA expression following the transfection with siRNA vs. NCLX (siNCLX) as determined by qRT-PCR. After 2 days, GAPDH or NCLX mRNA expression was evaluated by quantitative RT-PCR (qRT-PCR). Values are based on duplicates and are shown as mean ±SEM. ***(D)*** Western blot analysis of crude mitochondrial fractions from microglial cells 3 days after treatment with different concentrations of siNCLX, control non-targeted siRNA or untreated, probed with NCLX antibody. As loading markers, antibodies against mitochondrial proteins ANT and Cytochrome C Oxidase were used (*lower panels*).

Next, I analyzed the effect of NCLX gene knock down on the expression of NCLX protein. Unfortunately, the effect was not seen clearly in all experiments. The most successful results for this part are presented in Figure 4.5D. Crude mitochondrial fractions from microglia either untreated, transfected with non-targeted control siRNA, or transfected with 10 or 50 nM siRNA were immunoblotted with NCLX antibody (*upper panel* Figure 4.5D) and with ANT or Cytochrome C antibodies as mitochondrial loading markers (*lower panels* Figure 4.5D). Protein levels were determined by normalizing to ANT protein expression. A decrease of NCLX protein levels was seen only when microglia were transfected with 50 nM siNCLX. The amount of NCLX protein was decreased to 64.4% compared to the cells transfected with control siRNA. Microglia transfected with 10 nM siNCLX did not show any decrease in NCLX protein levels. Of notice, levels of Cytochrome C oxidase dropped with each treatment. If Cytochrome C oxidase level in microglia treated with control siRNA was set to 100.0%, its level in the untreated control was 200.0%. Microglia treated with 10 and 50 nM siNCLX had 49.9% and 17.9% of Cytochrome C Oxidase, respectively. Taken together, siNCLX could knock down NCLX protein expression in microglia. However, this set of experiments also revealed that the siRNA transfection procedure affects one of the components of the respiratory chain, cytochrome C oxidase, and this effect was exacerbated by NCLX knock down.

Optimization of knock-down conditions in primary astrocytes

To assess the role of NCLX in modulating astrocytic Ca^{2+} homeostasis and astrocytic function, the expression of the exchanger was knocked down with siNCLX. The fluorescently tagged siRNA siGLO was used as a co-transfection marker to determine optimal conditions for effective NCLX silencing and to detect transfected cells, while calcein live cell staining was applied to assess cell viability. Cells treated with siRNA (siGLO + siNCLX) showed punctate red staining, consistent with intracellular accumulation of the transfection marker siGLO (*right column* Figure 4.6A). More than 85% of the cells received siRNA as determined by the siGLO signal while control untreated cells showed only dim autofluorescence. All astrocytes showed a similar accumulation of calcein-AM regardless whether they were treated with siRNA or were untreated controls (*left column* Figure 4.6A), indicating that the siRNA transfection procedure did not affect cell viability.

Next, to assess the efficiency of genetic RNAi mediated knock-down in astrocytes, cells were transfected with 10 nM siGAPDH by different amounts of Lipofectamine RNAiMAX or DharmaFECT 4 and GAPDH knock-down was measured 2 days after the transfection by qRT-

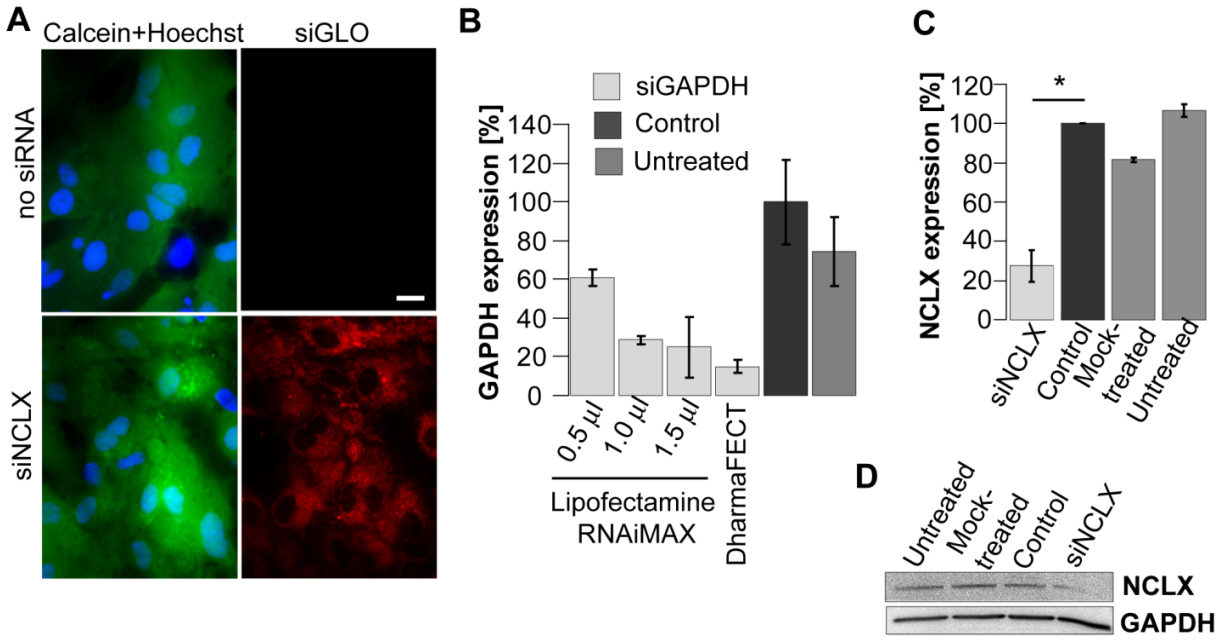

Figure 4.6. ***NCLX knock-down in astrocytes***

(*A*) Astrocytes are viable after 100% efficient siRNA transfection. *Upper row* shows data for untreated cells (no siRNA), while *bottom row* shows data for astrocytes treated with siGLO along with siNCLX (siGLO+siNCLX). Astrocytic nuclei were stained using the cell permeant nuclear stain Hoechst 33342 (blue color, *left column*). All tested astrocytes accumulated calcein (green color, *left column*), indicating their viability. Cells were transfected with siGLO to estimate siRNA delivery. Control untreated cells show dim and diffuse autofluorescence, while siRNA (siGLO + SiNCLX) treated cells show punctate stain, consistent with intracellular accumulation of the transfection marker siGLO (red color, *right column*). Scale bar 20 µm. (The images were provided by Dr. V. Montana and Prof. V. Parpura, University of Alabama, Birmingham, USA) ***(B)*** quantitative RT-PCR analysis of GAPDH mRNA expression for optimization of the transfection conditions. Astrocytes were untreated or transfected with 10nM siGAPDH or control non-targeted siRNA by 2 different transfection reagents and RNA was harvested after 2 days. ***(C)*** qRT-PCR analysis of NCLX mRNA expression following the co-transfection with mtRP and siNCLX or non-targeted siRNA (Control), respectively. Untreated and mock-treated (transfection agent only) cells were used as further controls (N=4 experiments, experiments were done in triplicates). Values are shown as mean ±SEM. (*p<0.05, Wilcoxon-Mann-Whitney U-test). ***(C)*** Western blot analysis showing NCLX protein expression in untreated, mock-transfected or astrocytes transfected with non-targeted siRNA (Control) or siNCLX *(upper panel)*. GAPDH served as an internal loading control *(lower panel).*

PCR. GAPDH expression was reduced from 100±21.7% in control-transfected astrocytes to 60.7±4.5%, 28.6±2.0% and 25.0±5.5% corresponding to Lipofectamine RNAiMAX amount of 0.5 µl, 1.0 µl or 1.5 µl/1200 µl, respectively (Fig 4.6B). SiGAPDH transfection by DharmaFECT 4 (1.6 µl/400 µl) achieved very efficient knock-down to 14.9±3.6%. SiRNA transfection increased GAPDH expression from 74.4±18.0% to 100±21.7%. Although I could achieve a better knock down by DharmaFECT 4, I decided to continue working with Lipofectamine RNAiMAX, because it did not affect on cell morphology.

The efficiency of NCLX silencing in astrocytes via siRNA was assessed by quantitative RT-PCR. Optimal NCLX gene silencing via siRNA was achieved at three days using 10nM siRNA vs. NCLX (siNCLX). NCLX expression in the presence of siNCLX was reduced to 24.9±1.3% of the expression level seen in astrocytes transfected with non-targeted control siRNA (Figure 4.6C, N=4 experiments, *p<0.05). NCLX mRNA expression levels remained almost unchanged in cells treated only with transfection agent (mock-treated) and untreated cells (84.0±13.9%, and 101.7±4.5%, respectively). Consequently, all experiments described in the following were performed on astrocytic cultures three days after siRNA treatment with 1.0 µl Lipofectamine RNAiMAX per 1,200 µl of medium.

NCLX silencing on mRNA level also affected the expression of the NCLX protein. To be able to see the protein changes as the effect of NCLX knock-down, the protocol was slightly modified, and after the first exposure of the immunoblot to the ECL substrate, the membrane was washed, re-blocked and exposed again to ECL substrate. Western blot analysis of astrocytic extracts showed a reduction in NCLX protein levels in astrocytes transfected with siNCLX compared to astrocytes transfected with control siRNA, mock-treated or untreated cells (Figure 4.6D).

NCLX influences glial mitochondrial Ca^{2+} signaling

Transduction of primary microglia with ratiometric pericam

To investigate mitochondrial Ca^{2+} handling in microglia, I induced expression of the mitochondrially targeted Ca^{2+} sensor ratiometric pericam (mtRP) (Nagai et al., 2001) in primary microglia. Initially mtRP was in the pcDNA3.1plus vector; the vector's map is shown in Figure 4.7A. The mtRP insert consists of cytochrome C oxidase targeting sequence (CoxIV), Ca^{2+}-

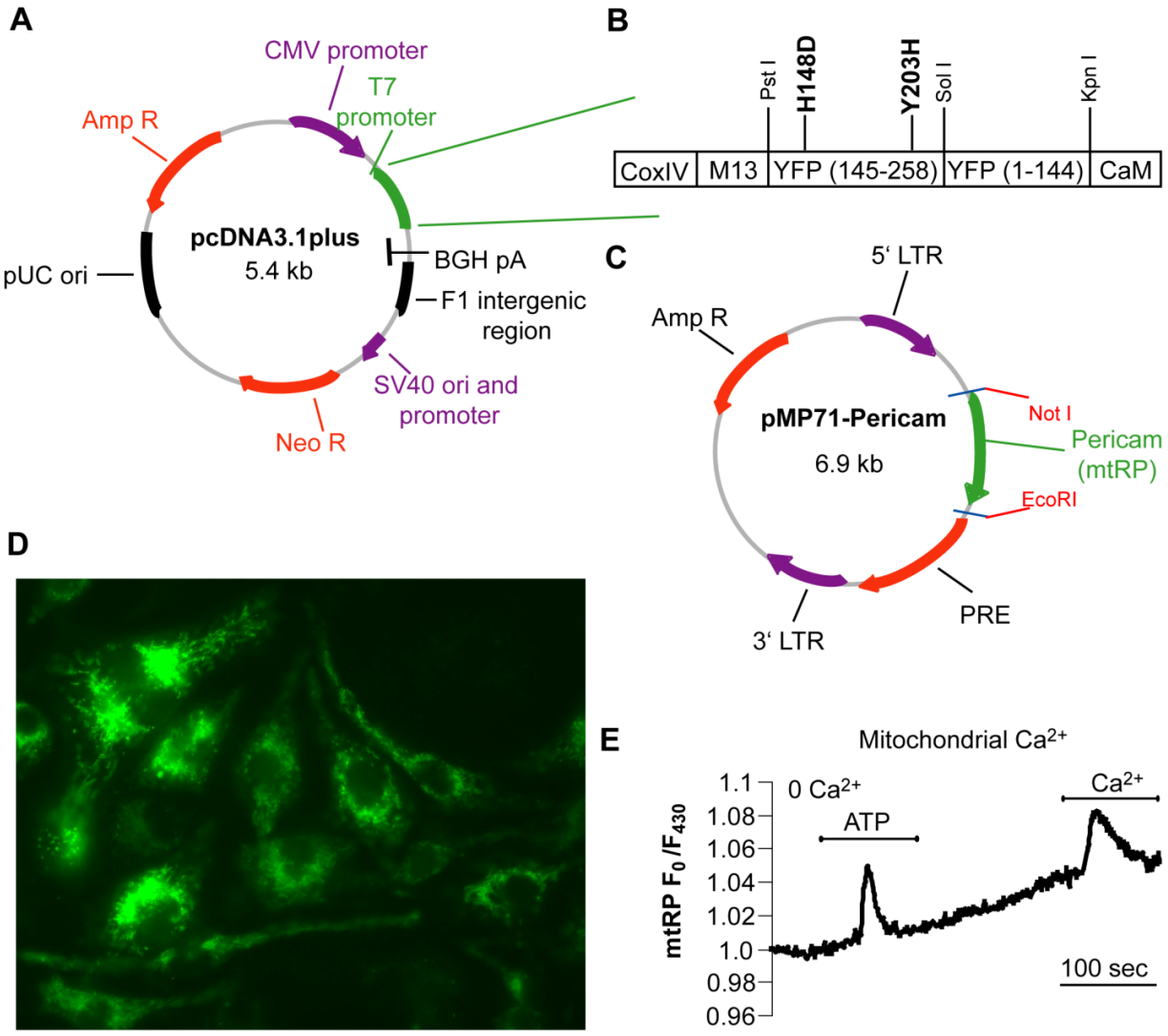

Figure 4.7. ***Mitochondrial ratiometric pericam allows recording of mitochondrial Ca^{2+} changes in microglia***

(***A***) Vector map of pcDNA3.1-mtRP plasmid, from which the mitochondrially targeted pericam insert (mtRP) was cut with HindIII and EcoRI. AmpR and Neo R correspond to regions responsible for ampicillin and neomycin resistance. ***(B)*** Map of mitochondrially-targeted pericam insert consisting of the mitochondrial targeting motif, Cytochrome C Oxidase subunit IV (Cox IV), calmodulin (CaM) at the C-terminus and its target peptide M13, and yellow fluorescent protein (YFP). ***(C)*** The map of the retroviral plasmid pMP71-mtRP. Ampicillin resistance gene (Amp R), long terminal repeat derived from murine myeloproliferative sarcoma virus (LTR), and woodchuck hepatitis virus posttranscriptional regulatory element (PRE) are shown. ***(D)*** Murine primary microglia were transfected with pMP71-mtRP, fluorescence microscopy image taken after 2 days reveals a mitochondrial expression pattern. ***(E)*** Representative curve from mitochondrial Ca^{2+} imaging experiment. Mt-RP expressing microglia were perfused with Ca^{2+}-free HEPES buffer. 100µM ATP or 5 mM Ca^{2+} were applied as indicated by the bars.

binding protein calmodulin (CaM), which attaches M13 protein upon Ca^{2+} binding (Figure 4.7B). This conformational change in mtRP evokes a shift in fluorescence of yellow fluorescent protein (YFP), which is measured to assess Ca^{2+} changes.

For transduction of microglia, mtRP was subcloned into the retroviral vector backbone pMP71 (Engels et al., 2003) (Figure 4.7C). Microglia, the immune cells of the brain, react to any infection, including viral. Therefore, it was important to know whether microglia were activated by the pMP71 retrovirus. Microglial cultures infected with pMP71 mtRP did not show any changes in cell morphology indicative of cell activation. This was confirmed by a study performed in the Cellular Neuroscience group (Seifert et al.). The level of microglial activation was determined via measuring the release of proinflammatory cytokines and nitric oxide (NO), as well as microglial proliferation. Thus pMP71 is a suitable vector for the transduction of microglial cells. In my experiments, microglial transduction efficiency with pMP71-mtRP and the intensity of the mitochondrial signal varied between different days of experiments; the transduction rate (percentage of pericam expressing cells) under optimal conditions could reach 60% (Figure 4.7D), but was in most cases lower.

Mitochondrial Ca^{2+} imaging was performed as described in mtRP (pericam) expressing microglial cells that were stimulated with 100 µM ATP in Ca^{2+}-free buffer, followed by application of 5 mM Ca^{2+}, either in the presence or absence of the pharmacological inhibitor of NCLX, CGP37157. Application of ATP or Ca^{2+} evoked fast rise in mitochondrial Ca^{2+} followed by a decline (Figure 4.7E). Generally, the amplitudes of the mitochondrial Ca^{2+} responses were very small and usually combined with noise. This lead to small signal to noise ratio that did not allow a reliable analysis of the mitochondrial Ca^{2+} answers.

Mitochondrial Ca^{2+} responses in primary astrocytes

To monitor mitochondrial Ca^{2+} responses in primary astrocytes, subconfluent cultures were transfected with the mitochondria-targeted ratiometric Ca^{2+} sensor pericam (mtRP) in pcDna3.1plus vector. Expression of mtRP reached its maximal intensity ~48-72 hrs after transfection and could still be detected until 96 hrs following transfection. This allowed me to measure the mitochondrial Ca^{2+} at the siRNA optimal silencing time of 3 days. MtRP expression pattern appeared as a typical mitochondrial distribution (Figure 4.8A).

To test whether the NCLX inactivation affects the basal mitochondrial Ca^{2+} levels, I compared mtRP ratios during the 100 sec pre run phase before ATP application of NCLX-silenced versus

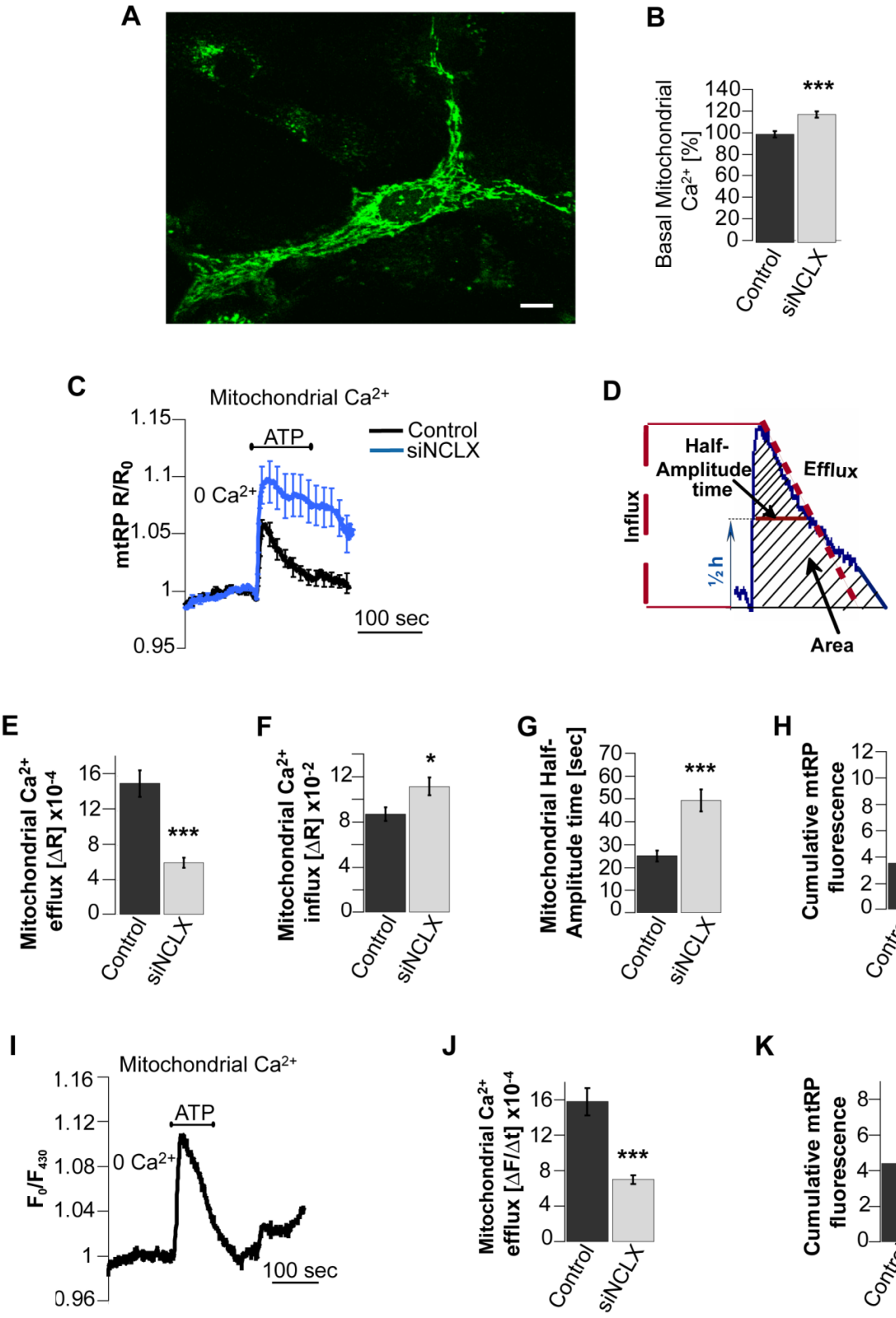
A
B
Basal Mitochondrial Ca2+ [%]
***
Control
siNCLX
C
Mitochondrial Ca2+
ATP
0 Ca2+
Control
siNCLX
mtRP R/R0
100 sec
D
Half-Amplitude time
Efflux
Influx
½ h
Area
E
Mitochondrial Ca2+ efflux [ΔR] x10-4
F
Mitochondrial Ca2+ influx [ΔR] x10-2
*
G
Mitochondrial Half-Amplitude time [sec]
H
Cumulative mtRP fluorescence
I
Mitochondrial Ca2+
ATP
0 Ca2+
F0/F430
100 sec
J
Mitochondrial Ca2+ efflux [ΔF/Δt] x10-4
K
Cumulative mtRP fluorescence
**

Figure 4.8. NCLX is an essential component of the mitochondrial Ca^{2+} efflux in astrocytes.

Primary astrocytes were co-transfected with mitochondrial ratiometric pericam (mtRP) and siNCLX or non-targeted siRNA (control) and were analyzed after 3 days. ***(A)*** 2-Photon microscopy image of astrocytes transfected with mtRP reveals typical mitochondrial expression pattern of the fluorescent sensor. Scale bar 10 μm. ***(B-K)*** Effect of NCLX gene silencing on basal mitochondrial Ca^{2+} levels and mitochondrial Ca^{2+} efflux. ***(B)*** Statistical analysis of basal mitochondrial Ca^{2+} levels calculated from the imaging experiments of control and siNCLX-transfected astrocytes (N=5 culture preparations, n=140 and 122 regions of interest (ROIs), respectively). ***(C-K)*** Astrocytes were perfused with Ca^{2+}-free HEPES buffer and 100 μM ATP was applied as indicated. ***(C)*** Averaged curves ± SEM of the mitochondrial Ca^{2+} imaging experiments from the control (N=10) and siNCLX-transfected astrocytes (N=11), utilizing F_{480}/F_{430} ratio to assess mitochondrial Ca^{2+}. ***(D)*** A scheme showing a mitochondrial Ca^{2+} imaging curve and graphical representation of different parameters used to characterize mitochondrial Ca^{2+} handling. ***(E-H)*** Statistical analysis of the ***(E)*** mitochondrial Ca^{2+}efflux (slopes),***(F)*** influx (amplitudes) ***(G)*** half-amplitude time and ***(H)*** cumulative mtRP fluorescence (area) in control and siNCLX-transfected astrocytes, comparing N=10 (n=38 ROIs) and N=11 (n=64 ROIs) experiments for each condition respectively (***p<0.001, *p<0.05, Wilcoxon-Mann-Whitney U-test). ***(I)*** An example of mitochondrial Ca^{2+} imaging curve, utilizing only Ca^{2+}-sensitive F_{430} wavelength to assess changes in mitochondrial Ca^{2+}. Statistical analysis of the ***(J)*** mitochondrial Ca^{2+}efflux and ***(K)*** cumulative mtRP fluorescence (area) in control and siNCLX-transfected astrocytes, comparing N=10 (n=57 ROIs) and N=12 (n=79 ROIs) experiments for each condition respectively (***p<0.001, **p<0.01, Wilcoxon-Mann-Whitney U-test).

unsilenced astrocytes (control). As shown in Figure 4.8 B there is a significant increase in the basal mitochondrial Ca^{2+} from 100.0±3.1% to 118.2±3.1% when NLCX activity is blocked (N=5 cultures, n=140 and 122 regions for control and siNCLX-transfected astrocytes, respectively, ***p<0.001).

Application of ATP (100 μM) to astrocytes in Ca^{2+}-free HEPES buffer for 100 seconds elicited a fast rise in the mitochondrial Ca^{2+} concentration corresponding to the Ca^{2+} uptake phase followed by a slower efflux (Figure 4.8C, N=10 and 11 experiments for control and siNCLX-transfected astrocytes, respectively). For each imaging curve efflux, influx, half-amplitude time and cumulative response (area) were calculated as presented in Figure 4.8D. Comparison of the efflux rates of the ATP-elicited mitochondrial Ca^{2+} responses in siNCLX versus non-targeted siRNA (control) treated cells showed that the mitochondrial efflux rate was decreased by 60.2% in siNCLX treated cells compared to control astrocytes (from (15.1±1.5) $x10^{-4}$ sec^{-1} to (6.0±0.6) $x10^{-4}$ sec^{-1}, N=10 and 11 experiments and n=38 and 64 regions for control and siNCLX

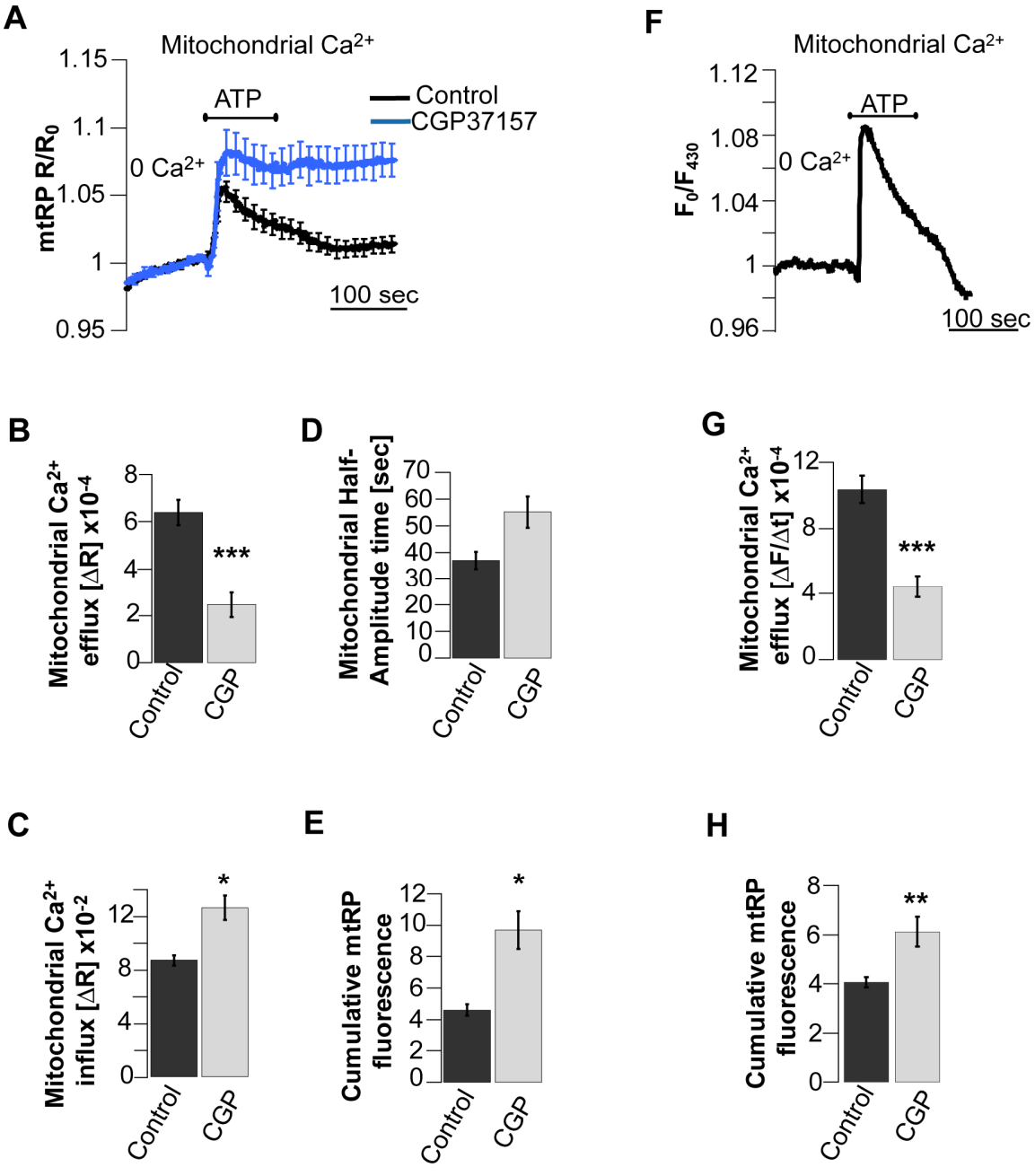
A
Mitochondrial Ca2+
mtRP R/R0
1.15
1.1
1.05
1
0.95
ATP
0 Ca2+
Control
CGP37157
100 sec
F
Mitochondrial Ca2+
F0/F430
1.12
1.08
1.04
1
0.96
ATP
0 Ca2+
100 sec
B
Mitochondrial Ca2+ efflux [ΔR] x10-4
***
Control
CGP
D
Mitochondrial Half-Amplitude time [sec]
Control
CGP
G
Mitochondrial Ca2+ efflux [ΔF/Δt] x10-4
***
Control
CGP
C
Mitochondrial Ca2+ influx [ΔR] x10-2
*
Control
CGP
E
Cumulative mtRP fluorescence
*
Control
CGP
H
Cumulative mtRP fluorescence
**
Control
CGP

Figure 4.9. Pharmacological inhibition of NCLX impairs mitochondrial Ca^{2+} efflux in astrocytes

Primary astrocytes were transfected with mitochondrial ratiometric pericam (mtRP) and were analyzed after 2 days. Effect of CGP37157 on mitochondrial Ca^{2+} efflux. Cells were superfused with Ca^{2+}-free HEPES buffer ± 20 µM CGP37157and 100µM ATP was applied as indicated. ***(A)*** Averaged curves ± SEM of the mitochondrial Ca^{2+} imaging experiments from control (N=15) and CGP37157-treated astrocytes (N=11), utilizing F_{480}/F_{430} ratio to assess mitochondrial Ca^{2+}. Statistical analysis of ***(B)*** mitochondrial Ca^{2+} efflux, ***(C)*** influx, ***(D)*** half-amplitude time and ***(E)*** cumulative mtRP fluorescence ± CGP37157. Values are given as means ± SEM for N=15 (n=106 ROIs) control and N=11 (n=75 ROIs) CGP37157 experiments, respectively (***p<0.001, *p<0.05, Wilcoxon-Mann-Whitney U-test). ***(F)*** An example of mitochondrial Ca^{2+} imaging curve, utilizing only Ca^{2+}-sensitive F_{430} wavelength to assess changes in mitochondrial Ca^{2+}. Statistical analysis of the ***(G)*** mitochondrial Ca^{2+}efflux and ***(H)*** cumulative mtRP fluorescence (area) in control and CGP37157-treated astrocytes, comparing N=11 (n=56 ROIs) and N=15 (n=74 ROIs) experiments for each condition respectively (***p<0.001, **p<0.01, Wilcoxon-Mann-Whitney U-test).

conditions, respectively, ***p<0.001) (Figure 4.8E). Moreover, silencing of NCLX significantly increased the net mitochondrial Ca^{2+} influx by 28.1 % compared to control condition (from (8.7±0.6)x10^{-2} to (11.1±0.7)x10^{-2}; N=10 and 11 experiments with control- and siNCLX-transfected astrocytes, *p<0.05) (Figure 4.8F). Half-amplitude time increased from 25.08±2.42 seconds to 49.41±4.80 seconds as a result of NCLX knock-down (N=10 and 11 experiments with control- and siNCLX- transfected astrocytes, ***p<0.001) (Figure 4.8G). Consequently, NCLX knock-down significantly enhanced net cumulative mitochondrial Ca^{2+} signaling from

3.52±0.40 to 8.10±1.00 (N=10 and 11 experiments with control- and siNCLX- transfected astrocytes, ***p<0.001) (Figure 4.8H).

The results described in the last paragraph were derived from the analysis of the ratiometric recording of the pericam-expressing astrocytes (F_{480}/F_{430}). Next I asked whether this would be different when non-ratiometric recordings from Ca^{2+}-dependent F_{430} wavelength are analyzed. As expected, similar results were achieved. An example of an imaging trace is shown in Figure 4.8I. RNAi knock-down of NCLX significantly reduced mitochondrial Ca^{2+} efflux from (15.8±1.6) x10^{-4} sec^{-1} to (7.0±0.5) x10^{-4} sec^{-1} (N=10 and 12 experiments and n=57 and 79 regions for control and siNCLX conditions, respectively, ***p<0.001) (Figure 4.8J) and increased mitochondrial cumulative Ca^{2+} response in 71% (from 4.39±0.25 to 7.49±0.65) (N=10 and 12 experiments and n=57 and 79 regions for control and siNCLX conditions, respectively, **p<0.01) (Figure 4.8K). Both types of analysis show that NCLX knock-down impairs mitochondrial Ca^{2+}

efflux and elevates overall mitochondrial Ca^{2+} during Ca^{2+} signaling, confirming NCLX involvement in mitochondrial Ca^{2+} machinery in astrocytes.

As benzothiazepine compound CGP37157 is the most specific pharmacological inhibitor of the mitochondrial Na^+/Ca^{2+} exchanger, I asked whether it has the same effect as NCLX knock-down. Application of CGP37157 (20 μM) resulted in a 62.4% reduction of the ATP-induced mitochondrial Ca^{2+} efflux in treated cells compared to cells treated with vehicle (DMSO) (control $(6.4\pm0.5)x10^{-4}$ sec^{-1} , N=15, n=106; CGP37157 treated group $(2.5\pm0.5)x10^{-4}$ sec^{-1} , N=11, n=75, ***p<0.001) (Figure 4.9A,B). The average net mitochondrial Ca^{2+} influx was increased from (8.6 ± 0.4) $x10^{-2}$ sec^{-1} to (12.5 ± 0.9) $x10^{-2}$ sec^{-1} in the presence of CGP37157 (N=15 and 11 experiments with control- and CGP37157- treated astrocytes, respectively, *p<0.05) (Figure 4.9C). Half-time amplitude grew from 36.96±3.28 sec to 55.12±5.87 sec (N=15 and 11 experiments with control- and CGP37157- treated astrocytes, respectively, p>0.05) (Figure 4.9D) and mitochondrial cumulative Ca^{2+} increased from 4.60±0.36 to 9.67±1.19 (N=15 and 11 experiments with control- and CGP37157- treated astrocytes, respectively, *p<0.05) (Figure 4.9E). This result was confirmed by analysis of single wavelength measurements (F_{430}). The pharmacological blocker as in the ratiometric mode significantly inhibited the efflux rate from $(10.4\pm0.8)x10^{-4}$ sec^{-1} to $(4.5\pm0.6)x10^{-4}$ sec^{-1} (***p<0.001) (Figure 4.9G,H). In conclusion, NCLX inhibition either by molecular inhibition with the specific siRNA or by the pharmacological inhibitor significantly reduced mitochondrial Ca^{2+} extrusion, thereby indirectly increasing also the net Ca^{2+} influx. These data indicate that NCLX mediates mitochondrial Ca^{2+} efflux in astrocytes and thereby shapes the mitochondrial Ca^{2+} transients.

4.2 NCLX is involved in maintaining glial Ca^{2+} homeostasis

Mitochondrial Ca^{2+} has been shown to affect cytosolic Ca^{2+} handling in a variety of cells (Ardon et al., 2009; Boitier et al., 1999; Demaurex et al., 2009; Kim et al., 2012). As shown above, the Na^+/Ca^{2+} exchanger NCLX is responsible for mitochondrial Ca^{2+} efflux. Next, I was interested to know whether this element of the mitochondrial Ca^{2+} machinery shapes the cytosolic Ca^{2+} responses in glial cells.

NCLX inhibition decreases metabotropic Ca^{2+} signaling in glia

NCLX involvement in microglial metabotropic Ca^{2+} signaling

Microglia express a variety of metabotropic receptors linked to Ca^{2+} release from intracellular stores and influx from the extracellular space (Farber and Kettenmann, 2006; Verkhratsky et al., 1998). In order to test the involvement of NCLX in metabotropic signaling I chose C5a and ATP as a stimulus to induce Ca^{2+} signals. C5a is a potent mediator of inflammation (Brown, 1992; Greer, 1985; Huber-Lang et al., 2003; March et al., 2004; Mastellos et al., 2005; Strachan et al., 2000). In microglia C5a and ATP was shown to evoke Ca^{2+} response via G-protein coupled receptors (GPCR) (Moller et al., 1997) and induce microglial motility (Nolte et al., 1996). For cytoplasmic Ca^{2+} imaging microglial cells on coverslips were loaded with Fura-2 AM and stimulated with 2 nM C5a or 100 µM ATP. 20 µM CGP37157 was applied to inhibit the activity of NCLX in microglia. Due to the side effect of the siRNA transfection on the level of Cytochrome C oxidase and possibly other proteins involved in the mitochondrial ion homeostasis, the experiments investigating NCLX function via inhibition by more specific siRNA approach were not performed in microglia.

Fura-2 AM loaded primary murine microglia showed the typical biphasic Ca^{2+} responses to C5a described previously (Figure 4.10A), consisting of a fast and a slow phase of decline. The activity of NCLX affected the overall Ca^{2+} response, as defined by the areas below the Ca^{2+} curves (Cumulative Fura-2 fluorescence). The average value for the control at each day of experiments was taken as 100%. In the presence of 20 µM CGP37157 the overall response was significantly decreased (Figure 4.10B) by 25.5% (from 100.0±1.6% to 74.5±1.5%, N=12 and 9 experiments, n=513 and 456 cells for control and CGP37157-treated microglia, ***p<0.001). This decrease was mostly due to a reduction in the half-amplitude time to C5a (Figure 4.10C) by 59.7% (from 100.0±2.4% to 40.3±0.9%, N=12 and 9 experiments, n=513 and 456 cells for control and CGP37157-treated microglia, ***p<0.001). These results indicate that the activity of NCLX prolongs the Ca^{2+} response of C5a-stimulated microglia.

ATP-evoked Ca^{2+} response of microglia in Ca^{2+} free HEPES buffer consisted of a very fast rise in cytosolic Ca^{2+} followed by a slower decrease (Figure 4.10D). As obvious from the imaging curves, the NCLX inhibitor affected the Ca^{2+}-response. Cumulative Fura-2 fluorescence was decreased by 38.4% (from 12.32±0.70 to 8.82±0.97, N=10 and 15 experiments for control and CGP37157-treated microglia, **p<0.01) (Figure 4.10E). Similarly to the effect of CGP37157 on

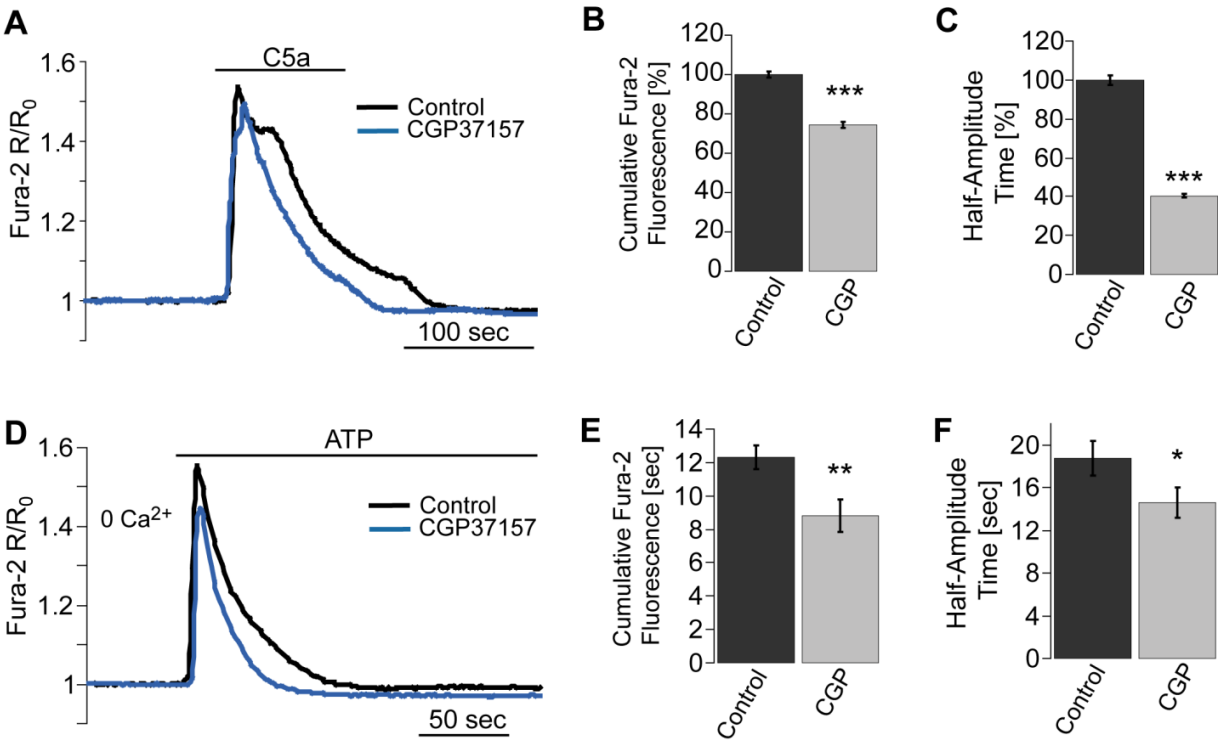

Figure 4.10. Pharmacological inhibition of NCLX attenuates metabotropic Ca^{2+} signaling in microglia

Changes in cytoplasmic Ca^{2+} of Fura-2 AM loaded primary murine microglia after stimulation with metabotropic ligands. ***(A-C)*** Fura-2 AM stained microglia grown on coverslips were perfused in HEPES buffer without (control) or with 20 µM CGP37157. 2 nM C5a was added as indicated by the bar. ***(A)*** Averaged responses from individual coverslips, containing 40-50 cells are given. Statistical analysis of the ***(B)*** cumulative fluorescence (integral below the curve) and ***(C)*** half-amplitude time of C5a response with or without CGP37157 (CGP). Values are given as mean ± SEM summarized from 12 control experiments (N=12, n=482 cells) and 9 experiments with CGP37157 (N=9, n=437 cells) (***p<0.001, Wilcoxon-Mann-Whitney U-test). ***(D-F)*** Microglia loaded with Fura-2 AM were incubated in Ca^{2+}-free HEPES buffer with or without 20 µM CGP37157; 100 µM ATP was applied as indicated. ***(D)*** Averaged curves from individual experiments containing 40-50 cells. ***(E, F)*** Statistical analysis of the ***(E)*** cumulative fluorescence (integral below the curve) and ***(F)*** half-amplitude time of the Ca^{2+} response following ATP with or without CGP37157 (CGP). Values are given as mean ± SEM summarized from 3 different cell preparations, 10 control experiments (N=10) and 12 experiments with CGP37157 (N=12). (**p<0.01, Student's unpaired t-test, *p<0.05, Wilcoxon-Mann-Whitney U-test).

the C5a-evoked Ca^{2+} response (see above), the decrease in ATP-evoked overall response was mostly due to a reduction in the half amplitude time from 18.75±1.66 sec to 14.63±1.43 sec (N=10 and 15 experiments for control and CGP37157-treated microglia, *p<0.05) (Figure 4.10F). These data show that NCLX inhibition shortens the purinergic metabotrobic Ca^{2+} response in microglia.

NCLX involvement in astrocytic metabotropic Ca^{2+} signaling

Mitochondrial Ca^{2+} transport has been shown to participate in intracellular Ca^{2+} signaling in different cell types (Hajnoczky et al., 1999; Hoth et al., 1997; Malli et al., 2003; Parekh, 2008). The finding in this study that NCLX is the mitochondrial Na^{+}/Ca^{2+} exchanger in astrocytes provided me with a molecular handle to determine how mitochondria respond to or shape cytosolic Ca^{2+} responses in astrocytes and what is the specific role of NCLX in this process. Astrocytes were co-transfected with control siRNA or siNCLX together with the transfection marker siGLO red. After three days, cells were loaded with Fura-2 AM and cytoplasmic Ca^{2+} signals in response to application of 100 µM ATP were monitored from siGLO red positive cells, either in Ca^{2+} containing (Figure 4.11A-D) or Ca^{2+} free buffer (Figure 4.11E-H). As described previously (Kresse et al., 2005), application of ATP in Ca^{2+}-containing buffer evoked a rapid increase of cytosolic Ca^{2+} followed by an initial rapid decline and a slower decaying phase of an "elevated Ca^{2+} plateau" associated with Ca^{2+} influx from the extracellular space. The averaged Ca^{2+} transients indicate that the slower decaying phase is reduced in NCLX-silenced astrocytes (Figure 4.11A, N=12 and 11 experiments for control and siNCLX-transfected astrocytes). To quantify the effect of NCLX silencing on the cytosolic Ca^{2+} transients, I determined the cumulative Fura-2 fluorescence, peak amplitude and half-amplitude time in control vs. siNCLX-treated astrocytes. The cumulative fluorescence was reduced by 39.3 % in NCLX-silenced astrocytes (Figure 4.11B), the peak amplitude was reduced by 13.4% (Figure 4.11C) and half-amplitude time of the signal was reduced by 9.8% (Figure 4.11D) in NCLX silenced astrocytes compared to control siRNA treated astrocytes (N=12 and 11 experiments, n=294 and 222 astrocytes for control and siNCLX-transfected astrocytes (n)) (***p<0.001, **p<0.01).

To determine the contribution of the mitochondrial exchanger to the regulation of Ca^{2+} signals that originate from the ER stores only, I superfused astrocytes with Ca^{2+}-free buffer and measured the ATP-induced cytosolic Ca^{2+} signals in NCLX silenced and control astrocytes. ATP triggered a fast rise followed by a fast decline of the cytoplasmic Ca^{2+} signal as described before. The elevated plateau phase, seen when Ca^{2+} containing buffer was applied was reduced. While there was no marked difference in the averaged Ca^{2+} transients following NCLX

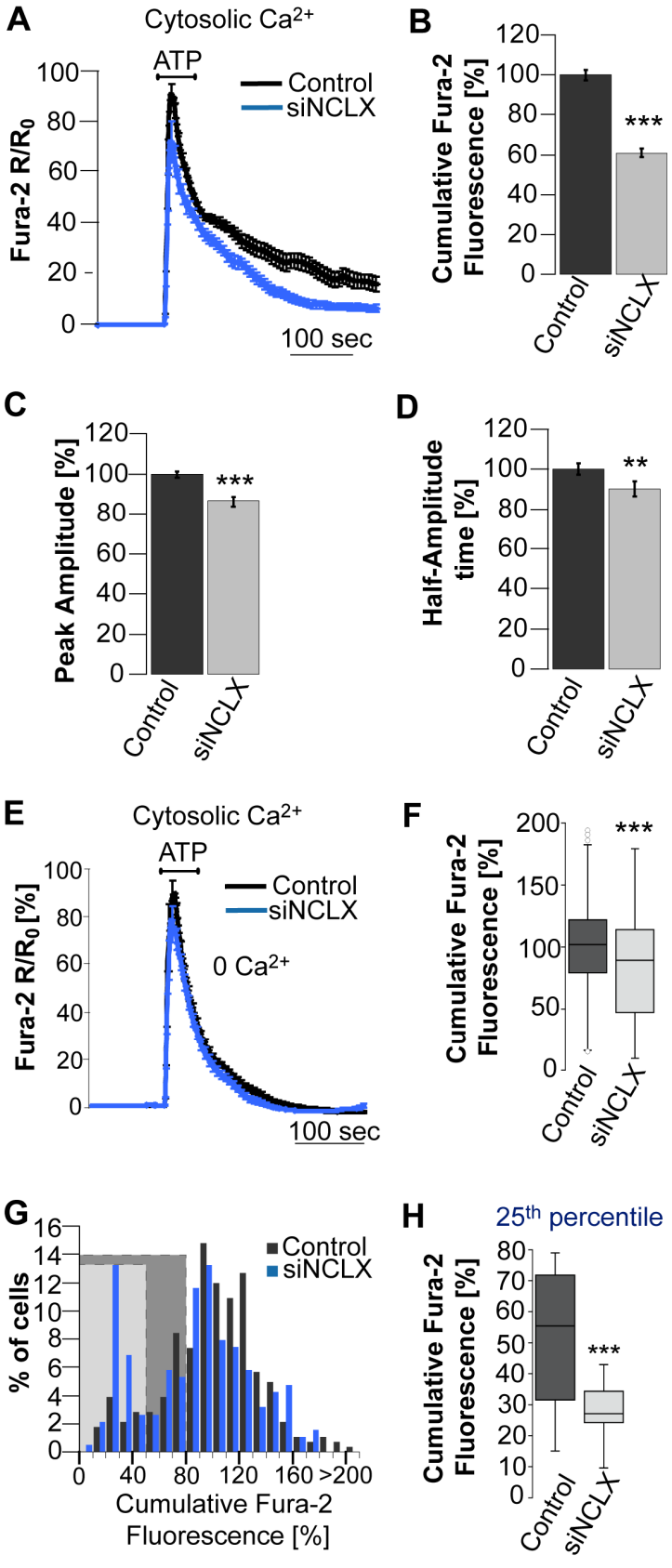

Figure 4.11. NCLX modulates ATP-induced Ca^{2+} response in astrocytes

Primary murine astrocytes were co-transfected with non-targeted siRNA (Control) or siNCLX and siGLO red indicator. Cells were loaded with Fura-2 AM and cytoplasmic Ca^{2+} signals were monitored from siGLO red positive cells. ***(A,E)*** Time lapse of average Fura-2 AM fluorescence, reporting on changes in cytoplasmic Ca^{2+}, for control and siNCLX- transfected astrocytes in Ca^{2+}-containing ***(A)***, and Ca^{2+}-free buffer ***(E)***, 100 µM ATP was added as indicated. ***(B-D)*** Statistical analysis of ***A***: ***(B)*** cumulative response ***(C)*** amplitudes and ***(D)*** half amplitude time of the ATP-evoked Ca^{2+} responses. Values are given as mean ± SEM (N=12 experiments, n=294 cells and N=11, n=222 experiments for control and siNCLX-transfected astrocytes (n)).(***p<0.001, **p<0.01, Wilcoxon-Mann-Whitney U-test). ***(F-H)*** Statistical analysis of the cumulative Ca^{2+} responses corresponding to ***E***: ***(F)*** Boxplot indicating median (dark line), 25th and 75th percentiles (upper and lower hinges, respectively) of the cumulative Fura-2 fluorescence for the whole population. ***(G)*** Histogram representing the proportion of ATP-evoked Ca^{2+} responses (cumulative Fura-2 fluorescence) in the cells presented in ***E*** (bin size 10%) showing a bimodal distribution for the population treated with siNCLX (N=9, n=189) but not with control siRNA (N=11, n=284) (dotted box). ***(H)*** Boxplot as in previous panel for the 25th percentile of the population (***p<0.001, Wilcoxon-Mann-Whitney U-test).

knock down (Figure 4.11E), statistical analysis of the cumulative Fura-2 fluorescence in control vs. siNCLX transfected astrocytes revealed a slight, but significant reduction of the mean cumulative Ca^{2+} signal in NCLX-silenced astrocytes. The median of the population shifted from 102.1% in the control population to 89.4% (***p<0.001) (Figure 4.11F). Interestingly, the difference became more apparent when looking at the 25th percentile of the box plot (Figure 4.11F). Here, following NCLX knock down, cumulative Ca^{2+} responses shifted from 79% to 47.4%. When normalized cumulative responses were presented as distribution histograms (Figure 4.11G), I observed an unimodal distribution in the control group (N=11, n=284) (Figure 4.11G), whereas data originating from NCLX silenced astrocytes showed a bimodal distribution. This additional population, which appeared in NCLX-inhibited cells, was apparent within the 20-30% range of cumulative Ca^{2+} responses, had an overall lower cumulative ATP-evoked Ca^{2+} response (N=9, n=189) (Figure 4.11G). Consequently, the further statistical analysis of the data corresponding to the first quartile in the histogram exposed the effect of NCLX silencing on the net Ca^{2+} release from the ER stores, namely a reduction of the cumulative Ca^{2+} response in this subpopulation of cells (median 27.1%, n=44 vs. 55.5%, n=71 in control; ***p<0.001) (Figure 4.11H).

In conclusion, these results indicate that stimulus-induced cytoplasmic Ca^{2+} signals in astrocytes, both caused by the entry of Ca^{2+} from the extracellular space or by release from the ER store, are distinctly modulated by the activity of the mitochondrial Na^{+}/Ca^{2+} exchanger NCLX.

NCLX contributes to the activity of store-operated Ca^{2+} entry

The store operated Ca^{2+} entry (SOCE) is a major Ca^{2+} influx pathway in glial cells (Toescu et al., 1998; Verkhratsky et al., 2011). Interaction of this entry pathway with the mitochondrial Ca^{2+} shuttling machinery has been documented in T-lymphocytes, RBL-1, and HeLa cells (Glitsch et al., 2002; Hoth et al., 1997; Varadi et al., 2004). The close local connection of mitochondria with Ca^{2+} influx pathways in the plasma membrane allows mitochondria to capture a substantial fraction of Ca^{2+} entering the cells and thereby maintain Store-Operated Ca^{2+} Channels (SOC) activity. Interestingly, the prolonged influx through SOC not only relies on the mitochondrial Ca^{2+} uptake, but also on an efficient mitochondrial Ca^{2+} efflux, as shown by a pharmacological approach with the mitochondrial exchanger inhibitor CGP37157 (Malli et al. 2003). However, the

role of mitochondria in regulating SOC activity, both, in microglia and astrocytes is poorly understood, and NCLX could provide a specific molecular handle.

NCLX involvement in SOCE in microglia

To investigate whether the activity of the mitochondrial Na^+/Ca^{2+} exchanger modifies SOCE in microglial cells, SOCE was induced by different paradigms. Microglial cells were loaded with Fluo-4 AM, placed in Ca^{2+} free buffer and perfused with 1 µM thapsigargin, an irreversible inhibitor of the sarcoplasmic/ER Ca^{2+} ATPase (SERCA). Thapsigargin causes constant leakage of Ca^{2+} from the ER which leads to the activation of SOCE. SOCE-mediated Ca^{2+} influx was monitored upon repetitive perfusion with buffer containing 2 mM Ca^{2+} (Figure 4.12 A-F). I exploited the fact that CGP37157 is a reversible drug; CGP37157 or DMSO (vehicle) for a control experiment were applied only during the induction of the second SOCE and then washed out during the third one. The first SOCE response was taken as 100 % for each cell, and other responses were calculated accordingly. During the control experiment the amplitude of SOCE decreased from 100% to 91.2±1.7% for the second SOCE (application of vehicle DMSO) and to 91.6±2.5% for the third peak (N=4 experiments and n=205 cells, NS $p>0.05$) (Figure 4.12B). For the SOC entry rates, the slopes of the Ca^{2+} influx were calculated. During the control experiment, SOC entry diminished from 100% for the first response to 88.4±4.1% during the second response and 89.4±6.5 for the third response (N=4 and n=205 cells) (Figure 4.12C), indicating that there is a certain run down of the Ca^{2+} response during repetitive stimulation. To analyze the effect of CGP37157 on thapsigargin-induced SOCE, I compared the amplitude and the slope of the influx of the 3rd SOC signal (after the washout of CGP37157) with the 2nd response elicited in the presence of 20 µM CGP37157. The SOC amplitude in microglia was reduced by 26.1% following the perfusion with the inhibitor (from 72.8±0.9% during the 3rd SOC signal to 46.7±0.6% during the 2nd peak) (N= 9 experiments and n=415 cells, ***$p<0.001$) (Figure 4.12E). SOC entry rate was reduced to 18.7±0.6% in the presence of CGP37157 (2nd peak) and returned to 47.5±1.0% during the washout (3rd peak) (N=9 experiments and n= 415 cells, ***$p<0.001$) (Figure 4.12F).

To confirm the effect of NCLX activity on SOCE I used another experimental paradigm to induce SOCE. Microglia were loaded with Fura-2 AM and then placed in Ca^{2+}-free HEPES solution. ER Ca^{2+} stores were depleted by purinergic receptor activation, specifically via perfusion with 100 µM ATP for 200 sec. SOCE was induced by application of 5 mM Ca^{2+} (Figure 4.12G). Experiments were performed either in the presence or absence of 20 µM CGP37157. Looking at

Ca^{2+} changes via analyzing ratios of Fura-2 AM R/R_0 values showed that the SOCE amplitude was reduced by 65.1% (from 0.249±0.008 to 0.087±0.004) (N=7 control experiments n=368 cells, N=4 experiments n=229 CGP37157-treated cells, ***p<0.0001) in the presence of CGP37157 (Figure 4.12H). These results indicate that NCLX is the major contributor to SOCE in microglial cells.

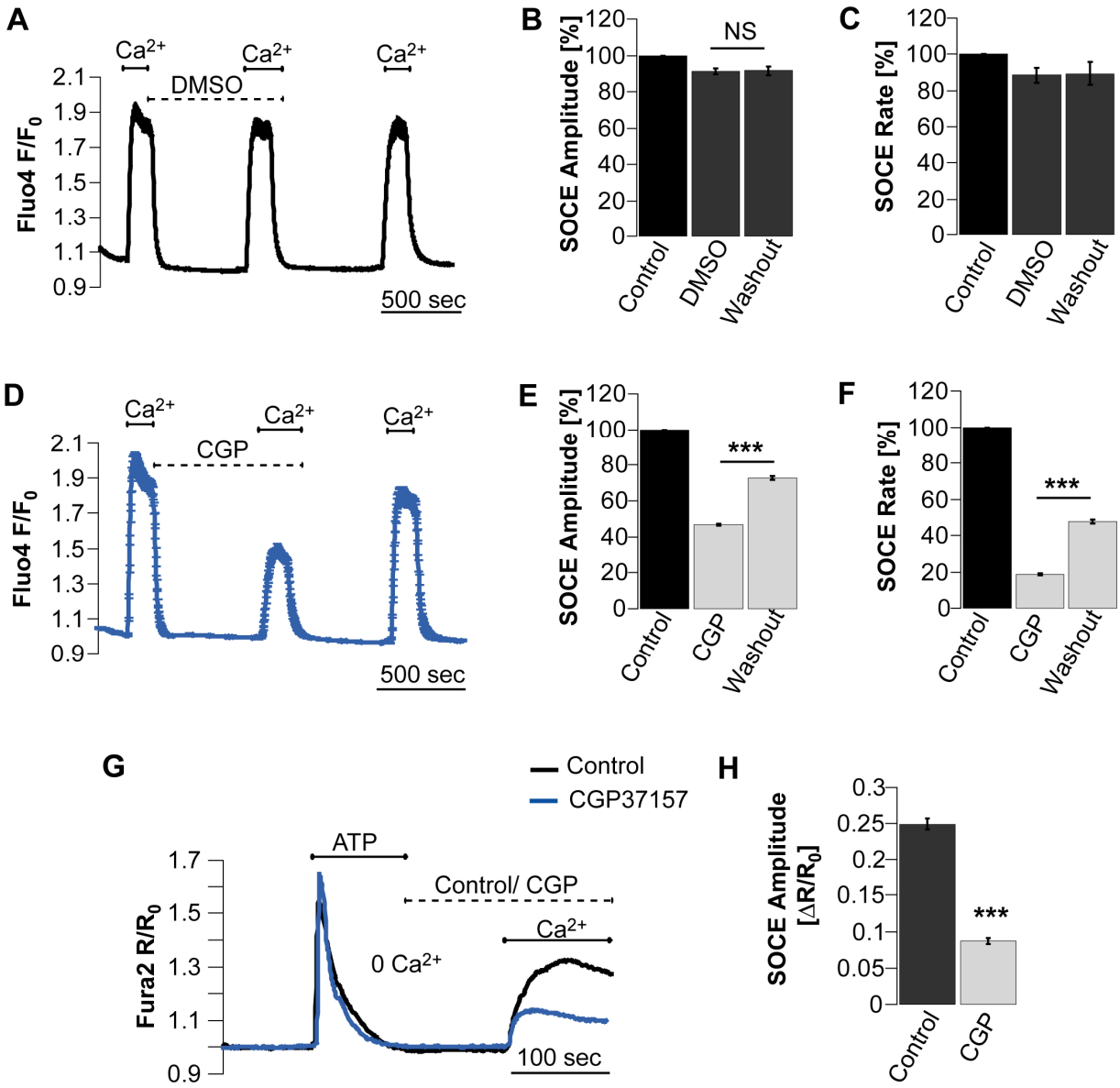

Figure 4.12. Pharmacological inhibition of NCLX diminishes Ca^{2+} entry via Store-Operated Channels (SOC) in microglia

(A-F) Stimulation paradigm to repetitively evoke SOC entry: primary murine microglia were loaded with Fluo-4 AM indicator. Prior to the recording, ER Ca^{2+} stores were depleted with 1 µM thapsigargin in Ca^{2+}-free buffer. While monitoring cytosolic Ca^{2+}, cells were perfused in Ca^{2+}-free solution, and SOC entry was repetitively elicited by application of 2mM Ca^{2+} via the perfusion buffer as indicated. CGP37157 or vehicle (DMSO) was applied only before and during the second SOC induction, followed by washout. ***(A,D)*** Averaged curves ±SEM from individual experiments containing 50-60 cells for ***(A)*** control experiment or ***(D)*** experiment with CGP37157-treated cells. Statistical analysis of ***(B, E)*** amplitudes of the responses and ***(C,F)*** the entry rate via SOC for ***(B,C)*** control and ***(E,F)*** CGP37157-treated microglia. Values are given as mean ± SEM (N=5 experiments, n=194 cells, N=9 experiments, n=395 cells for control and CGP37157-treated cells, respectively). (NS $p>0.05$, ***$p<0.001$, Wilcoxon-Mann-Whitney U-test). ***(G,H)*** Ca^{2+} re-addition protocol to visualize SOC entry: changes in cytosolic Ca^{2+} were monitored from Fura-2 AM-loaded microglia. To empty the ER Ca^{2+} stores, 100 µm ATP was applied as indicated, while perfusing cells in Ca^{2+}-free buffer, followed by a switch to 5mM Ca^{2+}- perfusion buffer containing either 20µM CGP37157 (blue) or vehicle (black). 5mM Ca^{2+} was re-added via the perfusion as indicated to distinguish SOC entry. ***(G)*** Averaged curves from individual experiments for control and CGP37157 (CGP)-treated microglia. ***(H)*** Statistical analysis of the amplitudes of SOC responses summarized from N=7 control experiments, n=368 cells and N=4 experiments with CGP37157, n=229 cells. (***$p<0.001$, Wilcoxon-Mann-Whitney U-test).

NCLX involvement in SOCE in astrocytes

To investigate the involvement of NCLX in SOCE in astrocytes, I applied both pharmacological and molecular approach (siRNA) to inhibit the activity of the exchanger. By knocking down NCLX expression and monitoring cytosolic and mitochondrial Ca^{2+} fluxes I investigated if there is a functional crosstalk between SOC and mitochondria and if NCLX can modulate mitochondrial Ca^{2+} fluxes and SOCE.

Astrocytes were transfected with the red siGLO transfection marker along with control non-targeted siRNA or siNCLX. To monitor changes in cytosolic Ca^{2+} cells were loaded with Ca^{2+}-sensitive dye Fura-2 AM, and signals were acquired from siGLO-positive cells. SOCE was activated using a common procedure described above for microglia (Kresse et al., 2005). Briefly, ER stores were initially depleted by application of ATP in the absence of extracellular Ca^{2+} and then superfused with Ca^{2+}- containing buffer. Re-addition of Ca^{2+} either in control or in siNCLX-transfected cells produced the corresponding increase in cytosolic Ca^{2+}, which is mediated by SOCE (Figure 4.13A, N=9 for both groups). Importantly, the amplitude of the SOCE response was strongly decreased after silencing of NCLX from 100.0±5.1% to 59.9± 3.1% (N=9, n=175 and 131 for control and siNCLX-transfected astrocytes, ***$p<0.001$) (Figure

4.13B). Moreover, SOCE entry rate was reduced from 100.0±3.6% to 68.0± 3.7% by NCLX silencing (***p<0.001) (Figure 4.13C), indicating that NCLX activity up regulates Ca^{2+} influx via SOC.

A similar impairment on SOC function in astrocytes was found, when NCLX was pharmacologically inhibited with 20 μM CGP3715. This blocker reduced SOCE amplitude by 25.5% and SOCE entry rate by 34.2% compared to vehicle-treated control (N=8 and 7 experiments, n=376 and 425 cells for control and CGP37157-treated astrocytes, ***p<0.001) (Figure 4.13D-F), confirming the strong involvement of NCLX activity in regulation of SOCE in astrocytes.

To substantiate the effect of mitochondria in the handling of Ca^{2+} from SOCE, I used the protonophore carbonyl cyanide 4-(trifluoromethoxy)phenylhydrazone (FCCP).This pharmacological agent disrupts the mitochondrial H^+ gradient, thus depolarizing the mitochondria and inactivating mitochondrial Ca^{2+} uniporter, the major route of mitochondrial Ca^{2+} uptake. In the presence of 1 μM FCCP, SOCE amplitude dropped by 43.7% (N=8 and 5 experiments, n=376 and 168 cells for control and FCCP-treated astrocytes, ***p<0.001) (Figure 4.13E). SOC entry rate was decreased by 54.4% (***p<0.001) (Figure 4.13D-F).

I then asked if Ca^{2+} influx via the SOC evokes mitochondrial Ca^{2+} transients and if NCLX is regulating this crosstalk. I adapted the Ca^{2+} re-admission protocol (described above) to mtRP expressing astrocytes. In this set of experiments I measured only the wavelength F_{430} of the mtRP signal because ratiometric measurements of mtRP fluorescence F_{480}/F_{430} during SOCE in most experiments displayed a decrease in signal to noise ratio. SOCE evoked a fast rise in the mitochondrial Ca^{2+} followed by a gradual efflux (Figure 4.13G). Interestingly, there were a minor proportion of cells that responded only to ATP and others that responded only to SOCE. Mitochondrial Ca^{2+} efflux rate was greatly diminished in siNCLX-transfected cells compared to control-transfected cells (1.67±0.22) $x10^{-4}$ sec^{-1} and (0.28±0.26) $x10^{-4}$ sec^{-1} respectively, N=9 experiments; ***p<0.001). (Figure 4.13H). Similarly to the effect of NCLX inhibition on the ATP-evoked mitochondrial Ca^{2+}, NCLX inhibition during SOCE led to a significant increase (48.8%) of the net mitochondrial Ca^{2+} influx (***p<0.001) (Figure 4.13I) and to a 60.3% increase of the cumulative mitochondrial Ca^{2+} (***p<0.001) (Figure 4.13J).

In summary, these results indicate that an active crosstalk exists between SOC and mitochondria, and that mitochondrial Ca^{2+} extrusion through NCLX is crucial for augmenting a strong SOCE activity.

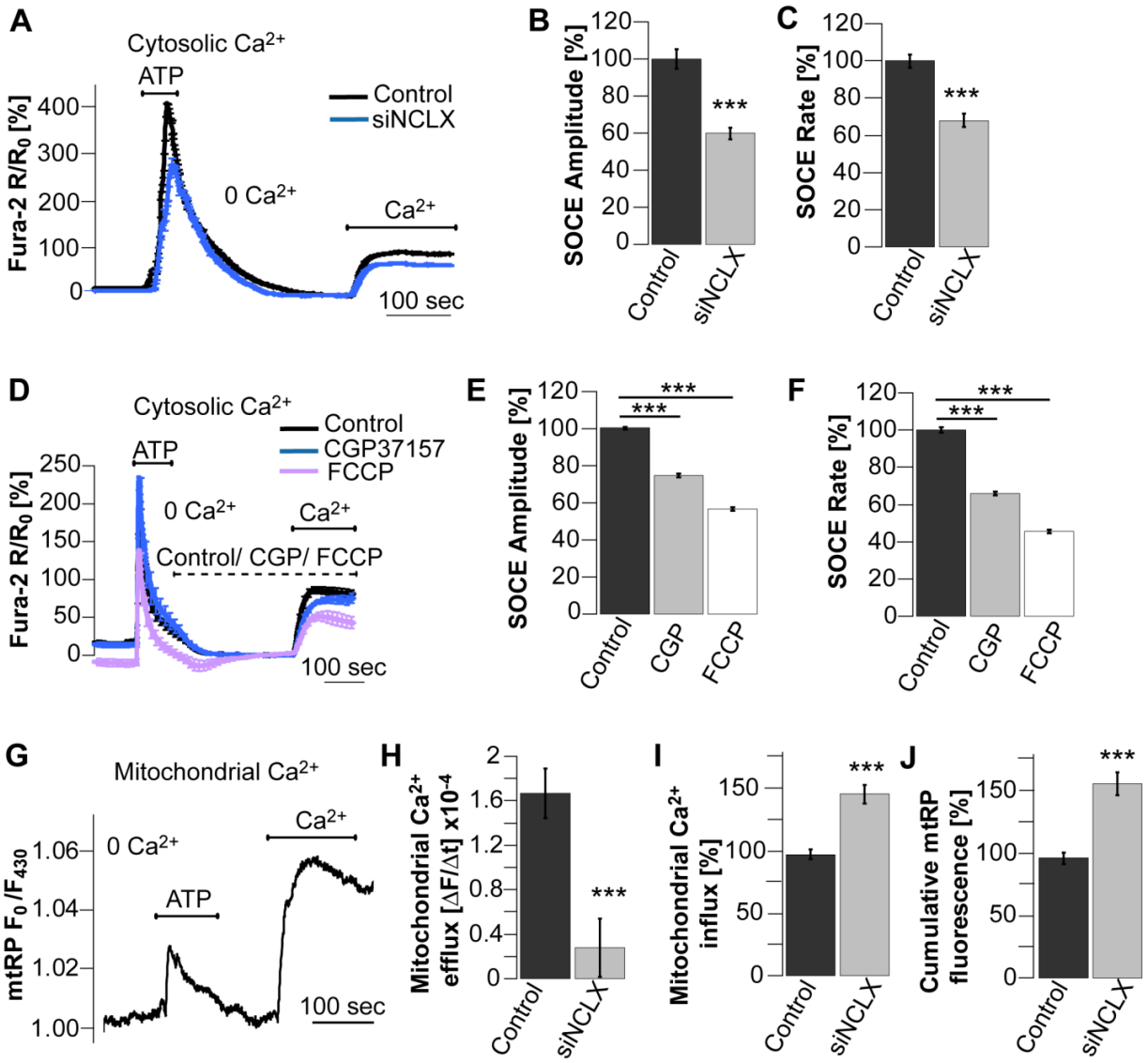

Figure 4.13. ***NCLX contributes to the activity of the store-operated Ca^{2+} entry in astrocytes***

(A-F) *Changes in cytoplasmic* Ca^{2+} in Fura-2 AM loaded primary murine astrocytes. ***(A-C)*** Astrocytes were co-transfected with non-targeted siRNA (Control) or siNCLX and siGLO red indicator. Cells were perfused in Ca^{2+} -free HEPES buffer and 100 µM ATP was applied as indicated by the bar to empty Ca^{2+} stores; 5 mM Ca^{2+} was re-added to distinguish SOCE. (***A)*** Time lapse of average Fura-2 fluorescence, reporting on changes in cytosolic Ca^{2+} *,* average Fura-2 response curve± SEM (normalized averages). Statistical analysis of the ***(B)*** amplitudes and ***(C)*** rates of SOCE in control (N=9, n=175) and siNCLX-transfected (N=9, n=131) astrocytes. Values are given as mean± SEM (***p<0.001, Wilcoxon-Mann-Whitney U-test). ***(D-F)*** Untransfected astrocytes were perfused in Ca^{2+}-free HEPES buffer without (Control) or with 20 µM CGP37157 (CGP) or with 1 µM FCCP. 100 µM ATP and 5 mM Ca^{2+} were added as indicated. ***(D)*** Mean Ca^{2+} response curve of all experiments ± SEM (normalized averages). Statistical analysis of the ***(E)*** amplitudes and ***(F)*** SOC entry rates in astrocytes treated with CGP37157*(CGP)*, FCCP, or without any drug *(Control)*. Values are given as mean ± SEM summarized from N=8 (n=376 cells), N=7 (n=425 cells), and N=5 (n=168 cells) experiments for control, CGP37157 and FCCP-treated astrocytes, respectively (***p<0.001, Kruskal-Wallis Rank Sum Test followed by Bonferonni's post-test and Wilcoxon test pair comparisons). ***(G-J)*** SOC-induced mitochondrial Ca^{2+} signals in astrocytes co-transfected with mtRP and non-targeted siRNA (control) or siNCLX. Cells were perfused with Ca^{2+}-free HEPES buffer, 100 µM ATP was applied as indicated and 5mM Ca^{2+} were re-added to induce SOCE. ***(G)*** Representative curve showing the mitochondrial Ca^{2+} response averaged from all ROIs of one experiment. Statistical comparison of the ***(H)*** mitochondrial Ca^{2+} efflux, ***(I)*** influx and ***(J)*** cumulative fluorescence from N=9 experiments (n=59 and n=43 ROIs for siNT- and siNCLX-transfected astrocytes, respectively (***p<0.001, Student t-test for unpaired samples, two-tailed and Mann-Whitney U-test)).

4.3 Glial function is shaped by NCLX activity

NCLX plays a role in microglial secretory functions and chemotaxis

Ca^{2+} plays an essential role in microglial function, and is involved in cytokine release, migration, proliferation, and activation. As NCLX modulates microglial Ca^{2+} signaling I sought to determine its role in microglial executive functions, namely microglial chemotaxis, release of cytokines, nitric oxide (NO) and reactive oxygen species (ROS).

Influence of NCLX on cytokine and chemokine secretion by microglia

A dependence of cytokine release on Ca^{2+} levels in microglia has been described before (Hoffmann et al., 2003). Therefore, mitochondria as important players in Ca^{2+} signaling may also affect cytokine secretion. To analyze the contribution of the mitochondrial Na^{+}/Ca^{2+} exchanger to this secretory activity in microglia, cytokine release was triggered by application of inflammatory stimuli. Bacterial lipopolysaccharide (LPS) and Interferon γ (IFNγ) have been shown to be potent stimuli (Hausler et al., 2002; Mertsch et al., 2001; Prinz et al., 1999; Stohwasser et al., 2000).

Microglia on 96-well plates were stimulated to secrete cytokines either by LPS alone (100 ng/ml) or by combination of 100 ng/ml LPS and 10 Units/ml IFNγ for 18 hours, either in the presence or in the absence of 20 µM CGP37157. IL-6, IL-12, TNFα and MCP-1 release were evaluated by enzyme-linked immunosorbent assay (ELISA) from the supernatants. NCLX inhibition by CGP37157 reduced LPS-triggered IL-6 release by 24.1% (from 100±2.72% to 75.87±2.84%) (N=3 independent cultures, n=11 and 12 replicates for control and CGP37157-treated microglia, ***p<0.001) (Figure 4.14A). Release of IL-12 was moderately increased in LPS activated microglia in the presence of the NCLX inhibitor (to 113.74±11.76%) (N=6 cultures, *p<0.05), as well as in LPS and IFNγ-stimulated microglia (from 173.06±36.61% to 214.63±45.45%) (N=6 cultures, *p<0.05) (Figure 4.14B). TNFα release, however, was not influenced by CGP37157 (100±2.66% and 103±4.24% for control and CGP37157-treated mciroglia, respectively, N=3 cultures, n=12 replicates, NS p>0.05) (Figure 4.14C). Chemokine monocyte chemoattractant protein-1 (MCP-1) release was slightly but significantly reduced upon NCLX blockade. Interestingly, basal release of MCP-1 from non-activated microglia was reduced upon CGP37157 application by 66.5% from 7.77±1.24% to 2.60±1.19%, while in LPS-triggered microglia the MCP-1 secretion was diminished from 100±0.71% to 94.29±0.83% and in microglia activated by combined stimuli of LPS and IFNγ the secretion was reduced from 108.95±1.87% to 93.62±3.25% upon NCLX inhibition (N=3 cultures, n=10 replicates, **p<0.01, ***p<0.001) (Figure 4.14D). These data show that NCLX activity modifies the secretion pathways of specific cytokines in microglia, like IL-6, IL-12, and MCP-1, while some are not affected.

Influence of NCLX on microglial chemotaxis

These results suggest NCLX involvement in the release pathway of specific cytokines and not in the general release activity of microglia. To investigate NCLX role in microglial chemotaxis, I used the Boyden chamber assay. The Boyden chamber consists of lower and upper parts separated by a porous membrane with 8μm holes (Figure 4.15A). Lower wells contain medium with chemoattractant, the upper wells contain the cell suspension. During the assay, cells migrate through the porous membrane towards the chemoattractant, allowing the quantification of cell migration. As chemoattractants, 100 μM ATP or 2 nM C5a were applied to the lower wells. Cells were added to the upper compartment and migration rates in the presence or absence of CGP37157 were analyzed. Indeed, CGP37157 diminished ATP-evoked chemotaxis by 47.8%: from 2007.00±288.64% to 1048±118.00% of the migration rate of control (N=4 experiments, n=41 and 38 replicates for control and CGP37157-treated microglia, **p<0.01) (Figure 4.15B). In contrast, chemotaxis induction by C5a was less strong and not reduced in the presence of CGP37157 (378.80±55.43% without CGP37157 and 405.15±51.42% with CGP37157) (N=4, NS p>0.05). In conclusion, NCLX inhibition reduces chemotaxis evoked by some agonists, suggesting its involvement in specific agonist-evoked pathways as opposed to the general migration ability impairment.

Influence of NCLX on the release properties of microglia

Activated microglial cells have been shown to upregulate reactive oxygen species (ROS) generation via NADH oxidases (Kettenmann et al., 2011) and to increase their nitric oxide (NO) release, causing neurotoxicity. Therefore I was interested to study NCLX involvement in microglial ROS and NO generation. Microglia on 96 well-plates were stimulated with 1mg/ml opsonized zymosan or 100ng/ml LPS for 18 hours either in the presence or in the absence of 20 μM CGP37157, H_2DCFDA was added and the generation of ROS was measured fluorimetrically (Eruslanov and Kusmartsev, 2010). While both zymosan and LPS induced 2.0 and 1.3 fold increase in ROS levels, respectively, the inhibition of NCLX by CGP37157 did not influence ROS generation in LPS- and zymosan-activated microglia (204.72±10.05% and 210.71±12.23% for control and CGP37157-treated LPS-triggered microglia, respectively; 132.09±14.76% and 138.95±15.03% for control and CGP37157-treated zymosan-triggered microglia, respectively, N=3 cultures, n=18 replicates, NS p>0.05) (Figure 4.15C).

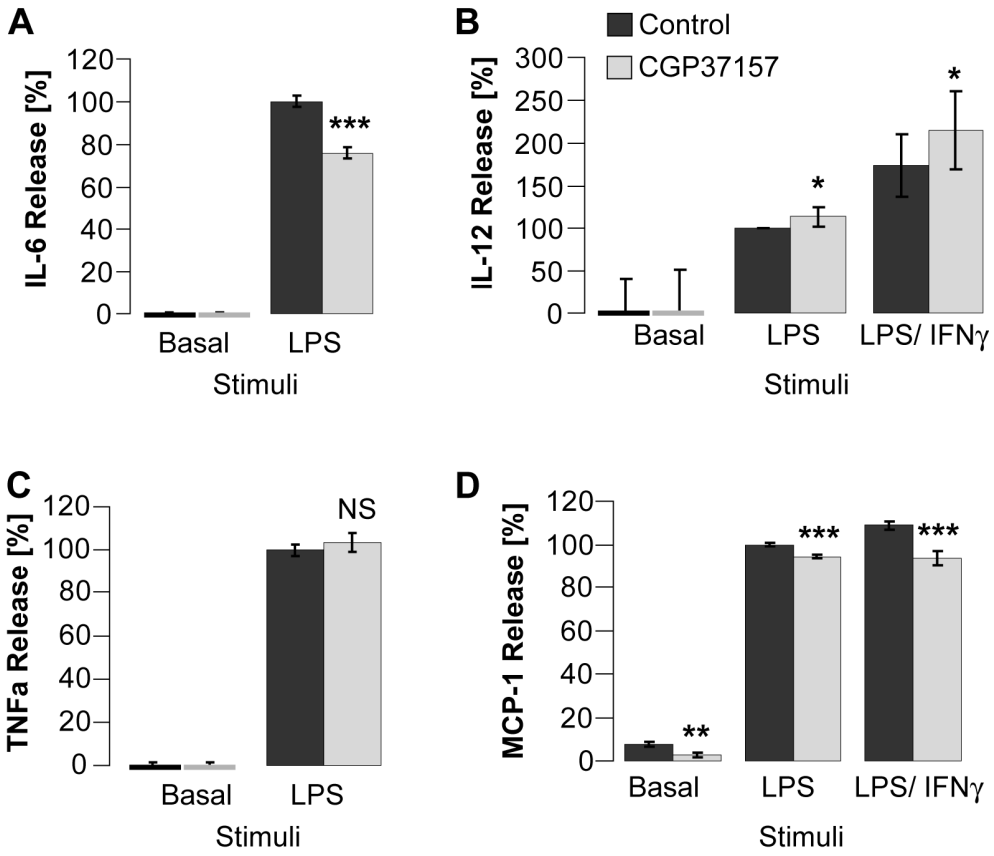

Figure 4.14. Microglial cytokine release is modulated by inhibition of NCLX

Microglia were stimulated for 18 h with LPS (100 ng/ml) and/or IFNγ (10 U/ml) either in the presence or absence of 20µM CGP37157, and IL-6, IL-12, TNFα or MCP-1 release into the supernatants was determined by ELISA. Cytokine release was normalized to protein concentration. Values were normalized to % of LPS-stimulated control experiment and given as mean ± SEM summarized from ***(A)*** 3 independent experiments (N=3) for IL-6 release, n=11 and 12 replicates for control and CGP37157 treated microglia (Student t-test unpaired double-tailed, ***p<0.001), ***(B)*** N=6 independent experiments for IL-12 release (Mann-Whitney U-test, *p < 0.05), ***(C)*** N=3 independent experiments and n=12 replicates for TNFα release (Student t-test unpaired double-tailed, NS p≥0.05), and ***(D)*** N=3 independent experiments and n=10 replicates for MCP-1 release (Student t-test unpaired double-tailed, ***p<0.001).

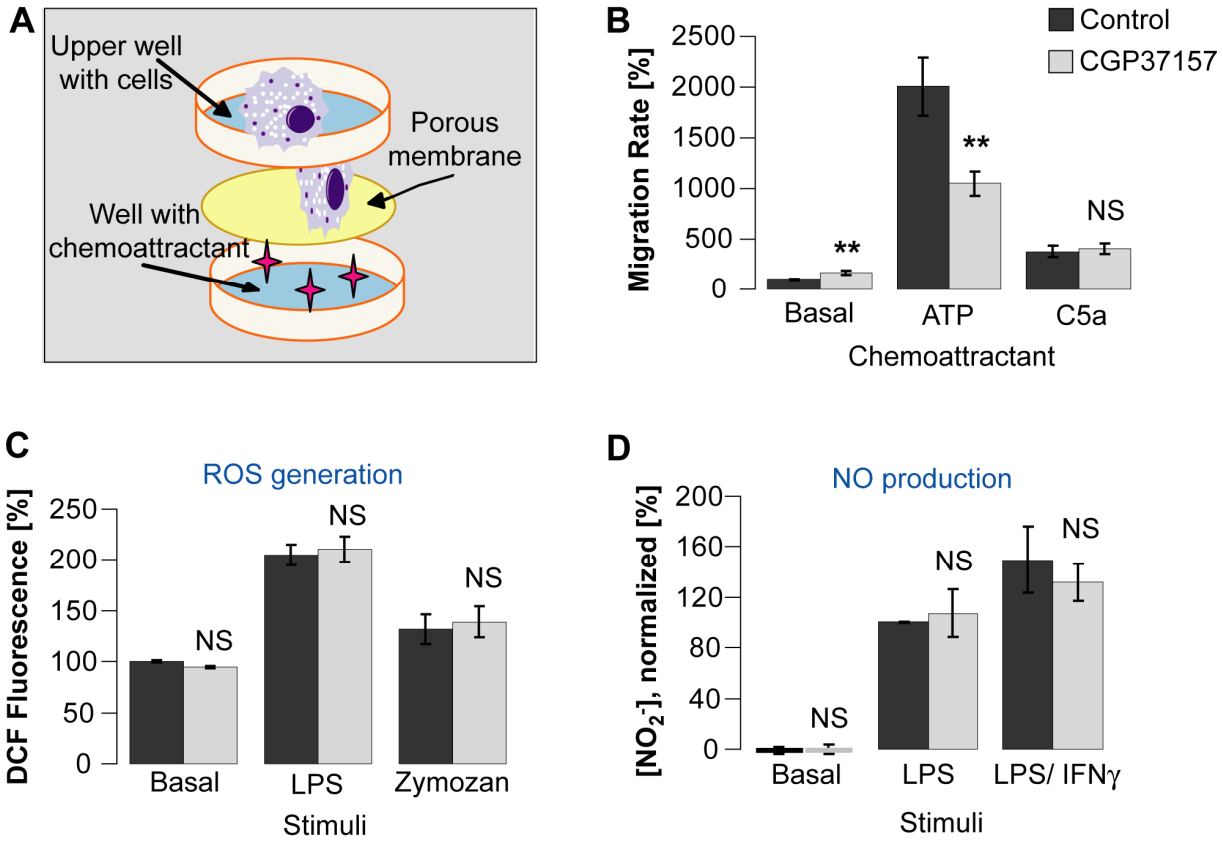

***Figure 4.15.* NCLX inhibition impairs microglial chemotaxis, but does not affect release of NO or ROS**

(A-B) Microglial chemotaxis was measured in a multiwell microchemotaxis Boyden chamber assay. ***(A)*** Scheme of assay, in which filter with pores of 5 µm diameter separates the upper and lower wells. Chemoattractive agents (100 µM ATP or 5 nM C5a) were added to the lower wells. Cell suspensions were added to the upper wells and allowed to migrate towards the chemoattractant for 3h. ***(A-D)*** CGP37157 was applied at final concentration of 20 µM to both wells for all the experiments. ***(B)*** Data is given as mean ± SEM summarized from 4 independent experiments (N=4, n=41 and 38 replicates for control and CGP37157-treated microglia). ***(C)*** Microglia were stimulated for 18 h with LPS (100 ng) or 1mg/ml Zymosan in the presence or absence of 20 µM CGP37157, and reactive oxygen species (ROS) generation was determined by measurement of DCF fluorescence as described. Data is given as mean ± SEM summarized from N=4 independent experiments (n=18 replicates for each condition) (Student t-test unpaired double-tailed, NS $p \geq 0.05$). **(D)** Cultured microglial cells were treated with LPS (100 ng/ml) and/or IFNγ (10 U/ml), either in the presence or absence of 20 µM CGP37157, and NO production was determined by Griess reaction after 18 h. Values are given as mean ± SEM summarized from N=5 independent experiments (Student t-test unpaired double-tailed, NS $p \geq 0.05$).

For determination of NO release, supernatants of LPS- or LPS/IFNγ-activated microglia were analyzed by Griess reaction (Kim et al., 1997). NO production was not significantly altered by pharmacological NCLX inhibition (Figure 4.15D). LPS-stimulated microglia produced 100±0.01% and 107.30±18.80% NO for control and CGP37157-treated cells, respectively (N=5 cultures, NS p>0.05). Microglia stimulated with combined LPS and IFNγ stimuli produced 149.70±26.37% and 131.74±14.74% NO for control and CGP37157-treated cells, respectively (N=5 cultures, NS p>0.05).

These data show NCLX involvement in chemotaxis and secretory properties of microglia.

NCLX affects astrocytic communication, secretory and wound healing abilities

NCLX influence on Ca^{2+} wave propagation in astrocytes

Astrocytes communicate with each other via Ca^{2+} waves, and astrocytic Ca^{2+} wave propagation depends on the purinergic signalling (Haas and Kettenmann, 2009). Therefore, I next tested the impact of NCLX on astrocytic Ca^{2+} wave propagation.

For this purpose, control- or siNCLX-transfected astrocytic monolayers were loaded with Fluo-4 AM Ca^{2+} dye and Ca^{2+} waves were induced mechanically by touching one astrocyte with a micropipette (Cornell-Bell et al., 1990). The bright field image of the stimulation and the series of the consecutive fluorescent images following such a mechanical stimulation are shown in Figure 4.16A. To calculate the effect of NCLX silencing on the wave propagation, fluorescent intensity vs. time was analyzed in 3 concentric circles with radiuses of 23.45, 117.81, and 212.19 µm (Figure 4.16B,C). Time points where the intensity reached the maximum were taken for each area between the circles and the wave velocity in this area was calculated according to the equation in Figure 4.16C. Silencing of NCLX resulted in not significant decelerated wave propagation in the middle area (from 23 to 118 µm from the stimulation point) by 12% (from 11.12±1.67 µm/sec to 9.80±1.33 µm/sec) and by 14% (from 9.32±1.43 µm/sec to 8.05±1.22 µm/sec) in the large area (from 118 to 213 µm from the stimulation point) (N=6 independent cultures, n=24 and 21 experiments for control and siNCLX-transfected astrocytes, NS p>0.05) (Figure 4.16D). However, the area of the Ca^{2+} wave was significantly diminished from 100% for control-transfected astrocytic monolayers to 79.45±12.02% upon NCLX ablation (N=6 independent cultures, *p<0.05) (Figure 14.6E). The speed of Ca^{2+} wave propagation was

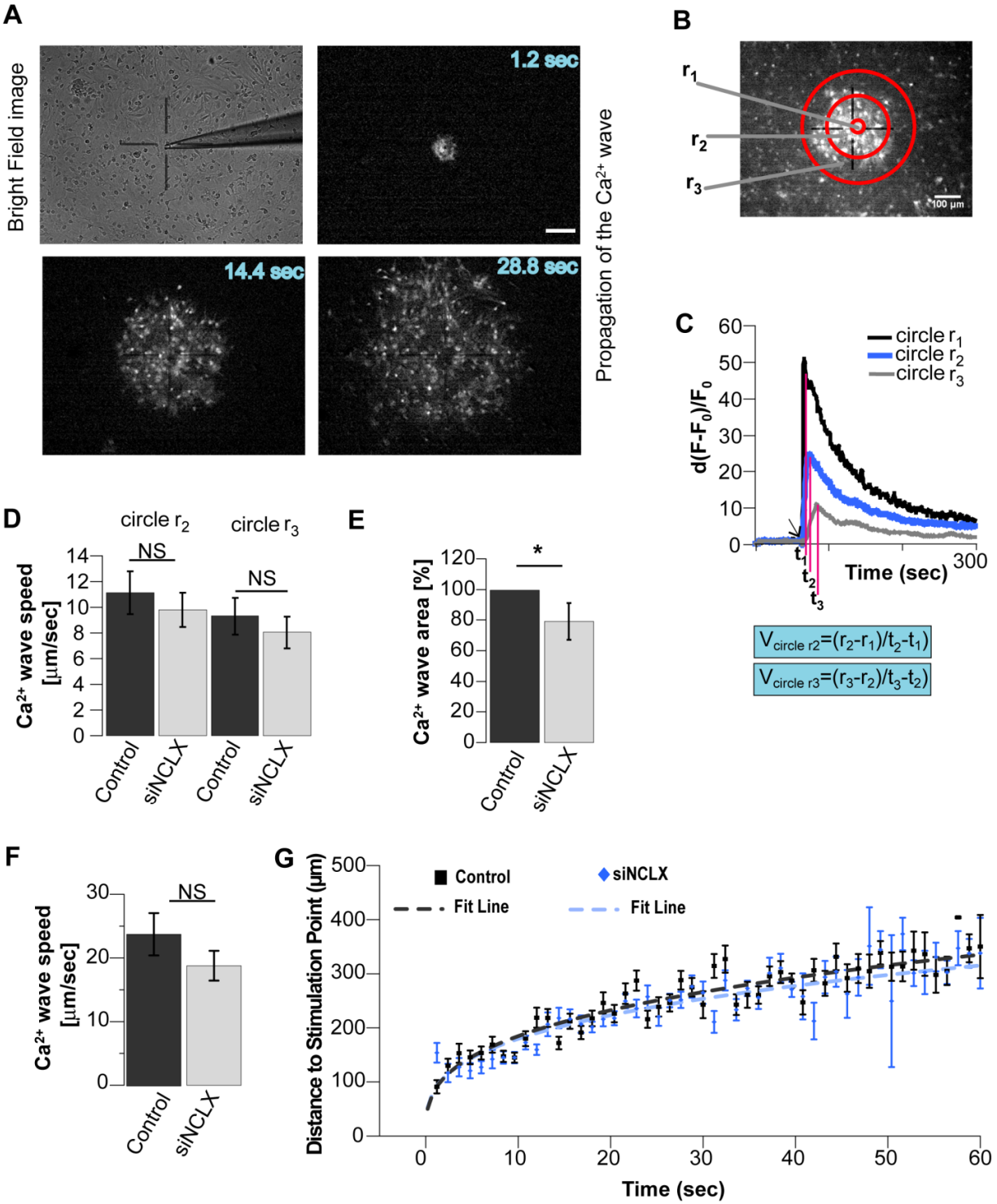
A
Bright Field image
1.2 sec
14.4 sec
28.8 sec
Propagation of the Ca2+ wave
B
r1
r2
r3
100 µm
C
circle r1
circle r2
circle r3
d(F-F0)/F0
Time (sec)
t1
t2
t3
Vcircle r2=(r2-r1)/t2-t1)
Vcircle r3=(r3-r2)/t3-t2)
D
circle r2
circle r3
NS
NS
Ca2+ wave speed [µm/sec]
Control
siNCLX
Control
siNCLX
E
*
Ca2+ wave area [%]
Control
siNCLX
F
NS
Ca2+ wave speed [µm/sec]
Control
siNCLX
G
Control
Fit Line
siNCLX
Fit Line
Distance to Stimulation Point (µm)
Time (sec)

Figure 4.16. Effect of NCLX blockade on mechanically-evoked Ca^{2+} waves in astrocytes

Cytoplasmic Ca^{2+} waves were induced by mechanical stimulation in Fluo-4 AM loaded confluent astrocyte cultures that had been transfected with non-targeted siRNA (control) or siNCLX as described. ***(A)*** Series of subtraction images show the concentric propagation of a Ca^{2+} wave (*3 fluorescent images*) as induced by poking an astrocyte with a micropipette *(bright field image, top left)*. Scale bar 100 µm. ***(B)*** Wave propagation was analyzed in concentric circles of radiuses r_1=23.5 µm, r_2= 117.8 µm and r_3=212.2 µm. ***(C)*** Curves of fluorescence intensity vs. time were generated for each circle, time *(t)* for maximal fluorescence intensity for each circle was determined and speed was calculated according to the formula shown. Graph comparing the mean values ± SEM of the ***(D)*** averaged speed and ***(E)*** area of Ca^{2+} wave propagation in the control astrocytic monolayer vs. siNCLX-transfected astrocytic monolayer (N=6 astrocytic preparations, n=24 and 21 experiments, respectively) (Wilcoxon-Mann-Whitney U-test, NS p>0.05, *p>0.05). ***(F-G)*** An alternative method for calculation of Ca^{2+} wave speed (done in collaboration with Dr. I. Delgado-Martinez, MDC, Berlin, Germany). To calculate the velocity of the Ca^{2+} wave for each cell, distance from the stimulation point and time at which the wave reached the cell were determined by a self-made algorithm. ***(F)*** For each experiment Ca^{2+} wave propagation velocity was calculated by averaging the velocities at which the Ca^{2+} wave reached each of the cells on a coverslip. The analysis showed that propagation velocity was slower after blockade of NCLX, however this difference was not significantly different (Wilcoxon-Mann-Whitney U-test, p>0.05, N=5 astrocytic preparations, n=20 and 28 coverslips for control and siNCLX, respectively). ***(G)*** Average time course of the propagation of the Ca^{2+} wave. The wave was initiated as a fast burst which propagated centrifugally close to a linear velocity. Mean data points could be fitted to a power function: Distance=A x time^b. For control-treated astrocytes A = 82 ±6.7 µm and b = 0.35 ± 0.02 (R^2=0.92) and for siNCLX-treated astrocytes A = 74 ± 6.64 µm and b = 0.36 ± 0.02 (R^2=0.82). The values for A and for b are given as mean ± StDev. Values on the graph show mean ± SEM, fitting curves are presented as dashed lines.

analyzed more carefully. An algorithm identifying each cell in the astrocytic monolayer was developed in collaboration with Dr. Ignacio Delgado-Martinez. Then for each cell the algorithm determined the distance from the stimulation point and time after the beginning of the wave. This allowed calculating the speed of the wave seen by each individual cell. Calcium wave propagation after mechanical stimulation was slower, yet not significantly, in NCLX-disrupted astrocytes compared with control: 18.79±2.34 µm/sec to 23.85±3.33 µm/sec, respectively (N=6 independent cultures, n=20 and 28 experiments for control and siNCLX-transfected astrocytes, NS p>0.05) (Figure 4.16F). The effect could be observed also from the average time course of the propagation of the Ca^{2+} wave (Figure 4.16G). The wave was initiated as a fast burst which propagated centrifugally close to a linear velocity. To see the overall direction of the trace, mean velocities were matched to a power function. In control-treated astrocytic monolayers the wave

spread according to the formula: Distance = (82±6.7) x time$^{0.35\pm0.02}$ (R^2=0.92); and in NCLX-treated astrocytes the formula was: Distance = (74±6.6) x time$^{0.36\pm0.02}$ (R^2=0.82). This data indicates that NCLX may play a role in astrocytic communication by probably slowing down the wave propagation and by affecting the area of communication. Further experiments need to be performed in order to substantiate the effect.

NCLX affects astrocyte Ca^{2+} excitability and glutamate release

Mechanical stimulation of astrocytes induces the elevation of cytosolic Ca^{2+} and subsequently causes exocytosis of glutamate (Hua et al., 2004; Innocenti et al., 2000; Montana et al., 2004). The pharmacological inhibitor of mitochondrial Na^+/Ca^{2+} exchanger CGP37157 has been shown to diminish mechanically-induced Ca^{2+} responses and glutamate release from rat solitary astrocytes *in vitro* (Reyes and Parpura, 2008). Does specific molecular knock-down of NCLX affect astrocytic gliotransmission differently?

To answer this question, astrocytes were transfected with red siGLO transfection marker along with control non-targeted siRNA or siNCLX. To monitor Ca^{2+} changes cells were loaded with Ca^{2+}-sensitive dye Fluo-3 AM, and signals were acquired from siGLO-positive cells. Mechanical stimulation evoked a rapid increase in cytosolic Ca^{2+} followed by slower decline (n=15; peak dF/F_o= 478 ± 43%; paired t-test **p < 0.01) (Figure 4.17A). This Ca^{2+} elevation originates primarily from the ER store as well as from the extracellular space (Hua et al., 2004; Malarkey et al., 2008). Common efforts of the mitochondrial uniporter, rapidly taking up Ca^{2+} near open Ca^{2+} channels, and NCLX slowly releasing Ca^{2+} into the cytosol, could shape Ca^{2+} signals.

NCLX knock-down caused a significant 46% decrease in the amplitude of the response (n=15; peak dF/F_o= 283 ± 52%) and significant decrease in cumulative Ca^{2+} fluorescence (**p < 0.01) (Figure 4.17 A-C). Interestingly, NCLX knock-down was much more effective in the reduction of Ca^{2+} response than the pharmacological inhibition of this exchanger by CGP37157 (Reyes and Parpura, 2008).

To investigate the role of NCLX in exocytotic glutamate release from astrocytes, L-glutamate dehydrogenase (GDH)-linked assay was used. In this assay GDH creates fluorescent substrate nicotinamide adenine dinucleotide NADH from NAD^+ and released glutamate (Hua et al., 2004; Montana et al., 2004), therefore allowing measuring extracellular glutamate concentration as

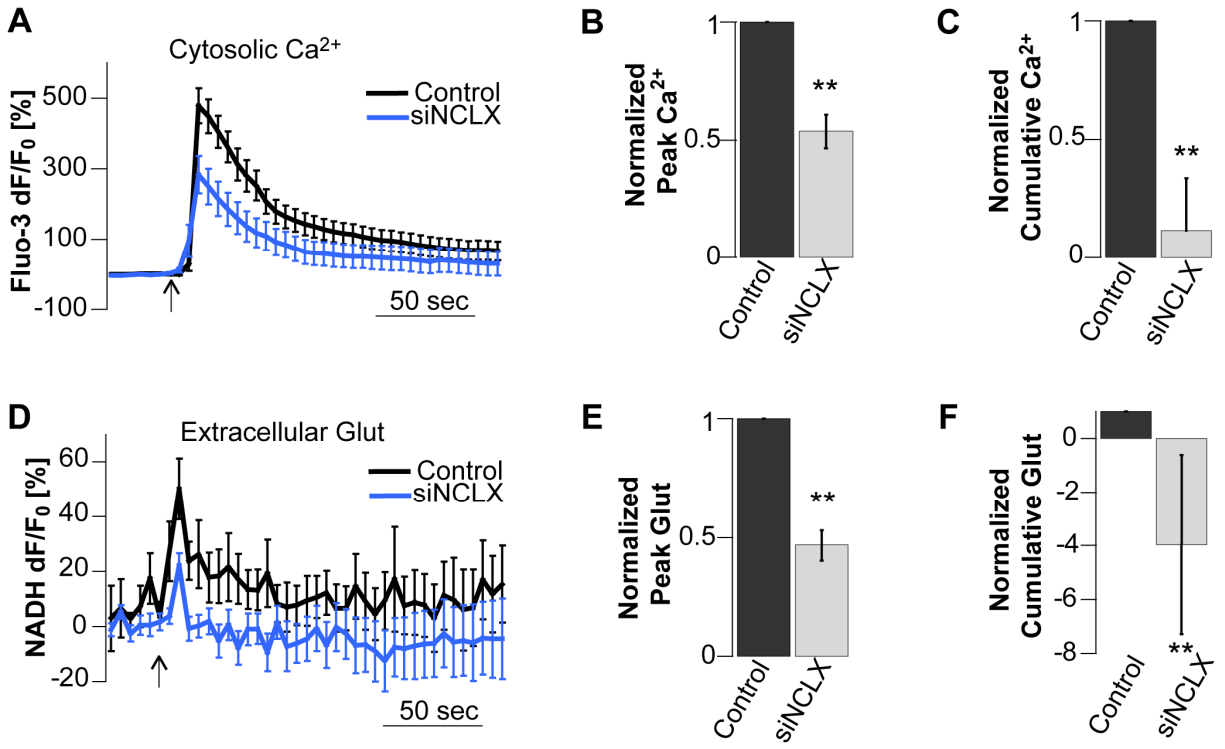

Figure 4.17. NCLX mediates cytoplasmic Ca^{2+} increase and exocytotic glutamate release in astrocytes after mechanical stimulation

(A-C) Cytosolic Ca^{2+} measurements. ***(A)*** Time lapse of average Fluo-3 fluorescence, reporting on changes in cytosolic Ca^{2+} in solitary astrocytes transfected with either non-targeted siRNA (Control) or siNCLX in response to mechanical stimulation; all cells were co-transfected with the red transfection marker siGLO. ***(B)*** Normalized Fluo-3 peak and ***(C)*** cumulative fluorescence values of mechanically stimulated solitary astrocytes in ***A***. ***(D-F)*** Extracellular glutamate measurements. ***(D)*** Average kinetics of extracellular NADH fluorescence, reporting on mechanically-induced changes in extracellular glutamate surrounding somata of solitary astrocytes that were transfected as in ***A***. ***(E)*** Normalized peak and ***(F)*** cumulative glutamate (Glut) release from mechanically stimulated solitary astrocytes in ***D***. Solitary astrocytes transfected with siNCLX displayed significantly (Mann-Whitney U-test, **$p < 0.01$) reduced mechanically-induced cytosolic Ca^{2+} increase and glutamate release when compared to control transfected cells. The points and bars represent means ± SEMs of measurements from individual astrocytes (N=15); Arrows in ***A*** and ***D*** represent the time when mechanical stimulation was applied to the cells. (The data and analysis were provided by Dr. V. Montana and Prof. V. Parpura, University of Alabama, Birmingham, AL, USA)

increase in fluorescent product NADH. Mechanical stimulation of astrocytes evoked an

increase in fluorescent NADH levels (n=15; peak dF/F_o= 50 ± 11%; paired t-test **p < 0.01) (Figure 4.17D), corresponding to astrocytic glutamate release. As was expected from the NCLX effect on mechanically-evoked Ca^{2+} signal, NCLX knock-down diminished the amplitude of the glutamate release by 53% (n=15, peak normalized=0.47±0.06, **p<0.01) and totally abolished cumulative glutamate secretion (n=15, from 1.0 for control to -3.98±3.10 for siNCLX-treated cells, **p<0.01) (Figure 4.17D-F). Molecular silencing of NCLX had a much greater effect on glutamate release than was previously reported using the pharmacological inhibition by CGP37157 (Reyes and Parpura, 2008). Probably, non-specific effects of CGP37157 (Neumann et al 2011, Czyz and Kiedrowski, 2003, Thu et al. 2006) could hide the actual effect of NCLX on astrocytic Ca^{2+} excitability and gliotransmission. These data show a key role of NCLX for mediating cytosolic Ca^{2+} signaling and exocytotic glutamate release.

NCLX affects wound healing in vitro and astrocyte proliferation

Astrocyte migration and proliferation play an important role in the brain's response to injury and during regeneration. Mitochondria and Ca^{2+} homeostasis are critical to the regulation of these cellular responses (Feldman et al., 2010; Valero et al., 2008; Wei et al., 2009; Xu et al., 2004).Therefore, I asked whether mitochondrial Na^+/Ca^{2+} exchanger NCLX may affect these functional parameters in astrocytes. To assess the effect of NCLX on migration and proliferation I used an *in vitro* astrocytic wound healing assay described previously (Matyash et al., 2002). Monolayers of astrocytes that had either been treated with NCLX siRNA or with CGP37157 were scratched and the closure of the open wound area was measured at 0 hrs and 48-72 hrs after wounding as described by Geback et al. (Geback et al., 2009) (Figure 4.18A-B). Both pharmacological inhibition of NCLX by CGP37157 and molecular silencing of NCLX via siRNA significantly impaired the astrocytic ability to close an open wound area (Figure 4.18C, D). While the wound area was closed to more than two thirds after 48-72h in control cultures, it remained significantly larger when NCLX was inhibited: mean open wound area at the end point was 62.8±3.7% for CGP37157-treated astrocytes (34.45±2.65% for control astrocytes, N=5 experiments, n=30 scratches, ***p<0.001) (Figure 4.18C). Open wound areas in NCLX silenced astrocytes were 48.5±2.6% on average compared to 24.6±2.5% for the control conditions, N=3, n=20, ***p<0.001) (Figure 4.18D).

The *in vitro* wound healing assay does not distinguish between migration and proliferation. To assess whether the effect of NCLX-inhibition was due to impaired cell proliferation, I performed

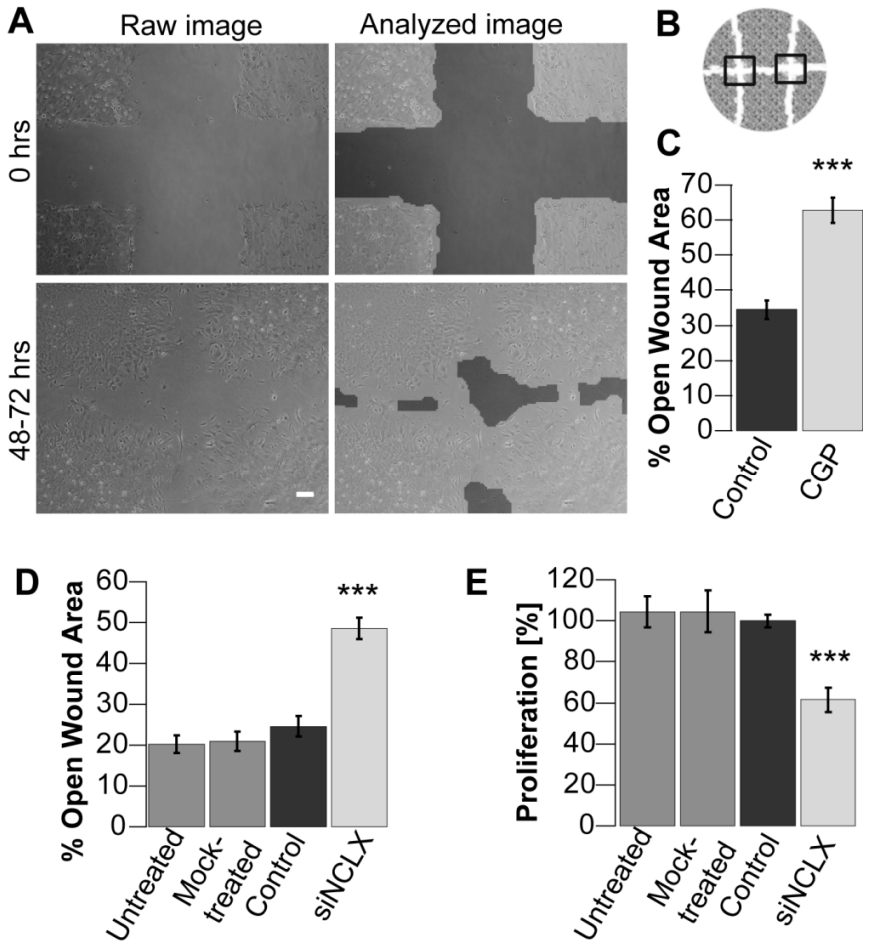

Figure 4.18. NCLX participates in astrocytic in vitro wound healing and proliferation

(A) Confluent astrocytic monolayers were wounded as described and phase contrast images were acquired at 0 hrs *(top row)* and after 48-72 hrs *(bottom row)* at low magnification. Left column shows raw images, and right column shows the same images after analysis with Tscratch software. Dark grey areas correspond to the open wound area; values at endpoint are normalized to 100% area at starting point (0 h). Scale bar 100 µm. ***(B)*** Scheme exemplifies how scratches *(white lines)* were applied to astrocytic monolayers *(grey areas)*. Black frames correspond to the analyzed area of interest. ***(C)*** % open wound area in monolayers that were untransfected, mock-transfected (only lipofectamine), transfected with control siRNA or siNCLX (N=3 cultures, n=18, 16, 20, 20 scratches, respectively). Values are given as mean ± SEM (***p<0.001, Student t-test for unpaired samples, two-tailed). ***(D)*** BrdU incorporation into proliferating astrocytes that were either untransfected, mock-transfected, or transfected with control siRNA or siNCLX, given as % proliferation normalized to control (N=3 cultures, n=15 wells) (***p<0.001, Mann-Whitney U-test).

cell proliferation ELISAs based on the measurement of BrdU incorporation. NCLX knock-down decreased astrocyte proliferation by 38.6% as compared to non-targeted siRNA-transfected astrocytes (control) (N=3, n=15 wells, ***p<0.001) (Figure 4.18E). This decrease was not due to a possible harmful effect of the transfection since the proliferation in both untransfected and mock-treated astrocytes was similar to control-transfected cells. Taken together, these findings indicate that the mitochondrial Na^+/Ca^{2+} exchanger NCLX is involved in control of astrocytic wound healing, most probably due to its effect on controlling cell proliferation.

Chapter 5

Discussion

Ca^{2+} signaling is the astrocyte form of excitability and is controlled by several families of Ca^{2+} transporting or buffering proteins in the plasma membrane, the cytoplasm and intracellular organelles, most notably the ER and the mitochondria. Mitochondria are critically involved in Ca^{2+} handling in glial cells, thereby modifying astrocytic function (Parpura and Verkhratsky, 2011; Verkhratsky et al., 2011). Here, I used cell fractionation, immunological assays, subcellular Ca^{2+} imaging and physiological assays combined with RNA_i-mediated inhibition of NCLX activity to address the specific role of NCLX, the recently identified mitochondrial Na^+/Ca^{2+} exchanger, on shaping glial mitochondrial and cytoplasmic Ca^{2+} signals and studied its impact on Ca^{2+}-dependent glial functions. I showed that NCLX is enriched in glial mitochondria and is a key component responsible for Ca^{2+} extrusion from the mitochondria in astrocytes. The exchanger's activity has a major impact on modulating cytoplasmic Ca^{2+} signals in astrocytes and microglia, as well as their functional output, exocytotic glutamate gliotransmission and wound healing capacities for astrocytes and secretory and migratory abilities for microglia. My findings furthermore suggest that the NCLX effect on cytoplasmic Ca^{2+} dynamics is mediated mainly via modulation of the store operated Ca^{2+} entry pathway, SOCE, in astrocytes, whereas the ER dependent Ca^{2+} release is less affected .

5.1 NCLX expression profile: Where, How, When and What?

Several approaches were used in this study to show NCLX expression: (i) histological approach allows to look for localization and architecture of NCLX expression in the brain only at the qualitative level; (ii) RT-PCR approach allows to see NCLX gene expression and quantify it; (iii) Western blot analysis reveals translation of NCLX with the possibility to quantify and to localize

protein expression to a certain region. However, Western blot cannot provide any information about architecture or the amount of cells expressing NCLX. All the techniques mentioned above do not provide any information about the functionality of the protein.

According to the previous studies, at the mRNA level NCLX is expressed both in mouse and in rat (Cai and Lytton, 2004). The richest expression in rat was found in the lung, followed by large intestine and then kidney and thymus. In mouse, NCLX expression was the highest in the lung, followed by skeletal muscle and heart. Protein NCLX expression was shown only in rat, where it was the highest in pancreas, followed by skeletal muscle, then stomach and skin (Palty et al., 2004). The same study revealed extremely low protein expression in the lung. Regarding the brain, mRNA expression was about an average level in both mouse and rat brains, NCLX protein levels in the rat brain were low compared with other tissues.

My study confirmed high NCLX protein expression in the pancreas and lower expression in the brain. However, the interesting observation was age-dependent regulation of NCLX expression: low at the late embryonic period and increasing towards the adulthood. Age-dependent changes in Ca^{2+} homeostasis in different tissues were shown on the protein and functional level (Buchholz et al., 2007; Delbono, 2011; Puzianowska-Kuznicka and Kuznicki, 2009; Squier and Bigelow, 2000; Toescu and Verkhratsky, 2004; Verkhratsky et al., 1994). Particularly, changes in mitochondrial Ca^{2+} handling were suggested to be linked to the physiological and pathological ageing processes in the brain, culminating in neurological age-dependent disorders (Buchholz et al., 2007; Toescu and Verkhratsky, 2004). My data show the first indication for the change in the expression of one of the major players in mitochondrial Ca^{2+} machinery in different brain regions with aging. The results of Xiong et al. (Xiong et al., 2002) suggest that during intense neuronal activity, characterized by repetitive Ca^{2+} rises, in the aged brain neuronal mitochondria cannot sufficiently restore their Ca^{2+} shuttling capacity. Although my data do not reveal what is happening in the aged brain, as adult mice in my study were two months of age, it strongly suggests that there are changes in the components of the mitochondrial Ca^{2+} machinery through the lifespan: NCLX expression becomes higher towards the adulthood with possibilities of alteration towards the elderliness. This raises many intriguing questions regarding the role of the mitochondrial Ca^{2+} handling in development and aging in different brain cell populations and their effect on the brain functions. However, to draw a more conclusive decision, these data should be confirmed and more thorough analysis should be applied.

NCLX immunohistochemistry of the brain revealed few cell populations expressing the exchanger. NCLX expression was clearly visible in different neuronal populations of the

cerebellum and brainstem, and neuronal expression is expected, as there is evidence of the existence of the functional mitochondrial Na^+/Ca^{2+} exchange in the excitable cells (Pizzo et al., 2012). The result concerning NCLX expression in the ependymal-like cells in the choroid plexus is new, however due to the powerful secretory activity of these cells and due to the existence of functional Ca^{2+} machinery (Genzen et al., 2009; Johansson et al., 2007) and stronger Ca^{2+} extrusion via the activity of the mitochondrial Na^+/Ca^{2+} exchange than H^+/Ca^{2+} exchange, high expression of the mitochondrial Ca^{2+} handling machinery and particularly NCLX could be anticipated in these cells. For example, such highly secretory cells as pancreatic β-cells express NCLX, and it is the exchanger responsible for the mitochondrial Ca^{2+} extrusion in these cells and affecting their secretory activities (personal communication with Prof. I.Sekler). These results raise numerous questions regarding the mechanism of Ca^{2+} signaling in these cells and the effect of mitochondrial Ca^{2+} handling on their physiology. In cultured astrocytes functional mitochondrial Na^+/Ca^{2+} exchange was shown (Bernardinelli et al., 2006), therefore I expected to see its expression, but to my surprise, NCLX expression was very heterogeneous in the astrocytes of different brain regions, with astrocytic immunolabeling in most regions of the brain not being above the background level. These results may indicate to astrocytic heterogeneity, which is known and has been reviewed by Matyash et al. (Matyash and Kettenmann, 2010). Thus, to be able better understand astrocytic function, this is important to focus the investigation of astrocytic function to a certain brain region and specific cell type. However, it may also be possible that this heterogeneous labeling is simply due to the technical reasons. For example, NCLX antibody could be less suitable for *in situ* immunolabeling, as it could recognize better the unfolded protein.

Much clearer results than in immunohistochemistry were seen with the Western blot analysis. I clearly proved the expression of NCLX protein in astrocytes and microglia. Astrocytes and the astrocytic cell line express probably two isoforms, the more abundant one with a molecular weight of about 55-60 kDa, which was also found in other brain cell types and total brain extracts, and a 100 kDa form that is related to as SDS resistant NCLX dimer. This is in accordance with the expected molecular weight of 60kDa according to the protein database (http://www.uniprot.org/uniprot/Q925Q3) and previous studies that identified isoforms about 55, 70, and 100 kDa, the latter being consistently related to an SDS resistant NCLX dimer (Palty et al., 2006; Palty et al., 2004).

When comparing NCLX expression in different organelle-enriched fractions of astrocytes, I found that NCLX was strongly enriched in mitochondria, indicating that it is primarily located in

these organelles. Interestingly, the molecular weight of mitochondrial NCLX was slightly reduced to about 50 kDa compared to the other cellular compartments. Reduction of molecular weight was also observed in mitochondrial fractions from HEK293T cells, murine heart and brain (Palty et al., 2010) and may be explained by the possible cleavage of NCLX by mitochondrial proteases during NCLX import and translocation into the mitochondrial membrane (Chacinska et al., 2009; Wiedemann et al., 2004). Although the physiological role of such processing is not yet clear, and we cannot rule out whether NCLX cleavage occurred during mitochondrial isolation, the reduction in molecular weight is consistent with the sensitivity of NCLX to mitochondrial proteases such as mitochondrial calpains. In endothelial cells it was previously documented that calpain1 cleaves the mitochondrial exchanger leading to mitochondrial Ca^{2+} accumulation (Smith and Schnellmann, 2012). Alternatively, because our antibody is targeted to the C-terminal domain of NCLX, cleavage is likely to occur on the N-terminal domain. The N-terminal domains usually harbor mitochondrial targeting sequence that is often removed during its mitochondrial insertion (Chacinska et al., 2009; Wiedemann et al., 2004). NCLX has a predicted signal peptidase cleavage site (Figure 1.5), which may serve as a mitochondrial targeting sequence. While this possibility needs to be tested further it raises interesting questions regarding the mechanism of NCLX import and cleavage in mitochondria. How are other proteins of mitochondrial Ca^{2+} machinery targeted to mitochondria? Is their cleavage and targeting a subject to activity-dependent regulation? However, the identification and enrichment of NCLX in mitochondrial fractions allows to conclude that NCLX is the mitochondrial exchanger in astrocytes, and thus the specific molecular tools employed in our previous work to inhibit NCLX (Palty et al., 2010), can also be effectively employed to study the role of NCLX for glial Ca^{2+} homeostasis and physiological functions.

5.2 Why is NCLX knock-down preferable to the pharmacological inhibition of the exchanger?

For more than 20 years CGP37157 was the most specific pharmacological inhibitor to study the mitochondrial Na^{+}/Ca^{2+} exchanger and its role in cellular Ca^{2+} homeostasis. The drug was employed in previous studies on mitochondrial regulation of astrocytic Ca^{2+} homeostasis and function. Recent reports, however, show that this benzothiazepine compound also affects other targets, involved in cellular Ca^{2+} handling. In sarcoplasmic reticulum (SR) of skeletal muscle,

CGP37157 in concentrations above 5μM decreased SERCA-mediated Ca^{2+} uptake into SR and increased the RyR-mediated Ca^{2+} leak from SR (Neumann et al., 2011). Other reports have suggested that CGP37157 affects L-type Ca^{2+} channels in myocytes (Thu le et al., 2006). These Ca^{2+}-regulating proteins are also instrumental for astrocytic Ca^{2+} homeostasis (Parpura and Verkhratsky, 2011; Verkhratsky et al., 2011). Therefore, high concentrations of CGP37157 used in the previous studies may have affected other Ca^{2+}-signaling molecules and consequently, may have masked the real contribution of the mitochondrial exchanger. After the molecular entity of the mitochondrial exchanger has been identified (Palty et al., 2010), a much more specific tool, namely specific siRNA, can be implemented to acutely knock-down NCLX. This allows for the first time to determine NCLX effect on astrocytic Ca^{2+} dynamics and consequences for its function.

The recent study by Palty et al. (Palty et al., 2010) used specific siRNA to knock-down NCLX expression and convincingly showed that siNCLX significantly reduces mitochondrial Ca^{2+} efflux from HEK293T cell line and dopaminergic neuronal cell line SH-SY5Y. I used this knowledge to knock-down NCLX function in glia. To ensure that siNCLX specifically inhibits NCLX expression I used the following controls during the optimization of NCLX knock-down and some of them throughout the study: (i) fluorescently-tagged siRNA (siGLO) was used to monitor siRNA delivery into the cells; (ii) as a positive control cells were transfected with siRNA vs. GAPDH, which is known to efficiently target this protein; (iii) an untreated control was used to examine the background levels of NCLX expression for each culture; (iv) a mock-transfected control was used to assess the effect of the transfection reagent on the level of NCLX expression for each culture; (v) as negative control cells were transfected with non-targeted siRNA. The latter is important for the evaluation of siRNA transfection on the NCLX expression and thus was used in all the experiments involving NCLX knock-down. While the siRNA transfection procedure on itself affected the NCLX expression levels in the murine macrophage cell line RAW264.7, it did not very much alter the NCLX expression level in primary murine astrocytes and microglia. Therefore, the molecular silencing procedure using siNCLX is eligible in primary glial cells to specifically knock-down the mitochondrial exchanger.

This study showed for the first time the difference in using specific molecular tools vs. pharmacological inhibitor. For example, the effect of molecular silencing of NCLX on the mechanically-induced cumulative Ca^{2+} signal and glutamate secretion in astrocytes was much larger than reported earlier for CGP37157 (Reyes and Parpura, 2008). Although the previous study used rat astrocytes and not mouse, and species differences cannot be excluded, it is

likely that the inhibitory effect of CGP37157 on the mitochondrial exchanger may have partially masked the full capacity of the mitochondrial exchanger NCLX by modulating the Ca^{2+} influx mediated by other Ca^{2+} transporters.

5.3 How does NCLX influence mitochondrial Ca^{2+} fluxes?

My data regarding NCLX involvement in mitochondrial Ca^{2+} handling was acquired only in astrocytes. The small amplitudes of the mitochondrial Ca^{2+} responses acquired in microglia combined with noise lead to a small signal/noise ratio that resulted in mitochondrial Ca^{2+} answers which were almost impossible to analyze. Further, tedious optimization of the transfection procedure for the mitochondrial Ca^{2+} sensor mtRP might possibly have lead to a better signal/noise ratio and might have helped to overcome this problem. However, as it is well known that primary cultures of the macrophage/monocytic lineage are extremely difficult to transfect, I decided rather to focus my efforts on astrocytic cells than on microglia.

In astrocytes I showed that blocking NCLX activity, both by molecular silencing via siRNA and by using CGP37157 strongly reduced mitochondrial Ca^{2+} efflux, therefore supporting the importance of NCLX in mitochondrial Ca^{2+} extrusion. Importantly, inhibition of the mitochondrial Na^{+}/Ca^{2+} exchanger not only resulted in a reduced Ca^{2+} efflux in astrocytes but at the same time in an increased mitochondrial Ca^{2+} influx, both during ATP stimulus and SOCE (Figures 4.8 and 4.9). Such an effect of inhibition of mitochondrial Ca^{2+} efflux on Ca^{2+} uptake has been previously reported to be specific for astrocytes (Bambrick et al., 2006) vs. neurons, when another protein participating in mitochondrial Ca^{2+} efflux, the mitochondrial permeability transition pore, was inhibited. Pharmacological inhibition of the exchanger with CGP37157 elevated the mitochondrial Ca^{2+} peak amplitude upon agonist stimulation in cell lines containing mitochondrial mutations that affect oxidative phosphorylation (Brini et al., 1999). In the study by Palty et al., knock-down of NCLX lead to the inhibition of mitochondrial Ca^{2+} extrusion combined with the elevation of mitochondrial Ca^{2+} uptake in HEK293T and SH-SY5Y cells (Palty et al., 2010). This effect was not reported in the study, but can be observed from the mitochondrial Ca^{2+} imaging curves of control vs. NCLX-silenced cells. In contrast, in malignant melanoma cell lines NCLX inhibition by CGP37157 decreased the mitochondrial Ca^{2+} uptake (Feldman et al., 2010). These results indicate that the effect of mitochondrial Ca^{2+} efflux inhibition may be cell-specific. What underlies the cell type specificity of such responses? Is this

connected to the role that oxidative phosphorylation plays in the cell? The observed mitochondrial Ca^{2+} increases are the net result of primarily Ca^{2+} uptake via the uniporter and Ca^{2+} extrusion via the exchanger (additional mitochondrial Ca^{2+} uptake and extrusion routes may also play a role). Therefore, when the exchanger is not fully active, net Ca^{2+} accumulation in the matrix may be increased. The interesting questions are to which extent the mitochondrial Na^{+}/Ca^{2+} exchanger regulates mitochondrial Ca^{2+} uptake in different cell types and what are the physiological consequences.

Another interesting observation from my study is an elevated basal mitochondrial Ca^{2+} level upon NCLX knock-down in astrocytes. Fast Ca^{2+} uptake into mitochondria occurs upon spontaneous activation of IP_3Rs (Cardenas et al., 2010), and constant transfer of Ca^{2+} from IP_3Rs to mitochondria supports the cell's pro-survival pathways via macroautophagy suppression. However, fast mitochondrial Ca^{2+} uptake is not the only mechanism for Ca^{2+} elevation in the mitochondria. In the quiescent state there is a slow Ca^{2+} uptake into mitochondria (Pizzo et al., 2012), and reduced mitochondrial Ca^{2+} efflux combined with the same uptake could result in the net elevated basal mitochondrial Ca^{2+}. Augmented mitochondrial Ca^{2+} could cause either higher sensitivity to apoptotic stimuli or increased pro-survival (Cardenas et al., 2010; Contreras et al., 2010).

5.4 How is NCLX involved in shaping cytosolic Ca^{2+} responses?

ATP and C5a-evoked responses

The spatial and temporal profile of the cellular Ca^{2+} responses triggered by metabotropic as well as mechanical stimulation plays a key role in regulating executive glial functions, such as gliotransmission (Parpura and Verkhratsky, 2011) or wound healing response for astrocytes or secretion of pro- or anti-inflammatory molecules from microglia (Kettenmann et al., 2011). Ca^{2+} transients in response to Ca^{2+}-mobilizing stimuli or as a consequence of mechanical stimulation were analyzed with regard to (i) peak amplitude/peak response, which is a result of an interplay between Ca^{2+} entry into the cytosol from the ER store and extracellular space and immediate sequestration by mitochondria; (ii) half-amplitude time, which includes primarily the declining phase of Ca^{2+} response, exposing Ca^{2+} clearance from the cytosol by PMCA on the plasma membrane and SERCA on the ER (Kim et al., 2005; Reyes et al., 2012), as well as on opposing

slow Ca^{2+} release by mitochondria (Reyes and Parpura, 2008; Reyes et al., 2011); (iii) the cumulative response, which combines all the parameters of both Ca^{2+} increase and decrease. To distinguish between responses originating from the ER or the extracellular space, I used Ca^{2+}-full or Ca^{2+}-free extracellular solution. In nominally Ca^{2+}-free external solution, Ca^{2+} elevation in response to cell stimulation with ATP could originate only from Ca^{2+} release from the internal stores into the cytoplasm. Under these conditions all contributions of extracellular Ca^{2+} influx into the cytoplasm, either through ionotropic purinergic receptors or through SOC could be virtually excluded. Mitochondrial involvement in shaping Ca^{2+} signals originating from ER is expected. First of all, the close interaction between ER and mitochondria is well documented (Csordas et al., 2010; Giacomello et al., 2010) and it has been shown that the proteins linking the surfaces of both organelles affect ER-mitochondrial Ca^{2+} transfer (de Brito and Scorrano, 2008; Kornmann et al., 2009). One of these proteins is IP_3R. Ca^{2+} increases via IP_3Rs were shown to create high Ca^{2+} microdomains, which were detected by mitochondria (Csordas et al., 2010; Giacomello et al., 2010). In turn, Ca^{2+} near IP_3Rs regulates its activity. Under IP_3-saturated conditions, Ca^{2+} stimulates IP_3R activity until a certain threshold of $[Ca^{2+}]$ Above this threshold Ca^{2+} inhibits IP_3R activity (Foskett et al., 2007). The threshold and the kinetics of this biphasic Ca^{2+} regulation depend on the cell-type and the IP_3R type (Foskett et al., 2007). Mitochondrial Ca^{2+} shuttling in the close proximity to IP_3Rs can therefore enhance or inhibit IP_3R mediated ER-Ca^{2+}-release into the cytoplasm (Hajnoczky et al., 1999; Landolfi et al., 1998).

Here I show that astrocytes and microglia with reduced mitochondrial Ca^{2+} efflux have impaired IP_3R-mediated Ca^{2+} signaling. Detailed statistical analysis of the cumulative ATP-evoked cytosolic Ca^{2+} responses in astrocytes revealed that NCLX knock-down results in the appearance of the second population of “low responders”, which could be observed from the bimodal distribution of Ca^{2+} responses. In the NCLX-deficient astrocytes the peak of the “low responders” appears in the range of 20-30% of cumulative Ca^{2+} responses (Figure 4.11G). NCLX knock-down therefore severely decreased IP_3R-mediated cytoplasmic Ca^{2+} signals only in a subpopulation of the astrocytes (about 25% of the population) while in the majority of astrocytes the net ER-Ca^{2+} release from IP_3Rs appeared to be less affected by knocking down the activity of the mitochondrial exchanger. Which astrocytes were more prone to this inhibition and why? There are several possibilities. First, the selective inhibitory effect may be due to the astrocytic heterogeneity, as the astrocytes in this study are derived from the whole cortices. For example, astrocytes from different brain regions differ in their morphology, communication via

Ca^{2+} waves and features of Ca^{2+} oscillations (Matyash and Kettenmann, 2010), indicating on the possibility of differential expression of Ca^{2+} signaling molecules and/or diverse subcellular arrangement. Another simple explanation arises that NCLX knock-down is not uniform in all the cells and actually, the measurable effect on IP_3-mediated Ca^{2+} transients may be visible only if NCLX knock-down reaches a certain threshold. In general, this effect may be explained by the effect of NCLX inhibition on the ER Ca^{2+} stores. Previous data show that blockade of the mitochondrial Na^+/Ca^{2+} exchanger decreases the ER Ca^{2+} content in various cell systems (Belmonte and Morad, 2008; Griffiths et al., 1997; Malli et al., 2005). However, it has to be considered that all the previous experiments were performed under non-specific pharmacological inhibition with possible "side" effects of the CGP37157 on ER Ca^{2+} stores via modulation of RyRs and SERCA (Neumann et al., 2011).

ER Ca^{2+} stores are thought to be refilled via SOCE pathway (Parekh and Putney, 2005; Putney, 2009). The effect of NCLX knock-down on the ER Ca^{2+} store refilling pathway, SOCE, was obvious from my results in both astrocytes and microglia. Reduced SOCE due to NCLX depletion may result in reduced Ca^{2+} content of the ER. The effect of NCLX knock-down on IP_3-triggered Ca^{2+} signaling may be different, however, in astrocytes *in vitro* and *in vivo* due to differences in ER architecture in both systems (Pivneva et al., 2008). In microglia the effect of NCLX inhibition on ATP-evoked Ca^{2+} signals was investigated using the pharmacological approach and seems to be larger than in astrocytes. The difference of NCLX inhibition on IP_3-mediated Ca^{2+} signaling in microglia and astrocytes may relate to their different cellular Ca^{2+} toolkit, difference in the subcellular arrangement and side effects of CGP37157 or/and possible side effects of siRNA treatment.

Stimulation with ATP or complement C5a in Ca^{2+}-full buffer triggers cytoplasmic Ca^{2+} entry from both intracellular and extracellular Ca^{2+} pools. The rise in $[Ca^{2+}]_{cyt}$ upon stimulation with ATP is contributed by metabotropic and ionotropic purinergic receptors, while complement C5a evokes metabotropic response in microglia. The decline in $[Ca^{2+}]_{cyt}$ is contributed via SERCA on the ER, PMCA and NCX on the plasma membrane. SOCE prolongs the declining phase, resulting in a biphasic decline with a plateau phase. In astrocytes, the larger effect of NCLX inhibition on ATP-evoked cytoplasmic Ca^{2+} transients in Ca^{2+}-full buffer than in Ca^{2+}-free buffer could be explained by the effect on SOCE and, possibly, also by a contribution of ionotropic P2X receptors. In microglia, the effect of NCLX inhibition on C5a-mediated Ca^{2+} transients was very large, mostly affecting the declining phase of the response. This outcome may be contributed by NCLX effect

on cytoplasmic Ca^{2+} entry pathways, like SOCE and IP_3Rs. Additionally, NCLX may regulate Ca^{2+} efflux from the cytosol via SERCA or PMCA.

SOCE

The store operated Ca^{2+} entry (SOCE) is the major Ca^{2+} influx pathway in glia (Kettenmann et al., 2011; Verkhratsky et al., 2012). Although Ca^{2+} influx through SOC is triggered by the depletion of Ca^{2+} from the ER, their gating is strongly regulated by the mitochondrial Ca^{2+} shuttling (Parekh, 2008) via several mechanisms: (i) mitochondrial uptake of Ca^{2+} released via IP_3Rs can stimulate the activity of IP_3Rs and therefore can enhance ER Ca^{2+} store depletion, augmenting SOC activity; (ii) Ca^{2+} shuttling via mitochondria can reduce the local $[Ca^{2+}]$ in subplasmalemmal microdomains below the open SOC channel, reducing Ca^{2+}-dependent slow inactivation of SOC and prolonging SOCE; (iii) mitochondria depolarized due to Ca^{2+} accumulation can negatively affect Stim1 mobility across the ER membrane, therefore preventing disengagement of Stim1 and Orai channels, which give rise to SOCE (Bakowski et al., 2012).

Ca^{2+} influx through SOC plays a role in prolonging intracellular Ca^{2+} responses and influencing numerous cellular activities, including neurotransmitter release (Berridge et al., 2003). Interaction of the SOC pathway with the mitochondrial Ca^{2+} shuttling machinery has been documented in many cell types (Ardon et al., 2009; Feldman et al., 2010; Glitsch et al., 2002; Hoth et al., 1997; Malli et al., 2003). Interestingly, not only a mitochondrial Ca^{2+} uptake, but also an efficient mitochondrial Ca^{2+} efflux is crucial to maintain the prolonged Ca^{2+} influx through SOC (Malli et al., 2003). For glia, the role of mitochondria in regulating SOC activity and downstream responses is poorly understood, and NCLX provides a specific molecular handle to address their role.

My work shows that an impaired mitochondrial Ca^{2+} efflux due to inhibition of NCLX reduces both the entry rate of Ca^{2+} through SOC as well as the peak amplitude of the SOC-induced cytoplasmic Ca^{2+} signals in astrocytes and microglia. As shown previously, mitochondrial Ca^{2+} shuttling decreases $[IP_3]$ needed to activate SOCE by a factor of two and increases the dynamic range of $[IP_3]$ for SOCE (Gilabert et al., 2001). Mitochondrial involvement in the facilitation of ER store depletion could be involved in the initial phase of SOCE, contributing to the entry rate of Ca^{2+} through SOC. However, contribution of other channels, like P2XRs for $[Ca^{2+}]_{cyt}$ elevation or Ca^{2+} clearance pathways cannot be excluded. The effect of NCLX on the amplitude of SOCE could be primarily explained by the mitochondrial involvement in the sustained Ca^{2+} influx via

SOC, either through the effect on slow Ca^{2+}-dependent inactivation of SOC or by affecting motility of Stim1. The full influence of NCLX on SOCE, however, may be masked by cytoplasmic Ca^{2+} extrusion mechanisms. For example, extrusion of cytosolic Ca^{2+} via PMCA has a flexible dynamic range, which increases following SOCE (Bautista et al., 2002).

Giacomello M. et al. (Giacomello et al., 2010) suggest that mitochondrial participation in SOCE regulation may be indirect. They show that mitochondria in the vicinity of SOC are not exposed to high Ca^{2+} microdomains, thus SOCE may not be directly affected by mitochondria. As I did not apply high resolution Ca^{2+} imaging techniques in my study, a direct effect of the mitochondrial Ca^{2+} on SOCE, although possible, cannot be concluded from the results. Similarly as described by Giacomello et al, one can speculate that the NCLX modulation of SOCE may be indirect via the effect on the ER Ca^{2+} stores, for example. To exactly define the control mechanism and make a stronger conclusion, direct measurements of the ER Ca^{2+} content upon NCLX silencing or high resolution imaging with membrane-tethered Ca^{2+} indicators would be needed. Reduction of SOCE due to NCLX inhibition could influence SOCE-dependent functions. For example, in astrocytes SOCE has been shown to affect ATP-evoked Ca^{2+} oscillations and glutamate release (Malarkey et al., 2008; Sergeeva et al., 2003). In rat astrocytoma cell line C6 SOCE participated in ATP-induced secretion of chemokines MCP-1 and IL-8 (Jantaratnotai et al., 2009). In human microglia, SOCE contributed to PAF-triggered IL-6 expression (Sattayaprasert et al., 2005). In human monocytic THP-1 cells, SOCE contributed to the release of neurotoxic factors, like TNFα, IL-6 and NO (Lee et al., 2010). Moreover, microglial SOCE is the Ca^{2+} pathway altered upon inflammation and in neurological diseases like Alzheimer disease (Beck et al., 2008; McLarnon et al., 2005). Why was SOCE in both glial cell types so strongly affected by the activity of NCLX, while IP_3R-mediated ER-Ca^{2+} signaling was only moderately influenced (see above)? Maybe, the hypothesized effect on the ER Ca^{2+} stores as discussed above more strongly affects SOCE than the IP_3R-mediated Ca^{2+}_{cyt} elevation. This difference can be also explained by the possibility of larger influence of the mitochondria to plasma membrane Ca^{2+} transporters due to mitochondrial distribution and properties. For instance, Kolikova et al. recently showed in astrocytes, that stimulation with ATP triggered a Ca^{2+}-dependent translocation of mitochondria to the plasma membrane (Kolikova et al., 2006). This could be another mode of how mitochondria regulate the perimembrane Ca^{2+} dynamics, and probably functional NCLX plays an important role in this process. Further experiments are required to dissect which regulatory mechanisms exactly account for the strong effect on SOC in glial cells.

Propagation of intercellular Ca^{2+} waves: does NCLX contribute?

Rapid Ca^{2+} waves are a major communication pathway of the astrocytic network and of neuronal astrocytic communication. The mechanisms responsible for the propagation of intercellular Ca^{2+} waves upon mechanical stimulation in astrocytes have been intensively studied and are reviewed by Haas et al. (Haas and Kettenmann, 2009). Briefly, mechanical stimulation evokes the release of ATP from astrocytes, followed by activation of metabotropic purinergic receptors on the neighboring cells. Simultaneously, IP_3 spreads intracellularly via gap-junctional communication into the astrocytic network. The intercellular ATP wave precedes the wave of Ca^{2+} elevation, indicating the importance of purinergic signaling for the propagation of Ca^{2+} between the astrocytes. Mechanical stimulation of astrocytes also evokes a Ca^{2+}-dependent glutamate wave, which propagates with a speed of 26 µm/sec, while the Ca^{2+} wave spreads with a speed of 10-30 µm/sec (Innocenti et al., 2000). However, the contribution of the glutamate wave to the propagation of astrocyte intercellular Ca^{2+} wave has to be shown. In my work I showed that NCLX silencing had no significant effect on the propagation speed of the astrocytic Ca^{2+} wave, although there was a slight decrease in the area of the wave, when NCLX function was blocked. Below I will discuss possible explanations for the slight influence of NCLX on the propagation of Ca^{2+} waves:

i. Decreased purinergic Ca^{2+} signaling may decrease the wave propagation. $P2Y_2R$ is the major receptor involved in the propagation of the astrocyte Ca^{2+} wave (Haas and Kettenmann, 2009). However, as shown here, the effect of NCLX knock-down on purinergic metabotropic signaling was only very moderate and affected only 25% of the astrocytes in the entire population (see above); this amount of “NCLX-impaired” cells is probably not sufficient to significantly down-modulate the propagation speed.
ii. The release of ATP upon stimulation could be decreased resulting in smaller Ca^{2+} wave’s propagation. This possibility is likely due to the severe impairment in the release of another gliotransmitter, glutamate following mechanical stimulation upon NCLX knock-down, although mitochondrial involvement in ATP and glutamate release from astrocytes may differ due to the difference in the secretion mechanism of both gliotransmitters (Coco et al., 2003).
iii. Mitochondrial Ca^{2+} changes may affect astrocyte communication via gap junctions
iv. Inhibition of the mitochondrial Ca^{2+} uptake via the dissipation of mitochondrial membrane potential with FCCP and oligomycin accelerated the propagation of Ca^{2+} signal inside an

astrocyte by 50% (Boitier et al., 1999). My results show that NCLX inhibition increases mitochondrial uptake, therefore possibly inhibiting the intracellular propagation of the Ca^{2+} signal.

5.5 How NCLX participates in the wound healing *in vitro*: connection between injury, astrogliosis and Ca^{2+}

Astrocytes respond to any CNS injury by a process, commonly referred as astrogliosis. Reactive astrogliosis is one of the players orchestrating the injury response in the CNS along with the regulation of inflammation and repair of the CNS. Moreover, dysfunction of reactive astrogliosis and scar formation can cause or contribute to various CNS diseases. During brain injury astrocytes change their phenotype, migrate into the damaged region and subsequently proliferate (Buffo et al., 2010; Sofroniew, 2009; Sofroniew and Vinters, 2010). Reactive astrocytes are ubiquitously present at all places of CNS pathology and have a strong impact on the ability of axons to regrow and form new synaptic connections (Buffo et al., 2010; Sofroniew, 2009). To test the involvement of NCLX in astrocyte scar formation, I used the cell monolayer ”scratch-wound” model, an established *in vitro* system, mimicking astrocytic response to CNS injury. Repopulation of the cell free area (“wound” closure) in this model is primarily due to astrocyte proliferation, although migration also can contribute to this process (Kornyei et al., 2000).

Upon injury, purines, pyrimidines and pro-inflamatory cytokines mediate astrocyte activation and possibly contribute also to the later astrocytic answers. Further factors that contribute to astrogliosis, like endothelin, growth factors, inflammatory molecules, advance astrogliosis till the time point, when the factors, inhibiting astrogliosis, like IFNβ, IL-10 and erythropoietin prevail (Buffo et al., 2010). My results show that NCLX inhibition either by CGP37157 or by siNCLX significantly impaired astrocytic wound closure abilities. This effect may be contributed by migration, proliferation, or apoptosis. All these functions are known to be Ca^{2+}-dependent (Berridge et al., 2003) and therefore may be influenced via P2Rs and/or SOCE. Since these Ca^{2+} pathways were more or less strongly modulated by the mitochondrial exchanger NCLX, an influence of mitochondrial impairment, more specifically, NCLX knockout, on the Ca^{2+} dependent functions, such as proliferation and/or migration was to be expected. Molecules involved in the proliferation of reactive astrocytes *in vivo* are epidermal growth factor, fibroblast

growth factor, endothelin1 and ATP (Sofroniew, 2009). One of the ionotropic receptors $P2X_7R$, reacts to pathologically high [ATP] with increases in cytoplasmic [Ca^{2+}], thereby changes the expression of cytokines, inflammatory molecules and purinoreceptors, and promotes astrogliosis (Buffo et al., 2010). Activation of $P2X_7R$ stimulates Akt and extracellular signal-regulated kinase 1/2 (ERK1/2) transcription factors, involved in cell proliferation (Buffo et al., 2010). *In vivo* and *in vitro* evidence demonstrates that ATP and its analogs promote astrocytic proliferation also via P2YRs (Buffo et al., 2010). An additional effect of P2YR stimulation is the activation of growth factor receptors, adding even more to the proliferative response (Buffo et al., 2010). During injury, endothelin1 is primarily secreted by astrocytes and the expression of type B endothelin receptor is being upregulated (Buffo et al., 2010). Endothelin1 can mobilize Ca^{2+} via the IP_3-dependent pathway in order to induce proliferation (Stanimirovic et al., 1995). Endothelin receptor agonists promote cytoskeletal changes, proliferation and modulation of metabolic properties (Buffo et al., 2010). Extracellular nucleotides, endothelin and growth factors mediate proliferation effects via triggering mitogen-activated protein kinase (MAPK)/ERK phosphorylation and subsequent upregulation of transcription factors like CREB, c-Jun and c-Fos (Buffo et al., 2010). P2YRs also mediate proliferative and anti-apoptotic responses via protein kinase B (PKB)/Akt system (Franke et al., 2009).

Involvement of SOCE in cellular proliferation has been shown for different cell types. For example, in vascular smooth muscle cells mitochondrial depolarization reduces cell proliferation via a decrease in SOCE (Munoz et al., 2011). In malignant myeloma cells, Feldman et al. (Feldman et al., 2010) showed that NCLX inhibition abolished SOCE, inactivated PKB/Akt, retarded cell growth and increased the vulnerability to apoptosis, a mechanism that could also play a role in regulation of detectable astrocytic proliferation.

Evidence indicates that the source of proliferating scar-forming astrocytes are mature astrocytes re-entering cell cycle, although other cells may participate (Sofroniew, 2009). One of the transcription factors, shown to be upregulated during astrocytic proliferation response is STAT3 (Herrmann et al., 2008; Sofroniew, 2009). STAT3 knock-down in astrocytes impaired mitochondrial functions: decreased ATP production, triggered mitochondrial membrane depolarization and increased the production of ROS (Sarafian et al., 2010). Mitochondrial impairment, evoked by STAT3 knock-down, coincided with the significant reduction in the proliferative abilities of astrocytes. STAT3 is also involved in astrocytic migration and glial scar formation (Buffo et al., 2010).

The strong effect of NCLX silencing in the wound-closure model, in which regrowth of astrocytes into the cell free area could be also contributed by migration, suggests a participation of NCLX in astrocytic migration. Although the migratory property was not studied independently, as for instance in a Boyden chamber model (Matyash et al., 2002), I would like to discuss a possible mechanism of action suggested by data from the literature..P2YRs, and particularly $P2Y_2R$, directly interact with integrins (Bagchi et al., 2005). This interaction is involved in Rho GTPase-mediated changes in the astrocytic cytoskeleton and migration. Indeed, stimulation of $P2Y_2R$ with UTP was found to increase astrocytic migration (Bagchi et al., 2005). In a similar in vitro wound healing model Rao et al. (Rao et al., 2006) proved the direct involvement of TRPC1, a constituent of SOC, in wound healing properties of epithelial cells. Their work provides the direct link between increased Ca^{2+} entry through SOC and enhanced cell migration necessary for resealing the intestinal wound. Such mechanism, through the NCLX-mediated modulation of SOCE and IP_3R-mediated Ca^{2+} signaling, may affect astrocytic migratory abilities.

Another possibility is the involvement of NCLX in RyR-mediated signaling. It has been demonstrated recently that functional RyRs control astrocytic wound healing via an effect on migration (Matyash et al., 2002). So far nothing is known about the interaction between mitochondria and RyRs-mediated Ca^{2+} signaling and the role of mitochondrial NCLX in this pathway needs to be explored in further studies.

Mitochondrial Ca^{2+} is a strong modulator of apoptosis (Contreras et al., 2010; Pinton et al., 2008). Ca^{2+} transferred from the ER to mitochondria can trigger apoptotic pathways and induce release of mitochondrial pro-apoptotic factors. It is plausible to assume that NCLX activity may influence apoptosis and thereby might have modulated the wound-closure properties. However, previous data indicate that astrocytes are quite resistant to apoptosis, which is supported by the lack of any effect of clonazepam, the inhibitor of the mitochondrial exchanger, on apoptosis (Ceruti et al., 2005; Chelli et al., 2004). Moreover, my preliminary experiments (not shown) suggest that NCLX knock-down does not significantly alter apoptosis. However, the role of NCLX in the modulation of apoptotic pathways is of major interest and requires further investigation.

5.6 How NCLX modulates migratory and secretory properties of microglia: a link to inflammation and homeostasis

Cytokines and chemokines secreted by microglia mediate a plethora of CNS activities including homeostatic brain functions, like regulation of body temperature or feeding behavior; organ development, synaptic pruning and CNS pathology (Guyon et al., 2008; Rostene et al., 2011). Cytokine and chemokine secretion is upregulated upon stimulation with inflammatory molecules, like LPS. Both, microglial secretory function and migration are Ca^{2+}-dependent processes (Kettenmann et al., 2011). Therefore, it is plausible to assume that the mitochondrial Na^{+}/Ca^{2+} exchanger NCLX may be involved in the inflammatory responses, mediated by microglia, defining the outcome of the inflammation.

LPS is a ligand of Toll-like receptor 4 (TLR4), which upon activation signals via adaptor protein MyD88 to transcription factor AP-1 and/or NFκB (Kettenmann et al., 2011). NFκB translocates to the nucleus, where it can activate transcription of different genes. LPS can elevate cytokine and NO levels also via acting on the transcription factor Notch1 (Cao et al., 2008). While LPS is a strong inflammatory stimulus, IFNγ is associated with neuroprotective function of microglia (Butovsky et al., 2005).

In neurodegenerative disease, such as multiple sclerosis, Alzheimer and Parkinson diseases, or glioma and stroke, the levels of imflammatory cytokines are deregulated. This applies, for example, to one prevalent cytokine, IL-6, which is also important for the regulation of physiological processes in the brain, like neuronal homeostasis, astrogliogenesis and neuronal differentiation (Spooren et al., 2011). In the brain, IL-6 is produced by microglia, astrocytes and neurons, and acts in a paracrine or autocrine fashion. Its secretion can be modulated by neurotransmitters, inflammatory stimuli and cytokines (Spooren et al., 2011). IL-6 secretion can be upregulated also through $P2Y_{2,4}R$ and $P2X_7R$ via activation of the P38 MAPK and NFκB pathway (Lee et al., 2011). Interestingly, the same paper also showed an involvement of SOCE in modulation of IL-6 secretion (Lee et al., 2011). It would be interesting to know whether NCLX is involved in IL-6 release via its contribution to these major Ca^{2+} pathways in microglia; however my results do not answer whether there is this causal link.

MCP-1 (MCP-1/CCL2) is a member of the CC chemokine family, secreted by inflammatory and stromal cells. The major origins of MCP-1 in the brain are microglia and astrocytes, while endothelial cells secrete it to a lesser extent (Deshmane et al., 2009; Savarin-Vuaillat and Ransohoff, 2007). MCP-1 is expressed constitutively and its expression is upregulated after

proinflammatory stimuli and tissue injury. MCP-1 controls the migration and infiltration of other immune cells, like microglia, monocytes, macrophages, T-lymphocytes, neutrophils and natural killer cells, thereby regulating the inflammation status in the brain (Deshmane et al., 2009; Savarin-Vuaillat and Ransohoff, 2007). MCP-1 is also important in normal brain physiology. MCP-1 mediates dopaminergic neuron signaling and development, promotes glial proliferation and growth, probably contributing to neurogenesis, and involved in the differentiation of neural precursor cells into neurons, astrocytes and oligodendrocytes (Semple et al., 2010). Its secretion can be mediated by UDP activation of $P2Y_6R$ and Ca^{2+}-activated transcription factors NFATc1 and c2 (Kim et al., 2011).

This study investigated the connection of LPS activation and cytokine/chemokine secretion. As shown previously, LPS evokes an increase in $[Ca^{2+}]_{cyt}$ after 40-50 min of the exposure, and the LPS-induced Ca^{2+} elevation continues for about 3 hrs an then returns to the basal level, combined with a constant downregulation of Ca^{2+} influx via SOC (Beck et al., 2008). Others have shown, that the basal cytosolic Ca^{2+} level in microglia is elevated even after longer periods of microglial exposure to LPS (Hoffmann et al., 2003), suggesting that there may be a biphasic elevation of basal cytosolic Ca^{2+} that through its temporal pattern may activate different Ca^{2+} dependent secretory pathways. Interestingly, the maximal expression levels of IL-6 and MCP-1 mRNAs have been described to occur within 4 hrs after LPS exposure (Lund et al., 2006). In my study, I assayed for cytokine/NO/ROS release only at one time point: after 18 hrs. It is tempting to speculate that NCLX exerts a differential, time dependent effect on different secretory pathways. The primary LPS-induced Ca^{2+} transient may regulate the secretion of both IL-6 and MCP-1. The mechanism leading to LPS-induced elevation of the basal cytosolic Ca^{2+} level is not really known. However, it may be related to the alkaline shift that is seen upon LPS-exposure and to the ~2.6 fold rise in $[Na^+]_{cyt}$, contributed by the activity of the Na^+/H^+ exchanger. Finally, Ca^{2+} elevation can occur due to plasmalemmal NCX working in the reverse mode (Liu et al., 2010). Elevation of $[Na^+]$ may activate the mitochondrial exchanger, and the uptake of Na^+ and extrusion of Ca^{2+} may be related to LPS-induced primary $[Ca^{2+}]_{cyt}$ rise and concomitant secretion of both MCP-1 and IL-6. In conclusion, NCLX, due to its effect on both Na^+ and Ca^{2+} homeostasis may be strongly involved in controlling basal cytosolic Ca^{2+} levels after exposure to inflammatory stimuli.

Under pathological conditions microglia become activated and migrate towards a source of injury. ATP content in the cells is extremely high and upon injury ATP is released and attracts microglia (Farber and Kettenmann, 2006; Honda et al., 2001). ATP-induced microglial migration

is mediated via $P2Y_{12}R$ and following activation of the PI_3K pathway and increased Akt phosphorylation and additionally via $P2X_4R$ (Kettenmann et al., 2011). C5a-induced migration proceeds via a different mechanism.

My results show that NCLX inhibition results in the downregulation of ATP- but not C5a-evoked chemotaxis. A likely scenario to explain this differential effect, depending on the chemotactic stimulus, is the involvement of NCLX in the sensing of specific chemoattractants. Extensive further experiments are required to test such possibility.

The immense reduction of ATP-induced microglial chemotaxis seen in my experiments, when NCLX was pharmacologically inhibited, could be related to the effect on the P2YR-mediated Ca^{2+} signaling, possibly $P2Y_{12}R$. The effect on $P2X_4R$ is also possible; however this has not been explored further in this study. Another possible explanation may involve the strong effect of NCLX on SOCE; however the role of SOCE in control of microglial migration is still unclear. The third possibility of NCLX involvement may be relates to the plasmalemmal NCX. Ifuku et al demonstrated that bradykinin-induced migration depends on Ca^{2+} influx via the reverse-mode activity of the NCX (Ifuku et al., 2007; Ifuku et al., 2011). Moreover, NCX1 expression and activity is increased in the microglia invading the infarct core 3 and 7 days after cerebral artery occlusion (Boscia et al., 2009). NCX1 activity, in combination with the activity of the mitochondrial Na^+/Ca^{2+} exchanger may regulate migratory abilities of microglia, a mechanism that needs to be explored further in the future.

5.7 How is NCLX linked to the astrocytic glutamate release and Ca^{2+} excitability and why is the effect of NCLX so large?

To investigate NCLX effect on glutamate release and Ca^{2+} excitability my collaborators Dr. Vedrana Montana and Prof. Vlad Parpura investigated two parameters of the Ca^{2+}_{cyt} dynamics in solitary astrocytes as a consequence of mechanical stimulation: i) the peak response, which reports on the mitochondrial sequestration of Ca^{2+} entering the cytosol upon stimulation and in case of glutamate release indicates the size of the ready releasable pool combined with the extent of the high $[Ca^{2+}]$ microdomain unlocking the release; and ii) the cumulative response, reporting on the decreasing Ca^{2+}_{cyt} phase, indicating Ca^{2+} clearance from the cytosol by PMCA

and SERCA and Ca^{2+} release into the cytosol by mitochondria (Kim et al., 2005; Reyes and Parpura, 2008; Reyes et al., 2011; Reyes et al., 2012).

In a previous study, before the molecular nature of the mitochondrial exchanger was revealed, the group of Prof. V. Parpura investigated the influence of the mitochondrial Na+/Ca^{2+} exchanger on astrocytic Ca^{2+} and glutamate by use of the pharmacological inhibitor CGP37157. They described that inhibition of the exchanger resulted in a reduction of mechanically-induced Ca^{2+} responses and glutamate release recorded from rat solitary astrocytes in culture (Reyes and Parpura, 2008). Here, we applied the more specific molecular approach to downregulate NCLX activity. The new data show the same effect of NCLX inhibition, however, to a much larger extent, revealing a profound role of the exchanger in the astrocytic Ca^{2+} excitability and a key role in astrocytic glutamate release. For comparison, pharmacological inhibition reduced the normalized Ca^{2+} peak to 77% of the control and the cumulative Ca^{2+} response to 49% of the control. RNA_i-mediated NCLX knock-down, however, reduced the peak to 54% and the cumulative response to 12% of the control (Figure 2 from (Reyes and Parpura, 2008) and Figure 4.14). For glutamate release the difference between the pharmacological and molecular inhibition of the exchanger was even more drastic: pharmacological inhibition decreased the peak to 66% and the cumulative response to 61% of the control, while molecular NCLX knock-down decreased the peak to 47% and the cumulative response to **-398%** of the control (Figure 2 from (Reyes and Parpura, 2008) and Figure 4.14). In particular, the strong effect on cumulative glutamate release indicates that the basal glutamate release is completely eliminated when NCLX is not working.

It has been shown that glutamate release in astrocytes is strongly dependent on the cytosolic Ca^{2+} response (Parpura and Haydon, 2000). Treatment of astrocytes with high affinity Ca^{2+} chelator BAPTA-AM almost abolishes astrocytic glutamate release (normalized peak) upon mechanical stimulation (Innocenti et al., 2000). Therefore, a decrease in the total cytosolic Ca^{2+} levels may correlate with the decreased glutamate release in astrocytes due to NCLX knockout. However the “story” is more complex. BAPTA is much faster at binding Ca^{2+} than other Ca^{2+} chelators, like EGTA and its relatives. Therefore, during Ca^{2+} transients BAPTA is able to eliminate fast Ca^{2+} elevations and high Ca^{2+} microdomains at specific cellular locations, underlying Ca^{2+} entry, while EGTA for example cannot. For the exocytotic release to occur, fast sub-plasmalemmal Ca^{2+} elevation in the region of readily-releasable vesicles is required (Marchaland et al., 2008). Upon stimulation in astrocytes, mitochondria travel to the plasma membrane and become immobilized in high Ca^{2+} microdomains (Kolikova et al., 2006),

therefore being located just near readily-releasable pool of vesicles and influencing the release site much more than other elements of Ca^{2+} machinery do. For example, inhibition of plasmalemmal NCX decreased glutamate release to much lesser extent (to about 75% of the control) (Reyes et al., 2012). Moreover, mechanical stimulation in astrocytes induces Na^+ transient (Reyes et al., 2012), therefore the mitochondrial Na^+/Ca^{2+} exchanger would have a larger driving force to extrude Ca^{2+}, contributing even more to Ca^{2+} concentration in the release sites.

Another explanation for the influence of NCLX on glutamate release may be an effect on the size of the readily-releasable pool, which includes vesicle recycling, generation, docking and priming (Sudhof, 2004). All these processes are ATP-dependent. High mitochondrial $[Ca^{2+}]$ due to NCLX knock-down, however, would increase the rate of the Ca^{2+}-dependent TCA cycle and therefore [ATP], making this possibility implausible.

Vesicular content can also influence the amount of an exocytosed transmitter. A decrease in the glutamate content of the vesicles can be influenced by the cytosolic level of glutamate and glutamate loading into the vesicles. Cytosolic glutamate levels and vesicular glutamate content control the exocytotic glutamate release in astrocytes (Ni and Parpura, 2009), providing a possible explanation for unparalleled changes in $[Ca^{2+}]_{cyt}$ and Ca^{2+}- dependent glutamate release in NCLX-deficient astrocytes. Furthermore, glutamate synthesis relies on the mitochondrial matrix enzyme pyruvate carboxylase (Hertz et al., 1999), which is activated by Ca^{2+} (Civelek et al., 1996). This is, however, a less likely scenario to explain the effect, as my data showed elevated mitochondrial $[Ca^{2+}]$ in astrocytes with diminished NCLX activity. In astgrocytes, glutamate is loaded into the vesicles by vesicular glutamate transporter 3 (VGLUT3) (Ni and Parpura, 2009). The activity of this transporter strictly depends on the H^+ gradient across the vesicle membrane (Omote et al., 2011). NCLX therefore may affect intracellular Na^+ levels and consequently, Na^+/H^+ exchange in order to balance two ions may influence intracellular pH, influencing the driving force for glutamate vesicular loading.

Another possible explanation for differences in effects between the pharmacological vs. the targeted siRNA approach could be due to the “side” effects of CGP37157 and/or compensatory function of proteins, e.g., VGLUT3 and/or glutamine synthetase (an enzyme that converts glutamate to glutamine), discussed above. However, it should be noted, that in previous pharmacological studies controls were defined as untreated astrocytes, and here control astrocytes were exposed to negative non-targeting siRNA; this could account for some differences as well. It should also be noted that different animal models were used in two

studies: rat was utilized in the previous pharmacological work, while here mouse was used. Thus, differences between the two studies could be explained to some extent by species difference, which may include differences in functionality and utilization of a so-called downstream of Ca^{2+} modulation of exocytosis, as has been implicated elsewhere (Reyes et al., 2011). These differences do not detract from a general conclusion that NCLX can shape Ca^{2+}_{cyt} responses and subsequent exocytotic glutamate release in astrocytes. It is tempting to hypothesize that NCLX modulation of glutamate release from astrocytes would have consequences on synaptic transmission and plasticity at the tripartite synapse.

Chapter 6

Summary

Mitochondria are placed at the crossroad of the cellular demands and activities due to their major role in supply of cellular energy and global Ca^{2+} signaling. Ca^{2+} entering the cytosol is shuttled by mitochondria: it is rapidly taken up via a mitochondrial Ca^{2+} uniporter and slowly extruded via a mitochondrial Na^{+}/Ca^{2+} exchanger. While Ca^{2+} uptake shares common properties in diverse cell-types, Ca^{2+} extrusion mechanisms are different. This transmitochondrial Ca^{2+} transfer partially shapes the cytosolic Ca^{2+} signals, altering activation patterns of Ca^{2+}-dependent proteins, including Ca^{2+} transporters, residing nearby. Consequently, mitochondrial Ca^{2+} shuttling modifies different Ca^{2+}-dependent functions in various cell types. The role of the mitochondrial Ca^{2+} signaling in glial cells, closely participating in brain signaling in physiology and pathology, remains, however, poorly understood. The recent identification of the mitochondrial exchanger NCLX provided me with the possibility to devise the molecular tools to control its expression and activity.

Here, I investigated the role of NCLX in shaping glial mitochondrial and cytosolic Ca^{2+} responses and assessed how NCLX activity is linked to astroglial and microglial function *in vitro*. For this purpose I combined RNAi knockdown of NCLX expression or pharmacological inhibition by the benzothiazepine compound CGP37157 with cellular and mitochondrial Ca^{2+} imaging of murine primary astrocytes and microglia. Cytosolic Ca^{2+} levels were monitored from cells loaded with Ca^{2+}-sensitive dyes Fluo-4 AM or Fura-2 AM. Mitochondrial Ca^{2+} changes were recorded from cells transfected with Ca^{2+}-sensitive protein, specifically targeted to the mitochondrial matrix, mitochondrial ratiometric pericam.

Immunoblot analysis of organelle-enriched fractions from murine primary cultured astrocytes and microglia showed that NCLX is targeted to the mitochondria. ATP-induced cytosolic Ca^{2+} responses in astrocytes and microglia evoked mitochondrial Ca^{2+} transients, indicating that mitochondria participate in glial Ca^{2+} signaling. Silencing NCLX expression in astrocytes

inhibited mitochondrial Ca^{2+} extrusion and enhanced the net mitochondrial Ca^{2+} uptake, indicating that NCLX mediates mitochondrial Ca^{2+} efflux. Silencing or pharmacological blockade of NCLX activity diminished the biphasic, ATP-evoked cytosolic Ca^{2+} responses in astrocytes and microglia or complement C5a-induced Ca^{2+} transients in microglia. In microglia the reduction in Ca^{2+} answers was primarily due to the loss of the delayed component of the response, while in astrocytes the reduction was similarly contributed by the decrease in the amplitude and the time of the response. Moreover, in both types of glia, inhibition of NCLX activity significantly reduced Ca^{2+} entry via store-operated Ca^{2+} channels on the plasma membrane. These effects suggest that there is a functional interaction between the mitochondria, ER and plasma membrane, shaping glial Ca^{2+} responses and that NCLX is a critical component in this crosstalk in both astrocytes and microglia.

Pharmacological inhibition of NCLX in microglia resulted in modification of Ca^{2+}-dependent functions. It significantly reduced ATP-stimulated chemotaxis and attenuated the LPS-evoked secretion of Il-6, a cytokine involved in the inflammation process, and elevated basal levels of the chemokine MCP-1. However, NCLX inhibition did not affect other Ca^{2+}-dependent functions in microglia, like TNFα secretion, NO and ROS release. Remarkably, NCLX knockdown in astrocytes was followed by almost complete elimination of the secretion of the major transmitter in the brain, glutamate, and a marked inhibition of astrocytic wound healing and proliferation capacity. However, NCLX knockdown did not significantly alter the speed of the intercellular astrocyte Ca^{2+} wave propagation.

In conclusion, NCLX is the mitochondrial Na^{+}/Ca^{2+}exchanger in glial cells, and its activity affects glial Ca^{2+} homeostasis, in particularly, the major Ca^{2+} entry pathway, SOC. In microglia NCLX function via its participation in cellular Ca^{2+} homeostasis is connected to tuning the inflammatory profile and migratory properties of these cells. In astrocytes, NCLX appears to be a critical element in the crosstalk between mitochondria, ER and plasma membrane, thereby shaping cytoplasmic Ca^{2+} transients, required for a diverse array of astrocyte activities.

Chapter 7

Zusammenfassung

Mitochondrien sind ein Zellkompartiment, welches eine wichtige Schlüsselrolle für die Energieversorgung der Zelle sowie in globalen Kalziumsignalwegen darstellt. Kalzium-Ionen (Ca^{2+}), die in das Cytosol der Zelle gelangen, werden durch Mitochondrien weiterverteilt: sie werden schnell über einen mitochondrialen Ca^{2+} Uniporter aufgenommen und langsam über einen mitochondrialen Na^{+}/Ca^{2+}-Austauscher abgegeben. Während die Ca^{2+}-Aufnahme in diversen Zelltypen ähnliche Eigenschaften aufweist, sind die Extrusionsmechanismen unterschiedlich. Dieser transmitochondriale Ca^{2+}-Transfer moduliert partiell die intrazellulären Ca^{2+}-Signale, verändert die Aktivierungsmuster Ca^{2+}-abhängiger Proteine, einschließlich der sich in der Nähe der Mitochondrien befindlichen Ca^{2+}-Transporter. Folglich verändert der unterschiedliche mitochondriale Ca^{2+}-Transfer verschiedene Ca^{2+}-abhängige Funktionen in verschiedenen Zelltypen. Die Rolle des mitochondrialen Ca^{2+} in Gliazellen, welche unter physiologischen und pathologischen Bedingungen an Signalweiterleitungen im Gehirn beteiligt sind, ist bis jetzt wenig verstanden. Durch die kürzliche Identifizierung des mitochondrialen Ionentransporters NCLX war es mir möglich, die Expression und Aktivität des Kanals zu studieren.

In dieser Arbeit habe ich die Rolle des Ionentransporters NCLX in der Modulierung mitochondrialer und zytosolischer Ca^{2+}-Antworten sowie den Effekt von NCLX Aktivität auf astrogliale und mikrogliale Funktionen in vitro untersucht. Hierfür habe ich NCLX über die RNA-Interferenz-Technik oder pharmakologisch mithilfe der Benzothiazepinverbindung CGP37157 inhibiert. Anschließend habe ich sowohl zelluläres als auch mitochondriales Ca^{2+}-Imaging an murinen primären Astrozyten und Mikroglia durchgeführt. Intrazelluläre Ca^{2+}-Level wurden mithilfe der Ca^{2+}-sensitiven Farbstoffe Fluo-4 AM oder Fura-2 AM bestimmt. Für die Analyse der mitochondrialen Ca^{2+}-Veränderungen wurden die Zellen mit einem mitochondrialen Ca^{2+}-sensitiven Protein (Pericam) transfiziert.

Immunoblot-Analysen von verschiedenen Organellfraktionen aus murinen primären kultivierten Astrozyten und Mikroglia zeigten, dass NCLX mitochondrial exprimiert ist. ATP-induzierte zytosolische Ca^{2+}-Antworten in Astrozyten und Mikroglia riefen einen mitochondrialen Ca^{2+}-Einstrom hervor. Dies weist darauf hin, dass Mitochondrien an glialen Ca^{2+}-Signalwegen beteiligt sind.

Ein Silencing der NCLX Expression in Astrozyten verhindert den mitochondrialen Ca^{2+}-Ausstrom und erhöht die mitochondriale Netto-Ca^{2+}-Aufnahme. Daher liegt die Annahme nahe, dass NCLX den mitochondrialen Ca^{2+}-Ausstrom vermittelt. Silencing oder pharmakologische Blockade der NCLX - Aktivität vermindert weiterhin ATP-evozierte, bipasische intrazelluläre Ca^{2+}-Antworten in Astrozyten und Mikroglia oder Komplement C5a-induzierte Ca^{2+}-Einströme in Mikroglia. In Mikroglia-Zellen ergab sich die Reduktion der kumulativen Ca^{2+}-Antworten in erster Linie aus der Verringerung der langsamen Reaktionskomponente. In Astrozyten hingegen trugen sowohl eine Abnahme in der Amplitude als auch in der Zeit der Reaktion zur Verminderung der Ca^{2+}-Antworten bei. Darüber hinaus führt eine Hemmung der NCLX-Aktivität in beiden Arten von Gliazellen zu einem erheblich reduzierten Ca^{2+}-Einstrom über speicherregulierte Ca^{2+}-Kanäle (SOC) auf der Plasmamembran. Diese Effekte weisen darauf hin, dass es eine funktionelle Interaktion zwischen den Mitochondrien, dem ER und der Plasmamembran bei der Modulierung glialer Ca^{2+}-Antworten gibt und dass NCLX eine wichtige Komponente in dieser Interaktion in sowohl Astrozyten als auch Mikroglia ist.

Pharmakologische Inhibierung von NCLX in Mikroglia führte zu einer Veränderung von Ca^{2+}-abhängigen Funktionen. Es reduzierte signifikant die ATP-stimulierte Chemotaxis und führte zu einer Abschwächung der LPS-vermittelten Sekretion von IL-6, einem Zytokin, welches an Entzündungsprozessen beteiligt ist, sowie zu einem erhöhten basalen Level des Chemokins MCP-1. Allerdings hatte eine Inhibierung von NCLX keinen Einfluss auf andere Ca^{2+}-abhängige Funktionen in Mikroglia, wie TNFα-Sekretion oder NO- und ROS-Freisetzung. Bemerkenswerterweise wurde nach Knockdown von NCLX in Astrozyten die Ausschüttung des Hauptneurotransmitters des Gehirns, Glutamat, fast vollständig inhibiert. Weiterhin konnte ich ich eine deutliche Hemmung der astrozytären Wundheilung sowie der Proliferationskapazität messen. Allerdings verändert der NCLX-Knockdown die Geschwindigkeit der Ausbreitung von interzellulären astrozytären Ca^{2+} Wellen nicht wesentlich.

Zusammenfassend kann ich sagen, dass NCLX der mitochondriale Na^{+}/Ca^{2+}-Austauscher in Gliazellen ist. Seine Aktivität beeinflusst die gliale Ca^{2+}-Homöostase, insbesondere den Hauptweg des Ca^{2+}-Einstroms in die Zelle über SOC. In Mikroglia ist NCLX an der zellulären

Ca^{2+} Homöostase beteiligt und moduliert dadurch das inflammatorische Profil sowie die Migrationseigenschaften der Zellen. In Astrozyten scheint NCLX ein kritisches Element in der Interaktion zwischen den Mitochondrien, dem ER und der Plasmamembran zu sein, wodurch zytoplasmatische Ca^{2+} Einströme moduliert werden, was für vielfältige astrozytäre Aktivitäten erforderlich ist.

Chapter 8

References

Aguado, F., Espinosa-Parrilla, J.F., Carmona, M.A., and Soriano, E. (2002). Neuronal activity regulates correlated network properties of spontaneous calcium transients in astrocytes in situ. J Neurosci *22*, 9430-9444.

Agulhon, C., Petravicz, J., McMullen, A.B., Sweger, E.J., Minton, S.K., Taves, S.R., Casper, K.B., Fiacco, T.A., and McCarthy, K.D. (2008). What is the role of astrocyte calcium in neurophysiology? Neuron *59*, 932-946.

Andersson, M., Blomstrand, F., and Hanse, E. (2007). Astrocytes play a critical role in transient heterosynaptic depression in the rat hippocampal CA1 region. J Physiol *585*, 843-852.

Araque, A., Li, N., Doyle, R.T., and Haydon, P.G. (2000). SNARE protein-dependent glutamate release from astrocytes. J Neurosci *20*, 666-673.

Araque, A., Martin, E.D., Perea, G., Arellano, J.I., and Buno, W. (2002). Synaptically released acetylcholine evokes Ca2+ elevations in astrocytes in hippocampal slices. J Neurosci *22*, 2443-2450.

Araque, A., Parpura, V., Sanzgiri, R.P., and Haydon, P.G. (1998a). Glutamate-dependent astrocyte modulation of synaptic transmission between cultured hippocampal neurons. Eur J Neurosci *10*, 2129-2142.

Araque, A., Sanzgiri, R.P., Parpura, V., and Haydon, P.G. (1998b). Calcium elevation in astrocytes causes an NMDA receptor-dependent increase in the frequency of miniature synaptic currents in cultured hippocampal neurons. J Neurosci *18*, 6822-6829.

Ardon, F., Rodriguez-Miranda, E., Beltran, C., Hernandez-Cruz, A., and Darszon, A. (2009). Mitochondrial inhibitors activate influx of external Ca(2+) in sea urchin sperm. Biochim Biophys Acta *1787*, 15-24.

Attwell, D., Buchan, A.M., Charpak, S., Lauritzen, M., Macvicar, B.A., and Newman, E.A. (2010). Glial and neuronal control of brain blood flow. Nature *468*, 232-243.

Azarias, G., and Chatton, J.-Y. (2011). Selective Ion Changes during Spontaneous Mitochondrial Transients in Intact Astrocytes. PLoS One *6*, e28505.

Bagchi, S., Liao, Z., Gonzalez, F.A., Chorna, N.E., Seye, C.I., Weisman, G.A., and Erb, L. (2005). The P2Y2 nucleotide receptor interacts with alphav integrins to activate Go and induce cell migration. J Biol Chem *280*, 39050-39057.

Bakowski, D., Nelson, C., and Parekh, A.B. (2012). Endoplasmic reticulum-mitochondria coupling: local Ca(2+) signalling with functional consequences. Pflugers Arch.

Bambrick, L.L., Chandrasekaran, K., Mehrabian, Z., Wright, C., Krueger, B.K., and Fiskum, G. (2006). Cyclosporin A increases mitochondrial calcium uptake capacity in cortical astrocytes but not cerebellar granule neurons. J Bioenerg Biomembr *38*, 43-47.

Baughman, J.M., Perocchi, F., Girgis, H.S., Plovanich, M., Belcher-Timme, C.A., Sancak, Y., Bao, X.R., Strittmatter, L., Goldberger, O., Bogorad, R.L., *et al.* (2011). Integrative genomics identifies MCU as an essential component of the mitochondrial calcium uniporter. Nature *476*, 341-345.

Bautista, D.M., Hoth, M., and Lewis, R.S. (2002). Enhancement of calcium signalling dynamics and stability by delayed modulation of the plasma-membrane calcium-ATPase in human T cells. J Physiol *541*, 877-894.

Beattie, E.C., Stellwagen, D., Morishita, W., Bresnahan, J.C., Ha, B.K., Von Zastrow, M., Beattie, M.S., and Malenka, R.C. (2002). Control of synaptic strength by glial TNFalpha. Science *295*, 2282-2285.

Beck, A., Penner, R., and Fleig, A. (2008). Lipopolysaccharide-induced down-regulation of Ca2+ release-activated Ca2+ currents (I CRAC) but not Ca2+-activated TRPM4-like currents (I CAN) in cultured mouse microglial cells. J Physiol *586*, 427-439.

Beierlein, M., and Regehr, W.G. (2006). Brief bursts of parallel fiber activity trigger calcium signals in bergmann glia. J Neurosci *26*, 6958-6967.

Bekar, L.K., He, W., and Nedergaard, M. (2008). Locus coeruleus alpha-adrenergic-mediated activation of cortical astrocytes in vivo. Cereb Cortex *18*, 2789-2795.

Belanger, M., Allaman, I., and Magistretti, P.J. (2011). Brain energy metabolism: focus on astrocyte-neuron metabolic cooperation. Cell Metab *14*, 724-738.

Bell, C.J., Bright, N.A., Rutter, G.A., and Griffiths, E.J. (2006). ATP regulation in adult rat cardiomyocytes: time-resolved decoding of rapid mitochondrial calcium spiking imaged with targeted photoproteins. J Biol Chem *281*, 28058-28067.

Belmonte, S., and Morad, M. (2008). 'Pressure-flow'-triggered intracellular Ca2+ transients in rat cardiac myocytes: possible mechanisms and role of mitochondria. J Physiol *586*, 1379-1397.

Bernardinelli, Y., Azarias, G., and Chatton, J.Y. (2006). In situ fluorescence imaging of glutamate-evoked mitochondrial Na+ responses in astrocytes. Glia *54*, 460-470.

Berridge, M.J., Bootman, M.D., and Roderick, H.L. (2003). Calcium signalling: dynamics, homeostasis and remodelling. Nat Rev Mol Cell Biol *4*, 517-529.

Berridge, M.J., Lipp, P., and Bootman, M.D. (2000). The versatility and universality of calcium signalling. Nat Rev Mol Cell Biol *1*, 11-21.

Bezzi, P., Carmignoto, G., Pasti, L., Vesce, S., Rossi, D., Rizzini, B.L., Pozzan, T., and Volterra, A. (1998). Prostaglandins stimulate calcium-dependent glutamate release in astrocytes. Nature *391*, 281-285.

Boitier, E., Rea, R., and Duchen, M.R. (1999). Mitochondria exert a negative feedback on the propagation of intracellular Ca2+ waves in rat cortical astrocytes. J Cell Biol *145*, 795-808.

Boscia, F., Gala, R., Pannaccione, A., Secondo, A., Scorziello, A., Di Renzo, G., and Annunziato, L. (2009). NCX1 expression and functional activity increase in microglia invading the infarct core. Stroke *40*, 3608-3617.

Boucsein, C., Kettenmann, H., and Nolte, C. (2000). Electrophysiological properties of microglial cells in normal and pathologic rat brain slices. Eur J Neurosci *12*, 2049-2058.

Boucsein, C., Zacharias, R., Farber, K., Pavlovic, S., Hanisch, U.K., and Kettenmann, H. (2003). Purinergic receptors on microglial cells: functional expression in acute brain slices and modulation of microglial activation in vitro. Eur J Neurosci *17*, 2267-2276.

Bowser, D.N., and Khakh, B.S. (2004). ATP excites interneurons and astrocytes to increase synaptic inhibition in neuronal networks. J Neurosci *24*, 8606-8620.

Bozidis, P., Williamson, C.D., and Colberg-Poley, A.M. (2007). Isolation of endoplasmic reticulum, mitochondria, and mitochondria-associated membrane fractions from transfected cells and from human cytomegalovirus-infected primary fibroblasts. Curr Protoc Cell Biol *Chapter 3*, Unit 3 27.

Brini, M., Pinton, P., King, M.P., Davidson, M., Schon, E.A., and Rizzuto, R. (1999). A calcium signaling defect in the pathogenesis of a mitochondrial DNA inherited oxidative phosphorylation deficiency. Nat Med *5*, 951-954.

Brockhaus, J., and Deitmer, J.W. (2002). Long-lasting modulation of synaptic input to Purkinje neurons by Bergmann glia stimulation in rat brain slices. J Physiol *545*, 581-593.

Brown, E.J. (1992). Complement receptors, adhesion, and phagocytosis. Infect Agents Dis *1*, 63-70.

Buchholz, J.N., Behringer, E.J., Pottorf, W.J., Pearce, W.J., and Vanterpool, C.K. (2007). Age-dependent changes in Ca2+ homeostasis in peripheral neurones: implications for changes in function. Aging Cell *6*, 285-296.

Buffo, A., Rolando, C., and Ceruti, S. (2010). Astrocytes in the damaged brain: molecular and cellular insights into their reactive response and healing potential. Biochem Pharmacol *79*, 77-89.

Burkeen, J.F., Womac, A.D., Earnest, D.J., and Zoran, M.J. (2011). Mitochondrial calcium signaling mediates rhythmic extracellular ATP accumulation in suprachiasmatic nucleus astrocytes. J Neurosci *31*, 8432-8440.

Butovsky, O., Talpalar, A.E., Ben-Yaakov, K., and Schwartz, M. (2005). Activation of microglia by aggregated beta-amyloid or lipopolysaccharide impairs MHC-II expression and renders them cytotoxic whereas IFN-gamma and IL-4 render them protective. Mol Cell Neurosci *29*, 381-393.

Butt, A.M. (2011). ATP: a ubiquitous gliotransmitter integrating neuron-glial networks. Semin Cell Dev Biol *22*, 205-213.

Cai, X., and Lytton, J. (2004a). The cation/Ca(2+) exchanger superfamily: phylogenetic analysis and structural implications. Mol Biol Evol *21*, 1692-1703.

Cai, X., and Lytton, J. (2004b). Molecular cloning of a sixth member of the K+-dependent Na+/Ca2+ exchanger gene family, NCKX6. J Biol Chem *279*, 5867-5876.

Cao, Q., Lu, J., Kaur, C., Sivakumar, V., Li, F., Cheah, P.S., Dheen, S.T., and Ling, E.A. (2008). Expression of Notch-1 receptor and its ligands Jagged-1 and Delta-1 in amoeboid microglia in postnatal rat brain and murine BV-2 cells. Glia *56*, 1224-1237.

Cardenas, C., Miller, R.A., Smith, I., Bui, T., Molgo, J., Muller, M., Vais, H., Cheung, K.H., Yang, J., Parker, I.*, et al.* (2010). Essential regulation of cell bioenergetics by constitutive InsP3 receptor Ca2+ transfer to mitochondria. Cell *142*, 270-283.

Castonguay, A., and Robitaille, R. (2001). Differential regulation of transmitter release by presynaptic and glial Ca2+ internal stores at the neuromuscular synapse. J Neurosci *21*, 1911-1922.

Ceruti, S., Mazzola, A., and Abbracchio, M.P. (2005). Resistance of human astrocytoma cells to apoptosis induced by mitochondria-damaging agents: possible implications for anticancer therapy. J Pharmacol Exp Ther *314*, 825-837.

Chacinska, A., Koehler, C.M., Milenkovic, D., Lithgow, T., and Pfanner, N. (2009). Importing mitochondrial proteins: machineries and mechanisms. Cell *138*, 628-644.

Chelli, B., Lena, A., Vanacore, R., Da Pozzo, E., Costa, B., Rossi, L., Salvetti, A., Scatena, F., Ceruti, S., Abbracchio, M.P.*, et al.* (2004). Peripheral benzodiazepine receptor ligands: mitochondrial transmembrane potential depolarization and apoptosis induction in rat C6 glioma cells. Biochem Pharmacol *68*, 125-134.

Civelek, V.N., Deeney, J.T., Shalosky, N.J., Tornheim, K., Hansford, R.G., Prentki, M., and Corkey, B.E. (1996). Regulation of pancreatic beta-cell mitochondrial metabolism: influence of Ca2+, substrate and ADP. Biochem J *318 (Pt 2)*, 615-621.

Clapham, D.E. (2007). Calcium signaling. Cell *131*, 1047-1058.

Coco, S., Calegari, F., Pravettoni, E., Pozzi, D., Taverna, E., Rosa, P., Matteoli, M., and Verderio, C. (2003). Storage and release of ATP from astrocytes in culture. J Biol Chem *278*, 1354-1362.

Contreras, L., Drago, I., Zampese, E., and Pozzan, T. (2010). Mitochondria: the calcium connection. Biochim Biophys Acta *1797*, 607-618.

Cornell-Bell, A.H., Finkbeiner, S.M., Cooper, M.S., and Smith, S.J. (1990). Glutamate induces calcium waves in cultured astrocytes: long-range glial signaling. Science *247*, 470-473.

Cox, D.A., Conforti, L., Sperelakis, N., and Matlib, M.A. (1993). Selectivity of inhibition of Na(+)-Ca2+ exchange of heart mitochondria by benzothiazepine CGP-37157. J Cardiovasc Pharmacol *21*, 595-599.

Csordas, G., Varnai, P., Golenar, T., Roy, S., Purkins, G., Schneider, T.G., Balla, T., and Hajnoczky, G. (2010). Imaging interorganelle contacts and local calcium dynamics at the ER-mitochondrial interface. Mol Cell *39*, 121-132.

D'Ascenzo, M., Fellin, T., Terunuma, M., Revilla-Sanchez, R., Meaney, D.F., Auberson, Y.P., Moss, S.J., and Haydon, P.G. (2007). mGluR5 stimulates gliotransmission in the nucleus accumbens. Proc Natl Acad Sci U S A *104*, 1995-2000.

Davalos, D., Grutzendler, J., Yang, G., Kim, J.V., Zuo, Y., Jung, S., Littman, D.R., Dustin, M.L., and Gan, W.B. (2005). ATP mediates rapid microglial response to local brain injury in vivo. Nat Neurosci *8*, 752-758.

de Brito, O.M., and Scorrano, L. (2008). Mitofusin 2 tethers endoplasmic reticulum to mitochondria. Nature *456*, 605-610.

De Stefani, D., Raffaello, A., Teardo, E., Szabo, I., and Rizzuto, R. (2011). A forty-kilodalton protein of the inner membrane is the mitochondrial calcium uniporter. Nature *476*, 336-340.

Del Rio Hortega, P. (1919). El tercer elemento de los centros nerviosos I La microglia en estado normal II Intervencion de la microglia en los procesos patologicos III Naturaleza probable de la microglia. Bol de la Soc esp de biol, 69-120.

Del Rio Hortega, P. (1920). La microglia y su transformation en celulas an basoncito y cuerpos granulo-adiposos. Trab Lab Invest Biol Madrid, 37–82.

Delbono, O. (2011). Expression and regulation of excitation-contraction coupling proteins in aging skeletal muscle. Curr Aging Sci *4*, 248-259.

Demaurex, N., Poburko, D., and Frieden, M. (2009). Regulation of plasma membrane calcium fluxes by mitochondria. Biochim Biophys Acta *1787*, 1383-1394.

Deshmane, S.L., Kremlev, S., Amini, S., and Sawaya, B.E. (2009). Monocyte chemoattractant protein-1 (MCP-1): an overview. J Interferon Cytokine Res *29*, 313-326.

Dimmer, K.S., Navoni, F., Casarin, A., Trevisson, E., Endele, S., Winterpacht, A., Salviati, L., and Scorrano, L. (2008). LETM1, deleted in Wolf-Hirschhorn syndrome is required for normal mitochondrial morphology and cellular viability. Hum Mol Genet *17*, 201-214.

Ding, S., Fellin, T., Zhu, Y., Lee, S.Y., Auberson, Y.P., Meaney, D.F., Coulter, D.A., Carmignoto, G., and Haydon, P.G. (2007). Enhanced astrocytic Ca2+ signals contribute to neuronal excitotoxicity after status epilepticus. J Neurosci *27*, 10674-10684.

Dombeck, D.A., Khabbaz, A.N., Collman, F., Adelman, T.L., and Tank, D.W. (2007). Imaging large-scale neural activity with cellular resolution in awake, mobile mice. Neuron *56*, 43-57.

Drago, I., Pizzo, P., and Pozzan, T. (2011). After half a century mitochondrial calcium in- and efflux machineries reveal themselves. EMBO J.

Duffy, S., and MacVicar, B.A. (1994). Potassium-dependent calcium influx in acutely isolated hippocampal astrocytes. Neuroscience *61*, 51-61.

Emsley, J.G., and Macklis, J.D. (2006). Astroglial heterogeneity closely reflects the neuronal-defined anatomy of the adult murine CNS. Neuron Glia Biol *2*, 175-186.

Engels, B., Cam, H., Schuler, T., Indraccolo, S., Gladow, M., Baum, C., Blankenstein, T., and Uckert, W. (2003). Retroviral vectors for high-level transgene expression in T lymphocytes. Hum Gene Ther *14*, 1155-1168.

Eriksson, P.S., Nilsson, M., Wagberg, M., Hansson, E., and Ronnback, L. (1993). Kappa-opioid receptors on astrocytes stimulate L-type Ca2+ channels. Neuroscience *54*, 401-407.

Eruslanov, E., and Kusmartsev, S. (2010). Identification of ROS using oxidized DCFDA and flow-cytometry. Methods Mol Biol *594*, 57-72.

Fam, S.R., Gallagher, C.J., Kalia, L.V., and Salter, M.W. (2003). Differential frequency dependence of P2Y1- and P2Y2- mediated Ca 2+ signaling in astrocytes. J Neurosci *23*, 4437-4444.

Farber, K., and Kettenmann, H. (2006). Functional role of calcium signals for microglial function. Glia *54*, 656-665.

Farber, K., and Kettenmann, H. (2006). Purinergic signaling and microglia. Pflugers Arch *452*, 615-621.

Feldman, B., Fedida-Metula, S., Nita, J., Sekler, I., and Fishman, D. (2010). Coupling of mitochondria to store-operated Ca(2+)-signaling sustains constitutive activation of protein kinase B/Akt and augments survival of malignant melanoma cells. Cell Calcium *47*, 525-537.

Fiacco, T.A., Agulhon, C., Taves, S.R., Petravicz, J., Casper, K.B., Dong, X., Chen, J., and McCarthy, K.D. (2007). Selective stimulation of astrocyte calcium in situ does not affect neuronal excitatory synaptic activity. Neuron *54*, 611-626.

Fiacco, T.A., and McCarthy, K.D. (2004). Intracellular astrocyte calcium waves in situ increase the frequency of spontaneous AMPA receptor currents in CA1 pyramidal neurons. J Neurosci *24*, 722-732.

Fiacco, T.A., and McCarthy, K.D. (2006). Astrocyte calcium elevations: properties, propagation, and effects on brain signaling. Glia *54*, 676-690.

Foskett, J.K., White, C., Cheung, K.H., and Mak, D.O. (2007). Inositol trisphosphate receptor Ca2+ release channels. Physiol Rev *87*, 593-658.

Franke, H., Sauer, C., Rudolph, C., Krugel, U., Hengstler, J.G., and Illes, P. (2009). P2 receptor-mediated stimulation of the PI3-K/Akt-pathway in vivo. Glia *57*, 1031-1045.

Gallagher, C.J., and Salter, M.W. (2003). Differential properties of astrocyte calcium waves mediated by P2Y1 and P2Y2 receptors. J Neurosci *23*, 6728-6739.

Gandhi, S., Wood-Kaczmar, A., Yao, Z., Plun-Favreau, H., Deas, E., Klupsch, K., Downward, J., Latchman, D.S., Tabrizi, S.J., Wood, N.W.*, et al.* (2009). PINK1-associated Parkinson's disease is caused by neuronal vulnerability to calcium-induced cell death. Mol Cell *33*, 627-638.

Geback, T., Schulz, M.M., Koumoutsakos, P., and Detmar, M. (2009). TScratch: a novel and simple software tool for automated analysis of monolayer wound healing assays. Biotechniques *46*, 265-274.

Genzen, J.R., Yang, D., Ravid, K., and Bordey, A. (2009). Activation of adenosine A2B receptors enhances ciliary beat frequency in mouse lateral ventricle ependymal cells. Cerebrospinal Fluid Res *6*, 15.

Giacomello, M., Drago, I., Bortolozzi, M., Scorzeto, M., Gianelle, A., Pizzo, P., and Pozzan, T. (2010). Ca2+ hot spots on the mitochondrial surface are generated by Ca2+ mobilization from stores, but not by activation of store-operated Ca2+ channels. Mol Cell *38*, 280-290.

Gilabert, J.A., Bakowski, D., and Parekh, A.B. (2001). Energized mitochondria increase the dynamic range over which inositol 1,4,5-trisphosphate activates store-operated calcium influx. EMBO J *20*, 2672-2679.

Ginhoux, F., Greter, M., Leboeuf, M., Nandi, S., See, P., Gokhan, S., Mehler, M.F., Conway, S.J., Ng, L.G., Stanley, E.R.*, et al.* (2010). Fate mapping analysis reveals that adult microglia derive from primitive macrophages. Science *330*, 841-845.

Glitsch, M.D., Bakowski, D., and Parekh, A.B. (2002). Store-operated Ca2+ entry depends on mitochondrial Ca2+ uptake. EMBO J *21*, 6744-6754.

Gobbi, P., Castaldo, P., Minelli, A., Salucci, S., Magi, S., Corcione, E., and Amoroso, S. (2007). Mitochondrial localization of Na+/Ca2+ exchangers NCX1-3 in neurons and astrocytes of adult rat brain in situ. Pharmacol Res *56*, 556-565.

Golgi, C. (1873). Suella struttura della sostanza grigia del cervello (comunicazione preventiva). Gazetta Medica Italiana, Lombardia, 244-246.

Golgi, C. (1903). Opera Omnia Hoepli, Milano.

Gordon, G.R., Baimoukhametova, D.V., Hewitt, S.A., Rajapaksha, W.R., Fisher, T.E., and Bains, J.S. (2005). Norepinephrine triggers release of glial ATP to increase postsynaptic efficacy. Nat Neurosci *8*, 1078-1086.

Graham, F.L., and van der Eb, A.J. (1973). A new technique for the assay of infectivity of human adenovirus 5 DNA. Virology *52*, 456-467.

Greer, J. (1985). Model structure for the inflammatory protein C5a. Science *228*, 1055-1060.

Griffiths, E.J., Wei, S.K., Haigney, M.C., Ocampo, C.J., Stern, M.D., and Silverman, H.S. (1997). Inhibition of mitochondrial calcium efflux by clonazepam in intact single rat cardiomyocytes and effects on NADH production. Cell Calcium *21*, 321-329.

Grosche, J., Matyash, V., Moller, T., Verkhratsky, A., Reichenbach, A., and Kettenmann, H. (1999). Microdomains for neuron-glia interaction: parallel fiber signaling to Bergmann glial cells. Nat Neurosci *2*, 139-143.

Guyon, A., Massa, F., Rovere, C., and Nahon, J.L. (2008). How cytokines can influence the brain: a role for chemokines? J Neuroimmunol *198*, 46-55.

Haas, B., and Kettenmann, H. (2009). Calcium waves in glia. In Encyclopedia of Neuroscience (Elsevier Ltd.), pp. 567-574.

Hajnoczky, G., Hager, R., and Thomas, A.P. (1999). Mitochondria suppress local feedback activation of inositol 1,4, 5-trisphosphate receptors by Ca2+. J Biol Chem *274*, 14157-14162.

Hanisch, U.K. (2002). Microglia as a source and target of cytokines. Glia *40*, 140-155.

Hausler, K.G., Prinz, M., Nolte, C., Weber, J.R., Schumann, R.R., Kettenmann, H., and Hanisch, U.K. (2002). Interferon-gamma differentially modulates the release of cytokines and chemokines in lipopolysaccharide- and pneumococcal cell wall-stimulated mouse microglia and macrophages. Eur J Neurosci *16*, 2113-2122.

Herrmann, J.E., Imura, T., Song, B., Qi, J., Ao, Y., Nguyen, T.K., Korsak, R.A., Takeda, K., Akira, S., and Sofroniew, M.V. (2008). STAT3 is a critical regulator of astrogliosis and scar formation after spinal cord injury. J Neurosci *28*, 7231-7243.

Hertz, L., Dringen, R., Schousboe, A., and Robinson, S.R. (1999). Astrocytes: glutamate producers for neurons. J Neurosci Res *57*, 417-428.

Hirase, H., Qian, L., Bartho, P., and Buzsaki, G. (2004). Calcium dynamics of cortical astrocytic networks in vivo. PLoS Biol *2*, E96.

Hoffmann, A., Kann, O., Ohlemeyer, C., Hanisch, U.K., and Kettenmann, H. (2003). Elevation of basal intracellular calcium as a central element in the activation of brain macrophages (microglia): suppression of receptor-evoked calcium signaling and control of release function. J Neurosci *23*, 4410-4419.

Honda, S., Sasaki, Y., Ohsawa, K., Imai, Y., Nakamura, Y., Inoue, K., and Kohsaka, S. (2001). Extracellular ATP or ADP induce chemotaxis of cultured microglia through Gi/o-coupled P2Y receptors. J Neurosci *21*, 1975-1982.

Hoogland, T.M., Kuhn, B., Gobel, W., Huang, W., Nakai, J., Helmchen, F., Flint, J., and Wang, S.S. (2009). Radially expanding transglial calcium waves in the intact cerebellum. Proc Natl Acad Sci U S A *106*, 3496-3501.

Hooper, C., Taylor, D.L., and Pocock, J.M. (2005). Pure albumin is a potent trigger of calcium signalling and proliferation in microglia but not macrophages or astrocytes. J Neurochem *92*, 1363-1376.

Hoth, M., Fanger, C.M., and Lewis, R.S. (1997). Mitochondrial regulation of store-operated calcium signaling in T lymphocytes. J Cell Biol *137*, 633-648.

Hua, X., Malarkey, E.B., Sunjara, V., Rosenwald, S.E., Li, W.H., and Parpura, V. (2004). Ca2+-dependent glutamate release involves two classes of endoplasmic reticulum Ca2+ stores in astrocytes. J Neurosci Res *76*, 86-97.

Huang, G.N., Zeng, W., Kim, J.Y., Yuan, J.P., Han, L., Muallem, S., and Worley, P.F. (2006). STIM1 carboxyl-terminus activates native SOC, I(crac) and TRPC1 channels. Nat Cell Biol *8*, 1003-1010.

Huber-Lang, M.S., Sarma, J.V., McGuire, S.R., Lu, K.T., Padgaonkar, V.A., Younkin, E.M., Guo, R.F., Weber, C.H., Zuiderweg, E.R., Zetoune, F.S.*, et al.* (2003). Structure-function relationships of human C5a and C5aR. J Immunol *170*, 6115-6124.

Ifuku, M., Farber, K., Okuno, Y., Yamakawa, Y., Miyamoto, T., Nolte, C., Merrino, V.F., Kita, S., Iwamoto, T., Komuro, I.*, et al.* (2007). Bradykinin-induced microglial migration mediated by B1-bradykinin receptors depends on Ca2+ influx via reverse-mode activity of the Na+/Ca2+ exchanger. J Neurosci *27*, 13065-13073.

Ifuku, M., Okuno, Y., Yamakawa, Y., Izumi, K., Seifert, S., Kettenmann, H., and Noda, M. (2011). Functional importance of inositol-1,4,5-triphosphate-induced intracellular Ca2+ mobilization in galanin-induced microglial migration. J Neurochem *117*, 61-70.

Innocenti, B., Parpura, V., and Haydon, P.G. (2000). Imaging extracellular waves of glutamate during calcium signaling in cultured astrocytes. J Neurosci *20*, 1800-1808.

Ishii, K., Hirose, K., and Iino, M. (2006). Ca2+ shuttling between endoplasmic reticulum and mitochondria underlying Ca2+ oscillations. EMBO Rep *7*, 390-396.

Jantaratnotai, N., Choi, H.B., and McLarnon, J.G. (2009). ATP stimulates chemokine production via a store-operated calcium entry pathway in C6 glioma cells. BMC Cancer *9*, 442.

Jiang, D., Zhao, L., and Clapham, D.E. (2009). Genome-wide RNAi screen identifies Letm1 as a mitochondrial Ca2+/H+ antiporter. Science *326*, 144-147.

Johansson, P.A., Burnstock, G., Dziegielewska, K.M., Guida, E., McIntyre, P., and Saunders, N.R. (2007). Expression and localization of P2 nucleotide receptor subtypes during development of the lateral ventricular choroid plexus of the rat. Eur J Neurosci *25*, 3319-3331.

Jourdain, P., Bergersen, L.H., Bhaukaurally, K., Bezzi, P., Santello, M., Domercq, M., Matute, C., Tonello, F., Gundersen, V., and Volterra, A. (2007). Glutamate exocytosis from astrocytes controls synaptic strength. Nat Neurosci *10*, 331-339.

Kang, J., Jiang, L., Goldman, S.A., and Nedergaard, M. (1998). Astrocyte-mediated potentiation of inhibitory synaptic transmission. Nat Neurosci *1*, 683-692.

Kettenmann, H., Hanisch, U.K., Noda, M., and Verkhratsky, A. (2011). Physiology of microglia. Physiol Rev *91*, 461-553.

Kim, B., Jeong, H.K., Kim, J.H., Lee, S.Y., Jou, I., and Joe, E.H. (2011). Uridine 5'-diphosphate induces chemokine expression in microglia and astrocytes through activation of the P2Y6 receptor. J Immunol *186*, 3701-3709.

Kim, B., Takeuchi, A., Koga, O., Hikida, M., and Matsuoka, S. (2012). Pivotal role of mitochondrial Na(+)(-)Ca(2)(+) exchange in antigen receptor mediated Ca(2)(+) signalling in DT40 and A20 B lymphocytes. J Physiol *590*, 459-474.

Kim, H., Shim, J., Han, P.L., and Choi, E.J. (1997). Nitric oxide modulates the c-Jun N-terminal kinase/stress-activated protein kinase activity through activating c-Jun N-terminal kinase kinase. Biochemistry *36*, 13677-13681.

Kim, M.H., Korogod, N., Schneggenburger, R., Ho, W.K., and Lee, S.H. (2005). Interplay between Na+/Ca2+ exchangers and mitochondria in Ca2+ clearance at the calyx of Held. J Neurosci *25*, 6057-6065.

Kingham, P.J., Cuzner, M.L., and Pocock, J.M. (1999). Apoptotic pathways mobilized in microglia and neurones as a consequence of chromogranin A-induced microglial activation. J Neurochem *73*, 538-547.

Klegeris, A., Choi, H.B., McLarnon, J.G., and McGeer, P.L. (2007). Functional ryanodine receptors are expressed by human microglia and THP-1 cells: Their possible involvement in modulation of neurotoxicity. J Neurosci Res *85*, 2207-2215.

Koizumi, S., Shigemoto-Mogami, Y., Nasu-Tada, K., Shinozaki, Y., Ohsawa, K., Tsuda, M., Joshi, B.V., Jacobson, K.A., Kohsaka, S., and Inoue, K. (2007). UDP acting at P2Y6 receptors is a mediator of microglial phagocytosis. Nature *446*, 1091-1095.

Kolikova, J., Afzalov, R., Giniatullina, A., Surin, A., Giniatullin, R., and Khiroug, L. (2006). Calcium-dependent trapping of mitochondria near plasma membrane in stimulated astrocytes. Brain Cell Biol *35*, 75-86.

Kornmann, B., Currie, E., Collins, S.R., Schuldiner, M., Nunnari, J., Weissman, J.S., and Walter, P. (2009). An ER-mitochondria tethering complex revealed by a synthetic biology screen. Science *325*, 477-481.

Kornyei, Z., Czirok, A., Vicsek, T., and Madarasz, E. (2000). Proliferative and migratory responses of astrocytes to in vitro injury. J Neurosci Res *61*, 421-429.

Kozlov, A.S., Angulo, M.C., Audinat, E., and Charpak, S. (2006). Target cell-specific modulation of neuronal activity by astrocytes. Proc Natl Acad Sci U S A *103*, 10058-10063.

Kresse, W., Sekler, I., Hoffmann, A., Peters, O., Nolte, C., Moran, A., and Kettenmann, H. (2005). Zinc ions are endogenous modulators of neurotransmitter-stimulated capacitative Ca2+ entry in both cultured and in situ mouse astrocytes. Eur J Neurosci *21*, 1626-1634.

Kreutzberg, G.W. (1996). Microglia: a sensor for pathological events in the CNS. Trends Neurosci *19*, 312-318.

Kuchibhotla, K.V., Lattarulo, C.R., Hyman, B.T., and Bacskai, B.J. (2009). Synchronous hyperactivity and intercellular calcium waves in astrocytes in Alzheimer mice. Science *323*, 1211-1215.

Kuga, N., Sasaki, T., Takahara, Y., Matsuki, N., and Ikegaya, Y. (2011). Large-scale calcium waves traveling through astrocytic networks in vivo. J Neurosci *31*, 2607-2614.

Kulik, A., Haentzsch, A., Luckermann, M., Reichelt, W., and Ballanyi, K. (1999). Neuron-glia signaling via alpha(1) adrenoceptor-mediated Ca(2+) release in Bergmann glial cells in situ. J Neurosci *19*, 8401-8408.

Landolfi, B., Curci, S., Debellis, L., Pozzan, T., and Hofer, A.M. (1998). Ca2+ homeostasis in the agonist-sensitive internal store: functional interactions between mitochondria and the ER measured In situ in intact cells. J Cell Biol *142*, 1235-1243.

Lee, M., Jantaratnotai, N., McGeer, E., McLarnon, J.G., and McGeer, P.L. (2010). Mg2+ ions reduce microglial and THP-1 cell neurotoxicity by inhibiting Ca2+ entry through purinergic channels. Brain Res *1369*, 21-35.

Lee, W., Malarkey, E.B., Reyes, R.C., and Parpura, V. (2008). Micropit: A New Cell Culturing Approach for Characterization of Solitary Astrocytes and Small Networks of these Glial Cells. Front Neuroeng *1*, 2. doi:10.3389/neuro.3316.3002.2008

Lenhossek, M.V. (1891). Zur Kenntnis der Neuroglia des menschlichen Ruckenmarkes. Verh Anat Ges, 193-221.

Li, W., Shariat-Madar, Z., Powers, M., Sun, X., Lane, R.D., and Garlid, K.D. (1992). Reconstitution, identification, purification, and immunological characterization of the 110-kDa Na+/Ca2+ antiporter from beef heart mitochondria. J Biol Chem *267*, 17983-17989.

Liu, Q.S., Xu, Q., Arcuino, G., Kang, J., and Nedergaard, M. (2004a). Astrocyte-mediated activation of neuronal kainate receptors. Proc Natl Acad Sci U S A *101*, 3172-3177.

Liu, Q.S., Xu, Q., Kang, J., and Nedergaard, M. (2004b). Astrocyte activation of presynaptic metabotropic glutamate receptors modulates hippocampal inhibitory synaptic transmission. Neuron Glia Biol *1*, 307-316.

Liu, Y., Kintner, D.B., Chanana, V., Algharabli, J., Chen, X., Gao, Y., Chen, J., Ferrazzano, P., Olson, J.K., and Sun, D. (2010). Activation of microglia depends on Na+/H+ exchange-mediated H+ homeostasis. J Neurosci *30*, 15210-15220.

Lund, S., Christensen, K.V., Hedtjarn, M., Mortensen, A.L., Hagberg, H., Falsig, J., Hasseldam, H., Schrattenholz, A., Porzgen, P., and Leist, M. (2006). The dynamics of the LPS triggered inflammatory response of murine microglia under different culture and in vivo conditions. J Neuroimmunol *180*, 71-87.

Lyons, S.A., and Kettenmann, H. (1998). Oligodendrocytes and microglia are selectively vulnerable to combined hypoxia and hypoglycemia injury in vitro. J Cereb Blood Flow Metab *18*, 521-530.

Lytton, J. (2007). Na+/Ca2+ exchangers: three mammalian gene families control Ca2+ transport. Biochem J *406*, 365-382.

Maack, C., Cortassa, S., Aon, M.A., Ganesan, A.N., Liu, T., and O'Rourke, B. (2006). Elevated cytosolic Na+ decreases mitochondrial Ca2+ uptake during excitation-contraction coupling and impairs energetic adaptation in cardiac myocytes. Circ Res *99*, 172-182.

Malarkey, E.B., and Parpura, V. (2008). Mechanisms of glutamate release from astrocytes. Neurochem Int *52*, 142-154.

Malarkey, E.B., and Parpura, V. (2011). Temporal characteristics of vesicular fusion in astrocytes: examination of synaptobrevin 2-laden vesicles at single vesicle resolution. J Physiol *589*, 4271-4300.

Malarkey, E.B., Ni, Y., and Parpura, V. (2008). Ca2+ entry through TRPC1 channels contributes to intracellular Ca2+ dynamics and consequent glutamate release from rat astrocytes. Glia *56*, 821-835.

Malli, R., Frieden, M., Osibow, K., Zoratti, C., Mayer, M., Demaurex, N., and Graier, W.F. (2003). Sustained Ca2+ transfer across mitochondria is Essential for mitochondrial Ca2+ buffering, sore-operated Ca2+ entry, and Ca2+ store refilling. J Biol Chem *278*, 44769-44779.

Malli, R., Frieden, M., Trenker, M., and Graier, W.F. (2005). The role of mitochondria for Ca2+ refilling of the endoplasmic reticulum. J Biol Chem *280*, 12114-12122.

March, D.R., Proctor, L.M., Stoermer, M.J., Sbaglia, R., Abbenante, G., Reid, R.C., Woodruff, T.M., Wadi, K., Paczkowski, N., Tyndall, J.D.*, et al.* (2004). Potent cyclic antagonists of the complement C5a receptor on human polymorphonuclear leukocytes. Relationships between structures and activity. Mol Pharmacol *65*, 868-879.

Marchaland, J., Cali, C., Voglmaier, S.M., Li, H., Regazzi, R., Edwards, R.H., and Bezzi, P. (2008). Fast subplasma membrane Ca2+ transients control exo-endocytosis of synaptic-like microvesicles in astrocytes. J Neurosci *28*, 9122-9132.

Mastellos, D., Andronis, C., Persidis, A., and Lambris, J.D. (2005). Novel biological networks modulated by complement. Clin Immunol *115*, 225-235.

Matsuda, T., Nagano, T., Takemura, M., and Baba, A. (2006). Topics on the Na+/Ca2+ exchanger: responses of Na+/Ca2+ exchanger to interferon-gamma and nitric oxide in cultured microglia. J Pharmacol Sci *102*, 22-26.

Matyash, M., Matyash, V., Nolte, C., Sorrentino, V., and Kettenmann, H. (2002). Requirement of functional ryanodine receptor type 3 for astrocyte migration. FASEB J *16*, 84-86.

Matyash, V., and Kettenmann, H. (2010). Heterogeneity in astrocyte morphology and physiology. Brain Res Rev *63*, 2-10.

Matyash, V., Filippov, V., Mohrhagen, K., and Kettenmann, H. (2001). Nitric oxide signals parallel fiber activity to Bergmann glial cells in the mouse cerebellar slice. Mol Cell Neurosci *18*, 664-670.

McLarnon, J.G., Choi, H.B., Lue, L.F., Walker, D.G., and Kim, S.U. (2005). Perturbations in calcium-mediated signal transduction in microglia from Alzheimer's disease patients. J Neurosci Res *81*, 426-435.

Menaka, K.B., Ramesh, A., Thomas, B., and Kumari, N.S. (2009). Estimation of nitric oxide as an inflammatory marker in periodontitis. J Indian Soc Periodontol *13*, 75-78.

Mertsch, K., Hanisch, U.K., Kettenmann, H., and Schnitzer, J. (2001). Characterization of microglial cells and their response to stimulation in an organotypic retinal culture system. J Comp Neurol *431*, 217-227.

Minelli, A., Castaldo, P., Gobbi, P., Salucci, S., Magi, S., and Amoroso, S. (2007). Cellular and subcellular localization of Na+-Ca2+ exchanger protein isoforms, NCX1, NCX2, and NCX3 in cerebral cortex and hippocampus of adult rat. Cell Calcium *41*, 221-234.

Moller, T., Nolte, C., Burger, R., Verkhratsky, A., and Kettenmann, H. (1997). Mechanisms of C5a and C3a complement fragment-induced [Ca2+]i signaling in mouse microglia. J Neurosci *17*, 615-624.

Montana, V., Malarkey, E.B., Verderio, C., Matteoli, M., and Parpura, V. (2006). Vesicular transmitter release from astrocytes. Glia *54*, 700-715.

Montana, V., Ni, Y., Sunjara, V., Hua, X., and Parpura, V. (2004). Vesicular glutamate transporter-dependent glutamate release from astrocytes. J Neurosci *24*, 2633-2642.

Morita, S., Kojima, T., and Kitamura, T. (2000). Plat-E: an efficient and stable system for transient packaging of retroviruses. Gene Ther *7*, 1063-1066.

Muller, C.M., and Best, J. (1989). Ocular dominance plasticity in adult cat visual cortex after transplantation of cultured astrocytes. Nature *342*, 427-430.

Munoz, E., Valero, R.A., Quintana, A., Hoth, M., Nunez, L., and Villalobos, C. (2011). Nonsteroidal anti-inflammatory drugs inhibit vascular smooth muscle cell proliferation by enabling the Ca2+-dependent inactivation of calcium release-activated calcium/orai channels normally prevented by mitochondria. J Biol Chem *286*, 16186-16196.

Murchison, D., and Griffith, W.H. (2007). Calcium buffering systems and calcium signaling in aged rat basal forebrain neurons. Aging Cell *6*, 297-305.

Nagai, T., Sawano, A., Park, E.S., and Miyawaki, A. (2001). Circularly permuted green fluorescent proteins engineered to sense Ca2+. Proc Natl Acad Sci U S A *98*, 3197-3202.

Nagano, T., Kawasaki, Y., Baba, A., Takemura, M., and Matsuda, T. (2004). Up-regulation of Na(+)-Ca2+ exchange activity by interferon-gamma in cultured rat microglia. J Neurochem *90*, 784-791.

Navarrete, M., and Araque, A. (2008). Endocannabinoids mediate neuron-astrocyte communication. Neuron *57*, 883-893.

Nett, W.J., Oloff, S.H., and McCarthy, K.D. (2002). Hippocampal astrocytes in situ exhibit calcium oscillations that occur independent of neuronal activity. J Neurophysiol *87*, 528-537.

Neumann, J.T., Diaz-Sylvester, P.L., Fleischer, S., and Copello, J.A. (2011). CGP-37157 inhibits the sarcoplasmic reticulum Ca(2)+ ATPase and activates ryanodine receptor channels in striated muscle. Mol Pharmacol *79*, 141-147.

Newman, E.A. (2003). Glial cell inhibition of neurons by release of ATP. J Neurosci *23*, 1659-1666.

Newman, E.A. (2005). Calcium increases in retinal glial cells evoked by light-induced neuronal activity. J Neurosci *25*, 5502-5510.

Newman, E.A., and Zahs, K.R. (1998). Modulation of neuronal activity by glial cells in the retina. J Neurosci *18*, 4022-4028.

Ni, Y., and Parpura, V. (2009). Dual regulation of Ca2+-dependent glutamate release from astrocytes: vesicular glutamate transporters and cytosolic glutamate levels. Glia *57*, 1296-1305.

Nimmerjahn, A., Kirchhoff, F., and Helmchen, F. (2005). Resting microglial cells are highly dynamic surveillants of brain parenchyma in vivo. Science *308*, 1314-1318.

Nimmerjahn, A., Mukamel, E.A., and Schnitzer, M.J. (2009). Motor behavior activates Bergmann glial networks. Neuron *62*, 400-412.

Nolte, C., Moller, T., Walter, T., and Kettenmann, H. (1996). Complement 5a controls motility of murine microglial cells in vitro via activation of an inhibitory G-protein and the rearrangement of the actin cytoskeleton. Neuroscience *73*, 1091-1107.

Oliveira, J.M., and Goncalves, J. (2009). In situ mitochondrial Ca2+ buffering differences of intact neurons and astrocytes from cortex and striatum. J Biol Chem *284*, 5010-5020.

Omote, H., Miyaji, T., Juge, N., and Moriyama, Y. (2011). Vesicular neurotransmitter transporter: bioenergetics and regulation of glutamate transport. Biochemistry *50*, 5558-5565.

Palty, R., and Sekler, I. (2012). The mitochondrial Na(+)/Ca(2+) exchanger. Cell Calcium *52*, 9-15.

Palty, R., Hershfinkel, M., Yagev, O., Saar, D., Barkalifa, R., Khananshvili, D., Peretz, A., Grossman, Y., and Sekler, I. (2006). Single alpha-domain constructs of the Na+/Ca2+ exchanger, NCLX, oligomerize to form a functional exchanger. Biochemistry *45*, 11856-11866.

Palty, R., Ohana, E., Hershfinkel, M., Volokita, M., Elgazar, V., Beharier, O., Silverman, W.F., Argaman, M., and Sekler, I. (2004). Lithium-calcium exchange is mediated by a distinct potassium-independent sodium-calcium exchanger. J Biol Chem *279*, 25234-25240.

Palty, R., Silverman, W.F., Hershfinkel, M., Caporale, T., Sensi, S.L., Parnis, J., Nolte, C., Fishman, D., Shoshan-Barmatz, V., Herrmann, S.*, et al.* (2010). NCLX is an essential component of mitochondrial Na+/Ca2+ exchange. Proc Natl Acad Sci U S A *107*, 436-441.

Panatier, A., Theodosis, D.T., Mothet, J.P., Touquet, B., Pollegioni, L., Poulain, D.A., and Oliet, S.H. (2006). Glia-derived D-serine controls NMDA receptor activity and synaptic memory. Cell *125*, 775-784.

Parekh, A.B. (2008). Mitochondrial regulation of store-operated CRAC channels. Cell Calcium *44*, 6-13.

Parekh, A.B., and Putney, J.W., Jr. (2005). Store-operated calcium channels. Physiol Rev *85*, 757-810.

Parpura, V., and Haydon, P.G. (2000). Physiological astrocytic calcium levels stimulate glutamate release to modulate adjacent neurons. Proceedings of the National Academy of Sciences of the United States of America *97*, 8629-8634.

Parpura, V., and Verkhratsky, A. (2011). The astrocyte excitability brief: From receptors to gliotransmission. Neurochem Int.

Parpura, V., Heneka, M.T., Montana, V., Oliet, S.H., Schousboe, A., Haydon, P.G., Stout, R.F., Jr., Spray, D.C., Reichenbach, A., Pannicke, T.*, et al.* (2012). Glial cells in (patho)physiology. J Neurochem *121*, 4-27.

Parri, H.R., and Crunelli, V. (2003). The role of Ca2+ in the generation of spontaneous astrocytic Ca2+ oscillations. Neuroscience *120*, 979-992.

Parri, H.R., Gould, T.M., and Crunelli, V. (2001). Spontaneous astrocytic Ca2+ oscillations in situ drive NMDAR-mediated neuronal excitation. Nat Neurosci *4*, 803-812.

Pascual, O., Casper, K.B., Kubera, C., Zhang, J., Revilla-Sanchez, R., Sul, J.Y., Takano, H., Moss, S.J., McCarthy, K., and Haydon, P.G. (2005). Astrocytic purinergic signaling coordinates synaptic networks. Science *310*, 113-116.

Pasti, L., Volterra, A., Pozzan, T., and Carmignoto, G. (1997). Intracellular calcium oscillations in astrocytes: a highly plastic, bidirectional form of communication between neurons and astrocytes in situ. J Neurosci *17*, 7817-7830.

Paucek, P., and Jaburek, M. (2004). Kinetics and ion specificity of Na(+)/Ca(2+) exchange mediated by the reconstituted beef heart mitochondrial Na(+)/Ca(2+) antiporter. Biochim Biophys Acta *1659*, 83-91.

Pellerin, L., and Magistretti, P.J. (1994). Glutamate uptake into astrocytes stimulates aerobic glycolysis: a mechanism coupling neuronal activity to glucose utilization. Proc Natl Acad Sci U S A *91*, 10625-10629.

Perea, G., and Araque, A. (2005a). Glial calcium signaling and neuron-glia communication. Cell Calcium *38*, 375-382.

Perea, G., and Araque, A. (2005b). Properties of synaptically evoked astrocyte calcium signal reveal synaptic information processing by astrocytes. J Neurosci *25*, 2192-2203.

Perea, G., Navarrete, M., and Araque, A. (2009). Tripartite synapses: astrocytes process and control synaptic information. Trends Neurosci *32*, 421-431.

Peters, O., Schipke, C.G., Hashimoto, Y., and Kettenmann, H. (2003). Different mechanisms promote astrocyte Ca2+ waves and spreading depression in the mouse neocortex. J Neurosci *23*, 9888-9896.

Pfrieger, F.W., and Barres, B.A. (1997). Synaptic efficacy enhanced by glial cells in vitro. Science *277*, 1684-1687.

Piet, R., and Jahr, C.E. (2007). Glutamatergic and purinergic receptor-mediated calcium transients in Bergmann glial cells. J Neurosci *27*, 4027-4035.

Pinton, P., Giorgi, C., Siviero, R., Zecchini, E., and Rizzuto, R. (2008). Calcium and apoptosis: ER-mitochondria Ca2+ transfer in the control of apoptosis. Oncogene *27*, 6407-6418.

Pivneva, T., Haas, B., Reyes-Haro, D., Laube, G., Veh, R.W., Nolte, C., Skibo, G., and Kettenmann, H. (2008). Store-operated Ca2+ entry in astrocytes: different spatial arrangement of endoplasmic reticulum explains functional diversity in vitro and in situ. Cell Calcium *43*, 591-601.

Pizzo, P., Drago, I., Filadi, R., and Pozzan, T. (2012). Mitochondrial Ca(2+) homeostasis: mechanism, role, and tissue specificities. Pflugers Arch *464*, 3-17.

Pocock, J.M., and Kettenmann, H. (2007). Neurotransmitter receptors on microglia. Trends Neurosci *30*, 527-535.

Prinz, M., Kann, O., Draheim, H.J., Schumann, R.R., Kettenmann, H., Weber, J.R., and Hanisch, U.K. (1999). Microglial activation by components of gram-positive and -negative bacteria: distinct and common routes to the induction of ion channels and cytokines. J Neuropathol Exp Neurol *58*, 1078-1089.

Putney, J.W. (2009). Capacitative calcium entry: from concept to molecules. Immunol Rev *231*, 10-22.

Puzianowska-Kuznicka, M., and Kuznicki, J. (2009). The ER and ageing II: calcium homeostasis. Ageing Res Rev *8*, 160-172.

Rao, J.N., Platoshyn, O., Golovina, V.A., Liu, L., Zou, T., Marasa, B.S., Turner, D.J., Yuan, J.X., and Wang, J.Y. (2006). TRPC1 functions as a store-operated Ca2+ channel in intestinal epithelial cells and regulates early mucosal restitution after wounding. Am J Physiol Gastrointest Liver Physiol *290*, G782-792.

Reyes, R.C., and Parpura, V. (2008). Mitochondria modulate Ca2+-dependent glutamate release from rat cortical astrocytes. J Neurosci *28*, 9682-9691.

Reyes, R.C., Perry, G., Lesort, M., and Parpura, V. (2011). Immunophilin deficiency augments Ca2+-dependent glutamate release from mouse cortical astrocytes. Cell Calcium *49*, 23-34.

Reyes, R.C., Verkhratsky, A., and Parpura, V. (2012). Plasmalemmal Na+/ Ca2+ exchanger modulates Ca2+-dependent exocytotic release of glutamate from rat cortical astrocytes. ASN Neuro *In Press*.

Rieger, A., Deitmer, J.W., and Lohr, C. (2007). Axon-glia communication evokes calcium signaling in olfactory ensheathing cells of the developing olfactory bulb. Glia *55*, 352-359.

Ringer, S. (1883). A further Contribution regarding the influence of the different Constituents of the Blood on the Contraction of the Heart. J Physiol *4*, 29-42 23.

Robitaille, R. (1998). Modulation of synaptic efficacy and synaptic depression by glial cells at the frog neuromuscular junction. Neuron *21*, 847-855.

Rock, R.B., Gekker, G., Hu, S., Sheng, W.S., Cheeran, M., Lokensgard, J.R., and Peterson, P.K. (2004). Role of microglia in central nervous system infections. Clin Microbiol Rev *17*, 942-964, table of contents.

Rostene, W., Guyon, A., Kular, L., Godefroy, D., Barbieri, F., Bajetto, A., Banisadr, G., Callewaere, C., Conductier, G., Rovere, C.*, et al.* (2011). Chemokines and chemokine receptors: new actors in neuroendocrine regulations. Front Neuroendocrinol *32*, 10-24.

Sarafian, T.A., Montes, C., Imura, T., Qi, J., Coppola, G., Geschwind, D.H., and Sofroniew, M.V. (2010). Disruption of astrocyte STAT3 signaling decreases mitochondrial function and increases oxidative stress in vitro. PLoS One *5*, e9532.

Sattayaprasert, P., Choi, H.B., Chongthammakun, S., and McLarnon, J.G. (2005). Platelet-activating factor enhancement of calcium influx and interleukin-6 expression, but not production, in human microglia. J Neuroinflammation *2*, 11.

Savarin-Vuaillat, C., and Ransohoff, R.M. (2007). Chemokines and chemokine receptors in neurological disease: raise, retain, or reduce? Neurotherapeutics *4*, 590-601.

Sawada, M., Suzumura, A., Yamamoto, H., and Marunouchi, T. (1990). Activation and proliferation of the isolated microglia by colony stimulating factor-1 and possible involvement of protein kinase C. Brain Res *509*, 119-124.

Schipke, C.G., Haas, B., and Kettenmann, H. (2008). Astrocytes discriminate and selectively respond to the activity of a subpopulation of neurons within the barrel cortex. Cereb Cortex *18*, 2450-2459.

Schummers, J., Yu, H., and Sur, M. (2008). Tuned responses of astrocytes and their influence on hemodynamic signals in the visual cortex. Science *320*, 1638-1643.

Seifert, S., Pannell, M., Uckert, W., Farber, K., and Kettenmann, H. (2011). Transmitter- and hormone-activated Ca(2+) responses in adult microglia/brain macrophages in situ recorded after viral transduction of a recombinant Ca(2+) sensor. Cell Calcium *49*, 365-375.

Semple, B.D., Kossmann, T., and Morganti-Kossmann, M.C. (2010). Role of chemokines in CNS health and pathology: a focus on the CCL2/CCR2 and CXCL8/CXCR2 networks. J Cereb Blood Flow Metab *30*, 459-473.

Sergeeva, M., Strokin, M., Wang, H., Ubl, J.J., and Reiser, G. (2003). Arachidonic acid in astrocytes blocks Ca(2+) oscillations by inhibiting store-operated Ca(2+) entry, and causes delayed Ca(2+) influx. Cell Calcium *33*, 283-292.

Serrano, A., Haddjeri, N., Lacaille, J.C., and Robitaille, R. (2006). GABAergic network activation of glial cells underlies hippocampal heterosynaptic depression. J Neurosci *26*, 5370-5382.

Simard, M., Arcuino, G., Takano, T., Liu, Q.S., and Nedergaard, M. (2003). Signaling at the gliovascular interface. J Neurosci *23*, 9254-9262.

Smith, M.A., and Schnellmann, R.G. (2012). Calpains, mitochondria, and apoptosis. Cardiovasc Res.

Sofroniew, M.V. (2009). Molecular dissection of reactive astrogliosis and glial scar formation. Trends Neurosci *32*, 638-647.

Sofroniew, M.V., and Vinters, H.V. (2010). Astrocytes: biology and pathology. Acta Neuropathol *119*, 7-35.

Spooren, A., Kolmus, K., Laureys, G., Clinckers, R., De Keyser, J., Haegeman, G., and Gerlo, S. (2011). Interleukin-6, a mental cytokine. Brain Res Rev *67*, 157-183.

Squier, T.C., and Bigelow, D.J. (2000). Protein oxidation and age-dependent alterations in calcium homeostasis. Front Biosci *5*, D504-526.

Stanimirovic, D.B., Ball, R., Mealing, G., Morley, P., and Durkin, J.P. (1995). The role of intracellular calcium and protein kinase C in endothelin-stimulated proliferation of rat type I astrocytes. Glia *15*, 119-130.

Starkov, A.A. (2010). The molecular identity of the mitochondrial Ca2+ sequestration system. FEBS J *277*, 3652-3663.

Stevens, B., Allen, N.J., Vazquez, L.E., Howell, G.R., Christopherson, K.S., Nouri, N., Micheva, K.D., Mehalow, A.K., Huberman, A.D., Stafford, B.*, et al.* (2007). The classical complement cascade mediates CNS synapse elimination. Cell *131*, 1164-1178.

Stohwasser, R., Giesebrecht, J., Kraft, R., Muller, E.C., Hausler, K.G., Kettenmann, H., Hanisch, U.K., and Kloetzel, P.M. (2000). Biochemical analysis of proteasomes from mouse microglia: induction of immunoproteasomes by interferon-gamma and lipopolysaccharide. Glia *29*, 355-365.

Strachan, A.J., Woodruff, T.M., Haaima, G., Fairlie, D.P., and Taylor, S.M. (2000). A new small molecule C5a receptor antagonist inhibits the reverse-passive Arthus reaction and endotoxic shock in rats. J Immunol *164*, 6560-6565.

Strehler, E.E., and Treiman, M. (2004). Calcium pumps of plasma membrane and cell interior. Curr Mol Med *4*, 323-335.

Strehler, E.E., Caride, A.J., Filoteo, A.G., Xiong, Y., Penniston, J.T., and Enyedi, A. (2007). Plasma membrane Ca2+ ATPases as dynamic regulators of cellular calcium handling. Ann N Y Acad Sci *1099*, 226-236.

Sudhof, T.C. (2004). The synaptic vesicle cycle. Annu Rev Neurosci *27*, 509-547.

Takata, N., and Hirase, H. (2008). Cortical layer 1 and layer 2/3 astrocytes exhibit distinct calcium dynamics in vivo. PLoS One *3*, e2525.

Thu le, T., Ahn, J.R., and Woo, S.H. (2006). Inhibition of L-type Ca2+ channel by mitochondrial Na+-Ca2+ exchange inhibitor CGP-37157 in rat atrial myocytes. Eur J Pharmacol *552*, 15-19.

Toescu, E.C., and Verkhratsky, A. (2004). Ca2+ and mitochondria as substrates for deficits in synaptic plasticity in normal brain ageing. J Cell Mol Med *8*, 181-190.

Toescu, E.C., and Verkhratsky, A. (2007). The importance of being subtle: small changes in calcium homeostasis control cognitive decline in normal aging. Aging Cell *6*, 267-273.

Toescu, E.C., Moller, T., Kettenmann, H., and Verkhratsky, A. (1998). Long-term activation of capacitative Ca2+ entry in mouse microglial cells. Neuroscience *86*, 925-935.

Tsien, R.Y. (1981). A non-disruptive technique for loading calcium buffers and indicators into cells. Nature *290*, 527-528.

Ullian, E.M., Sapperstein, S.K., Christopherson, K.S., and Barres, B.A. (2001). Control of synapse number by glia. Science *291*, 657-661.

Valero, R.A., Senovilla, L., Nunez, L., and Villalobos, C. (2008). The role of mitochondrial potential in control of calcium signals involved in cell proliferation. Cell Calcium *44*, 259-269.

Varadi, A., Cirulli, V., and Rutter, G.A. (2004). Mitochondrial localization as a determinant of capacitative Ca2+ entry in HeLa cells. Cell Calcium *36*, 499-508.

Verkhratsky, A., Orkand, R.K., and Kettenmann, H. (1998). Glial calcium: homeostasis and signaling function. Physiol Rev *78*, 99-141.

Verkhratsky, A., Rodriguez, J.J., and Parpura, V. (2011). Calcium signalling in astroglia. Mol Cell Endocrinol *353*, 45-56.

Verkhratsky, A., Shmigol, A., Kirischuk, S., Pronchuk, N., and Kostyuk, P. (1994). Age-dependent changes in calcium currents and calcium homeostasis in mammalian neurons. Ann N Y Acad Sci *747*, 365-381.

Virchow, R. (1858). Die Cellularpathologie in ihrer Begründung auf physiologische and pathologische Gewebelehre. Zwanzig Vorlesungen gehalten während der Monate Februar, März und April 1858 im pathologischen Institut zu Berlin., First Edition edn (August Hirscwald, Berlin).

Waldeck-Weiermair, M., Jean-Quartier, C., Rost, R., Khan, M.J., Vishnu, N., Bondarenko, A.I., Imamura, H., Malli, R., and Graier, W.F. Leucine zipper EF hand-containing transmembrane protein 1 (Letm1) and uncoupling proteins 2 and 3 (UCP2/3) contribute to two distinct mitochondrial Ca2+ uptake pathways. J Biol Chem *286*, 28444-28455.

Wang, X., Lou, N., Xu, Q., Tian, G.F., Peng, W.G., Han, X., Kang, J., Takano, T., and Nedergaard, M. (2006). Astrocytic Ca2+ signaling evoked by sensory stimulation in vivo. Nat Neurosci *9*, 816-823.

Wei, C., Wang, X., Chen, M., Ouyang, K., Song, L.S., and Cheng, H. (2009). Calcium flickers steer cell migration. Nature *457*, 901-905.

Wiedemann, N., Frazier, A.E., and Pfanner, N. (2004). The protein import machinery of mitochondria. J Biol Chem *279*, 14473-14476.

Wing, M.R., Bourdon, D.M., and Harden, T.K. (2003). PLC-epsilon: a shared effector protein in Ras-, Rho-, and G alpha beta gamma-mediated signaling. Mol Interv *3*, 273-280.

Xu, H.T., Yuan, X.B., Guan, C.B., Duan, S., Wu, C.P., and Feng, L. (2004). Calcium signaling in chemorepellant Slit2-dependent regulation of neuronal migration. Proc Natl Acad Sci U S A *101*, 4296-4301.

Yagi, R., Tanaka, S., and Koike, T. (1999). Thapsigargin induces microglial transformation from amoeboid to ramified type in vitro. Glia *28*, 49-52.

Yang, Y., Ge, W., Chen, Y., Zhang, Z., Shen, W., Wu, C., Poo, M., and Duan, S. (2003). Contribution of astrocytes to hippocampal long-term potentiation through release of D-serine. Proc Natl Acad Sci U S A *100*, 15194-15199.

Yuan, J.P., Zeng, W., Huang, G.N., Worley, P.F., and Muallem, S. (2007). STIM1 heteromultimerizes TRPC channels to determine their function as store-operated channels. Nat Cell Biol *9*, 636-645.

Zhang, Z., Chen, G., Zhou, W., Song, A., Xu, T., Luo, Q., Wang, W., Gu, X.S., and Duan, S. (2007). Regulated ATP release from astrocytes through lysosome exocytosis. Nat Cell Biol *9*, 945-953.

Xiong, J., Verkhratsky, A., and Toescu, E.C. (2002). Changes in mitochondrial status associated with altered Ca2+ homeostasis in aged cerebellar granule neurons in brain slices. J Neurosci *22*, 10761-10771.

Curriculum Vitae

Mein Lebenslauf wird aus datenschutzrechtlichen Gründen in der elektronischen Version meiner Arbeit nicht veröffentlicht.

Publications

Parnis J, Montana V, Delgado-Martinez I, Matyash V, Parpura V, Kettenmann H, Sekler I*, Nolte C*. Mitochondrial exchanger NCLX plays a major role in the intracellular Ca^{2+} signaling, gliotransmission and proliferation of astrocytes. (submitted to J. Neurosci., * equal contribution)

Parnis J, Nolte C, Freyer N, Kettenmann H, Sekler I. Mitochondrial Na^{+}/Ca^{2+}exchanger NCLX affects microglial inflammatory properties. (manuscript in preparation)

Palty R, Silverman WF, Hershfinkel M, Caporale T, Sensi SL, **Parnis J**, Nolte C, Fishman D, Shoshan-Barmatz V, Herrmann S, Khananshvili D, Sekler I. 2010. NCLX is an essential component of mitochondrial Na^{+}/Ca^{2+} exchange. Proceedings of the National Academy of Sciences of the United States of America 107(1):436-441.

Ilouz N, Branski L, **Parnis J**, Parnas H, Linial M. 1999. Depolarization affects the binding properties of muscarinic acetylcholine receptors and their interaction with proteins of the exocytic apparatus. Journal of Biological Chemistry 274(41):29519-29528.

Abstracts and meetings

Selected scientific abstracts

Parnis J, Nolte C, Matyash V, Kettenmann H, Sekler I. 2011. NCLX is the mitochondrial Na^+/Ca^{2+}exchanger in astrocytes, modulates Ca^{2+} signaling and Ca^{2+} wave propagation. Glia 59: S51-S51.

Parnis J, Boschwitz H, Linial M. 1999. Studying stimulation of neurotransmitter release by monitoring synaptic vesicle pools and the stability of snare proteins. Neuroscience Letters:S32-S32.

Selected scientific meetings

Parnis J, Nolte C, Matiash V, Kettenmann H, Sekler I. 2011. Mitochondrial Na^+/Ca^{2+}exchanger NCLX: connecting mitochondria, calcium and physiology in astrocytes. Berlin Brain Days, December 2011, Berlin, Germany

Parnis J, Sekler I, Freyer N, Kettenmann H, Nolte C . 2010. The physiological role of mitochondrial Na^+/Ca^{2+} exchanger NCLX for microglial Ca^{2+} homeostasis. Berlin Brain Days, November 2010, Berlin, Germany

Parnis J, Sekler I, Kettenmann H, Nolte C . 2010. The physiological role of mitochondrial Na^+/Ca^{2+} exchanger NCLX for glial Ca^{2+} homeostasis. 7^{th} FENS meeting, July 2010, Amsterdam, Netherlands

Erklärung

„Ich, Julia Parnis, erkläre, dass ich die vorgelegte Dissertation mit dem Thema: „*The physiological role of mitochondrial Na^+/Ca^{2+} exchanger NCLX for glial Ca^{2+} homeostasis*“ selbst verfasst und keine anderen als die angegebenen Quellen und Hilfsmittel benutzt, ohne die (unzulässige) Hilfe Dritter verfasst und auch in Teilen keine Kopien anderer Arbeiten dargestellt habe.“

Berlin, den

_____

Julia Parnis